THE DISTRIBUTION OF DIAMONDS ON A LATE CAINOZOIC GRAVEL BEACH, SOUTHWESTERN NAMIBIA

by

Leonard Apollus

Thesis submitted in fulfilment of the requirements
for the degree of Master of Science in Geology

Department of Geology and Applied Geology
University of Glasgow
November 1995

ProQuest LLC.
789 East Eisenhower Parkway
P.O. Box 1346
Ann Arbor, MI 48106 – 1346

THESIS DECLARATION

The material contained in this thesis is the result of my own research carried out between October 1993 and November 1995, at Namdeb and the Department of Geology and Applied Geology, University of Glasgow. Any published or unpublished work from other sources has been duly referenced in the text.

L. Apollus

ACKNOWLEDGMENTS

This study was kindly sponsored by the Namdeb Diamond Corporation (Pty) Ltd., without whose generous financial support this opportunity would never have been possible. Prof. Brian Bluck and Dr. Jeffrey Harris from the Department of Geology and Applied Geology, University of Glasgow, and Dr. John Ward of Namdeb, jointly supervised this project.

I am greatly indebted to the management of Namdeb for allowing me the time away from work to complete this thesis at the University of Glasgow, in particular the Ore Reserves Manager Mike Lain and Graham Wheelock, who initiated this project and whose continuous support and encouragement has been a tremendous inspiration to me throughout this project. Special thanks go to Dr. John Ward who never hesitated to offer much valuable advice on many different aspects of this project, often during evenings and weekends, as well as encouragement, and also his impeccable arrangements for my trip to Glasgow.

This study has greatly benefitted from the many constructive suggestions of Prof. B.J. Bluck and Dr. J.W. Harris and I gratefully acknowledge their guidence. The numerous discussions that Prof. Bluck and I had on a wide range of aspects relating to gravel beaches and alluvial deposits in general has been a very enriching learning experience to me.

The technical support that I received was absolutely first class. Thanks to the Namdeb mining department for their support in providing the equipment for the excavation and treatment of the diamond samples, here I particularly thank John Kilham, Doc Smit, Manie Klaazen, Malan Gerber, and their teams. Johannes, the poclain operator for his patience in

excavating the samples carefully with me. Debbie, Miemie, Ronel and Elana from the Geology laboratory for helping with the handsorting of the diamond concentrate and providing biscuits for lunch. Verlece Anderson, Edna van Blerk and Gill Parker from Harry Openheimer House (Kimberley) assisted with the diamond descriptions at CSO Valuations Namibia (Windhoek) who kindly allowed me to use their facilities. Gill helped with the photography of the excellent quality diamond photographs. Sydney from the Geological Survey of Namibia prepared the petrographic thin sections. Andre Fourie and Francois Prinsloo of the survey section helped with the theodolite surveys of the shore platforms. Many thanks to Louw Maritz from the drawing office who produced super quality diagrams for this thesis as well as Dave Farrow and his team who provided excellent computer backup. Also Dr. J. Vogel of the Council for Scientific and Industrial Research (CSIR) in South Africa for the radiometric dating of the shell samples.

I want to thank the Department of Geology and Applied Geology for allowing me the use of its facilities, and also the technical staff in this department for their assistance in many different ways. Also Chris McKeown for being so kind in helping to make my data compatible to the Apple Macintosh and sorting out many of my computer problems despite the pressures of his own studies.

I also want to thank all my colleages in the Ore Reserves Department who offered help and encouragement in many different ways throughout this project. Particularly Renato Spaggiari, Alex Warne and Jurgen Jacob, who showed so much patience when at times I seemed to have lost a few nuts as I tried to unravel some of the mysteries of the "shiny rounded pebbles lying on the Chameis beach".

Lots of thanks go to Brian and Mary Bluck for their endless hospitality in making my stay in Glasgow so enjoyable and also for introducing me to its wonderful culture!! Charles Rennie McIntosh, will always feature strongly in my future discussions with those that are architecturally inclined.

Finally I thank my family and friends for their support and Cynthia for all her understanding throughout this study.

CONTENTS

ABSTRACT

The Late Cainozoic diamondiferous pocket beach deposits studied here are exposed in the Chameis area along 8.8km of the storm-dominated, Atlantic coastline of the Sperrgebiet of southwestern Namibia, 100km north of the mouth of the Orange River. Several pocket beaches are present in the area, but only the deposits of the most extensive pocket beach (number 4) were studied. The main aim is to derive a model for the concentration of diamond placers in pocket beaches. In persuit of this aim the characteristics of the sediments and the shore platform on which they rest were recorded across and along the beach, and within that sedimentary framework, variations in both concentration and size of diamonds were recorded. In addition, the general characteristics, as well as the abrasion textures of the diamonds recovered from these sediments were described in detail for possible evidence of their original source and subsequent transport history. The exposures available for study were largely dependent on the progress of the mining operations in the study area which strip open the diamond bearing marine sediment otherwise buried under thick modern aeolian and beach sand. The sediment in the most southern part of the pocket beach was mined-out before this study commenced, nonetheless information about this part of the beach could be obtained from in-house reports.

Two sharply bounded lithostratigraphic units are recognized and are subdivided into an eastward (landward) red unit, Eemian in age, and a westward (seaward) Holocene grey unit. Both units comprise of a basal gravelly unit interpreted to represent the transgressive phase of beach accretion and an upper finer regressive phase. The downward progradational offlapping gravels of the red unit are interpreted as beachface (intertidal) facies with a more sandy and thicker seaward shoreface facies. The westward grey unit is interpreted to be wholly of the shoreface

(subtidal) facies. Both the mean and maximum grain size of the gravel fraction of both units increase towards the northern end of the pocket beach as does the sorting of the red unit gravel fraction. The high specific density banded ironstone formation, Orange River derived, exotic clasts also increase in abundance in the same direction as well as the relative concentration of diamonds. This trend indicates an increasing energy response towards the northern end of the pocket beach.

The Chameis deposits largely record the regressive phases of a sequence of transgressions and regressions. On the basis of the stratigraphic data from these deposits, the general sequence of the Namibian (Sperrgebiet) beaches and the global Pleistocene sea-level records, the following sequence of events is deduced:

6) Deposition of dune sand (TOP)

5) Regression and deposition of grey unit

4) Transgression and partial erosion of red unit

3) Sheetflows and mass-wasting from land: subaerial exposure

2) Regression and deposition of red unit, c. 130 000 BP

1) A major transgression: recutting and/or modification of shore platform (BASE)

During these phases of erosion and deposition normal to the coastline, diamonds were thought to be moving northwards along the shore and probably from the offshore, to be trapped in these raised marine terraces.

The shore platform morphology suggests it to be an inherited feature formed at least partly by marine transgressions during Middle to Late Pleistocene. As a result of a rapid sea-level rise during the last interglacial

highstand, the shore platform has probably remained relict. The most important factors that probably influenced the present morphology of the shore platform are the rate of sea-level rise and bedrock geology. Because the morphology of the shore platform is considered to be highly sensitive to local conditions the commonly accepted alongshore correlation of shore platforms on the basis of similar heights is rejected until the morphology and genesis of the shore platform in each area has been studied in some detail.

There is no significant spatial variation in the general characteristics and abrasion features of the diamonds in the study area but the diamond characteristics are consistent with patterns reported from other studies of southern African alluvial diamond populations. It is therefore concluded that the diamonds were presorted before being introduced into the study area and therefore the distribution of their characteristics was independent of the sedimentary processes operating in the pocket beach. However, the maximum diamond concentration is in the beachface (intertidal) facies of the red unit beach. In the grey unit diamonds concentrate best in areas with the highest intensity of gullies and potholes. Therefore sedimentary processes are more important mechanisms for the entrapment of diamonds in the red unit gravel whereas gullies and potholes take precedence in the subtidal grey unit.

This study has established a database which may be useful in comparing, the distribution of lithofacies and textural characteristics of the sediments, as well as the characteristics of the diamonds, with placer deposits from different parts of the Sperrgebiet with a view to determine their similarities and thus probable primary source. A comparison of the general characteristics of the Chameis diamond population with their offshore

counterparts may also be useful.

LIST OF FIGURES

CHAPTER 3

APPENDIX I

FIGURE

TABLES

APPENDIX II

TABLE

AII.A Bedrock structural orientation data

CHAPTER 1 INTRODUCTION

This study is concerned with the stratigraphy, sedimentation and diamond concentration in a pocket beach situated on the Atlantic Coast of Namibia. A pocket beach is defined as a small and local interruption in a normally continuous rocky headland area (Davis, 1985) (Fig.1.1).

1.1 LOCATION OF STUDY AREA

The Sperrgebiet in which the study area is wholly located is part of the coastal Namib desert on the western margin of southern Africa. The study area is situated at latitude 27° 59' S and longitude 15° 42' E, 100km north of the Orange River mouth along the Atlantic margin of southwestern Africa (Fig. 1.2). The area situated just south of Chameis Bay, and extending over 8.8km parallel to the coast comprises a series of embayments, arcuate in shape, bounded by rocky headlands (Fig. 1.3). These embayments represent Late Pleistocene-Holocene raised beaches which form part of a suite of alluvial diamondiferous placers of the Sperrgebiet (Diamond Area No.1) occurring along the coastal strip between the towns of Oranjemund in the south, and Luderitz in the north. The laterally most extensive embayment (2.2km long), pocket beach number 4, shown also in Fig. 1.4, was selected for study because mining excavations in this area provided extensive exposures of both beach deposits and the shore platform. In this setting the study of beach stratigraphy, beach and shore platform geometry, and beach accretion history in relation to the distribution of diamonds was possible.

Fig. 1.1 The important features of a typical pocket beach in the Sperrgebiet. Note the refraction of the incoming waves, particularly against the southern headland.

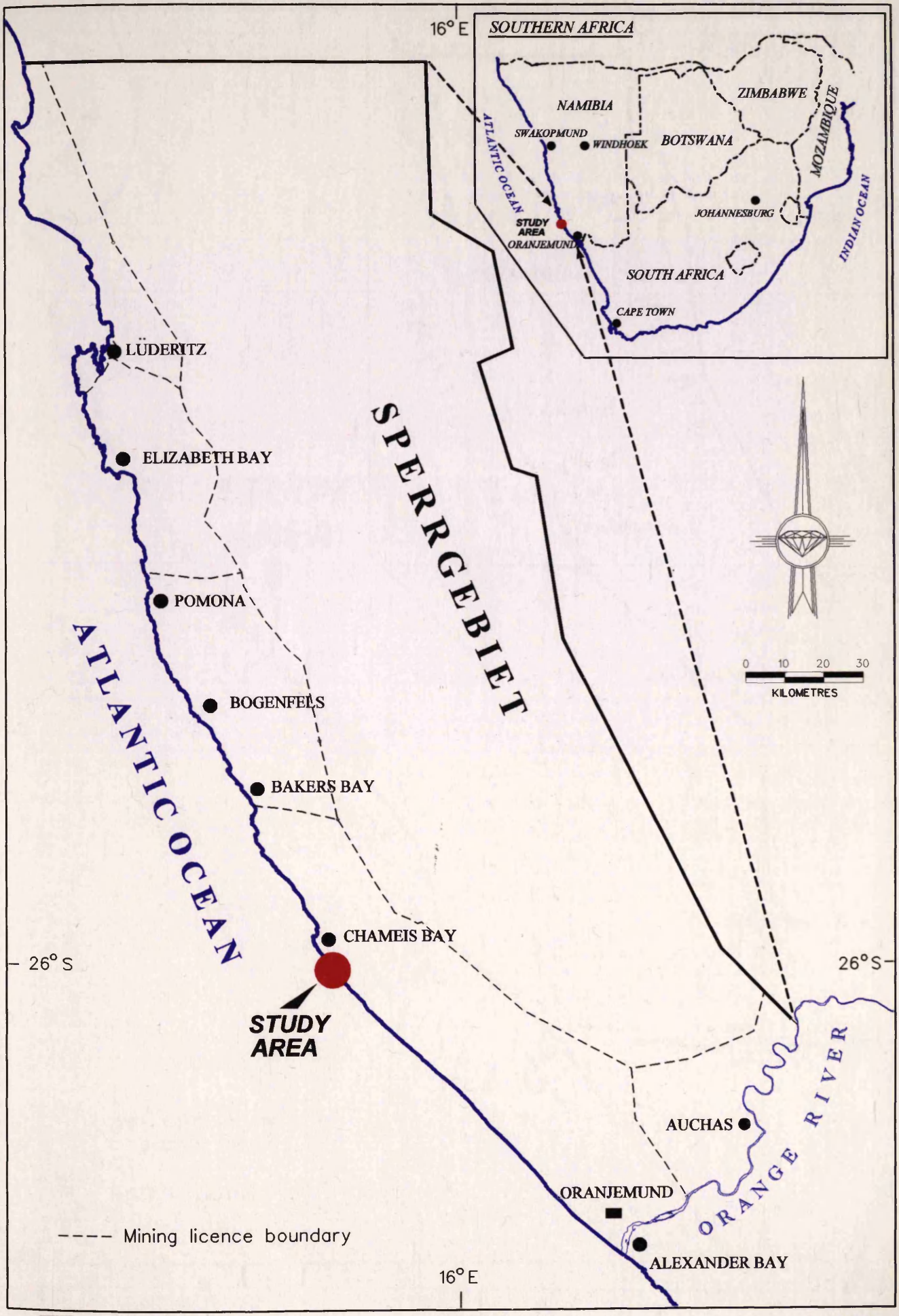

Fig. **1.2** Locality map of study area at Chameis within the Sperrgebiet, southwestern Africa.

NAMDEB

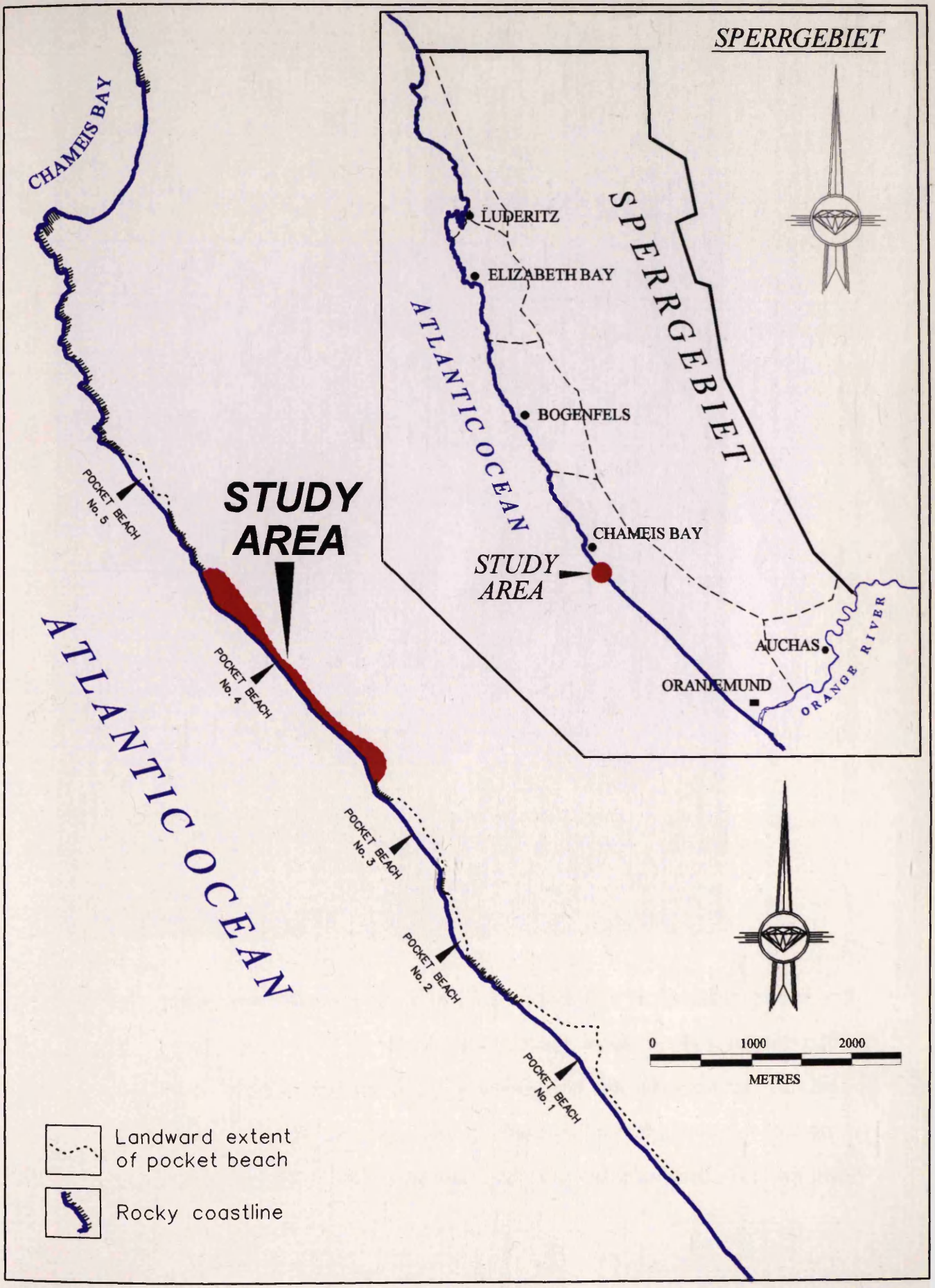

Fig. **1.3** Location of study area = pocket beach no. 4 relative to the other four known pocket beaches at Chameis, Sperrgebiet.

NAMDEB

Fig. 1.4 Oblique aerial view looking to the south-east across the central and southern parts of the study area (pocket beach No 4), Chameis (dotted outline). Current mining operations and mined-out areas can be seen in the foreground. Late Cretaceous to Early Tertiary erosion surfaces in the south (arrowed). Mining vehicles and roads for scale.

Fig. 1.4 Oblique aerial view looking to the south-east across the central and southern parts of the study area (pocket beach No 4), Chameis (dotted outline). Current mining operations and mined-out areas can be seen in the foreground. Late Cretaceous to Early Tertiary erosion surfaces in the south (arrowed). Mining vehicles and roads for scale.

1.2 PROCESSES ACTING ON THE COASTLINE

The morphology and orientation of the coastline of southwestern Africa play an important role in the distribution of sediments and diamonds on the continental margin.

The coastal region of Chameis represents the transition zone from the fairly straight coastline of the linear beaches of the southern Sperrgebiet to the more irregular or embayed coastal areas, associated with variable rock resistance, starting at Chameis and continuing northwards (see also Fig. 1.2). The coastline of southwestern Africa is dominated by persistent periodically high energy storm waves (Davies, 1964), approaching the coastline obliquely under the influence of strong south-to southwesterly winds from the south Atlantic Ocean. The average incident wave angle is ± 8.2°, while the maximum incident wave angle is ± 23.2° (CSIR, 1995). Here the waves are concentrated along the narrow coastal zone with a mean spring tidal range of 1.8m (microtidal) and the strong longshore Benguela current flowing northwards with typical speeds between 0.1 and 0.3m/s (CSIR, 1995). The average wave height for this coast is ± 2m, with wave heights and periods of up to 5m and 13 seconds, respectively, being recorded at times (CSIR, 1995). The force and constancy of the dominant south- to southwesterly winds increases from south to north, from an average of ± 26 km/h at Oranjemund to ± 38 km/h at Luderitz (see Fig. 1.1 for localities) in the afternoon (Lancaster and Ollier, 1983) (also shown later in Fig. 2.3). These winds originating in the south Atlantic high pressure system off the southwest African coastline are the driving force for the extensive Namib sand sea extending all along the west coast of southern Africa (Lancaster and Ollier, 1983), from just north of the study area.

As a result of the uneven outline of this part of the coastline, and thus also the

pocket beaches, the energy of the incoming long period waves approaching the coastline obliquely concentrate mostly on the southern headland and is refracted as shown in Fig. 1.1. This results in a decrease in wave energy in the bay bounded between the headlands as a consequence of which the free movement of sediment and diamonds, transported up the coast and having by-passed the linear beaches to the south, is hampered. Large quantities of this sediment together with the material generated locally by wave erosion of the headlands are then deposited in the pocket beaches with the rest being transported further north along the coast. The implications of this wave refraction around headlands for the transport of sediments and diamonds in the study area are further considered and illustrated in Chapter 5.

Southwestern Africa has a wide continental shelf with a gentle slope as opposed to the east coast which has a narrow shelf with a steep slope (Dingle *et al.*, 1983). The continental margin of the Sperrgebiet also has a submerged geological history which is thought to be represented by a series of post-Eemian beaches below present sea-level which overlie Tertiary sediments of the Orange River Basin. According to Murray *et al.*, (1970), the most prominent of these submarine beaches occurs at - 20m below present sea-level and is estimated to be ± 8 000-9 000 BP in age. Other less distinct submarine beaches have also been located at -30m, -40m, -60m, with an extensive, presumably wave-cut feature at -75m, and another submarine beach at -100 to -120m.

1.3 PREVIOUS WORK ON DIAMOND CONCENTRATION IN BEACHES

Considerable attention has been given to the study of different aspects of the littoral and aeolian diamond deposits of the west coast of southern Africa because of their wide distribution and considerable economic importance.

Most of these studies concentrated on the description of particular aspects of local deposits, and those addressing the general history of accretion are not publicly available. Notable among those studies that focus on aspects of the deposits are those of Merensky, 1904; Lotz, 1909; Wagner, 1914; Kaizer & Beetz, 1926; Reuning, 1931; Haughton, 1931; Hallam, 1964; Stocken, 1978; and Rouffaer, 1980. In general, these workers focussed on the regional sedimentological setting of these deposits with a view to provide a model for their mode of origin and source, for effective definition of prospecting targets. These authors postulated many different theories for the source of the diamonds along the Namibian west coast which included:

a) Merensky and Wagner (1914), amongst others that the diamonds were derived from a submarine kimberlite source

b) Lotz (1909), that the diamonds were transported by the Orange River and then concentrated on the beaches as placers

c) Kaizer (1926), that the diamonds were derived from the Kaapvaal craton

d) Beetz (1926), that the diamonds originated from the Namibian interior, and were then transported to the coast by north-south flowing rivers

e) Reuning (1931), that the diamonds from the northern areas were derived from the Late Cretaceous escarpment

f) Haughton (1931), used zone fossils to constrain the age of the older beaches as Lower Pleistocene and introduced the concept of downwarping of these beaches to the north

g) Hallam (1959; 1964), provided an excellent summary of the general stratigraphy of the beach deposits of the west coast of Namibia. He also pointed out that these beaches were largely Late Pleistocene in age and subdivided them into two groups; an Upper Terrace, about 12-25 metres above present sea-level, and a Lower Terrace, 2-10 metres above present sea-level. Hallam further argued that the altitudes of these terraces could be correlated throughout most of the Namibian west coast.

h) Stocken (1962; 1978), confirmed some of Hallam's findings, but differed in that he further subdivided the beach into six different raised terraces which he explained as reflecting a successsion of marine transgressions each followed by a major regression. Each raised beach therefore represented a marine transgression according to Stocken.

i) Rouffaer (1980), suggested a Dwyka tillite host for these diamonds

Lotz (1909) is however, credited with being the first to suggest that these diamonds came from the interior of the subcontinent and were then redistributed along the coast by ocean currents. This theory is widely accepted today as the most plausible explanation for the origin of the alluvial diamonds of the west coast of Namibia.

Hallam (1964), subdivided the littoral diamond deposits of the west coast of Namibia into two major depositional settings, (1) the Pliocene - Quaternary raised beach deposits which occur at elevations less than 40 metres above mean sea-level and (2) the aeolian deposits of the principal wind corridor situated between Chameis Bay and Swakopmund (see Fig. 1.2). He postulated that diamonds in the raised beaches mainly occur in the top (landward) and bottom (seaward) parts of the beach, marine erosion platform and storm beach gravels. They also preferentially concentrate on the north side of south-opening bays, on the south side of headlands and in steep shoreline pocket bays. Hallam(1964), also reported on the size distribution and general characteristics of these diamonds and noted a general diamond size diminution northwards, away from their source in both marine and aeolian settings. This linear decrease in diamond size has subsequently been well documented by Sutherland (1982) not only for the Namibian coast but for other systems as well. Hallam believed that there was no appreciable difference in the shape and secondary characteristics of alluvial diamonds from different

localities in the Sperrgebiet.

The Namibian beaches have been classified on the basis of their height above mean sea-level. Hallam (1964) and Stocken (1978) recorded six beaches which are considered in detail in Chapter 2 (see particularly Fig. 2.6). Recently attempts have been made to date these beaches. The beaches are generally referred to by letters A to F, with A being the youngest and F being the oldest. Corvinus (1983), used the stratigraphic context of archaeological finds from early to late Stone Age as a constraint. She suggested that, the older beach complex (F,E & D) in which no artefacts were found is considerably older than 800 000 BP , the 8 m (C-beach) has a minimum age of 400 000 BP, the 4m (B - beach) middle Pleistocene age (c. 130 000 BP) and the 2 m (A - beach) Holocene (c. 5000BP).

More recently, emphasis has been increasingly laid on the understanding of the stratigraphic context, ages, depositional environments, sedimentary response to rising and lowering of sea-levels and tectonic settings of these Late Cainozoic marine deposits as seen mainly in prospecting and mine excavations. Pether (1986), describing the late Tertiary and early Quaternary marine deposits of the west coast of South Africa, intimated that the ~ 30 metres above sea-level, seaward-thickening wedge of sediments (30 m Package) at Hondeklipbaai were the likely regional correlates of the D, E and F beaches of the west coast of Namibia because both contained the warm water zone fossils *Donax rogersi* and *Fissurella glarea*, and occur at similar elevations (9-25m). The younger beaches (< 10m above present sea-level) are characterized by the cold water zone fossil *Donax serra*.

In spite of the economic importance of these deposits and the extensive excavations which have been made into them, no detailed account of the

sedimentology, the shore platforms and their relationship to diamond distribution from the study area has been published. However, descriptions of general aspects relating to the geology and information about diamond concentrations are contained in many internal company reports.

1.4 AIMS

The main aims of this study are:

1) To establish the stratigraphic succession of the Chameis beach sediments as well as, outline the geological history of this coastal tract

2) To characterize the sedimentary deposits; recognize their facies, environment of deposition, geometry and internal structure

3) To examine the textural parameters of the beach, and determine how texture, form and structure of the sediments are related to varying energy levels on the beach

4) Deduce the nature and evolution history of the shore platform

5) Establish within the sedimentary and erosional history, the distribution of diamonds, thereby attempt to understand the mechanisms of placer formation in pocket beaches

6) To characterize the diamonds with a view to determining their origin.

The study area was selected because pocket beaches in the Sperrgebiet area are historically known to be good diamond placers, and therefore represent an important resource. In addition, pocket beaches have also generally been poorly studied, worldwide.

Before the methods used to achieve the aims set out above are outlined in section 1.6, it is important to point out some of the mining methods, as the approach followed during this study was largely controlled by the mining operations.

1.5 MINING METHODS

Mining in the study area comprises (i) overburden stripping to expose diamondiferous gravel or ore, (ii) excavation of this gravel and finally, (iii) hauling to the treatment plant.

Before excavation of the diamond-bearing gravel, a sandwall or seawall is built on the seaward side of the beach to keep the sea out of the area to be mined. Once an area has been stripped of overburden, which in the Chameis area mainly constitutes windblown and beach sand, the bulk of the gravel containing the diamonds is excavated by bulldozers and hydraulic excavators. Final cleaning of the bedrock is by either large vacuum suction units or by workers who physically sweep the bedrock to ensure that no gravel is left behind in the potholes or crevices. As soon as this process is completed, maintenance of the seawall and the pumping of sea water from the mining area stops, and the mined-out area is then flooded. The mining operations ideally advance in a carefully planned sequence, with only one or two mining blocks (approximately 30 000m^2) being mined at a time. This procedure,

however at times has to be adapted to changing physical conditions. A fleet of haul trucks carries the ore from the mine blocks to the screening plant at Chameis where sand and boulders are removed before the remaining +2 to -25 mm material is transported to a dense media separation plant for further concentration. Concentration of the heavy fraction in the +2 to -25 mm material relies on the density differential between diamond (3.5) and gangue (2.6). In this process water is mixed with finely ground ferrosilicon. The concentrate obtained represents about 0.1% of the original ore and is fed through X-ray sorting machines, at the Central Recovery Plant, under which diamonds fluoresce and are detected by a photomultiplier tube which activates air jets that blow the diamonds into a concentrate bin. This final product which represents around 0.001% of the original ore is then screened and hand sorted.

1.6 METHODOLOGY

Different aspects of sections of the study area were described, measured and sampled as they became exposed during mining operations. This mainly involved the characterization of lateral and vertical variations in stratigraphy, sedimentary facies, texture, fabric and diamond content across and along the pocket beach. These parameters were systematically recorded as a particular mining block being worked at a time progressively receded and the changes observed were documented. Table 1.1 shows most of the parameters that were measured during this study, whilst in Fig. 1.5 their relative location is shown. The sites chosen for measurement of these parameters were not on a regular grid as the areas accessible for study depended on practical considerations associated with the mining process. Care was however taken to as far as

TABLE: **1.1** Parameters measured at selected sites in the study area (pocket beach number 4), Chameis.

PARAMETERS	SITES																								
	1	2	3	4	5	6	7	8	9	10	11	12	13	14	15	16	17	18	19	20	21	22a	22b	23	24
Mean clast size						X					X	X	X	X		X	X					X	X	X	X
Maximum clast size						X					X	X	X	X		X	X					X	X	X	X
Framework clast size						X					X				X				X	X	X			X	X
Matrix grain size						X					X				X				X	X	X	X		X	X
Clast composition						X					X	X	X	X		X	X					X	X	X	X
Exotic clast composition							X						X	X		X	X								
Clast shape						X					X	X	X	X		X	X					X	X	X	X
Roundness						X																X	X	X	X
Thickness of unit											X									X	X	X	X	X	X
Elevation of unit											X									X	X	X	X	X	X
Palaeocurrent																						X			
Sampling trench											X									X	X				
Grab sample							X																		
Subsample of facies																		X				X	X	X	X
Subsample of pothole										X															
Diamond grade (cpht)							X			X	X							X		X	X	X	X	X	X
Diamond size							X			X	X							X		X	X	X	X	X	X
Diamond characteristics							X			X	X									X	X				
Bedrock struct. measurement		X	X	X	X	X		X	X																
Gully/pothole elevation		X	X	X	X	X	X	X	X	X	X			X						X	X	X	X	X	X
Petrographic description	X	X	X					X	X		X									X	X				X

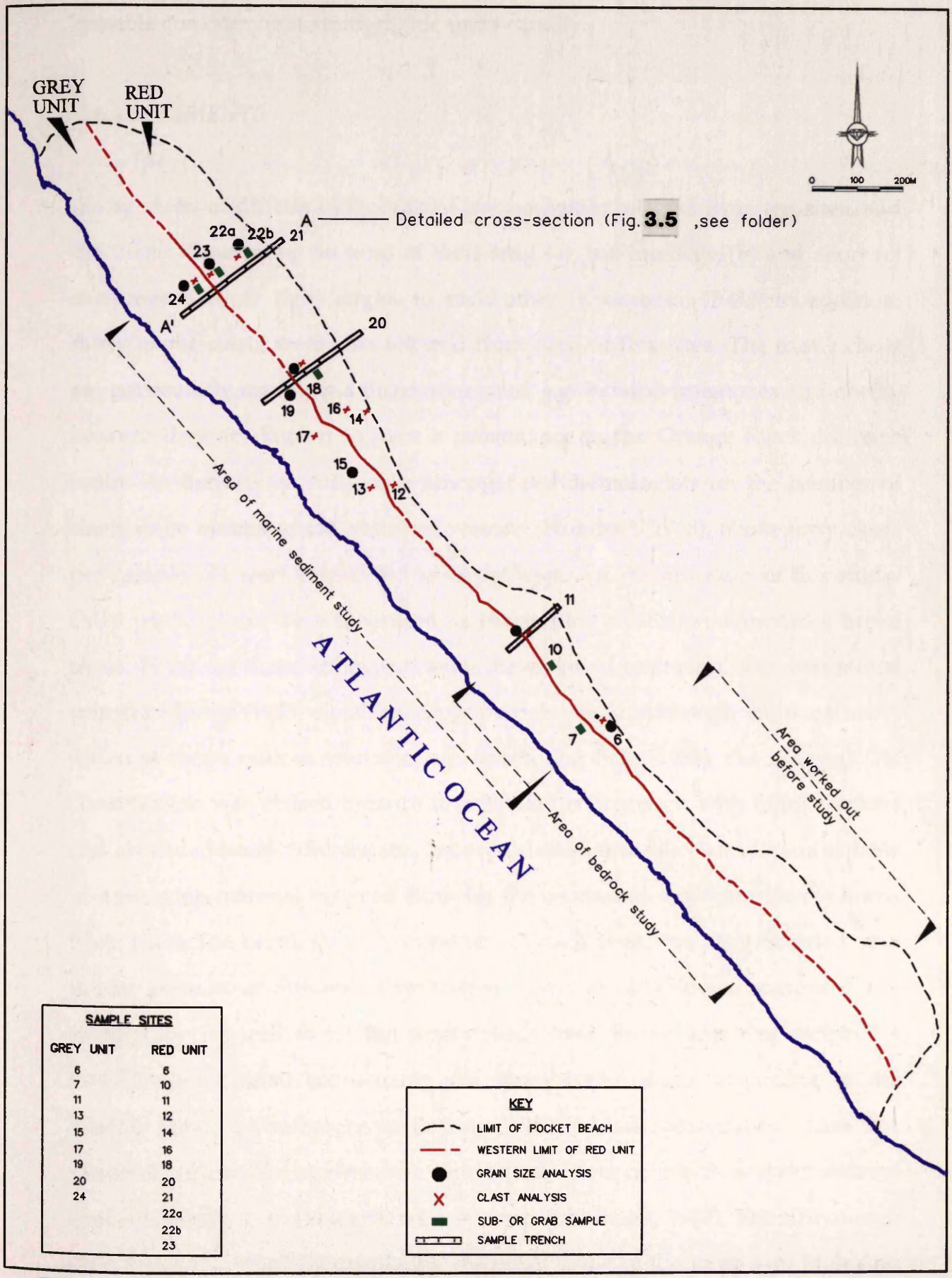

Fig. **1.5** Locality plan showing distribution of sample sites within the study area (pocket beach no. 4), Chameis.

NAMDEB

possible consider both stratigraphic units equally.

1.6.1 *SEDIMENTS*

Forty clasts of different lithologies were randomly selected from ten sites, and the linear dimensions (in mm) of their long (a), intermediate (b) and short (c) axes measured at right angles to each other (Krumbein, 1941). In addition, thirty exotic clasts were also selected from each of five sites. The exotic clasts are particularly useful as a distinctive suite, e.g. banded ironstones and cherts, because they are known to have a provenance in the Orange River drainage basin. As there is no consensus amongst sedimentologists on the number of clasts to be measured for statistical reasons (Humbert, 1968), about forty clasts per sample site were considered to be sufficient for the purposes of this study. Only whole clasts were measured as the mining operation sometimes broke clasts. From the three orthogonal axes, the shape of each clast was determined using the Zingg (1935) classification of particle shape. Although there are many different shape indices available, e.g. Sneed and Folk (1958), the Zingg (1935) classification was chosen because it facilitated comparison with other workers and also adequately differentiates between clast shapes. Special callipers capable of measuring material between 4mm for the c-axis and < 500mm for the a-axis were used. The lithology and roundness of each clast was also recorded, and the proportion of different clast shapes and clast lithologies computed per sample site, as well as for the whole study area. Roundness was assigned a visually determined score using the quantitative limits according to the Wadell index, by reference to Powers (1953) visual comparative chart. For maximum clast size analysis the ten largest clasts of the three predominant clast lithologies from each site, were selected (Lindholm, 1987). The size of each clast was determined by calculating the mean value of the three axes (a, b, and c) measured (Carr, 1969; Briggs, 1977).

For granulometric analysis, samples were collected from different sedimentary environments and facies at various sites. These samples were sieved through standard precision-made sieves into 1.0 phi size fractions ranging from -7.0phi (128mm) to 4.0phi (0.063mm), and put on a mechanical shaker for 15 minutes. The 1.0 phi sieve range was considered good enough for grain size determinations as palaeoenvironmental analysis on the basis of these grain size data alone, was not attempted. The weight retained on each sieve was recorded as a percentage of total sample weight and plotted as a cumulative frequency curve on logarithmic probability paper to facilitate computation of grain size parameters. For all grain size data the Udden-Wentworth scale was used. All statistical analyses were based on the graphic method of Folk and Ward (1957).

Palaeocurrent orientations of foreshore beach accretion surfaces were measured at site 22a only, because of poor exposure elsewhere. These surfaces were measured to determine the direction of beach growth.

For the sand fraction, the heavy and light minerals in three unconsolidated sand samples were separated by conventional methods using bromoform. Their mineral assemblages were then described and compared from thin sections mounted in resin and ground to the standard thickness of 0.3mm, using a petrographic microscope, with a view to provide information concerning their provenance. In addition, twenty quartz grains from each of the two stratigraphic units were randomly picked and the scanning electron microscope (SEM) used to study surface textures on them for information concerning their provenance and sedimentary history. The method used for the preparation and study of the quartz grains is the method described by Higgs (1979). The samples from the two stratigraphic units were washed in fresh

water and dried before the twenty monocrystalline, subrounded to well rounded whole quartz grains were picked under the binocular microscope. Angular grains were purposefully omitted because they were considered to be of local origin and therefore not reliable as indicators of transport. Only grains between 0.25-1.0mm were selected to reduce the bias of grain size on the surface features present. The selected grains were mounted on roughened SEM aluminium stubs and the grains coated twice with a film of gold. Individual grains were then viewed under different magnifications (up to x 1000) and impact features reported to be indicative of particularly marine environments (Nordstrom & Margolis, 1972; Higgs, 1979), recorded and photographed. Five garnet grains were also picked from each unit and studied under the SEM, using the same methods described briefly above. The terminology used to describe the surface textures in Chapter 3, section 3.2.3 was adopted from Higgs (1979). A statistical examination of many quartz sand grains was not attempted, as the objective here was merely to confirm the presence or absence of impact features to lend further evidence for lengthy transport. The roundness, shape and composition-assemblage of the unsorted sand grains observed under the binocular microscope were also noted for both stratigraphic units.

1.6.2 SHORE PLATFORMS

The basal and top elevations of 919 individual gullies and potholes were surveyed relative to present sea-level in different parts of the pocket beach where platforms have been exposed by mining. Wave-cut platforms developed on erodible lithology would be expected to faithfully record the associated sea-levels and therefore provide a temporal framework for the sea-level history of the area (Pether, 1986). A frequency curve was then plotted from these elevations and the differential of their top and basal elevations used to determine the depth of each gully or pothole.

Vertical aerial photographs taken from different heights by Dennis Barry and John Kilham, using the company helicopter, were used to compile a base map of the study area at a scale of 1:4000. The photographs were also used to determine the intensity of gullying and the orientation of gullies with respect to other structural features. The orientation of joints, as well as the schistosity of the bedrock were measured in some parts of the study area with a Brunton compass, and lower hemisphere equal area stereographic projections constructed using the method described by Ragan (1985).

Bedrock specimens were collected from different exposed parts of the area and thin sections (0.3mm thick) kindly prepared by the Geological Survey of Namibia. Petrographic descriptions of the thin sections were done to determine the relationship between the intensity of gully formation and the lithology of the bedrock.

1.6.3 SAMPLING

Three sampling trenches, each approximately 200 metres long, were mechanically excavated in different parts of the pocket beach after the sand overburden was stripped off to bedrock peaks or first gravel. The trenches were orientated at right angles to the present beach strike and partitioned into sections varying between 50 - 100 metres in length and 10 metres wide (Fig. 1.6). Each section constituted a separate sample of ± 500 to 1000 tons. Samples of between 8 and 15 tons referred to herein as subsamples, were taken from discrete sedimentary facies to provide an insight into the vertical distribution of diamonds (Fig. 1.7). Grab samples (± 160 tons) were also taken from a pothole and a particularly agate-rich (exotic clast) section of the pocket beach. The distribution of the diamond sampling sites is also shown in Fig. 1.5. Each

Fig. 1.6 Sampling trench across the beach at site 11. The east-west oriented trench is partitioned into three 10m wide, 50m long sampling paddocks, as marked by white survey pegs.

Fig. 1.7 Excavation of discrete sedimentary facies subsamples into multibuckets (arrowed) on haul truck at site 22.

resulting sample was treated separately for its diamond content at either one of the treatment plants or at the modular sampling plant. The treatment plants were flushed clean in between different samples and this process was supervised personally to prevent or minimize contamination.

1.6.4 DIAMONDS

The general characteristics as well as the surface textures of a sample of 1250 diamonds selected from a total of 2 821 recovered as part of this thesis, were described in detail using the Anglo American Research Laboratories descriptive scheme of Robinson (1979). This classification scheme considers such physical properties as, for example colour, shape, transparency and such surface features as for example terraces and lamination lines, and determines the proportion of these characteristics as a function of diamond size. Thus all the diamonds were initially sieved into sizes ranging from -6+5 (2.16-1.83 mm aperture diameter) up to +23 (10.31 mm aperture diameter). From the 2821 diamonds recovered, 1250 were initially randomly selected in proportion to the number of diamonds from the different sample sites. The 1250 diamonds were then further slightly reduced to omit samples of less than 20 stones and this final reduction allowed equal numbers of diamonds to be examined between the diamonds of the same sieve sizes at the different sites. From the 1093 stones overall, 243 diamonds were selected for direct comparison between the two stratigraphic units (see Tables 5.1 & 5.2, Chapter 5). The data obtained from the observations were tabulated and the frequency of occurrence of the features converted to percentages and the more important characteristics depicted as piecharts. The general characteristics of the diamonds as well as their surface features were then photographed with the aid of a binocular microscope, using a daylight source on a white backround.

CHAPTER 2 GEOLOGICAL SETTING OF STUDY AREA

The present day and Cainozoic beaches are only part of a geological history which extends beyond the Jurassic to a time when the south Atlantic began to open. The development of the continental shelf, the shelf energy regime and the climate are all partly related to the opening of the south Atlantic Ocean and therefore form a part of the history of the southwest African coastline. In addition, as with processes extending back to the Jurassic or earlier, the older basement of Africa has a marked effect on the final morphology of this coastline. It follows therefore that a brief description of the geological history of the region is needed to better understand the broad context in which this study is made.

2.1 REGIONAL GEOLOGY

The study area coincides with basement rocks of the Pan-African Gariep Belt shown in Fig. 2.1, which form part of a larger network of Late Proterozoic to Early Palaeozoic orogenic belts of equatorial and southern Africa. Frimmel and Hartnady (1992) divided the Gariep Belt into an eastern passive continental margin zone, the Port Nolloth zone, and a western allochthonous ophiolitic terrain, the Marmora Terrane. These two zones are joint along the arcuate, north-south to southwest trending Schakalsberge Thrust. The Chameis pocket beaches occur within the Marmora Terrane, which according to Frimmel and Hartnady (1992) is subdivided into three tectonostratigraphic units, namely: (i) the Schakalsberge Complex (ii) the Oranjemund Complex and (iii) the Chameis Complex (Fig. 2.1). The Oranjemund Complex to the south, within which the beach studied here occurs, consists of interbedded metagreywackes, phyllites and quartzites. The Chameis Complex to the north is interpreted to be

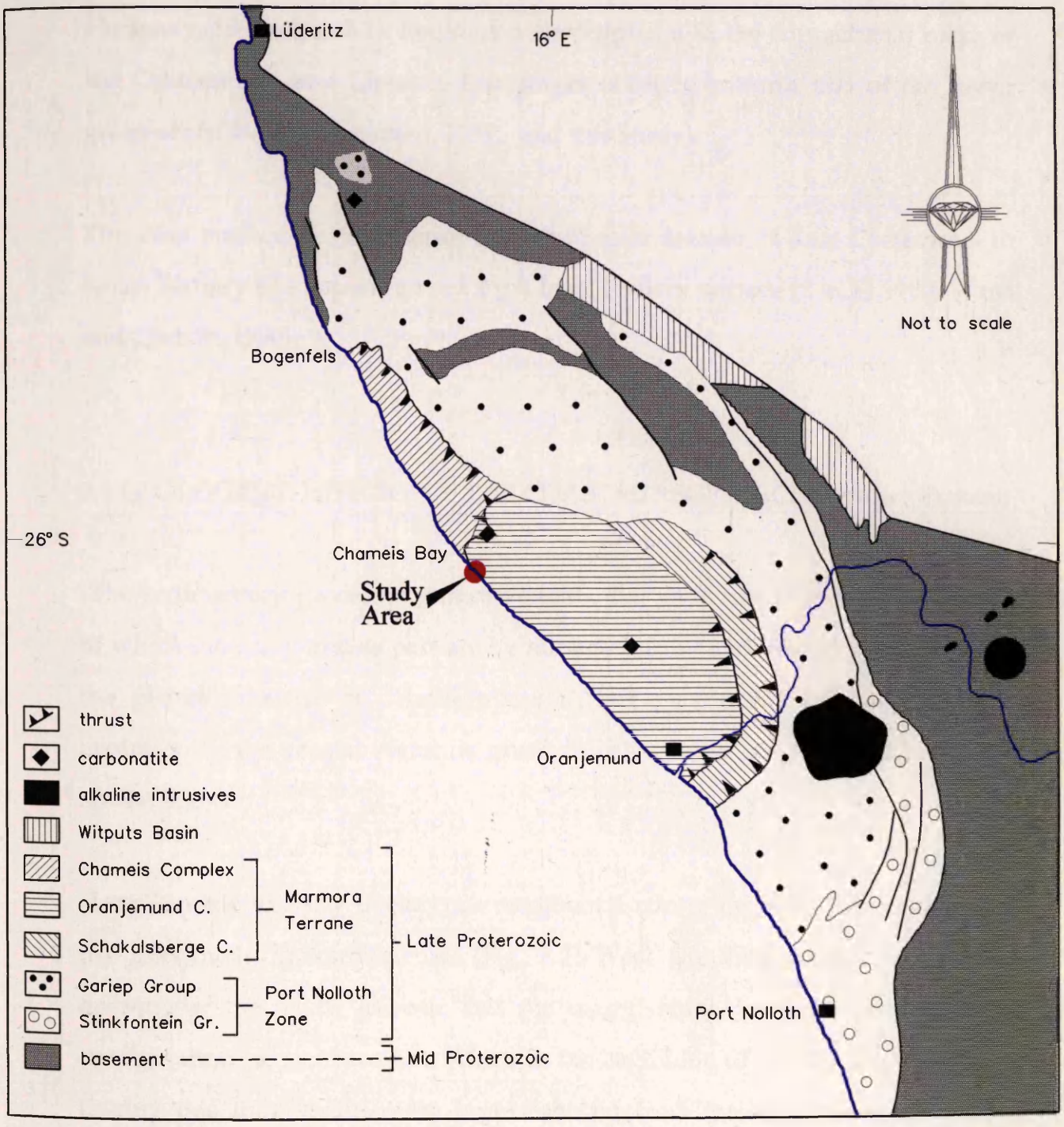

Fig. **2.1** Geological map of the Late Proterozoic Gariep Province, southwestern Africa (modified after Frimmel and Hartnady, 1992).

NAMDEB

a heterogeneous melange zone and is juxtaposed to the Oranjemund complex along a northwest-vergent thrust in the Chameis coastal area (Frimmel and Hartnady, 1992) (Fig. 2.1). Regional metamorphism in the supracrustal rocks of the Oranjemund and Chameis Complexes is fairly uniform and of the lower green-schist facies (Greenman, 1967, and this study).

The land surface of the interior is a composite feature of Late Cretaceous to Early Tertiary age superimposed by a Late Tertiary surface (SACS, 1980; Ward and Corbett, 1990).

2.2 GEOLOGICAL HISTORY OF THE COASTAL REGION (Cretaceous - Present)

The sedimentary process-response systems that gave rise to the coastal region of which the study area is part are by no means fully understood yet because of the general absence of datable material, but a summary of the geological evolution of the coastal region is given from a review of published literature on the subject.

Late Jurassic to Early Cretaceous continental rifting initiated the break-up of the previously intercontinental (Fig. 2.2) West Gondwana, resulting in the opening of the south Atlantic and the establishment of the present coastal configuration of southwestern Africa at the beginning of the Tertiary (Fig. 2.2). During this time sedimentary basins shifted from intercratonic areas to the developing continental margin zones (Dingle, Siesser and Newton, 1983). According to de Wit (1993), the Orange River drainage system started to evolve during Middle to Late Cretaceous times, but recent evidence suggests that the Orange River probably originated sometime during Jurassic times (personal communication, Bluck, 1995).

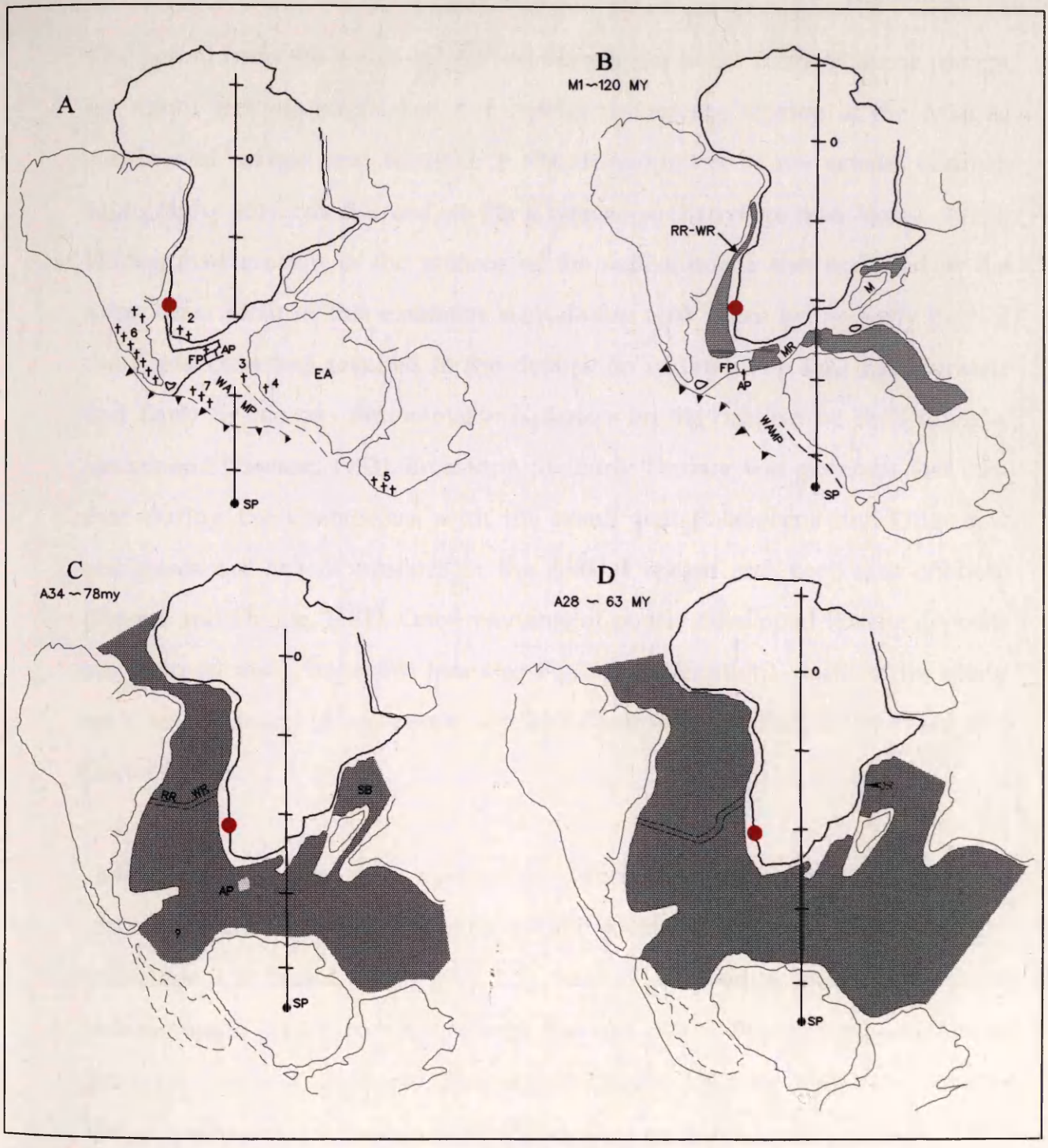

Fig. **2.2**

Gondwana palaeogeographies from Dingle, Siesser and Newton (1983) based on Norton & Sclater (1979) from the original refits of Elliot (1975a) and de Wit (1977) with modifications from Scrutton (1976a), Simpson *et al.* (1979), Segoufin & Patriat (1980), Miller (1981), Tucholke *et al.* (1981), Watts & Bramall (1981) and Martin *et al.* (1982a). The time scale is that of van Hinte (1976a). Details NE of Madagascar, are sketched (i.e. no attempt to refit Seychelles Plateau). Oceanic crust is shaded, Mesozoic orogenic belts shown by crosses, subduction zones shown by solid triangles. Abbreviations and key: FP - Falkland Plateau; AP - Agulhas Plateau; MR - Mozambique Ridge; M - Madagaskar; WAMP - West Antarctica microplates (e.g. Ellsworth, Thurston, Marie Byrd Land); EA - East Antarctica; SB - Somali Basin; RR - Rio Grande Rise; WR - Walvis Ridge; SP - South Pole; DR - Davie Ridge. Orogenic features: 1- Sierra de la Ventana; 2 - Cape Fold Belt; 3 - Ellsworth Mountains; 4 - Pensacola Mountains; 5 - East Australia; 6 - Andes; 7 - Antarctic Peninsula; Red dot - location of study area.

A. Pre-drift (early Triassic); B. Anomaly M1, ca.120 my (early Barremian); C. Anomaly A34, ca. 78 my (late Santonian/early Campanian); D. Anomaly A.28 ca. 63 my (early Palaeocene).

Projection is Lambert equal area.

NAMDEB

The period from the break-up of West Gondwana to the Early Miocene (except for minor tectonic interludes) was marked by intense erosion of the Atlantic continental margin and resulted in the development of the coastal bedrock topography towards the end of the Cretaceous (Partridge and Maud, 1987). Widespread erosion in the interior of the subcontinent also occurred at the same time. Most of this extensive denudation took place in the early part of the Cretaceous and resulted in the deposition of thick (4-6 km) Late Jurassic and Early Cretaceous sedimentary sequences on the continental shelf (Dingle, Siesser and Newton, 1983). Erosion in the Early Tertiary was generally less then that during the Cretaceous, with the result that Palaeocene and Oligocene sediments are absent onshore in the coastal region and very rare offshore (Siesser and Dingle, 1981). Only remnants of poorly developed Eocene deposits are exposed near Bogenfels (see also Fig. 1.2 for location), north of the study area, at elevations of approximately 160m and 40m (Martin, 1973; Ward and Corbett, 1990).

Asymmetrical uplift of the subcontinent during Early Miocene, ranging from 250m near the western continental margin to 1150m near the eastern margin (Partridge and Maud, 1987) (Fig. 2.3), lead to renewed erosion and offshore sedimentation which continued until the end of the Pliocene when climatic conditions became more arid (Siesser and Dingle, 1981; de Wit, 1993). Middle Miocene deposits are known from Proto- Orange River terrace gravels, while Middle and Late Miocene deposits occur on the continental shelf off southwestern Africa (Siesser and Dingle, 1981). A second major uplift took place at the end of the Pliocene resulting in the rejuvenation of the Orange River and the transport of large pulses of terrigeneous material to the Atlantic Ocean.

Sea-level fluctuations associated with climatic changes during the Pleistocene

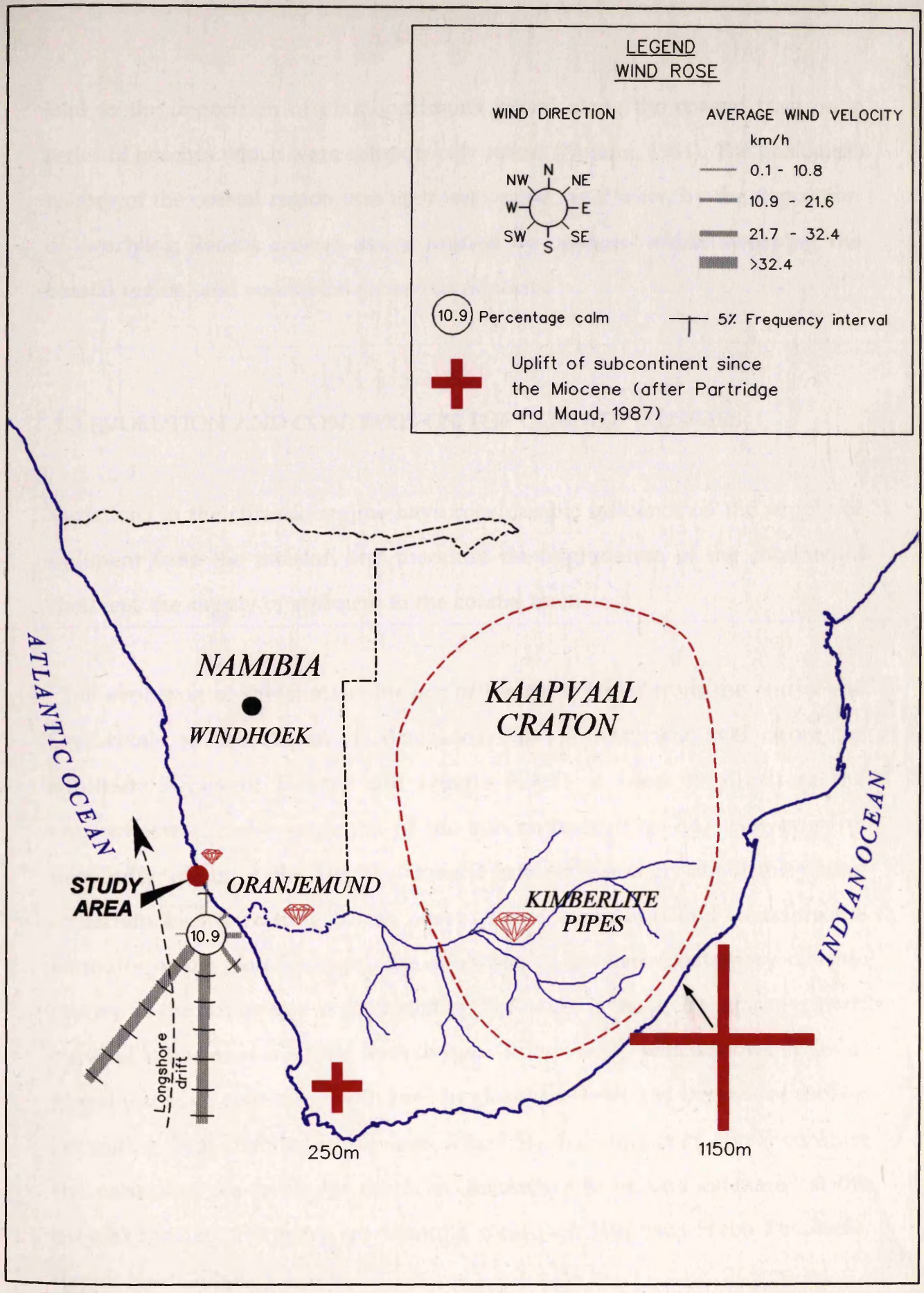

Fig. **2.3** Map showing the transport of diamonds from kimberlitic sources on the Kaapvaal craton by the Orange river to the west coast of southwestern Africa. Also shown are the dominant southerly and southwesterly winds, the resulting longshore drift and the degree of tectonic uplift (after Partridge and Maud, 1987) along the western and eastern coasts of Southern Africa.

lead to the deposition of diamondiferous gravel along the coastal tract on a series of beaches which were subsequently raised (Hallam, 1964). The geological history of the coastal region was then terminated, as it were, by the deposition of overlying Recent coastal dunes formed by onshore winds sweeping the coastal region, and superficial terrestrial deposits.

2.3 EVOLUTION AND CONTROLS ON THE CLIMATIC REGIMES

Variations in the climatic regime have considerable influence on the supply of sediment from the interior, and therefore the aggradation of the continental shelf and the supply of sediment to the coastal tract.

The evolution of the climatic history of the Sperrgebiet from the end of the Cretaceous to the Present is discussed. The Tertiary sea-level curve for southern Africa of Siesser and Dingle (1981) is used to illustrate the approximate climatic evolution of the subcontinent (Fig. 2.4). However, no unanimity, exists on the Tertiary climatic history, especially about the timing of certain events relating to the onset of arid conditions and therefore the antiquity of the Namib desert. The evolution of the Late Quaternary climatic history of the study area is discussed on the basis of the global glacio-eustatic curve of Williams *et al.* (1981) from oxygen isotope data, which shows cycles of global warming coinciding with rises in global sea-level and periods of cooling coinciding with lowering of sea-level (Fig. 2.5). Williams, *et al.* (1981) consider the pattern of sea-levels for the Late Quaternary to be best estimated at the present time by this curve representing coral-reef data from Huon Peninsula, Papua New Guinea.

Two different views exist about the maximum age of the onset of aridification

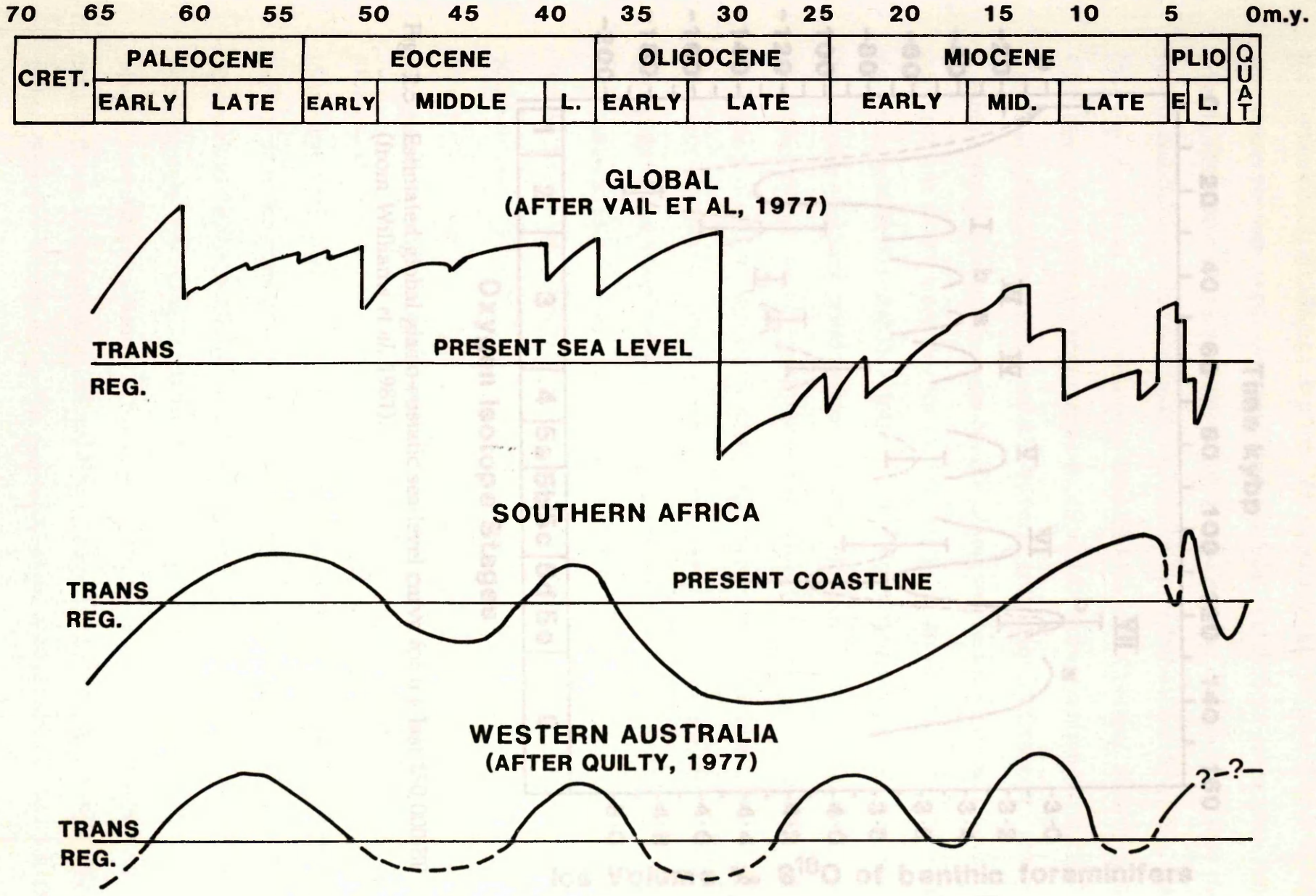

Fig. 2.4 Comparison of the global, southern African and western Australian Mesozoic sea-level changes (from Siesser and Dingle, 1981).

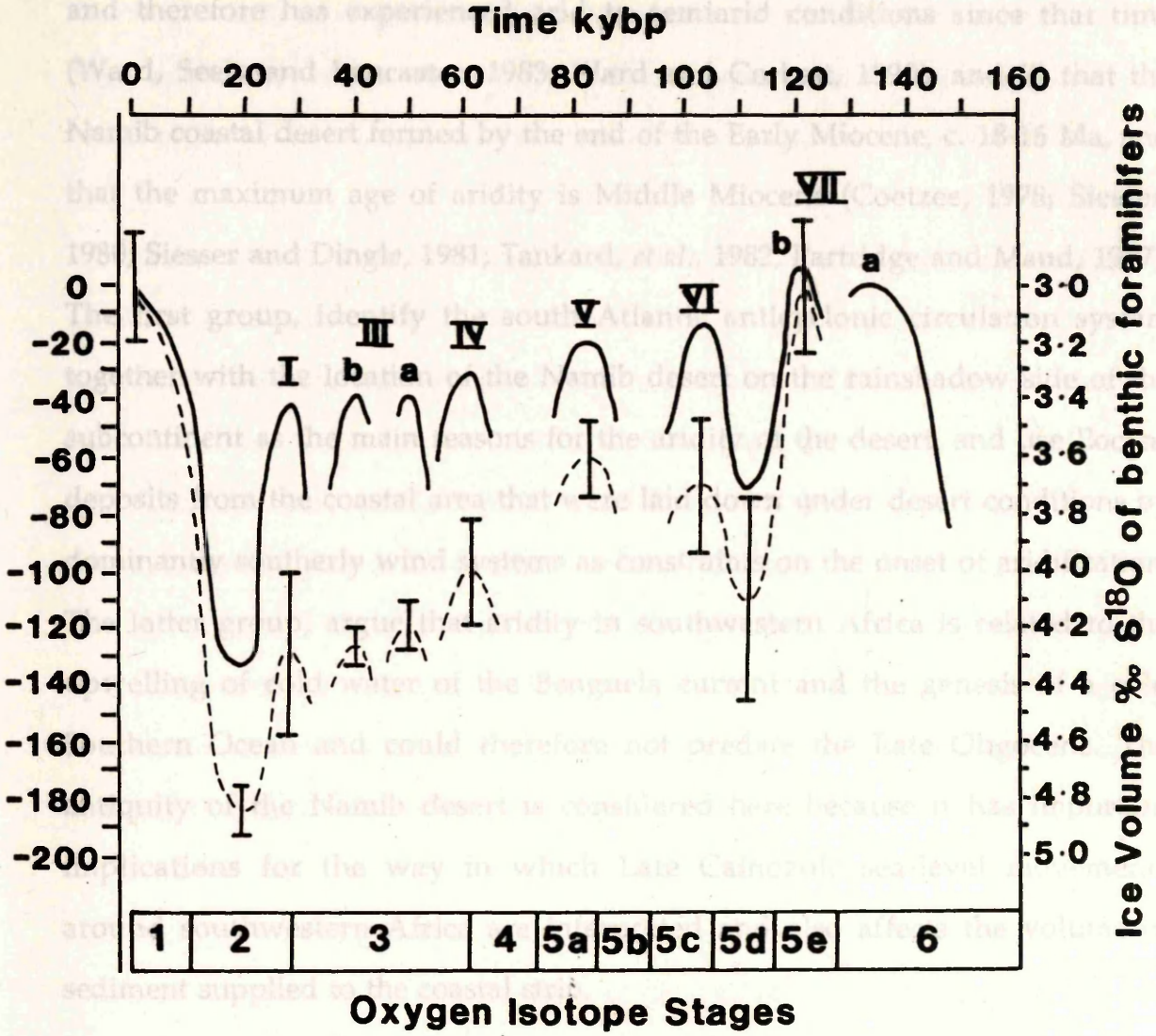

Fig. 2.5 Estimated global glacio-eustatic sea-level curve for the last 150 000 BP (from Williams *et al.* 1981).

for the Namib coastal tract: i) that the Namib coastal area formed by the end of the Cretaceous, c. 65 Ma ago and that the maximum age of aridity is c. 80 Ma and therefore has experienced arid to semiarid conditions since that time (Ward, Seely and Lancaster, 1983; Ward and Corbett, 1990), and ii) that the Namib coastal desert formed by the end of the Early Miocene, c. 18-16 Ma, and that the maximum age of aridity is Middle Miocene (Coetzee, 1978; Siesser, 1980; Siesser and Dingle, 1981; Tankard, *et al.*, 1982; Partridge and Maud, 1987). The first group, identify the south Atlantic anticyclonic circulation system together with the location of the Namib desert on the rainshadow side of the subcontinent as the main reasons for the aridity of the desert, and use Eocene deposits from the coastal area that were laid down under desert conditions by dominantly southerly wind systems as constraints on the onset of aridification. The latter group, argue that aridity in southwestern Africa is related to the upwelling of cold water of the Benguela current and the genesis of a cold Southern Ocean and could therefore not predate the Late Oligocene. The antiquity of the Namib desert is considered here because it has important implications for the way in which Late Cainozoic sea-level movements around southwestern Africa are interpreted and also affects the volume of sediment supplied to the coastal strip.

Following the break-up of West Gondwana, the South Atlantic anticyclonic circulation system was established by the end of the Cretaceous, c. 80 Ma (Simpson, 1977) with the full opening of the south Atlantic Ocean, as discussed earlier. It is the pressure gradient formed by the south Atlantic High that is responsible for the persistent southeasterly tradewinds, which in turn created the Benguela upwelling (current) system in the Late Miocene off the coast of southwestern Africa (Siesser, 1980) and the onshore winds of the coastal region which drive large amounts of sediment onshore to make the coastal dune fields. Effective winds along the coastal tract as also shown in Fig. 2.3, are

generally from the south or southwest for most of the year and result in a strong longshore current along the coastline. Water-mass movement along the west coast of southern Africa is mostly in the form of upwelling (de Decker, 1988) therefore the water circulation pattern on the coast is mainly the result of incoming swells and the wind driven longshore current.

de Decker (1988) gives a summary of wave data for the southwestern African coastline from a comprehensive review of wave data from southern Africa by Rossouw, 1984. The distribution of wave heights along the west coast ranges from 2.5m near Cape Town to 1.75m at Oranjemund (close to the study area) and 1.4m at Swakopmund (see Fig. 1.2, for location of towns), the most prevalent wave period at Oranjemund ranges from 10sec in winter to 7sec during summer. Tides are semi-diurnal and have a mean spring range of 1,8m at Oranjemund, placing this part of the coast in the microtidal (< 2m) range (Davis, 1964). Swell heights in excess of 5m are however, experienced during periodic storms (CSIR, 1995).

The average annual precipitation in this coastal desert area is about 40-50mm of which a large portion is in the form of dew associated with frequent fog. The Benguela current flowing northwards along the coast has a moderating influence on the coastal climate with the average maximum daily air temperature about 19° C.

Dingle (1992), argues that the climate of the coastal zone and therefore its depositional environment would not have changed significantly since the Miocene, except during periods of glaciation when the loci of cell upwelling would have been moved further offshore by low sea-levels and changed oceanic and atmospheric circulation. Therefore it is considered to be reasonable to assume that present climates largely resemble that of the recent past.

2.4 THE ORANGE RIVER AND THE DISTRIBUTION OF DIAMONDS ALONG THE COAST

It is now widely accepted that the Orange River acted as the major conduit for the transport of diamonds from the interior of the subcontinent to the Atlantic Ocean on the west coast of southern Africa (Fig. 2.3). They were then dispersed northward by longshore drift. Kimberlite or lamproite is the source rock for practically all diamonds and the diamond-bearing kimberlite intrusions in southern Africa are confined to or immediately adjacent to the stable parts of the crust, known as cratons (Gurney, 1993). The off-craton kimberlite intrusions do not carry diamonds. The cratons are at least 1.0 Ga old at their edges, while their core age is > 2.4 Ga (Mitchell, 1986). Most of the known kimberlite pipes within the Orange River drainage area are on the Kaapvaal craton (also Fig. 2.3) and their eruption age is mostly Middle to Late Cretaceous (Harris, 1992).

de Wit (1993) subdivided the evolution of the Orange River drainage network into three climatic time periods, the Middle to Late Cretaceous, the Early to Middle Cainozoic and the Late Cainozoic. The Orange River broke through to the Atlantic Ocean during Late Cretaceous and its course shifted north and south until its present course was established during the Pliocene (de Wit, 1993, figures 8.5 and 8.6). The Late Cretaceous period was characterised by deep incision and lowering of the base level of the Orange River as a result of uplift of the subcontinent. Early to Late Miocene raised diamondiferous gravel terraces occur along the banks of the Orange River apparently related to epeirogenic uplift or climatic change during this period.

According to Partridge and Maud (1987), this period was followed by extreme aridity during the Early Pliocene as a result of which the river was choked up by aeolian sediments. Fluvial conditions returned in the Late Pliocene to Early Pleistocene, and together with periods of relative uplift during the same period, the rejuvenated Orange River flushed its bed, straightened its course and transported large quantities of terrigeneous material together with the diamonds eroded from kimberlite pipes along its drainage into a sink, i.e its delta. This delta off the southwest African Atlantic coastline formed a huge reservoir of diamondiferous gravel which was continuously tapped and then dispersed northward along the Sperrgebiet coastline, initially by longshore drift under the influence of the strong prevailing south-to southwesterly winds (Hallam, 1964) (also Fig. 2.3). The diamonds together with the gravel were then subsequently reworked by wave turbulence mainly in the surf zone and deposited, during glacio-eustatic sea-level changes of the Pleistocene discussed elsewhere in this text. Here the diamonds are preserved in raised beaches where they are interspersed with or overlain by marine sediments, which in turn are overlain by often thick successions of generally barren terrestrial and aeolian sediment (Fig. 2.6). North of the study area the winds become stronger and are therefore able to transport diamonds which by then are much smaller (Fig. 2.7), northwards to form extensive deflation placer deposits as far north as Conception Bay, ± 120km south of Swakopmund (Fig. 2.7).

2.5 DEVELOPMENT OF SHORE PLATFORMS AND DEPOSITS

The shore platform and the marine sediments on them act as hosts for the diamonds which are transported northward from the mouth of the Orange River or from the continental shelf. The generation of both is significant not only for the insight it gives on the later evolution of southwestern Africa, but

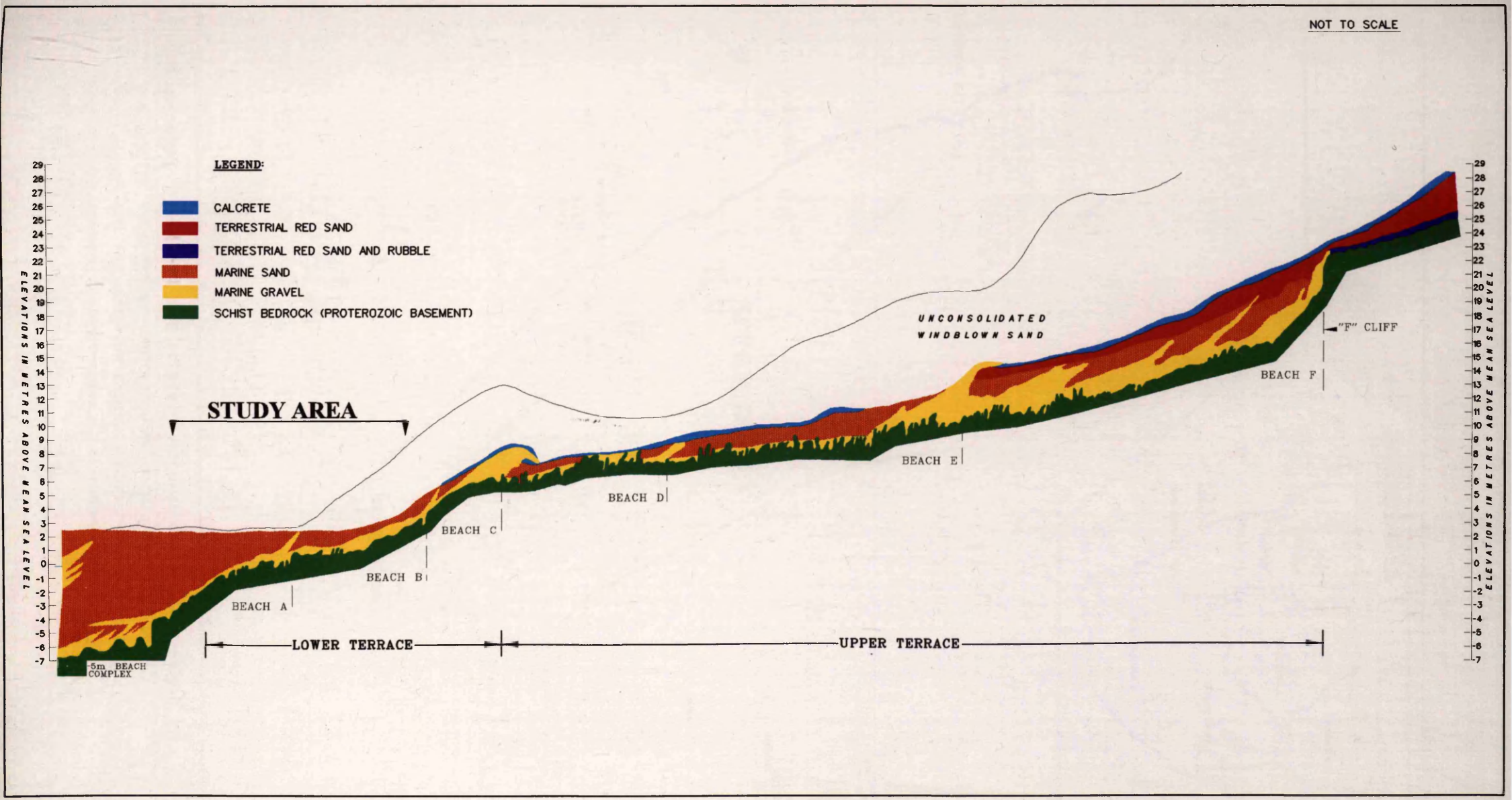

Fig. **2.6** Typical cross section through the raised beach deposits along the coast of southwestern Namibia (modified after Corvinus, 1983).

NAMDEB

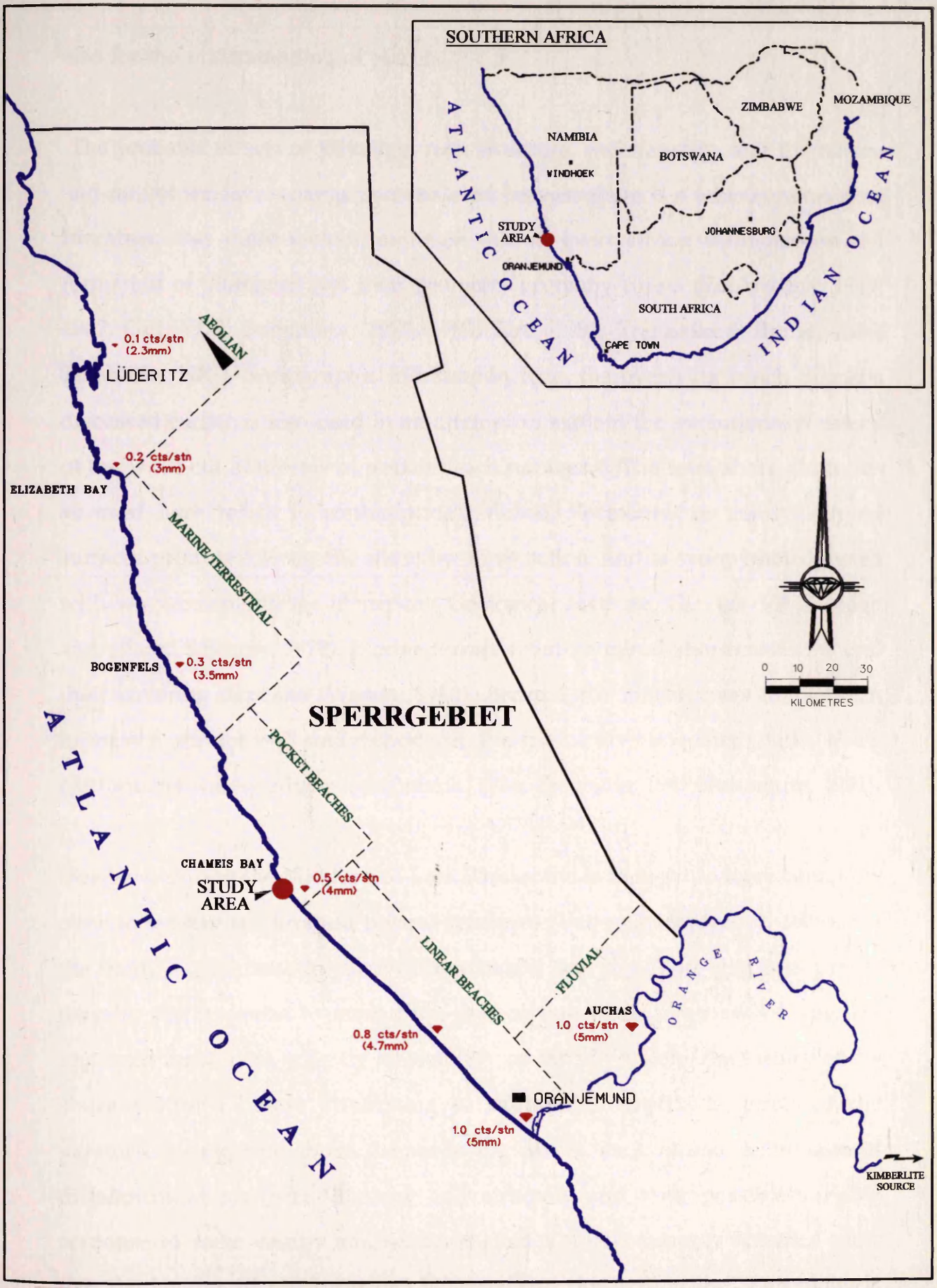

Fig. **2.7** Decrease in diamond size (cts/stn) northward from the mouth of the Orange River (after Hallam, 1964 and Sutherland, 1982). Also shown are the different diamond placer types of the Sperrgebiet, southwestern Namibia. Conversion carats to mm are approximate.

NAMDEB

also for the understanding of placers.

The probable effects of lithology, rock structure, wave energy, and the nature and rate of sea-level change is considered because there is a wide consensus in literature that these factors, amongst others, exert strong influence on the formation of platforms and their geometry on many coasts (Zenkovitch, 1949, 1967; Gill, 1972; Sunamura, 1975, 1992; Bird, 1984; Trenhaile & Byrne, 1986; Trenhaile, 1987). Stratigraphic information from the overlying beach deposits discussed earlier is also used in an attempt to explain the evolutionary history of the wave-cut platforms of pocket beach number 4. The term shore platforms as used here refers to contemporary/raised, horizontal or gently sloping surfaces produced along the shore by wave action, and is synonymously used with wave-cut platforms (American Geological Institute, Glossary of Geology and related Sciences, 1972). Marine terrace refers to raised shore platforms and their covering deposits (Woods, 1980). Because the mechanisms of platform formation are not well understood yet, the use of the non-genetic term, shore platforms is widely advocated (Pethick, 1984; Trenhaile, 1987; Sunamura, 1992).

Sea-level during the Middle and Late Pleistocene is thought to have been very close to present sea-level on several occasions (Vail and Hardenbol, 1979), but the many fluctuations in sea-level has meant that the shore platform profile may be the response to more than one cutting event. In view of this, the approach made here is firstly to establish, as far as possible, the history of the shore platform before attempting to explain its profile in terms of the parameters suggested above (i.e sea-levels, waves, etc.). Moreover, because of differences in platform lithology and structure and their possible variable response to wave energy and sea-level change, the commonly accepted view that the heights of platforms can be correlated throughout the Sperrgebiet is now rejected (*cf.* Hallam, 1964; Stocken, 1978). The elevations are therefore

relevant to the study area alone until such time as when the shore platform profiles of the other beaches are considered in a more rigorous way.

Six raised Pleistocene wave-cut platforms at heights between 2m and 25m above present sea-level have been recognized along the coastal tract of the Sperrgebiet of Namibia (Fig. 2.6). Remnants of Eocene terraces preserved in shallow basement depressions from 40m to 160m above present sea-level are also known from two localities (Kaiser, 1926; Martin, 1973). Most of the shore platforms have a sedimentary cover of beach sediment, covered in turn by terrestrial and aeolian sediment which often obscures their topography. However, over most of the coastal strip of the Sperrgebiet, the shore platforms have been exposed by the diamond mining operations and the shore platforms and their associated sediment cover have been correlated over the entire coastal strip using continuity, elevation and stratigraphic position. Beaches and platforms have been shown to become progressively older with increasing altitude (Hallam, 1964). The highest preserved marine terrraces abut a well defined cliff (see Fig. 2.6) which decreases in elevation northward, while the lower terraces (< 8m above present sea-level) (see also Fig. 2.6) essentially remain horizontal so that at about 60km north of the Orange River, the younger terraces truncate the older terraces (Stocken, 1978). This is interpreted to be the result of northward tilting of the older Late Pleistocene terraces, which had stopped before the younger terraces formed (Hallam, 1964; Stocken, 1978).

CHAPTER 3 SEDIMENTS

3.1 GENERAL LITHOSTRATIGRAPHY

Two distinctive stratigraphic units in superposition are recognized along and across the beach in the study area (Figs. 3.1 & 3.2). The older red unit, whose name is derived from its colour has a thickness of between 0.2-2m. It overlies Late Proterozoic basement rocks of the Gariep Complex along a major unconformity. Grey sediments of the grey unit, 0.2-1m thick, overlie in places, those of the red. On the westward beach margin, sediments of the grey unit rest directly on the shore platform. The red unit is in turn overlain by either an older sheetwash unit (up to 0.5m) or by the grey unit along a sharp erosional contact. Recent sheetwash (0.2m), marine sand (± 5m) and aeolian sand (± 3m) overlie the grey unit (Figs. 3.3 & 3.4 and Table 3.1). The transition from the grey unit to the overlying marine sand is not clear. These units are interpreted to represent successive transgressions and regressions as will be discussed later.

3.2 RED UNIT

3.2.1 DISTRIBUTION OF LITHOFACIES

Distinctive sedimentary facies, interpreted to correspond to the intertidal (beachface), subtidal (upper shoreface) and lower shoreface (zone seaward of the surf zone) subenvironments are preserved at only one locality in the study area, site 21 (Fig. 3. 5, see folder). Here the red unit deposits are preserved in a topographic depression.

Table: 3.1 Lithostratigraphy of the study area (pocket beach no. 4), Chameis.

EPOCH	AGE	STRATIGRAPHIC UNIT	DESCRIPTION	THICKNESS (APPROX)
Recent		Windblown Sand	Medium to fine-grained sand	3m
Recent	< 5 000 BP	Beach Sand	Medium-grained sand	5.0m
Recent		Sheetwash	Poorly sorted angular rubble	0.2m
Holocene	c. 5 000 BP	Grey Unit	Well sorted, cobble-pebble gravel set in fine pebble to coarse sand matrix	1.0m
Late Pleistocene *unconformity*	c. 5 000 BP to c. 130 000BP	Sheetwash	Angular vein quartz rubble	0.3m
Late Pleistocene (Eemian) *unconformity*	c. 5 000 BP to c. 130 000 BP	Red Unit	Moderately to well sorted, pebble gravel set in grit to very coarse sand matrix	0.5m
Proterozoic	900 - 600 Ma	Gariep Complex (local basement)	Interbedded quartzitic and phyllitic schist	

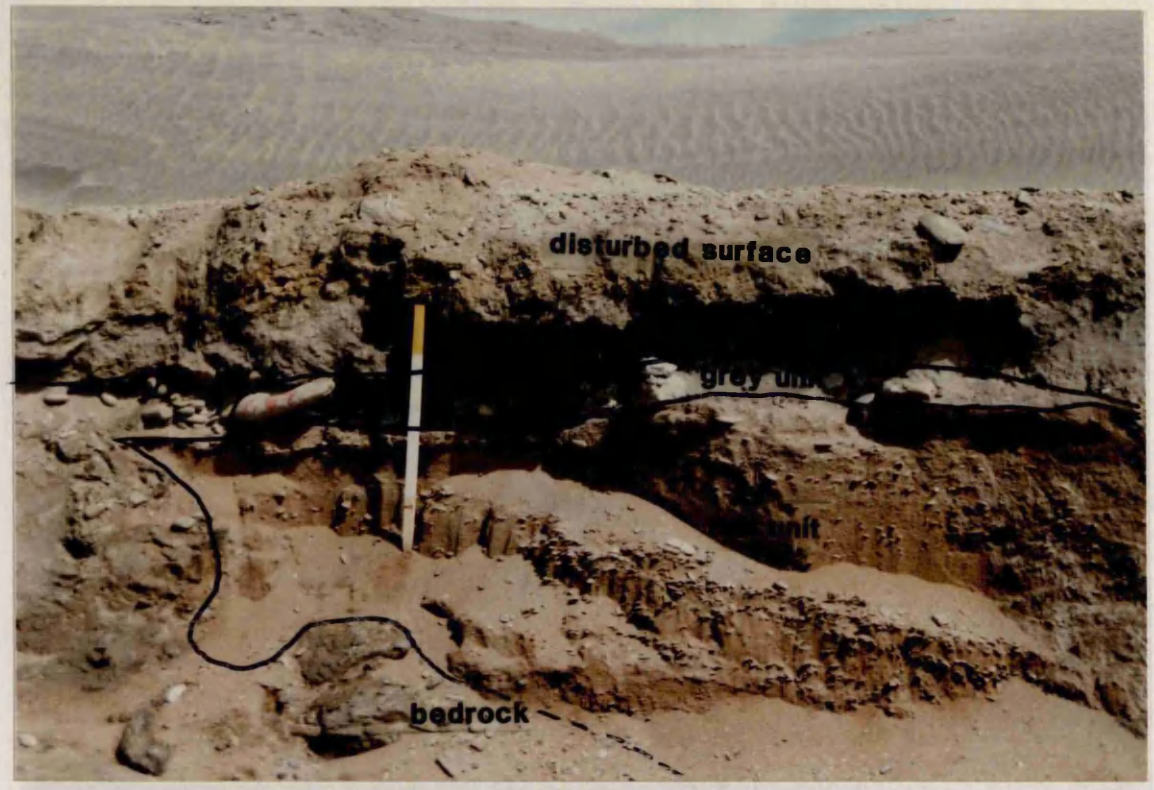

Fig. 3.1 Thin **grey unit** gravel bed overlying shell-rich, sandy, basal **red unit** gravel at site 20. Note road surface above grey unit. Scale 150cm.

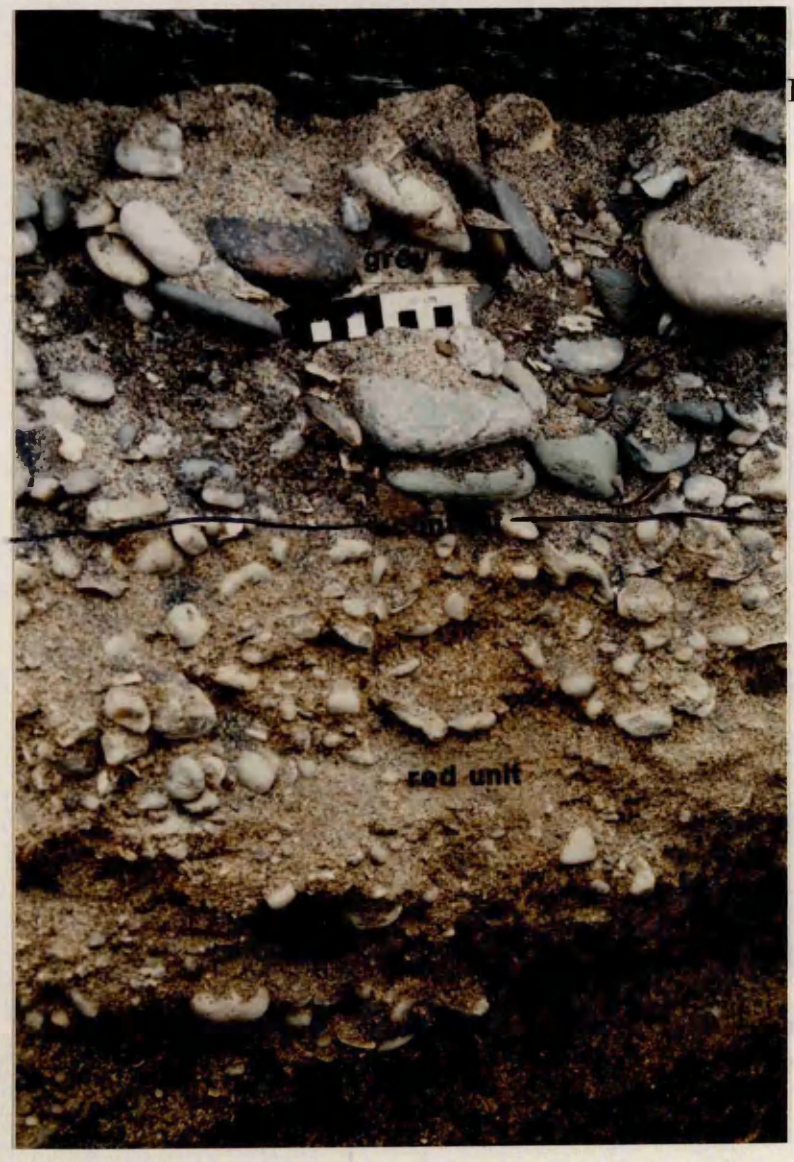

Fig. 3.2 **Grey unit** gravel overlying **red unit** gravel in a gully at site 16. Scale 10cm.

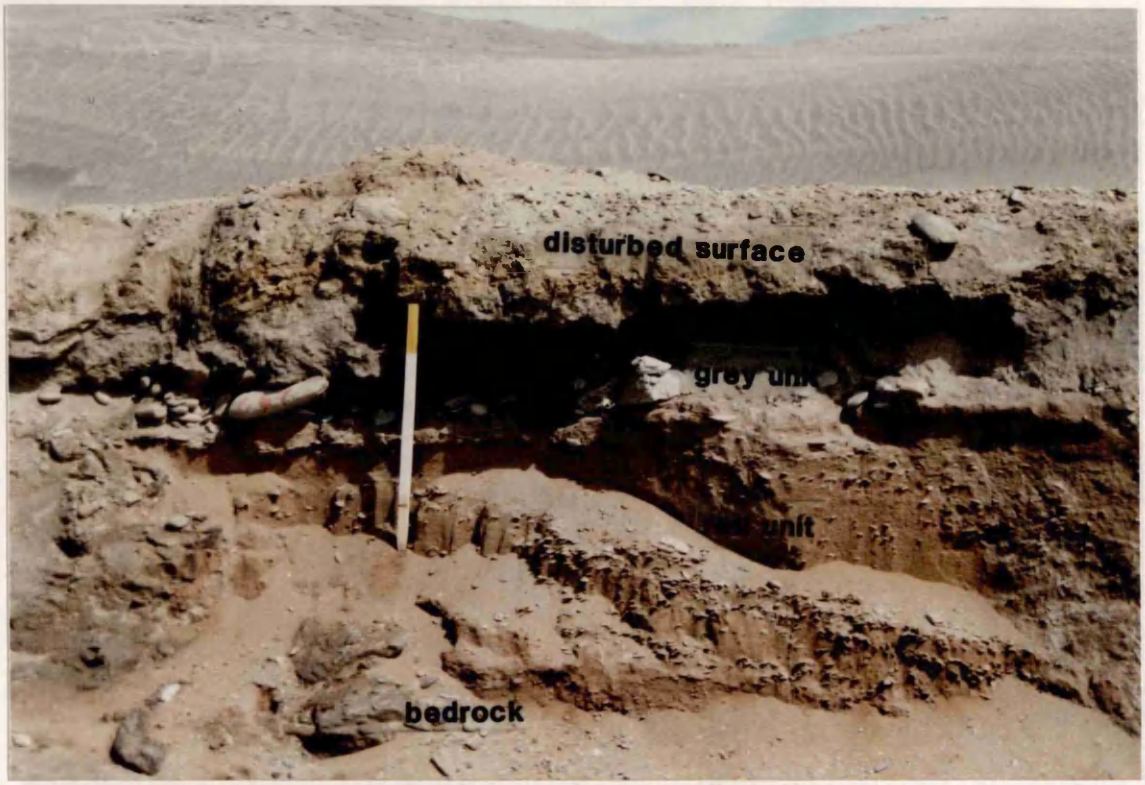

Fig. 3.1 Thin **grey unit** gravel bed overlying shell-rich, sandy, basal **red unit** gravel at site 20. Note road surface above grey unit. Scale 150cm.

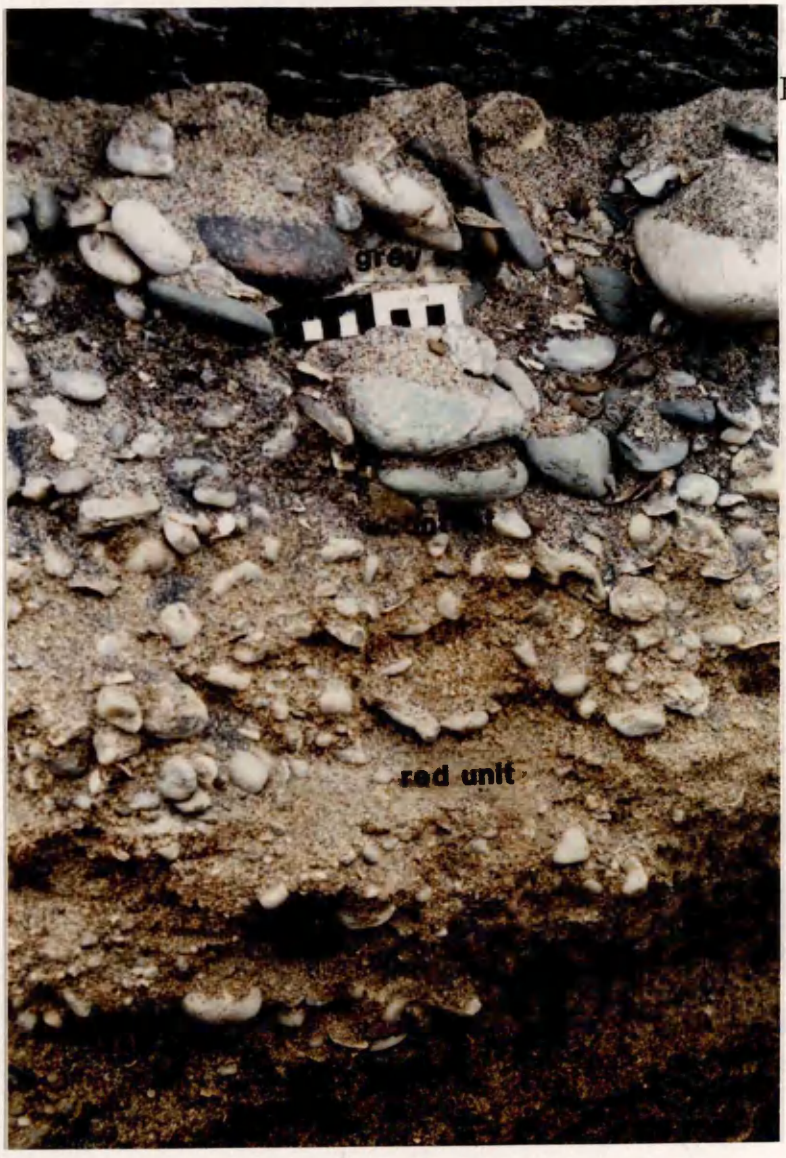

Fig. 3.2 **Grey unit** gravel overlying **red unit** gravel in a gully at site 16. Scale 10cm.

Fig. 3.3 Planar cross-stratified beach sand overlain by large- scale landward dipping planar cross-stratified windblown sand at site 24. Spade in top left corner for scale.

Fig. 3.4 Sub-horizontal landward-dipping plane beds of alternating light and heavy mineral aeolian sand overlying the **grey unit** at site 24. Scale 10cm.

Recognition or characterization of these beach facies follow criteria used by Massari & Parea (1988) and Postma & Nemec (1990) in similar sedimentary settings. These criteria are largely based on the relative position of the facies on the beach, textural characteristics of the sediments, nature of stratification and the average dip angle of beds.

The intertidal red unit comprises a thin basal lag of mainly discoidal and bladed clasts of locally derived schist and quartzite boulder-cobble gravel, and minor subrounded vein-quartz. These gravels deposited in water depths of 2-3m are interpreted as transgressive lag deposits and are infilled with and covered by shelly, low-angle, seaward dipping, gravel which is rich in vein-quartz. The calculations of palaeo-water depths are based on Dupre (1984), who pointed out that palaeo-water depth can be approximated by the vertical distance a deposit occurs below sediment deposited at sea-level (Fig. 3.5, see folder), assuming no change in relative sea-level and no compaction of the sediment after deposition. It is argued here that relative sea-level as well as compaction during deposition of these relatively thin beach sediments would have been minimal.

Westward of the sediments with a low-angle of dip (intertidal zone), the deposits of the red unit grade into thicker, gently seaward-dipping, shell-rich interfingering sand and gravel couplets wedging out landwards and with a downdip increase in grain size (also Fig. 3.5). These strata resemble those of the upper parts of the beach where each stratum is the deposit of a single beach surface. The inclination of beach accretion surfaces is higher here than in the intertidal zone of the red unit. This vein-quartz pebble gravel covers a similar basal lag gravel as described for the intertidal zone which drapes over the basement rock (bedrock) across the entire beach (also Fig. 3.5). The spatial arrangement and geometry of the vein-quartz gravel beach indicate eastward

beach progradation (also Figs. 3.5). At the seaward end of this facies shells often concentrate in lenses or coquinas. This zone is interpreted as the upper shoreface marking the concentration of shells often seen in this position on the recent beaches of the Namibian coast. The high variability in facies associations possible in the upper shoreface according to Massari & Parea (1988), makes facies identification difficult.

The red unit gravel, seaward (west) of the upper shoreface facies comprises thick, clean sheets of coarse to very coarse, shell-rich, parallel laminated sand deposited in water depths of about 4-5m. The sand contains scattered, flat-lying or slightly seaward imbricated discoidal pebbles, and is inferred to represent the lower shoreface facies of the red unit (Fig. 3.5).

3.2.2 COMPOSITION AND PROVENANCE

a) *Gravel fraction*

Schist, quartzite and vein quartz are the most abundant lithologies of the red unit gravel with subordinate silcrete and gneiss clasts (Fig. 3.6). Vein quartz shown in Fig. 3.7, predominates in the progradational beach gravel of the red unit. Local bedrock erosion supplied most of the common clasts. The silcrete clasts are probably derived from the adjacent Late Cretaceous escarpment and are generally better rounded than the locally derived quartzites. Therefore the silcrete clasts have either been transported from further south up the coast or have been sourced from an older Eocene beach which is known to have once existed between the present Late Cretaceous escarpment and the Eemian red unit beach. Orange River derived exotic clasts are extremely rare in the red unit, i.e their presence is not statistically significant (Fig. 3.8). The common clast lithologies are shown in Fig. 3.8.

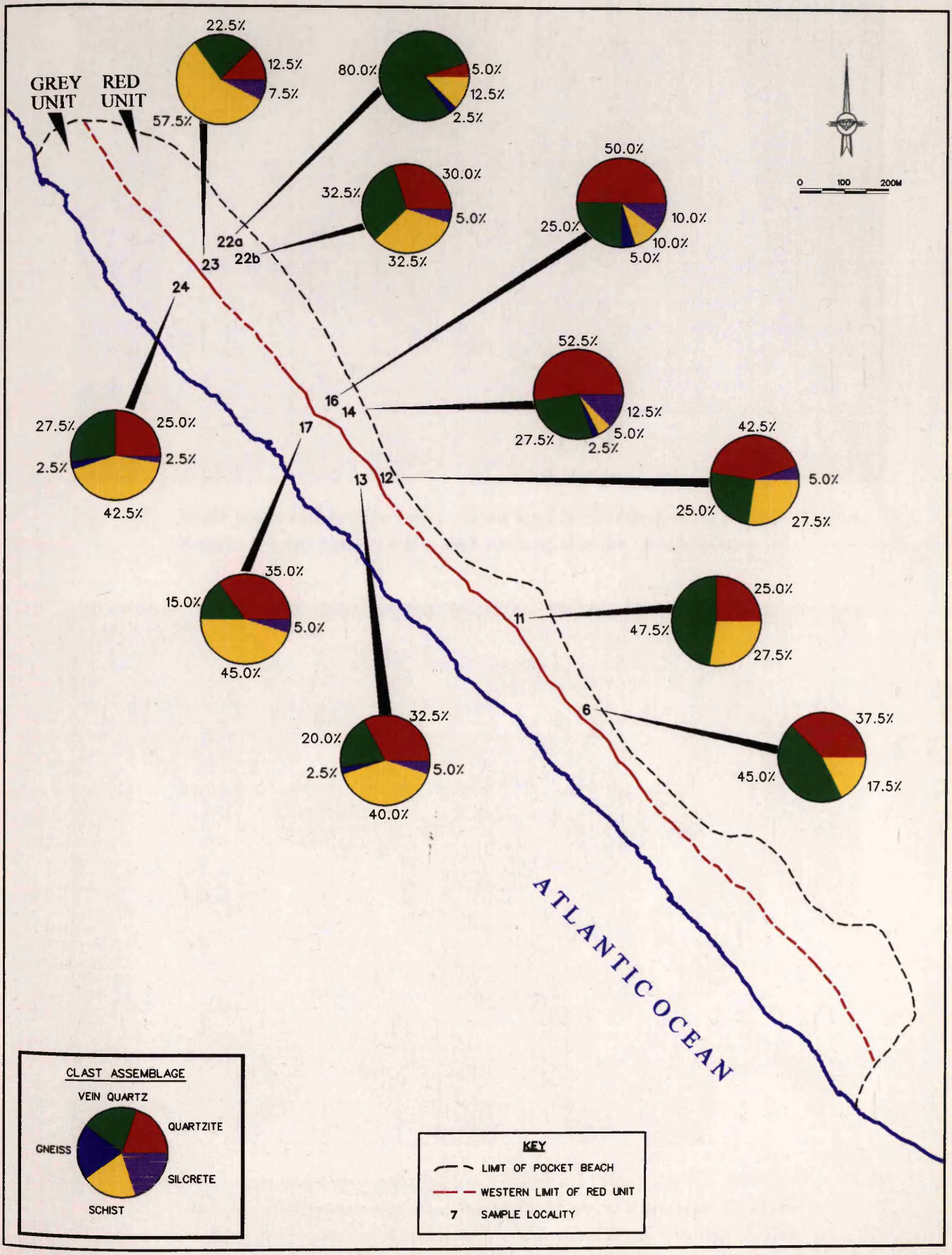

Fig. **3.6** The distribution of the clast composition-assemblage in the grey and red units within the study area (pocket beach no. 4), Chameis.

NAMDEB

Fig. 3.7 Well rounded schist (sch) clasts and subrounded to rounded vein quartz (vqtz) clasts of the **red unit** at site 20. Scale 10cm.

Fig. 3.8 Predominant clast lithologies and shell types found within the study area (pocket beach no. 4), Chameis. 1) yellow quartzite; 2) dark quartzite; 3) gneiss; 4) schist; 5) vein quartz; 6) Orange River quartzite; 7) banded ironstone formation; 8) jasper; 9) shells; 10) silcrete; 11) quartz porphyry; 12) riebeckite; 13) agate and 14) epidosite. Scale 10cm.

b) *Sand fraction*

Red unit sand is largely made up of quartz and feldspar grains, with minor amounts of heavy mineral grains (Fig. 3.9). The red colour of the sand is attributed to subaerial exposure which the presence of calcareous nodule development towards the top contact of the red unit is interpreted to indicate. This will be discussed in a later section. There is no obvious explanation for the relative rarity of heavy minerals, like garnets, etc. in the red unit sand compared to their abundance in the grey unit. Walker, *et al.* (1978) ascribe the genesis of red colouration in sands to the weathering of Fe-bearing detrital grains and there is the possibility that the heavy minerals in the red unit may have been lost by this means. However the scarcity of exotic clasts also, reported earlier, may suggest that there is an original difference in provenance between the two stratigraphic units. As diamonds, which generally occur in association with heavy minerals throughout the Sperrgebiet, are quite prevalent in the red unit as well, the general rarity of heavy minerals is therefore difficult to explain.

3.2.3 SEDIMENTARY TEXTURES

Grain size

Grain size on this beach was measured as it is a possible indicator of the energy of the longshore current and the waves that dispersed the sediment within the study area. The gravel and sand fractions were weighed separately because of the presence of large clasts which would have biased cumulative frequencies in favour of the gravel fraction.

a) *Gravel fraction*

The red unit gravel consists of moderately sorted, matrix-supported,

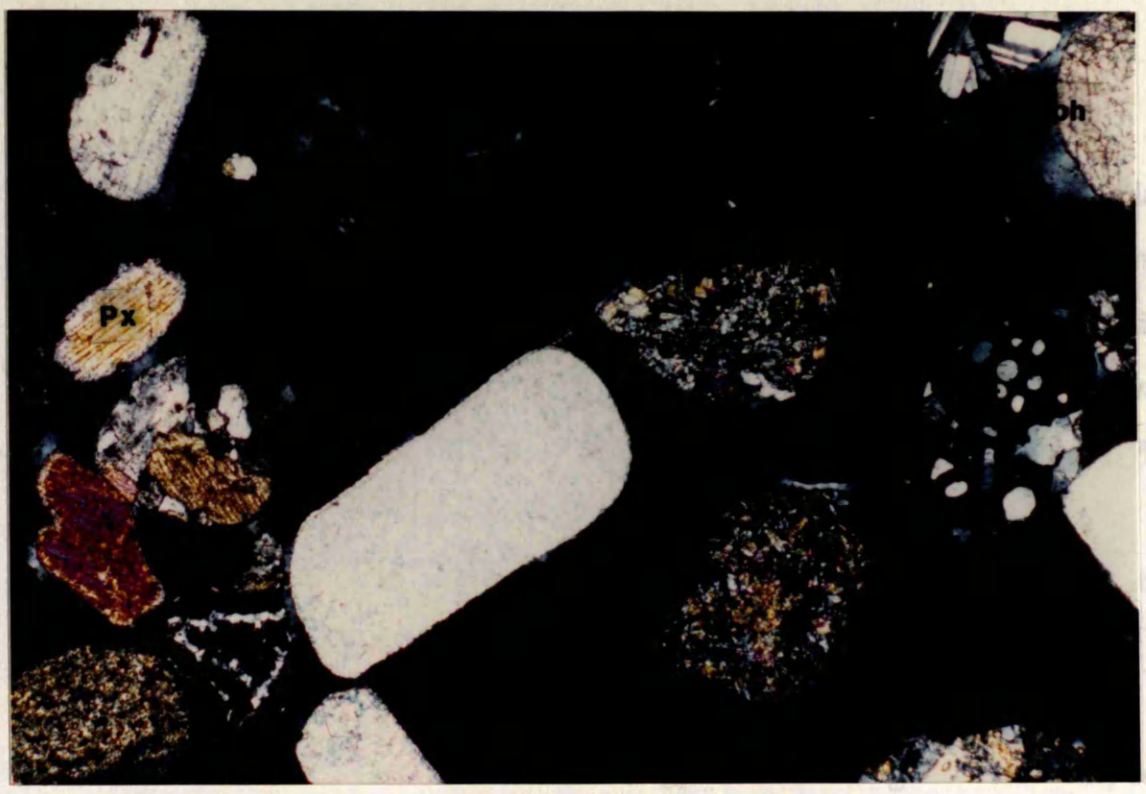

Fig. 3.9 Photomicrograph of the **red unit** heavy mineral sand fraction. Pyroxenes (Px), amphiboles (Amph), garnets (Grt) and opaque minerals are the most common. Also rock fragments. Crossed polars. Magnification (x 2.5).

Fig. 3.10 Moderately sorted, clast-supported shelly, local vein quartz pebble-cobble gravel of the **red unit** with scarce to absent sand matrix at site 16. Scale 10cm.

polymodal, shelly gravel (Figs. 3.10 & 3.11 and Table 3.2). Constituent clasts vary in size from medium boulders (< 1024mm) to coarse pebbles (16-32mm). The mean and average maximum clast size of the gravel range from medium boulders to large pebbles (Figs. 3.12 to 3.14). There is a general northward increase in both the mean clast size and the average maximum clast size (Figs. 3.12 & 3.13). The standard deviation of grain size decreases towards the northern end of the beach (Fig. 3.15). Both these observations indicate that energy levels were higher in the northern part of the beach compared to the southern part. The increase in grain size alone could either suggest that the gravel was generated here or that the energy level was higher. However, seen in conjunction with the improved sorting of the gravel, a more energetic system seems more likely (see subsection b, for the sand fraction).

b) *Sand fraction*

The red unit sand consists of moderately sorted, bimodal, shell-rich coarse to very coarse sand (Fig. 3.16). The sorting of the sand increases as its grain size increases, and as with the gravel fraction also shows better sorting towards the northern end of the beach (Fig. 3.15). This northward increase in grain size of the red unit gravel fraction and degree of sorting of the red unit as a whole, suggests a higher energy response in this region of the pocket beach.

Grain morphology

The morphology of gravel clasts was measured to determine the mechanisms involved in the sorting of differently shaped particles on the beach and the energy conditions asssociated with that sorting.

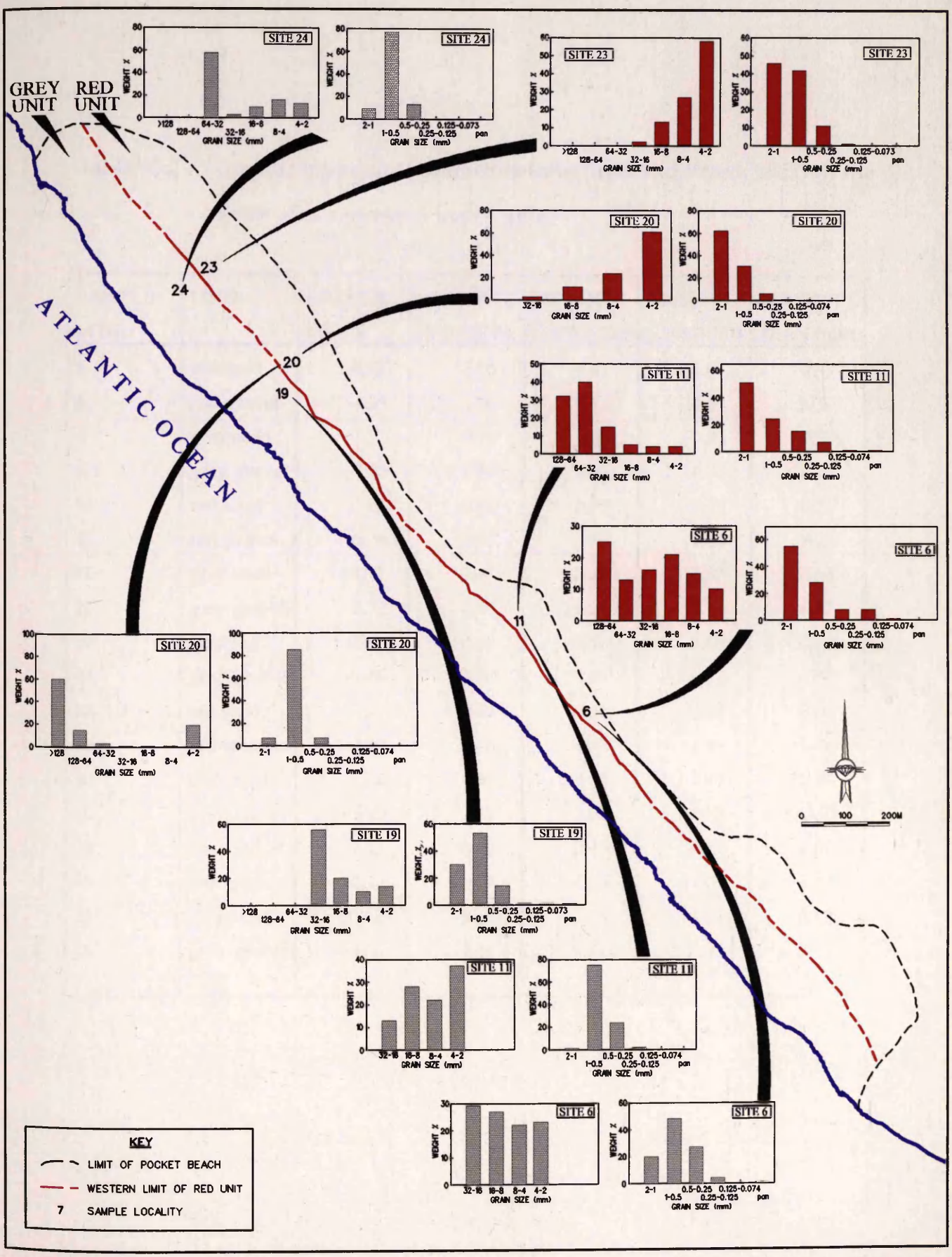

Fig. **3.11** Grain size distribution within the grey and red units of the study area (pocket beach no. 4), Chameis. Note as discussed in text, the gravel and sand size weight distributions calculated seperately. The grey unit overlies the red unit at sites 6, 11 and 20.

NAMDEB

Table: 3.2 Graphic grain size parameters (after Folk and Ward, 1957) of the study area expressed in phi units.

SAMPLE SITE	UNIT	GRAPHIC MEAN	GRAPHIC STD DEV	GRAPHIC SKEWNESS	GRAPHIC KURTOSIS	GRAPHIC MEAN (mm)
6	red sand	0.27	1.03	0.49	1.07	0.83
6	red gravel	-4.36	1.58	0.13	0.63	20.58
6	grey sand	0.77	0.75	0.05	0.84	0.59
6	grey gravel	-3.03	0.93	0.11	0.54	8.19
11	red sand	0.40	0.80	0.75	0.99	0.76
11	red gravel	-5.30	1.08	0.57	1.13	39.40
11	grey sand	0.84	0.44	0.23	1.37	0.56
11	grey gravel	-2.72	0.89	-0.30	0.68	6.57
19	grey sand	0.48	0.60	0.31	0.86	0.72
19	grey gravel	-3.45	0.86	0.83	1.02	10.93
20	red sand	0.15	0.44	0.66	1.13	0.90
20	red gravel	-2.18	0.66	-0.57	1.24	4.54
20	grey sand	1.22	0.62	0.08	0.96	0.43
20	grey gravel	-5.43	2.17	0.93	1.91	43.21
23	red sand	0.31	0.66	0.48	0.93	0.81
23	red gravel	-2.17	0.59	-0.57	1.05	4.49
24	grey sand	0.62	0.48	0.06	1.01	0.65
24	grey gravel	-4.31	1.26	0.81	0.85	19.79

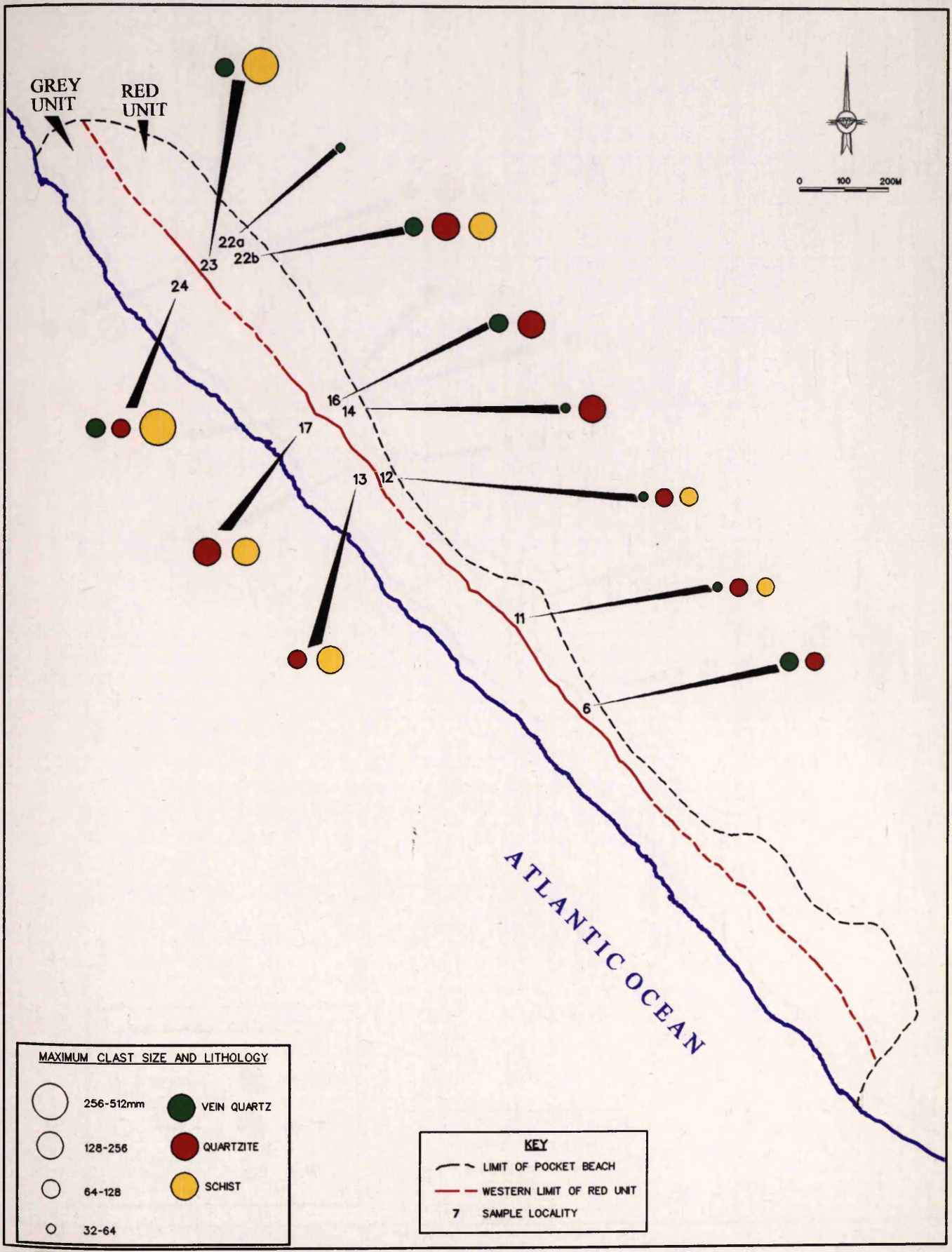

Fig.**3.12** The distribution of the average maximum clast size in the grey and red units within the study area (pocket beach no. 4), Chameis.

NAMDEB

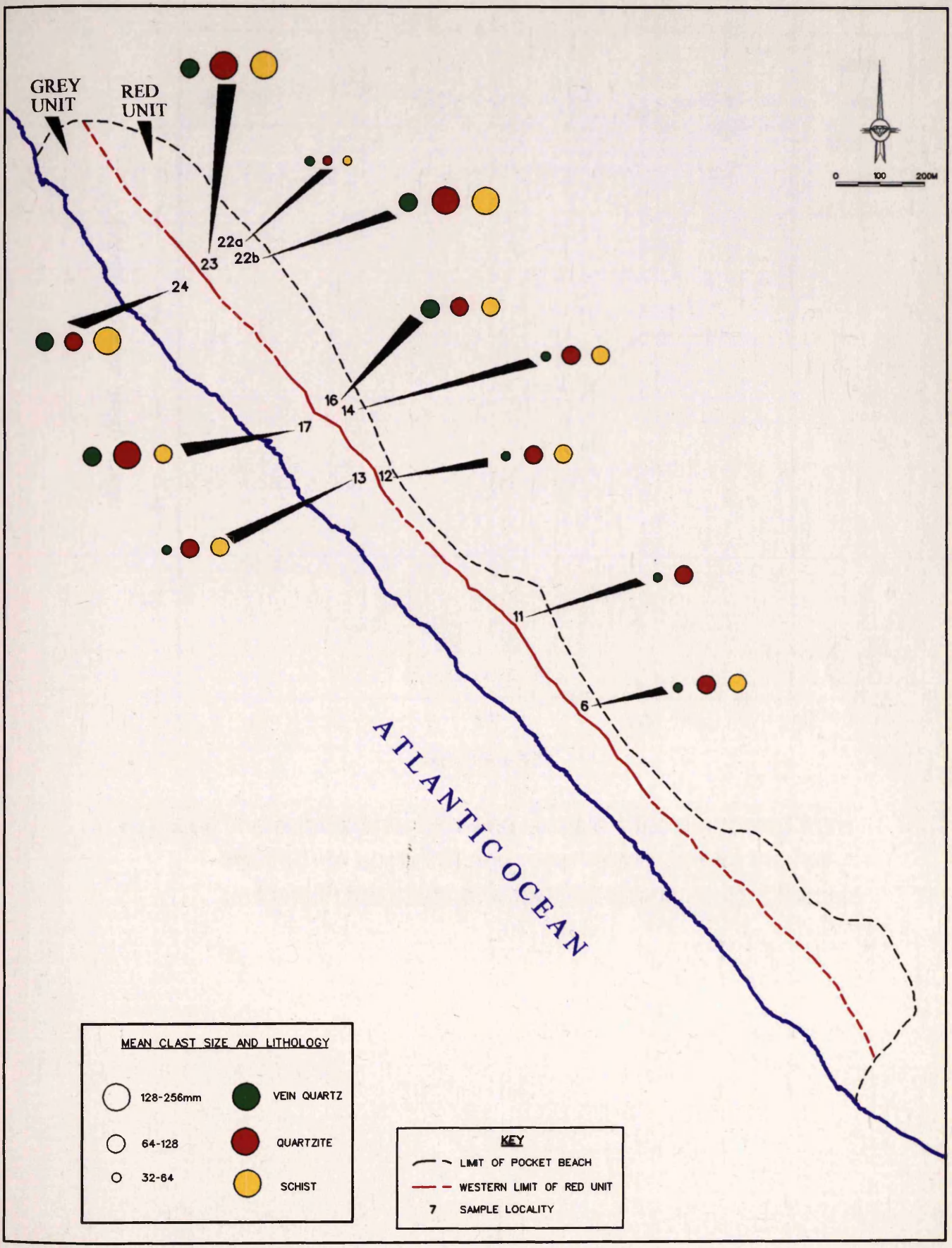

Fig. **3.13** Distribution of the mean clast size in the grey and red units within the study area (pocket beach no. 4), Chameis.

NAMDEB

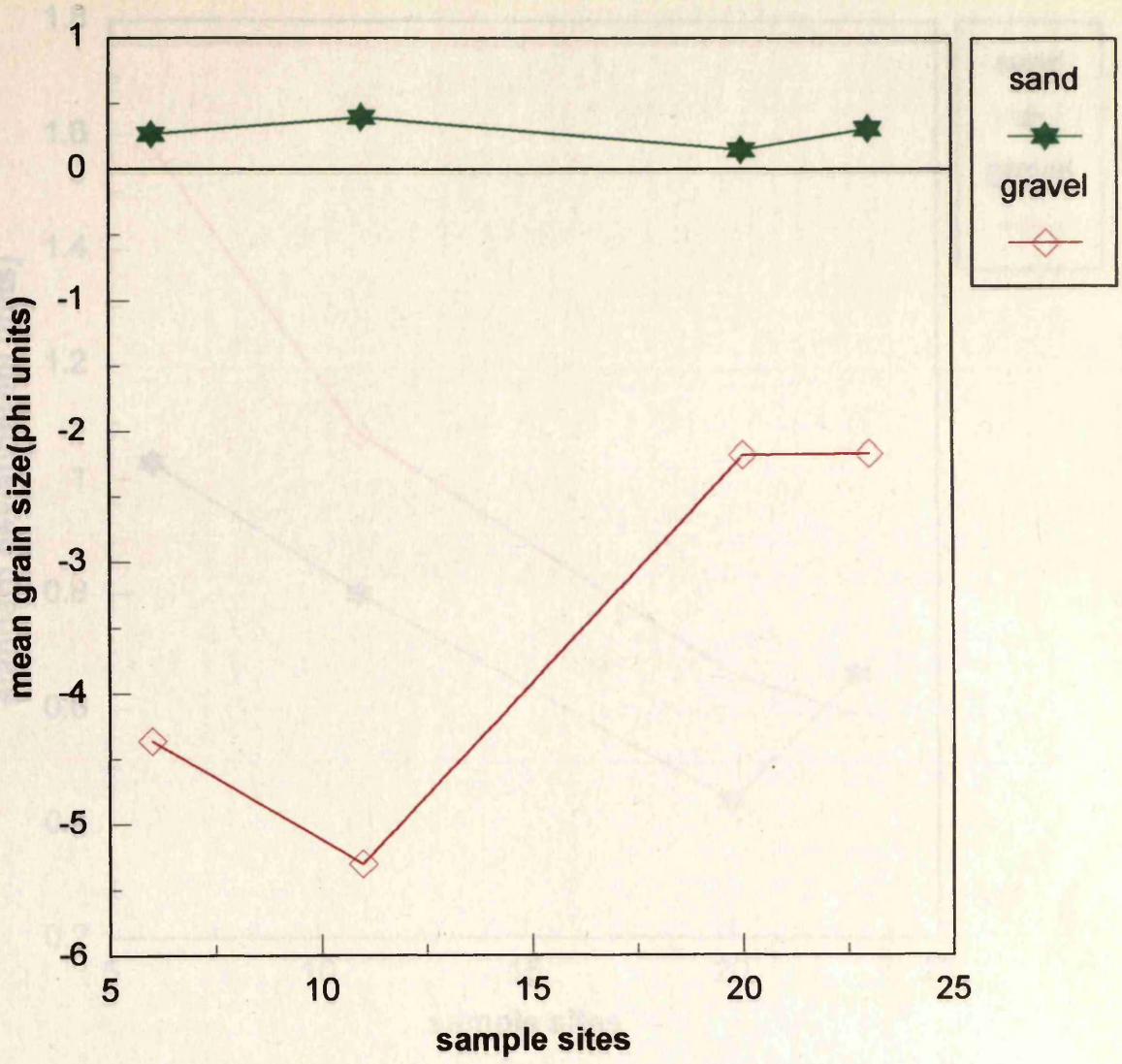

Fig. 3.14 The relationship between sample sites numbered from south(6) to north(23) and mean grain size for the red unit within the study area(pocket beach no.4), Chameis.

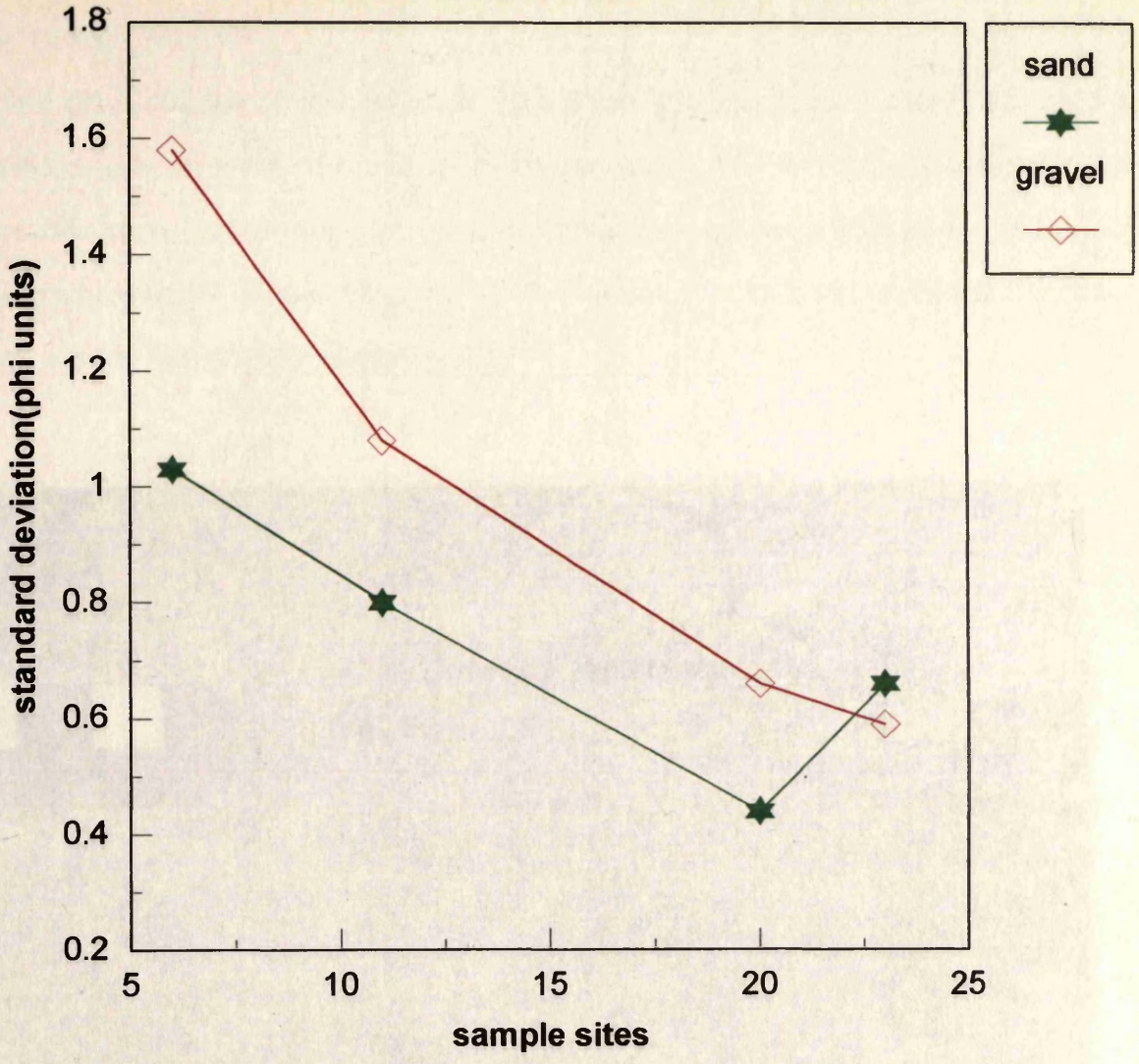

Fig. **3.15** The relationship between sample sites numbered from south(6) to north(23) and the standard deviation of grain size for the red unit within the study area(pocket beach no.4), Chameis.

Fig. 3.16 Coarse grained sand of the **grey unit** overlying very coarse-grained sand of the **red unit** at site 23. Scale intervals 1cm.

a) *Gravel fraction*

The clast shapes of the red unit gravel are predominantly discs and blades, with minor amounts of rods and spheres (Figs. 3.17 & 3.18). Quartzite clasts mostly form discs, vein quartz more discs than spheres and rods, and schist overwhelmingly blades (Fig. 3.19). The number of spheres of schist lithology are almost statistically insignificant.

It is very clear from the predominant lithologies present, and an examination of the effect of lithology on shape, that the lithological composition of the source exerts a commanding influence over the shape composition of these gravels (Fig. 3.20). There is no significant correlation between the shapes of quartzite and vein quartz, and their size, unlike for schist where the largest clasts form more blades. The internal structure of the schist, i.e the ease with which it splits along schistosity planes would explain the preponderance of blades in their shape composition. There is no discernable pattern of shape sorting across and along the beach (Fig. 3.18). One possible explanation of this is that all shapes were thrown up the beach during storm activity and the less mobile discs and blades were left behind on the beach together with the diamonds, while during backwash spheres and rods which move more readily in traction were moved down the beach into the offshore (Bluck, 1967). This would explain the striking abundance of discoidal and bladed clasts on this exposed part of the beach. From there they would then be moved further up the coast by longshore drift.

The average roundness value of the red unit gravel for the different lithologies lumped together is 0.6 (rounded). For a wide range of sizes (4-256mm) of vein quartz clasts, roundness decreases with an increase in mean clast size (Fig. 3.21). There is therefore a strong correlation between roundness and mean clast size as shown by measurements at site 22a (Figs. 3.22a&b),

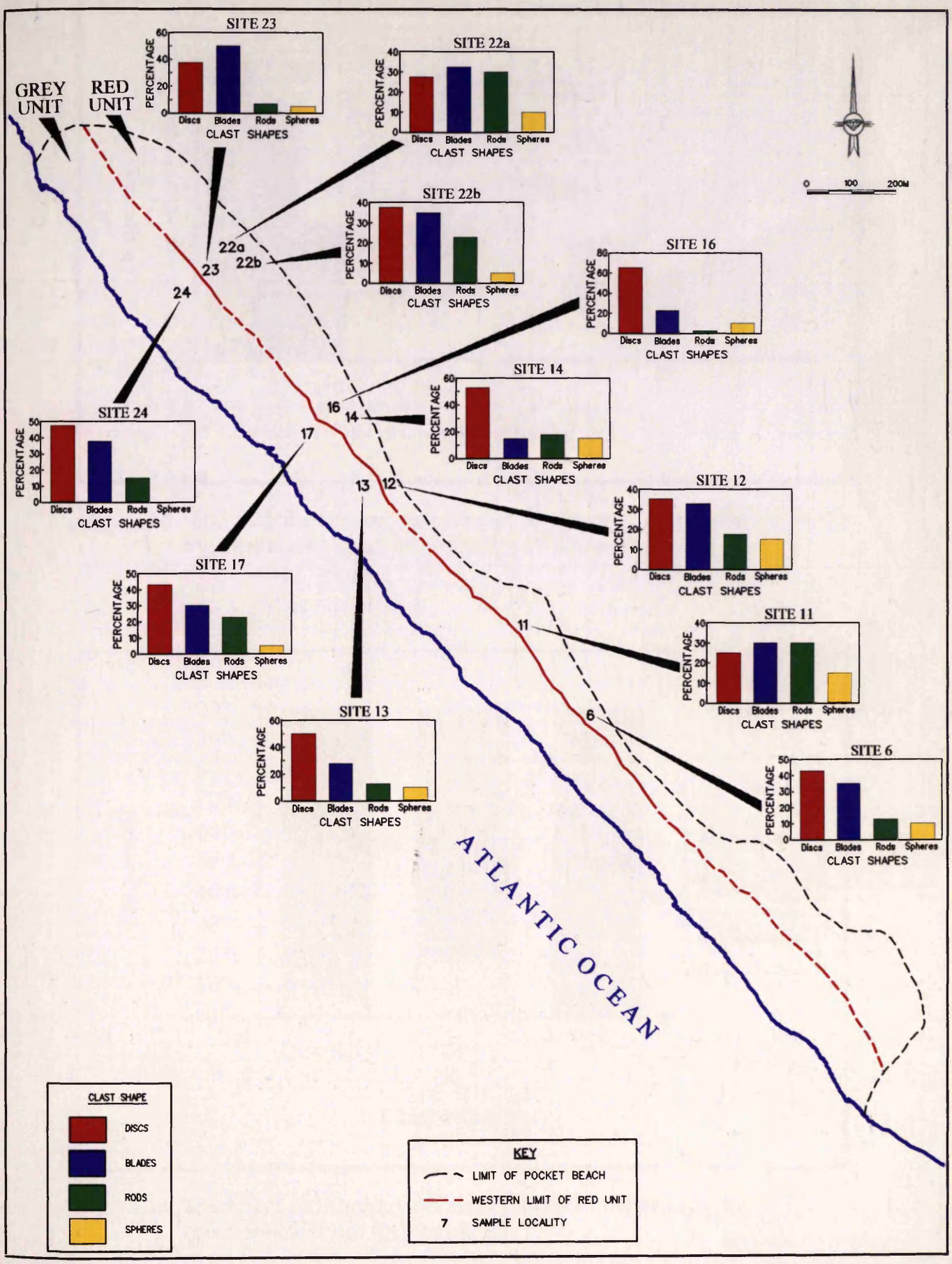

Fig.**3.17** The distribution of clast shapes in the study area (pocket beach no. 4), Chameis.

NAMDEB

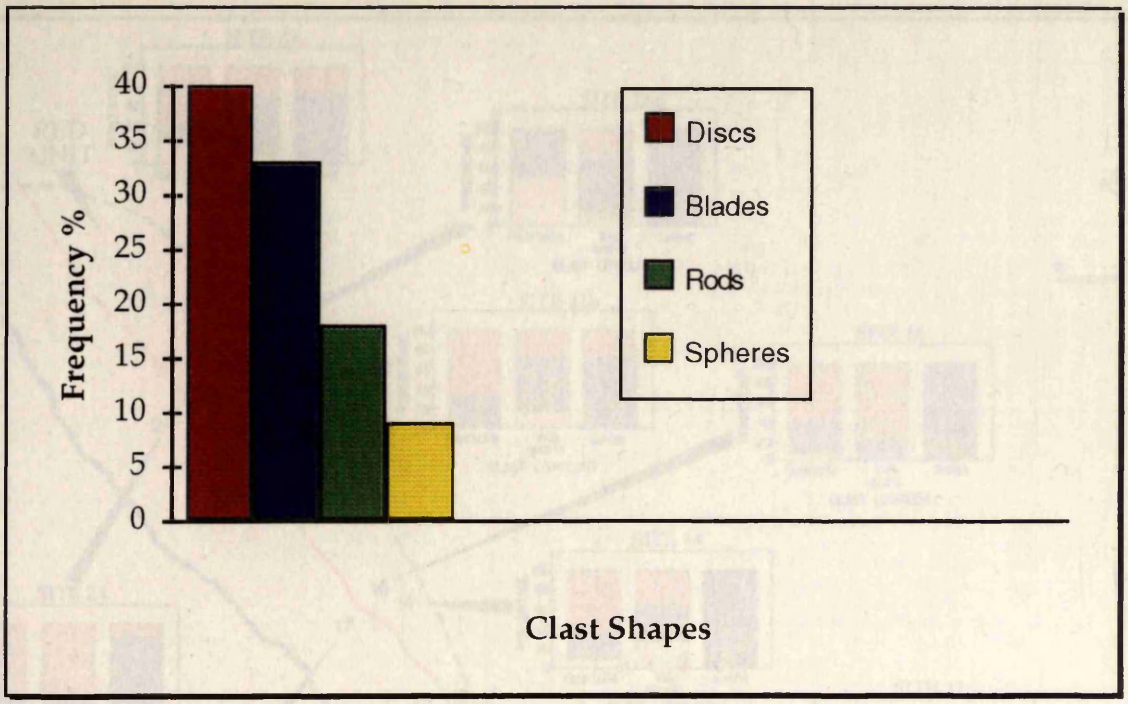

Fig. 3.18 The distribution of clast shapes in the grey and red units within the study area (pocket beach no. 4), Chameis.

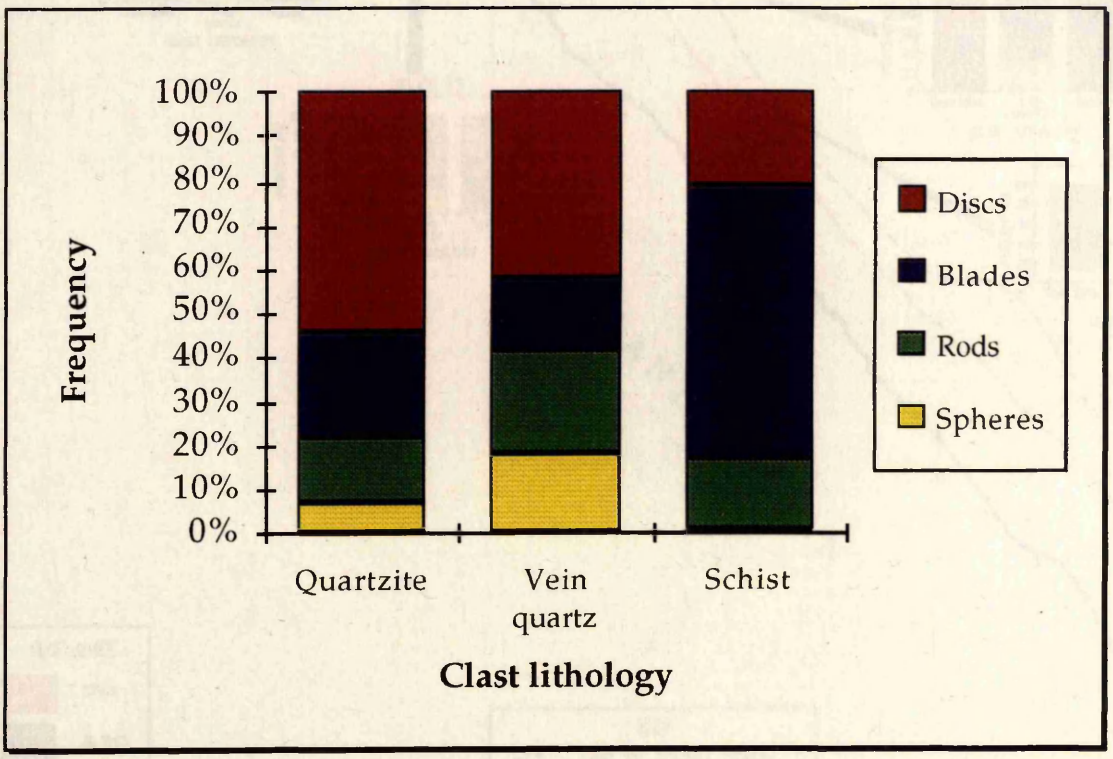

Fig. 3.19 The effect of lithology on clast shapes in the study area (pocket beach no. 4), Chameis.

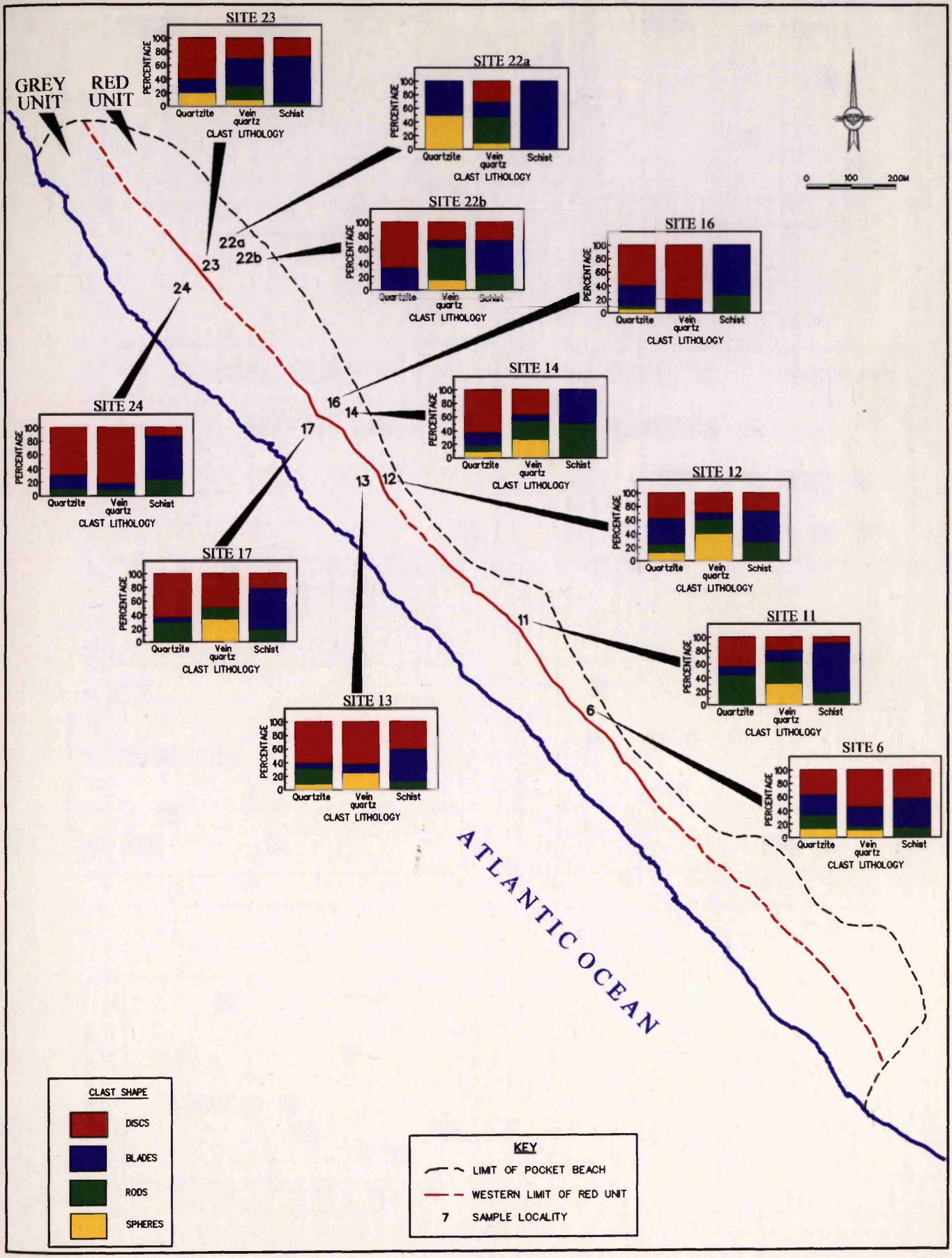

Fig.**3.20** The distribution of clast shapes in relation to composition in the grey and red units within the study area (pocket beach no. 4), Chameis.

NAMDEB

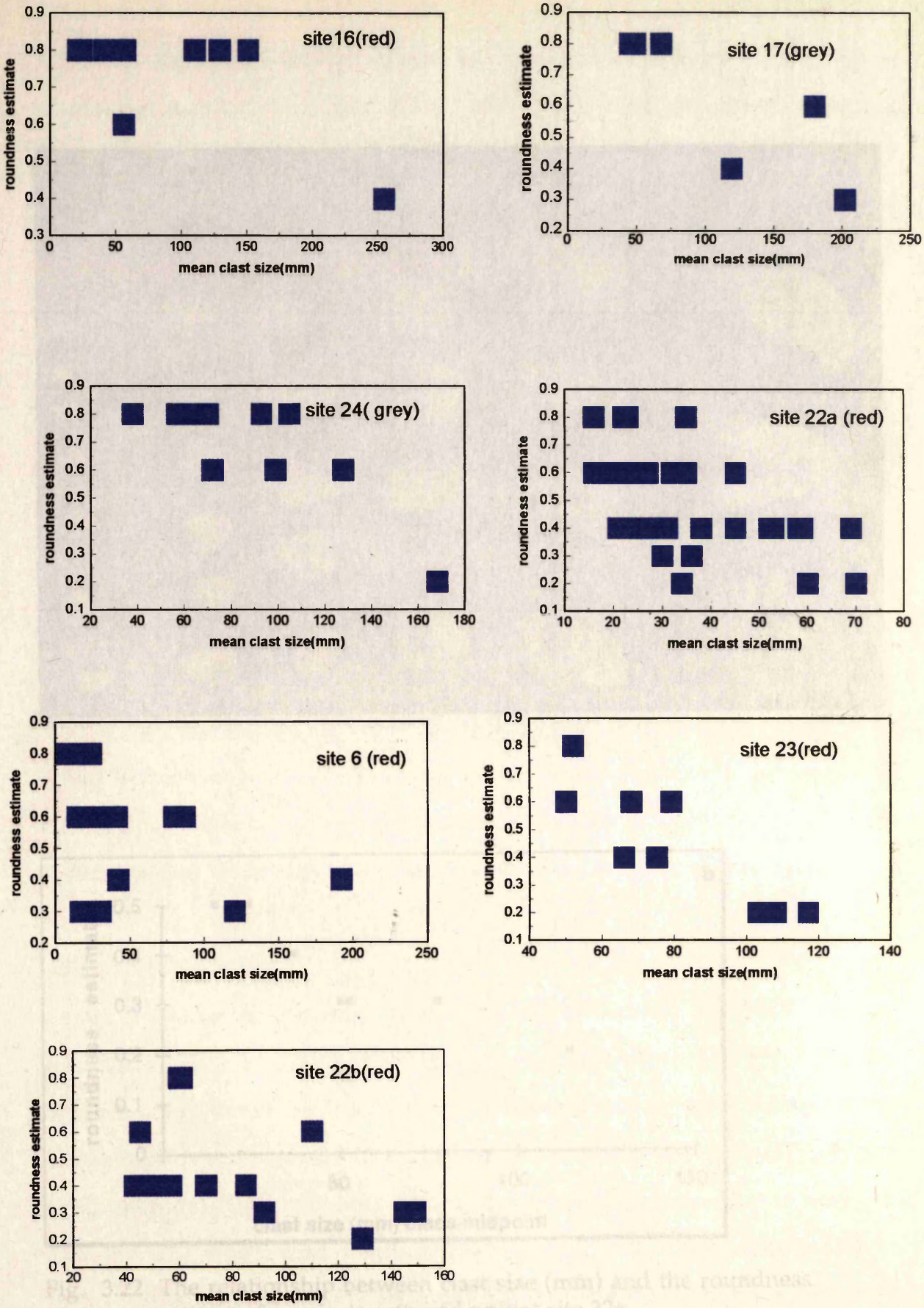

Fig. **3.21** The relationship between mean clast size and the roundness estimate of vein quartz for the grey and red units at different sites within the study area (pocket beach no.4) ,Chameis.

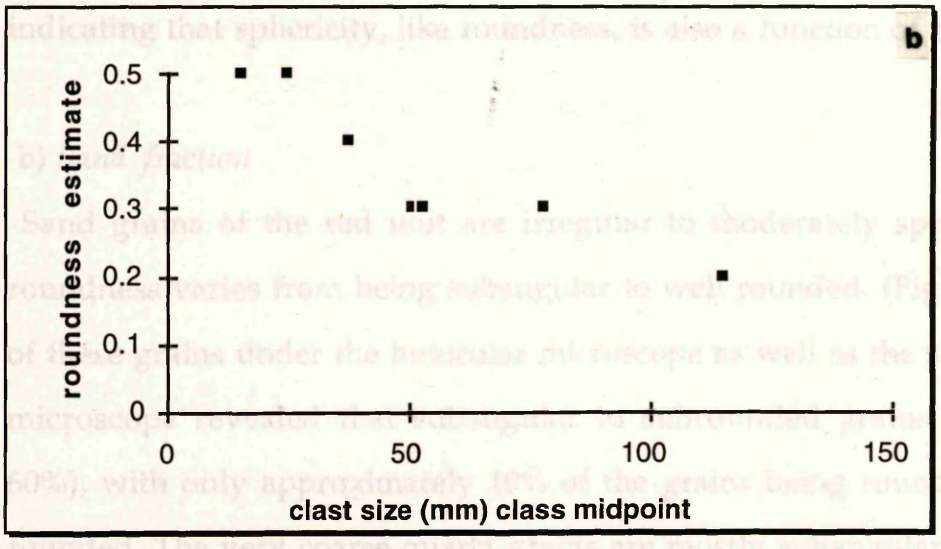

Fig. 3.22 The relationship between clast size (mm) and the roundness estimate for vein quartz: red unit at site 22a.

while no significant relationship exists between the standard deviation of roundness and the mean roundness value. The smaller vein quartz clasts (4-128mm) are generally better rounded than the larger vein quartz clasts (> 128mm) (Fig. 3.22b). The small vein quartz clasts are either fragments broken off the large clasts in the immediate environment or have migrated up the coast from beaches to the south.

Abrasion is more effective in the 16-128mm sizes than in the others, and is especially effective in the 64-128mm size range where the highest roundness values are recorded here and elsewhere (Pettijohn, 1957; Bluck, 1969, p.2). However the presence of quite angular clasts in this size range, as shown in Figs. 3.21 & 3.22a, indicates that breakdown processes are still operating (Bluck, 1969).

Quartzite and vein quartz clasts are more spherical (sphericity = 0.600) than schist (sphericity = 0.480). Sphericity is therefore a function of lithology, like clast shape. There is also a slight increase in sphericity as roundness increases indicating that sphericity, like roundness, is also a function of clast size.

b) *Sand fraction*

Sand grains of the red unit are irregular to moderately spherical and their roundness varies from being subangular to well rounded. (Fig. 3.9). Inspection of these grains under the binocular microscope as well as the scanning electron microscope revealed that subangular to subrounded grains predominate (± 60%), with only approximately 10% of the grains being rounded to very well rounded. The very coarse quartz grains are mostly subangular. Heavy mineral grains, e.g. garnet are mostly well rounded, but subrounded grains also occur. The sand fraction of the red unit is therefore clearly of mixed origin, with the rounded to well rounded, spherical grains probably having undergone

rigorous transport, while the subangular to subrounded less spherical grains appear to be texturally immature and are therefore most likely of local origin. Alternatively the well rounded grains had been in the intertidal environment for prolonged periods or are multicycled products of sedimentary rocks in the Orange River drainage area. These well rounded grains may also have been wind transported previously before being introduced into the marine environment.

Grain surface textures

a) *Gravel fraction*

Large quartzite boulders occasionally show crescentic impact scars or percussion marks, and imprints from fitted clast fabric (Fig. 3.23). These textures are attributed to high velocity flows during which clasts bounce against each other making impact scars (Conybeare & Crook, 1968), and where interlocked boulders abrade each other to form a fitted fabric (personal communication, Bluck, 1995).

b) *Sand fraction*

As shown in Fig. 3.25, the most common surface textures of the red unit sand are irregular pits of variable size (Fig. 3.25a), straight scratches and curved scratches (Fig. 3.25b), V's (Fig. 3.25c) and oriented etch pits (Fig. 3.25d). Most of the quartz grains studied have a moderate to low relief (Figs. 3.25). A surface texture called gullying identified for the first time by Higgs (1979, p. 608) can also be seen in Fig. 3.25c. According to Higgs (1979), irregular pits include any depression on the surface of grains and occur in a range of different sedimentary environments. Straight and curved scratches are believed to be indicative of grain movement in high-energy environments, while V's,

Fig. 3.23 Large (±0,8m along the a axis) percussion marks (p) ; imprints from fitted clast fabric (i). Quartzite boulder from the **red unit** at site 18. Note the degree of abrasion. Scale 0.5m.

Fig. 3.24 Steeply seaward dipping beach accretion surfaces of shell-rich **red unit** gravel at site 22. Scale 10cm.

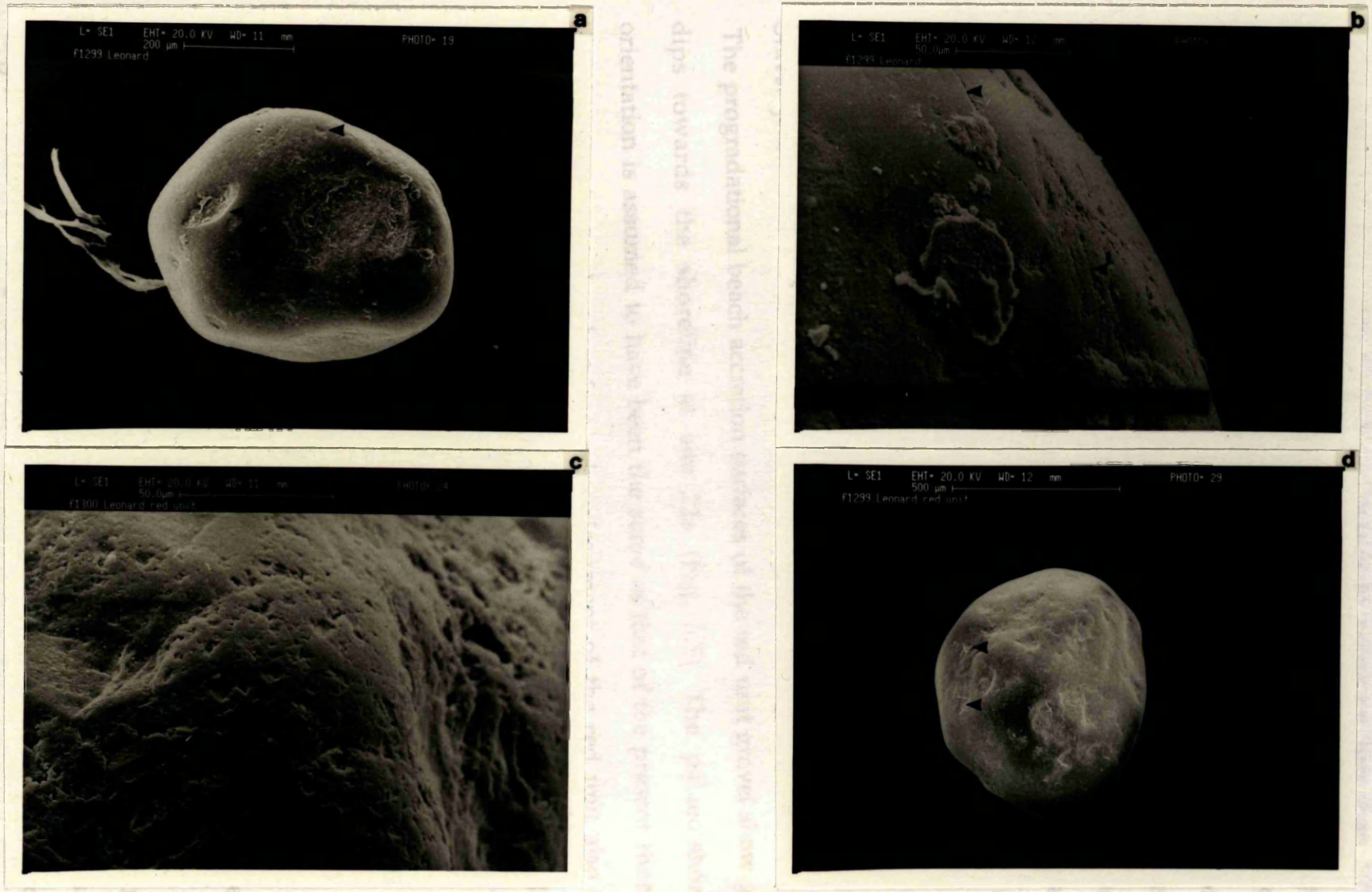

Fig. 3.25 Scanning electron microphotographs of the red unit quartz grain surface textures. a) Irregular pits of different sizes on a rounded quartz grain. b) Straight and curved scratches on a quartz grain with a rounded outline. Also note minor quartz overgrowths. c) V's and gullying. d) Oriented etch pits. Note the low to moderate relief in a-d.

triangular in outline, are also due to impact and form in subaqueous and aeolian environments. V's have been shown to occur on less than 50% of quartz grains from fluvial environments and on more than 50% of grains from high-energy beach environments (Nordstrom & Margolis, 1972). Although the results of this study are not statistically significant, most of the quartz grains studied exhibit V's. Oriented etch pits are dissolution products of quartz and are also believed to be indicative of marine environments. Gullying apparently results from both marine abrasion and weathering under acidic conditions.

Grain fabric

Gravel fraction

The progradational beach accretion surfaces of the red unit gravel show gentle dips towards the shoreline at site 22a (Fig. 3.5). The palaeo-shoreline orientation is assumed to have been the same as that of the present shoreline. Isolated pebbles in the shoreface subenvironment of the red unit also show gentle imbrication towards the sea. Red unit gravel in potholes and gullies occasionally shows bidirectional orientation which probably results from water turbulence inside these depressions.

3.2.4 SEDIMENTARY STRUCTURES AND GROWTH FORMS

The red unit is composed of a flat-lying, normally graded basal gravel bed slightly skewed towards the coarse fraction, which in the intertidal part of the beach grades upwards into gentle to steeply seaward dipping, pebble gravel medium-scale cross-beds with 0°-25° dip angles (Figs. 3.24 & 3.26). This high-angle cross-stratified gravel is in turn overlain by parallel-laminated sand with sharp erosional top contacts. Abundant shell debris often occur as interbedded

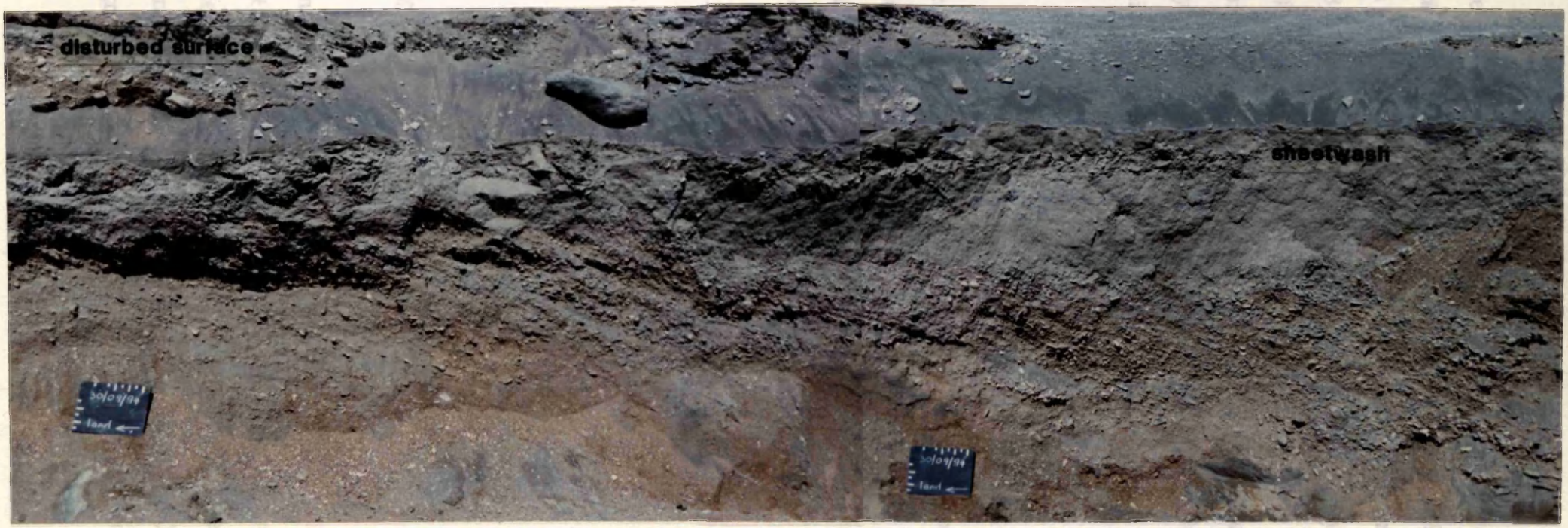

Fig. 3.26 Section normal to palaeo-shoreline showing steeply seaward dipping beach accretion surfaces of shelly, **red unit** gravel overlain by sheetwash, site 22.

layers or as scattered fragments within the red unit sediments (Figs. 3.26). There is no evidence of bioturbation or ripple cross-stratification in this sand and their absence is interpreted to be indicative of storm conditions (Swift *et al.*, 1983; Dupre, 1984), while the parallel laminated sand probably represents the waning stage of this storm event. However, the lack also of hummocky cross-stratification, considered to be characteristic of storm induced deposits, may be explained by the relative shallow water depths in which these deposits were, most likely, laid down.

3.2.5 SHELL TYPES

There is a low diversity and high abundance of marine macrofauna in the red unit. The typical shell types that occur in the red unit are shown in Fig. 3.27. The shells are generallly well fragmented indicating that energy conditions must have been moderately high periodically.

3.3 GREY UNIT

3.3.1 DISTRIBUTION OF LITHOFACIES

The westward lying grey unit mostly occurs in gullies and potholes cut by marine abrasion. It does also, however, form thin sheets of boulder-cobble gravel overlying the red unit in places and these possibly represent remnants of the maximum transgression of the grey unit (Figs. 3.1 & 3.2). The facies association of this gravel sheet cannot be established because it is poorly

Fig. 3.27 The common shell types in the **grey** and **red units** within the study area (pocket beach, no. 4), Chameis. Shell types identified by Dennis Kleinhans. 1) *Aulacomya ater* (ribbed mussel); 2) *Choromytilus meridionalis* (black mussel); 3) *Patella granatina*; 4) *Nucella squamosa*; 5) *Volutocorbis abyssicola*. Scale 8.5cm.

developed in those areas exposed by mining activities. The grey unit otherwise consists of a thin basal lag of mainly discoidal and bladed schist and quartzite boulder-cobble gravel. The framework of boulders and cobbles has been filled with finer gravel, suggesting deposition in the subaqueous zone of the beach (Masari & Parea, 1988). This basal lag (0.2m thick) is covered by an upward-fining succession (0.5m thick) of coarse to gritty sand with isolated pebble-sized clasts grading into subparallel to planar laminated, light and heavy mineral layers. The grey unit is interpreted to be subtidal, while the marine sand overlying it, probably represents the regressive phase of a recent marine transgression.

3.3.2 COMPOSITION AND PROVENANCE

a) *Gravel fraction*

The clast composition-assemblage of the grey unit is largely the same as that for red unit gravel (Figs. 3.6, 3.28 & 3.29). The grey unit in addition, contains abundant Orange River derived exotic clasts examples of which are shown in Fig. 3.31 (> 1% of assemblage is exotic clasts). Banded ironstone formation is the most common exotic clast, with agate, riebeckite, quartz porphyry, jasper, zeolite, chalcedony and epidosite being the other exotic clasts present (Fig. 3.30). There is an increase in the abundance of banded ironstone formation clasts (specific gravity = > 4.0) towards the northern end of the beach, while agate (specific gravity = ± 3.0) decreases in abundance in the same direction (Fig. 3.30). This suggests that the wave energy is greater towards the northern end of the study area and therefore supplements the average maximum clast size data discussed earlier.

Fig. 3.28 Subangular to subrounded, locally derived quartzite boulders from the **grey unit** at site 16. Scale is 50cm long.

Fig. 3.29 Large subrounded to rounded, mostly bladed locally derived schist clasts of the **grey unit**, with minor quartzite and vein quartz clasts: site 17. Broken clasts (angular) from mining. Scale 15cm.

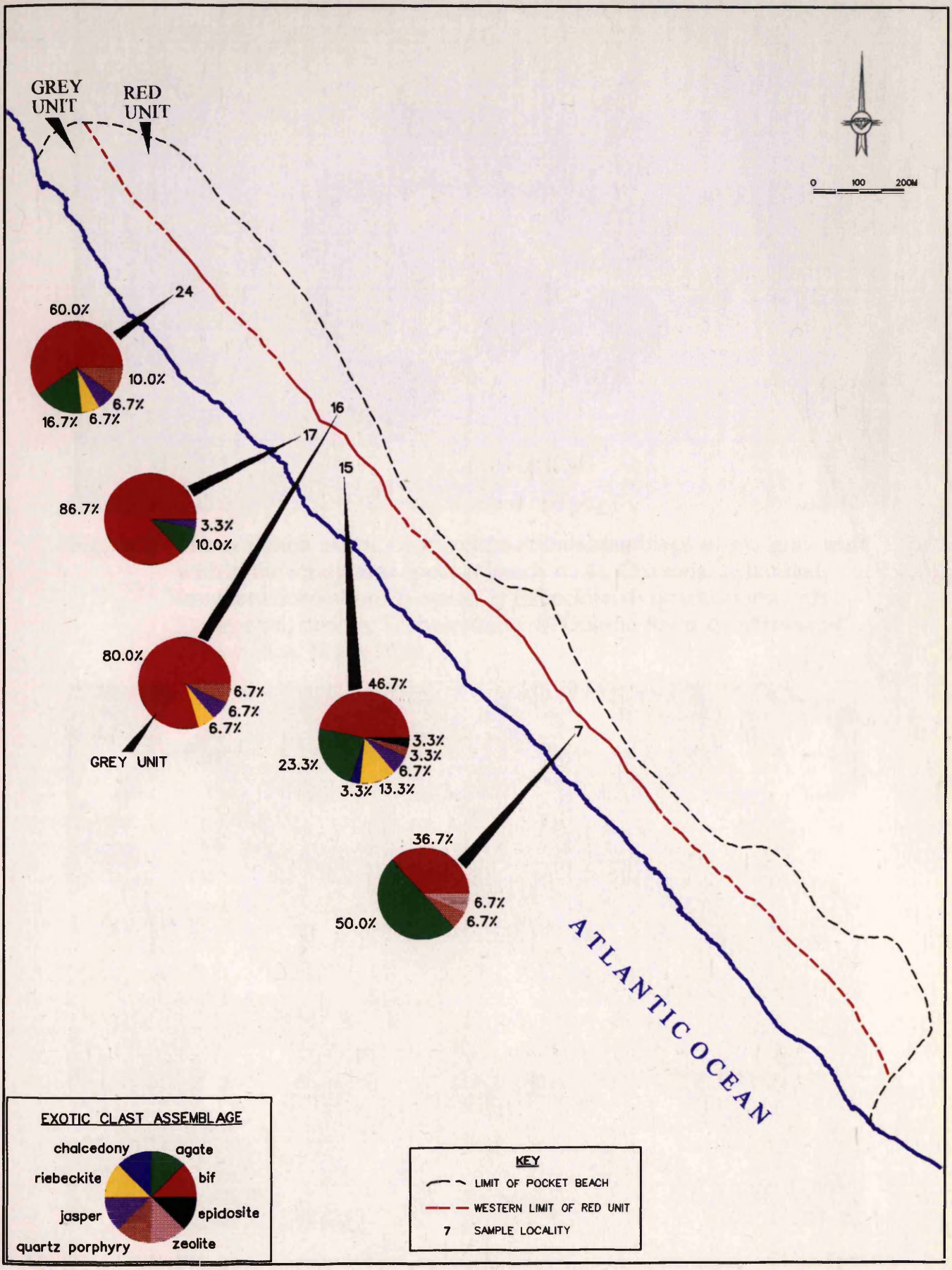

Fig.**3.30** The distribution of the exotic clast composition-assemblage within the study area (pocket beach no.4), Chameis. Note the absence of exotic clasts in the red unit, note also grey unit overlies red unit at site 16.

NAMDEB

Fig. 3.31 The common exotic clast composition-assemblage of the **grey unit** within the study area (pocket beach no.4), Chameis. 1) Banded ironstone formation; 2) agate; 3) riebeckite; 4) quartz porphyry; 5) jasper; 6) zeolite; 7) chalcedony; 8) Orange River quartzite and 9) cornelian. Scale 10cm.

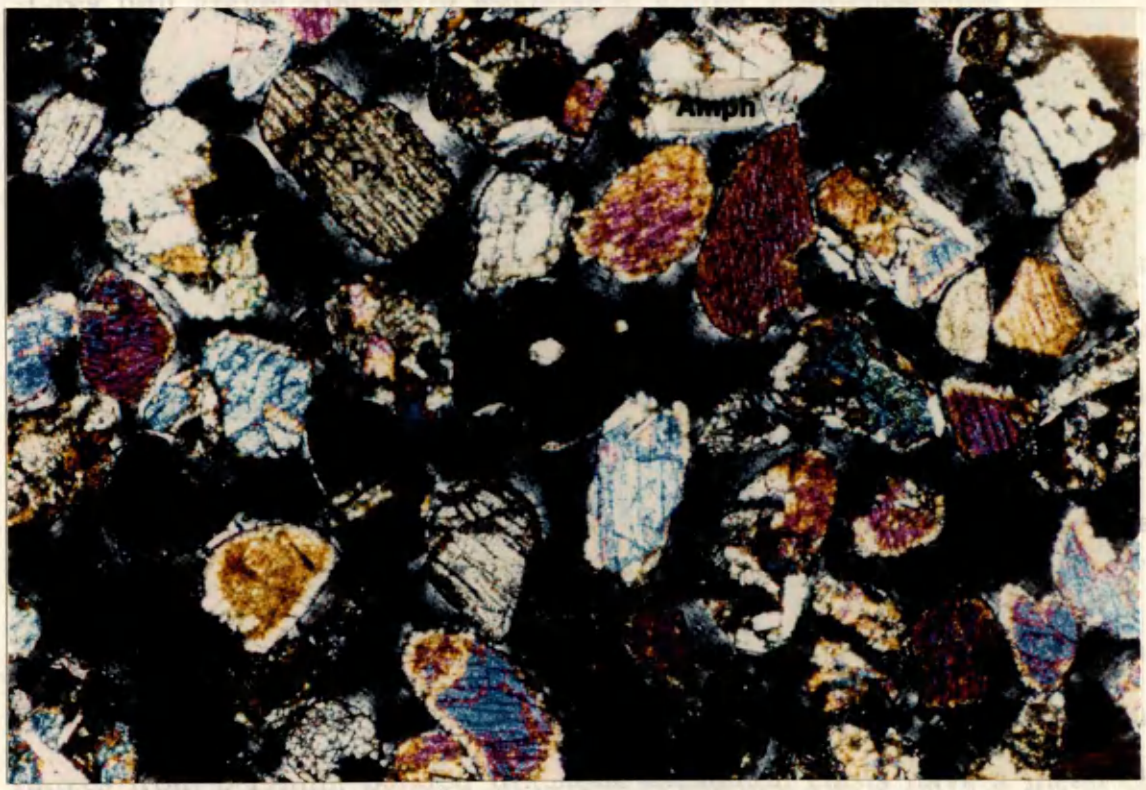

Fig. 3.32 Photomicrograph of the **grey unit** heavy mineral sand. Abundant pyroxenes, amphiboles, garnets and opaque minerals. Note abundance of heavy minerals compared to Fig. 3.9. Crossed polars. Magnification (x 2.5).

b) *Sand fraction*

Grey unit sand consists of quartz, feldspar and abundant heavy mineral grains. Clinopyroxene, garnet, and opaque minerals (magnetite, ilmenite, rutile, etc.) are the common heavy minerals (Fig. 3.32). The abundance of stable heavy minerals, like garnet would suggest that their provenance is probably at least partially, the Namaqualand Metamorphic Complex along the course of the Orange River. The study area hinterland is generally devoid of rocks of sufficient metamorphic grade to yield significant quantities of these heavy minerals.

3.3.3 SEDIMENTARY TEXTURES

Grain size

a) *Gravel fraction*

Grey unit gravel consists of moderately sorted, clast-supported, polymodal, shell-rich gravel (Table 3.2 and Figs. 3.2, 3.28 & 3.29). The size of the constituent clasts ranges from very large boulder to small pebble. In the grey unit gravel sheets, pebbles often concentrate around large boulder clasts as a result of the turbulence created by these boulders. Both the mean clast size and the average maximum clast size of the gravel are between medium boulder and large pebble (Figs. 3.13 & 3.14), and increase towards the northern end of the beach. Polymodal clast distribution in basal gravel most likely resulted from the mixing of grain size populations during storm activity following a fair-weather stage when earlier gravels were reworked (Bluck, 1967; Sherman *et al.*, 1993). Thus well-sorted gravel may only develop strongly if the supply of new material is low. For the Orange River derived exotic clasts the mean clast size ranges from 8-19mm. Banded ironstone formation clasts have a mean clast size of 19mm, agate 17mm, riebeckite 16mm and jasper 18mm. Chalcedony and zeolite have the smallest mean clast sizes, being 8mm and 9mm,

respectively. Quartz porphyry has a mean clast size of 31mm, but since quartz porphyry is also present in some of the local volcanic rocks, it is difficult to distinguish these from the Orange River derived quartz porphyry clasts. The mean clast size of the quartz porphyries compared to that of the more typical Orange River clasts would however suggest that most of the quartz porphyries are probably of local origin.

b) *Sand fraction*

The grey unit sand is moderately well-sorted, bimodal, shelly and medium to coarse grained (Fig. 3.16). Although there is no clear relationship between the mean grain size and the degree of sorting of the grey unit sand (Figs. 3.33 & 3.34), the sorting of the sand increases towards the northern part of the beach (Fig. 3.34). This again points to an increase in wave energy towards the northern end of the beach.

Grain morphology

a) *Gravel fraction*

The grain morphology of the locally derived clast lithologies described in a preceding section for the red unit also equally holds for the grey unit. However, the exotic clasts are only present in statistically significant numbers in the grey unit as indicated earlier. Banded ironstone formation clasts are mostly discoidal in shape, while the rest of the exotic clasts described earlier, are largely spherical.

b) *Sand fraction*

The grey unit sand grains also vary from being subrounded to very well rounded and are moderately spherical. Therefore the grey unit sand is probably slightly more texturally mature than that of the red unit, and also represent mixing of products of either different sources or energy levels. This further

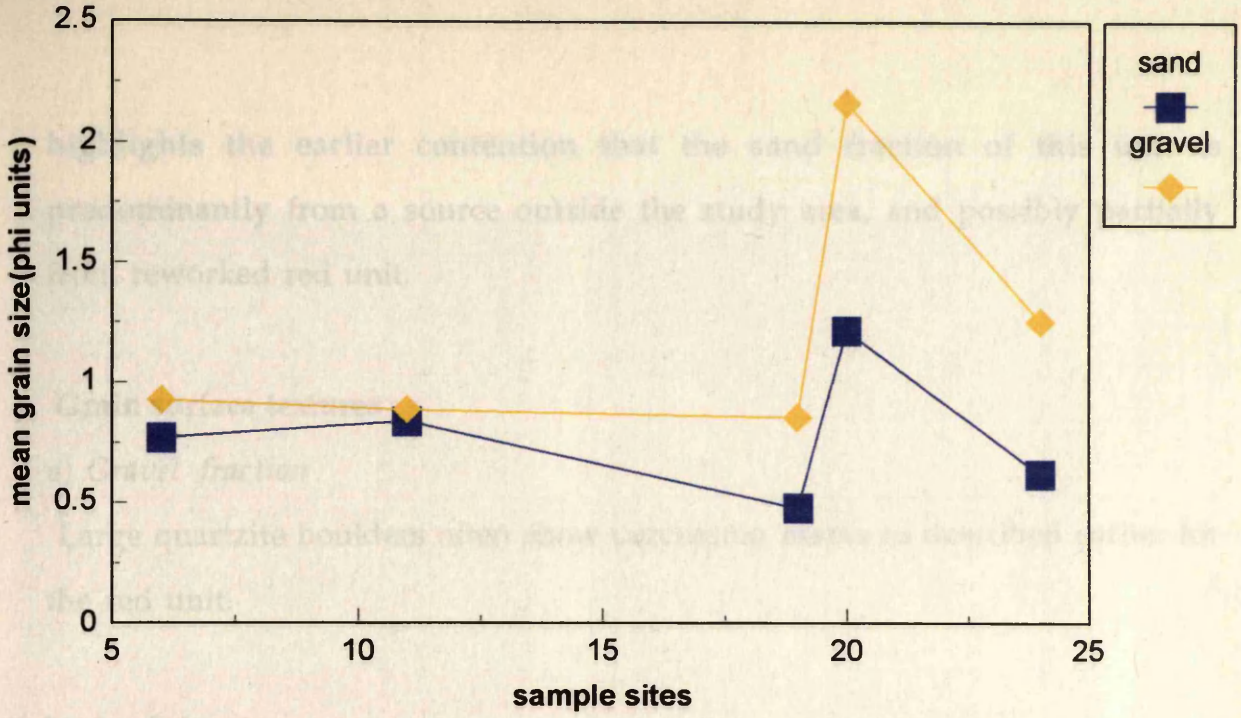

Fig. **3.33** The relationship between sample sites numbered from south(6) to north(24) and mean grain size for the grey unit within the study area(pocket beach no.4), Chameis.

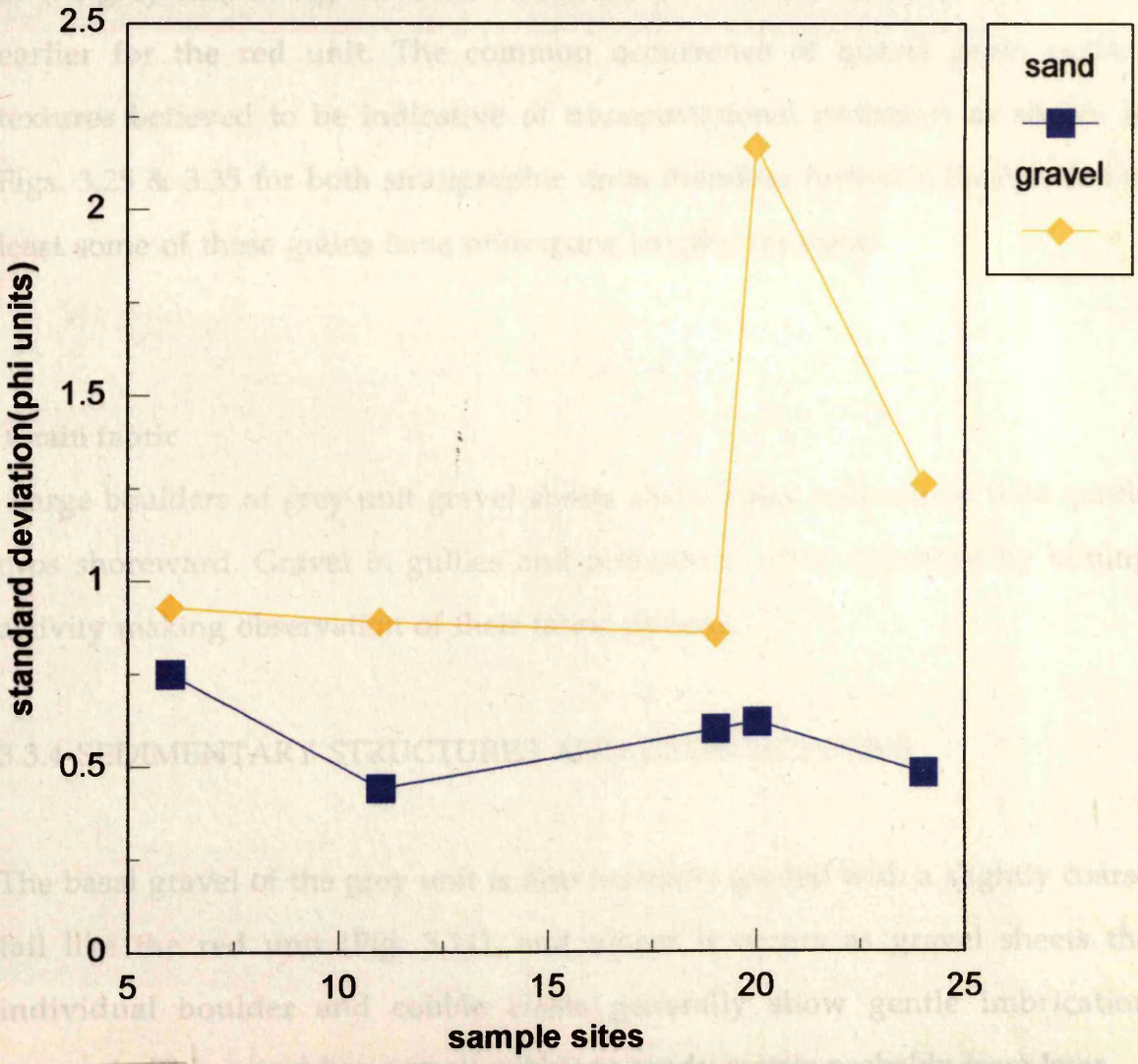

Fig. **3.34** The relationship between sample sites numbered from south(6) to north(24) and the standard deviation of grain size for the grey unit within the study area(pocket beach no.4), Chameis.

highlights the earlier contention that the sand fraction of this unit is predominantly from a source outside the study area, and possibly partially from reworked red unit.

Grain surface textures

a) *Gravel fraction*

Large quartzite boulders often show percussion marks as described earlier for the red unit.

b) *Sand fraction*

A comparison of the quartz grain surface textures shown in Fig. 3.25, with that of the grey unit in Fig. 3.35, shows similar surface textures as those reported earlier for the red unit. The common occurrence of quartz grain surface textures believed to be indicative of transportational processes as shown in Figs. 3.25 & 3.35 for both stratigraphic units therefore further indicates that at least some of these grains have undergone lengthy transport.

Grain fabric

Large boulders of grey unit gravel sheets also display imbrication with gentle dips shoreward. Gravel in gullies and potholes is often disturbed by mining activity making observation of their fabric difficult.

3.3.4 SEDIMENTARY STRUCTURES AND GROWTH FORMS

The basal gravel of the grey unit is also normally graded with a slightly coarse tail like the red unit (Fig. 3.11), and where it occurs as gravel sheets the individual boulder and cobble clasts generally show gentle imbrication seawards. This gravel has a small pebble to sandy matrix probably from later

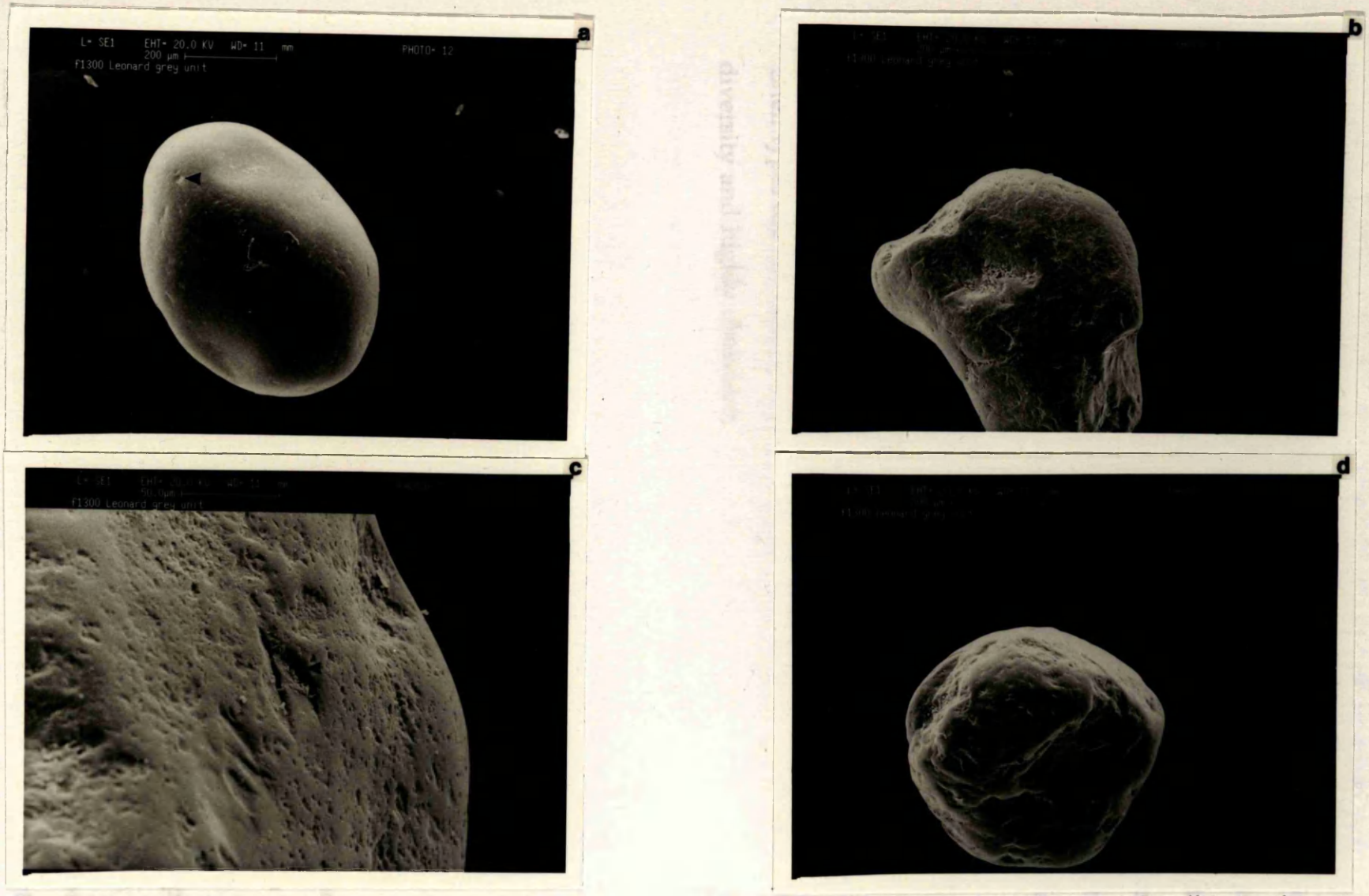

Fig. 3.35 Scanning electron microphotographs of the grey unit quartz grain surface textures. a) Small irregular pits on a well rounded grain with low relief. b) Curved scratches on subrounded grain with irregular outline. c)V's on grain with rounded outline. d) Oriented etch pits and V's on subrounded quartz grain. Again note the moderate relief in a-d.

infiltration by the overlying low-angle planar cross-stratified (also Fig. 3.2) seaward dipping alternating light and heavy mineral sand. The heavy mineral laminations merge landwards to form little heavy mineral placers. Sub-horizontal low to steep-angle landward dipping aeolian sand of alternating light and heavy mineral layers overlies the beach sand and its northwards orientation represent migration of the dunes as a result of the predominant north-northwesterly winds here (Figs. 3.3 & 3.4). Shell debris is most abundant in the bottom part of the grey gravel sequence, and again no bioturbation or ripple cross-stratification is discernable.

3.3.5 SHELL TYPES

Shell types are the same as those described for the red unit and are also of low diversity and highly abundant.

3.4 ACCRETION HISTORY OF BEACH

The Late Pleistocene to Holocene sea-level curve (Fig. 2.5) of Williams *et al.* (1981) is used to explain the evolution of the deposits in the study area as there are no known detailed sea-level curves for this period for the west coast of southern Africa. The following conceptual model is proposed to explain the accretion history of the red and grey unit deposits of the study area:

a) A rapid transgression occurred at c.130 000BP over a shore platform most likely to have already been in existence, for reasons discussed earlier, and accentuated during this transgression. Sea-level rose to about 3-6m (Fig. 3.37a).

Evidence for the age suggested comes from Corvinus (1983), maximum age of the *Donax serra* zone fossil, as well as the dating of a mammal fossil by Hendey and Cooke (1985) in similar elevation raised terraces along the west coast of South Africa. The c. 130 000BP highstand at 2-9m is also well known from many parts of the world and is a widely used Late Pleistocene datum (Williams, *et al.*, 1981).

b) This transgression was then followed by a major regression at c. 120 000BP until c. 20 000BP with interludes of minor transgressions each followed by a regression in between at about 103 000BP; 82 000BP; 60000BP; and 40 000BP (Fig. 3.37b). Radiometric dating of shell material collected from the red unit, using the ^{14}C method yielded an age of 25 690 ± 100 yrs BP (& ^{13}C - + 1.8%O) for sample analysis number Pta-6885. This age, which must be considered as a minimum age, suggests that the progradational Eemian red unit deposits were laid down during the later stages of this sea-level lowstand. Sediment supply would have been less abundant at this stage as the sources supplying the sediment would have been flushed clean. This may, at least partially, explain the relative scarcity of Orange River derived exotic clasts in the red unit.

c) The minor Late Quaternary transgressions mentioned above probably terminated the red unit depositional event. They were characterized intermittently by low sediment supply and increased shoreface erosion as a result of dryer periods (Imbrie, 1985). It is during this huge hiatus, in terms of marine deposition, that the red unit was subaerially exposed and reddened by oxidation. Although red colour due to iron staining is reported to also occur under subaqueous conditions, the presence of calcareous nodules towards the top contact of the red unit undoubtedly attests to incipient pedogenesis resulting from subaerial exposure (Figs. 3.36 & 3.37c). The pedotubules become progressively more weakly developed away from the top of the red unit

Fig. 3.36 **Red unit** sand, underlying **grey unit** sand at site 23, displays weak calcareous mottling and pedotubule formation. No bioturbation recognized. Scale 10cm.

succession (Fig. 3.36). Extensive floods generated large amounts of angular vein quartz and other terrestrial detritus (sheetwash) from the immediate hinterland and deposited them above the red unit deposits along a sharp erosional contact (Fig. 3.5). It is the sheetwash material that planed off the red unit to leave only a thin veneer below it on the landward side, except in areas where gullies and potholes prevented the red unit from being eroded (Fig. 3.5).

d) Holocene transgression (Fig. 3.37d) followed at c. 20 000 BP until c. 5 000BP during which most authors believe, there was a noticable and significant drop in the rate of sea-level rise (Davis and Clifton, 1987). It is inferred from the stratigraphic record that sea-level would have risen to about 3m above present level. The westward portion of the red unit was completely scoured out during this transgression (Fig. 3.37d). The eastward portion of the red unit was either protected by the sheetwash cover or was partially beyond the reach of this transgression and is therefore preferrentially preserved both in gullies as well as in some planated areas. The grey Holocene sediments of the grey unit contrasts greatly with the very apparent mottling and oxidation (red) of the Eemian red unit deposits as was shown earlier in Fig. 3.16.

e) A minor regression followed at c. 5 000BP during which the subtidal grey unit deposits overlain by recent beach sediments prograded over a thin basal transgressive basal lag gravel left by the preceeding transgression (Fig. 3.37e). ^{14}C dating of shell material from the grey unit yielded an age of 4850 ± 20 yrs BP (&^{13}C - 0 + 1.0%O) for sample analysis number Pta-6893. During this regression the more landward grey unit was overlain by a sheetwash sandwiched between the Holocene beach sediments (also Fig. 3.37e). As hinted earlier in the text, there is no noticable stratigraphic break between the grey unit sediments and the modern beach sediment. Therefore it is not clear whether the more recent marine sediments were part of the same regression

event ot postdated them.

f) Northward migrating dunes under the influence of the dominant south-southwesterly winds sweeping the beach as a consequence of the above regression then formed, and overlie the modern beach (Fig. 3.37f).

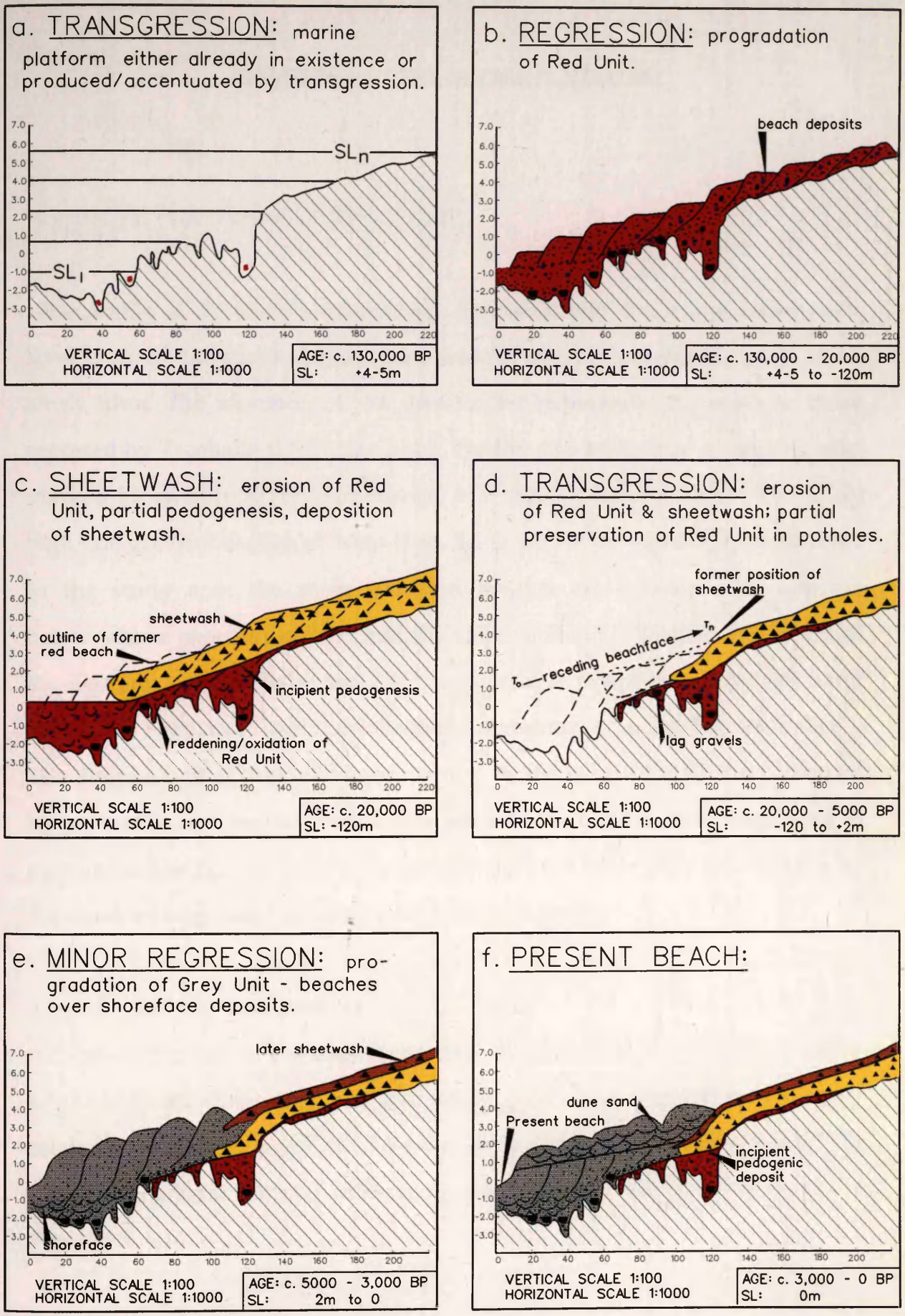

Fig. **3.37** Proposed accretion history of the grey and red unit deposits within the study area (pocket beach no.4), Chameis. SL_1 =sea level 1; SL_n =final sea level; T_o =time and T_n =final time.

CHAPTER 4 THE SHORE PLATFORM

4.1 SHORE PLATFORM MORPHOLOGY

The profile of the shore platform from approximately -2m below present sea-level to as far eastwards as practicable was surveyed across various parts of the study area. The elements of the profiles are essentially the same as those reported by Trenhaile (1987) for Gaspé, Quebec and include: a) a seaward edge marked by an abrupt gradient change; b) a gentle platform; and c) an abrupt high tide gradient change or ramp (Figs. 4.1 & 4.2). In the exposed bedrock areas in the study area the shore platform heights are between -2m and 6m below/above present sea-level and the slope is about 1:30m/m. The width of the platform is up to 300m and reaches its greatest extent just south and north of the two headlands within the sheltered embayment, pocket beach number 4. The morphology of the submerged, as well as, the part of the platform covered by terrestrial and aeolian sediment is not known. Drilling data were used to gain an insight into the coastal topography between those areas not exposed by diamond mining, and the Late Cretaceous escarpment.

Gullies (furrows) and potholes

Gullies and potholes are important traps for diamonds and associated heavy minerals in the study area and their development and orientation is strongly related to either the strike of schistosity or the directions of major joints. The common erosional features on shore platforms in the study area are shown in Figs. 4.3 to 4.10.

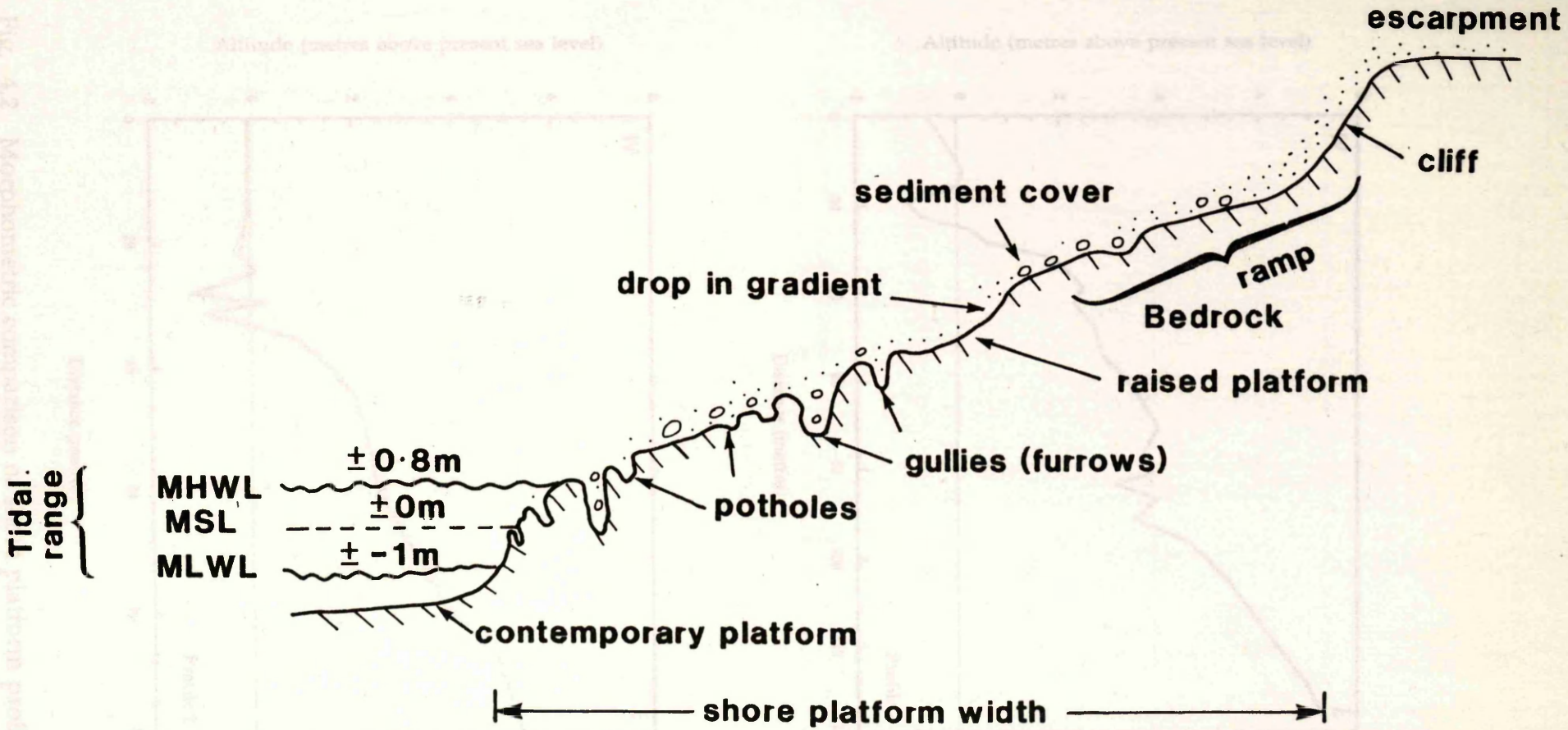

Fig. 4.1 Schematic representation of some of the important elements of shore platform morphology.

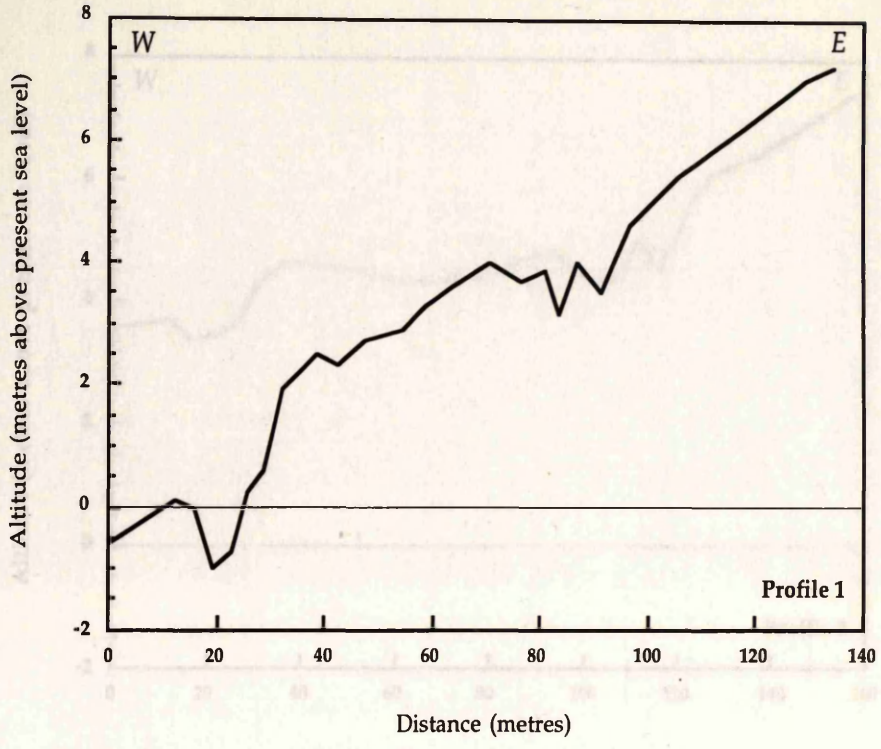

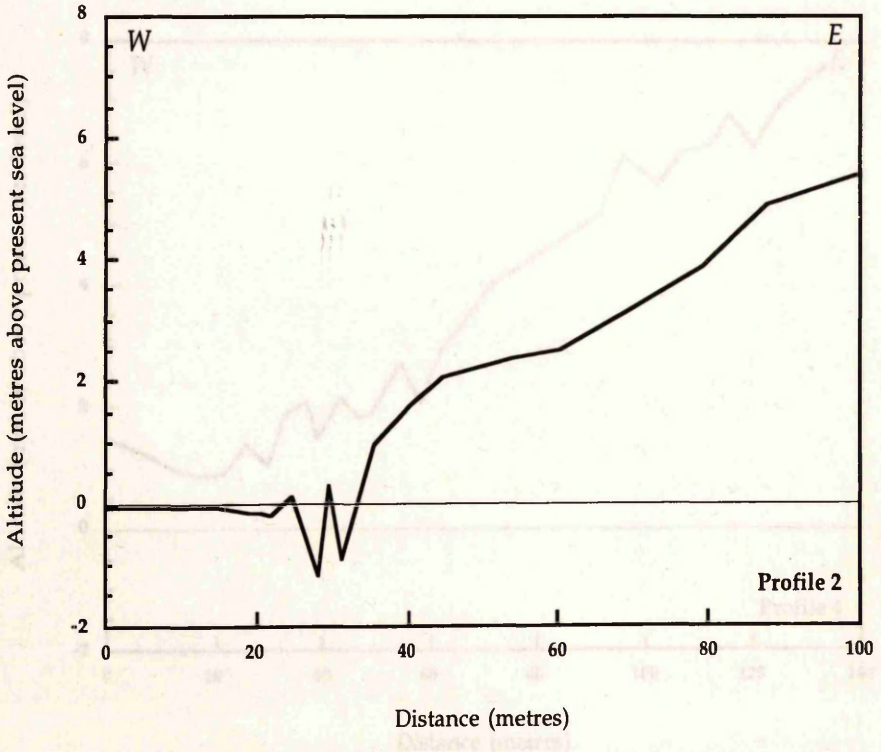

Fig. 4.2 Morphometric comparison of shore platform profiles (1-4) from different sites within the study area. Localities of profiles surveyed are shown in Fig. 4.12.

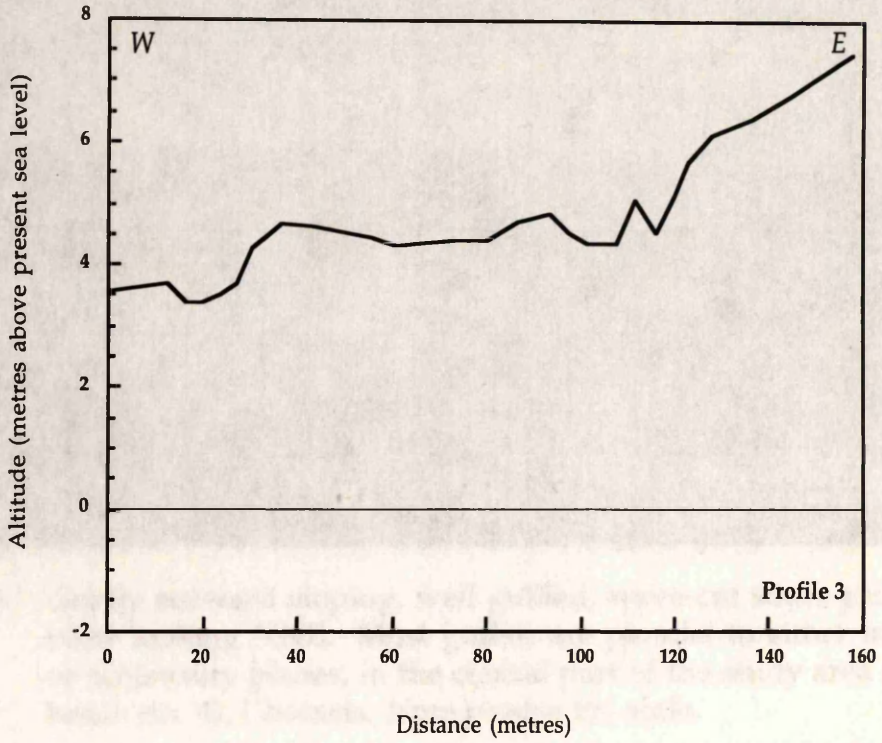
W
E
8
6
4
2
0
-2
Altitude (metres above present sea level)
Profile 3
0
20
40
60
80
100
120
140
160
Distance (metres)

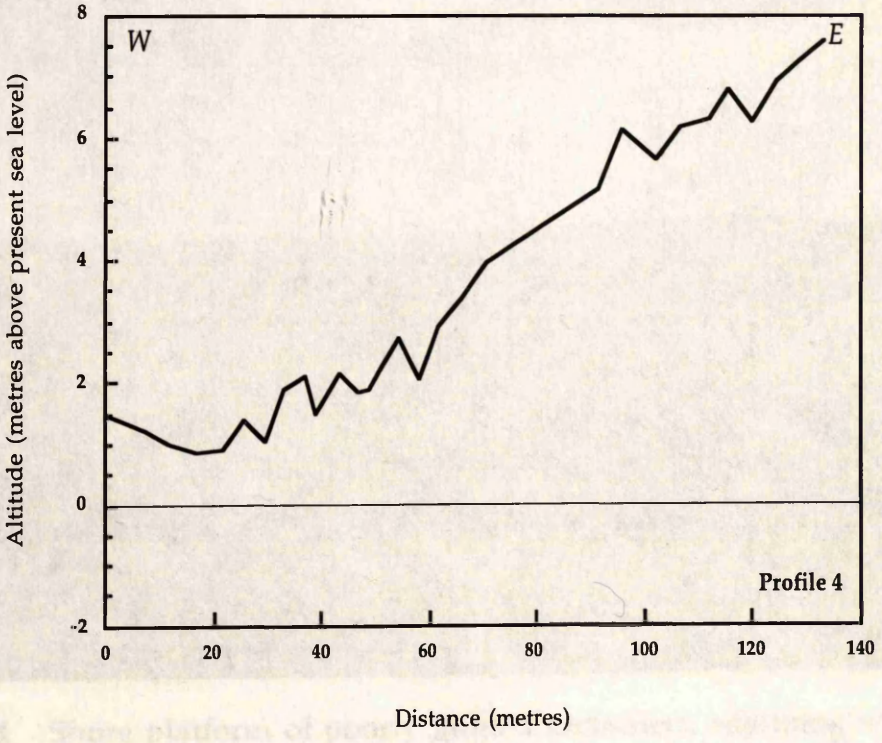
W
E
8
6
4
2
0
-2
Altitude (metres above present sea level)
Profile 4
0
20
40
60
80
100
120
140
Distance (metres)

Fig. 4.3 Gently seaward sloping, well gullied, wave-cut shore platform, with view looking NNE. Most gullies are parallel to either major joints or schistosity planes, in the central part of the study area (pocket beach no. 4), Chameis. Note people for scale.

Fig. 4.4 Shore platform of poorly gullied metachert, adjoining well gullied area of metagreywacke shown in Fig. 4.3, in the central part of study area (pocket beach no. 4), Chameis. Contact (dotted), view looking north. Note person for scale.

Fig. 4.3 Gently seaward sloping, well gullied, wave-cut shore platform, with view looking NNE. Most gullies are parallel to either major joints or schistosity planes, in the central part of the study area (pocket beach no. 4), Chameis. Note people for scale.

Fig. 4.4 Shore platform of poorly gullied metachert, adjoining well gullied area of metagreywacke shown in Fig. 4.3, in the central part of study area (pocket beach no. 4), Chameis. Contact (dotted), view looking north. Note person for scale.

Gullies

Gullies are longitudinal furrows of variable length and depth resulting from the vertical abrasion of the shore platform by waves (Figs. 4.5 to 4.7). Gullies often result from the coalescence of a series of adjoining potholes (Wright, 1964), with the most pronounced gullies being those that develop along joint planes in the more resistant lithologies (Fig. 4.7). However when the bedrock is homogeneous, highly resistant and with very few structural weaknesses, almost no gullies result as can be seen for the metachert in Fig. 4.4. The gullies in the study area are 3-4m deep and 1-3m wide, while the schistosity aligned gullies are usually smaller. Most of these gullies contain large clasts (up to cobble and boulder size) at their bottom, which would have acted as abrasives (Fig. 4.6).

Potholes

Sunamura (1992) defines marine potholes as usually roughly circular in outline, cylindrical or bowl-shaped depresssions formed on the shore platform by the grinding action of sand and gravel moved or rotated by wave turbulence (Figs. 4.8 to 4.10). He argues that where potholes are irregular in outline, they reflect either the adjoining of neighbouring depressions or differences in rock resistance. Potholes in the study area range from < 3 cm in diameter and depth (Fig. 4.9), to 18m in diameter and 2.5m in depth (Fig. 4.8), and their development is thought to be initiated by the presence of depressions which act as loci for the abrasive material (Sunamura, 1992). Many potholes seemingly form at the intersection of conjugate joint sets and are compatible with similar patterns reported for shore platforms south of Chameis by Tacier (1967).

Shore platform profiles from different parts of the study area are shown in Fig. 4.2, and clearly show composites of several levels although the general

Fig. 4.5 Joint-aligned gullies against break-in-slope with smooth wave-cut platform in the foreground. Gullies are approximately 1.5m deep, site 14.

Fig. 4.6 Gully, ±1.5m deep with well rounded clasts (abrasives) on the shore platform in the foreground, at site 18.

Fig. 4.7 Deep, steep-sided joint gully in poorly foliated metagreywacke. Person 1.8m high.

Fig. 4.8 Large circular pothole filled with **red unit** gravel, ± 18m wide and 2.5m deep at site 18. Also note oversize clasts (mostly quartzite) on gully floor. Scale 150cm.

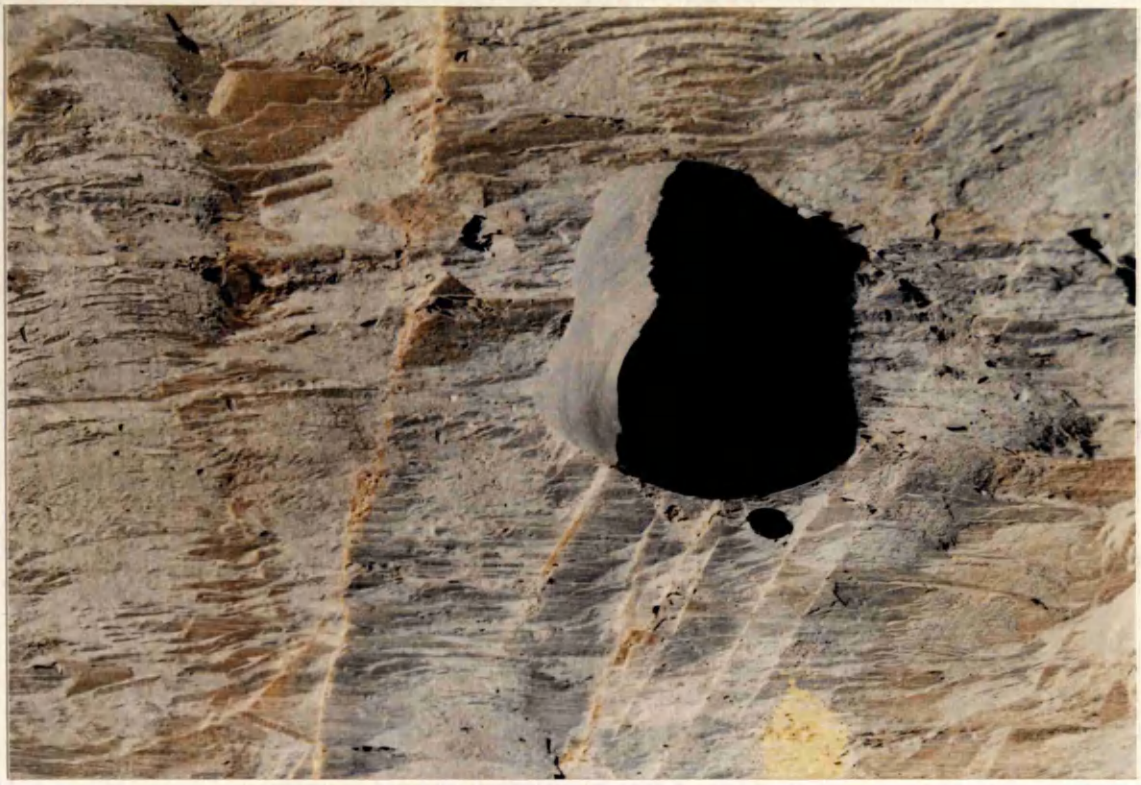

Fig. 4.9 Pothole developed in well jointed metagreywacke at site 18. Lens cap for scale (diameter = 5.5cm)

Fig. 4.10 Pothole in competent metagreywacke at site 15. Scale 50cm.

platform is included seaward. In explaining the general morphology of the shore platforms, the following parameters are thought to be the most important (Fig. 4.11, numbers 1a to 5c) (for any parameter considered the remaining parameters are assumed to be constant):

1) *Bedrock geology*

a) Lithology: uniform hard rock platforms will cut more slowly than soft platforms.

b) Structure: wave abrasion and quarrying will be more effective in well jointed and bedded rock platforms.

2) *Nature and rate of sea-level change*

a) Very rapid sea-level rise: produce original or near original platform profile.

b) Rapid sea-level rise: original platform profile inherited because wave erosion is less efficient as a result of rapid sea-level rise.

c) Slow sea-level rise: waves have more time to cut platform more effectively.

d) Change in rates of sea-level rise: parts of the platform where the rate of sea-level rise is relatively slower will be cut more efficiently than those areas where it is more rapid.

3) *Wave energy* (see Chapter 2 for wave parameters)

a) Wave intensity: cutting of shore platform increases with higher wave intensity.

b) Wave period: long period waves will be more effective in cutting the platform.

4) *Tidal range*

Widest intertidal platforms are formed by large tidal ranges, but depend on rise/fall of sea-level.

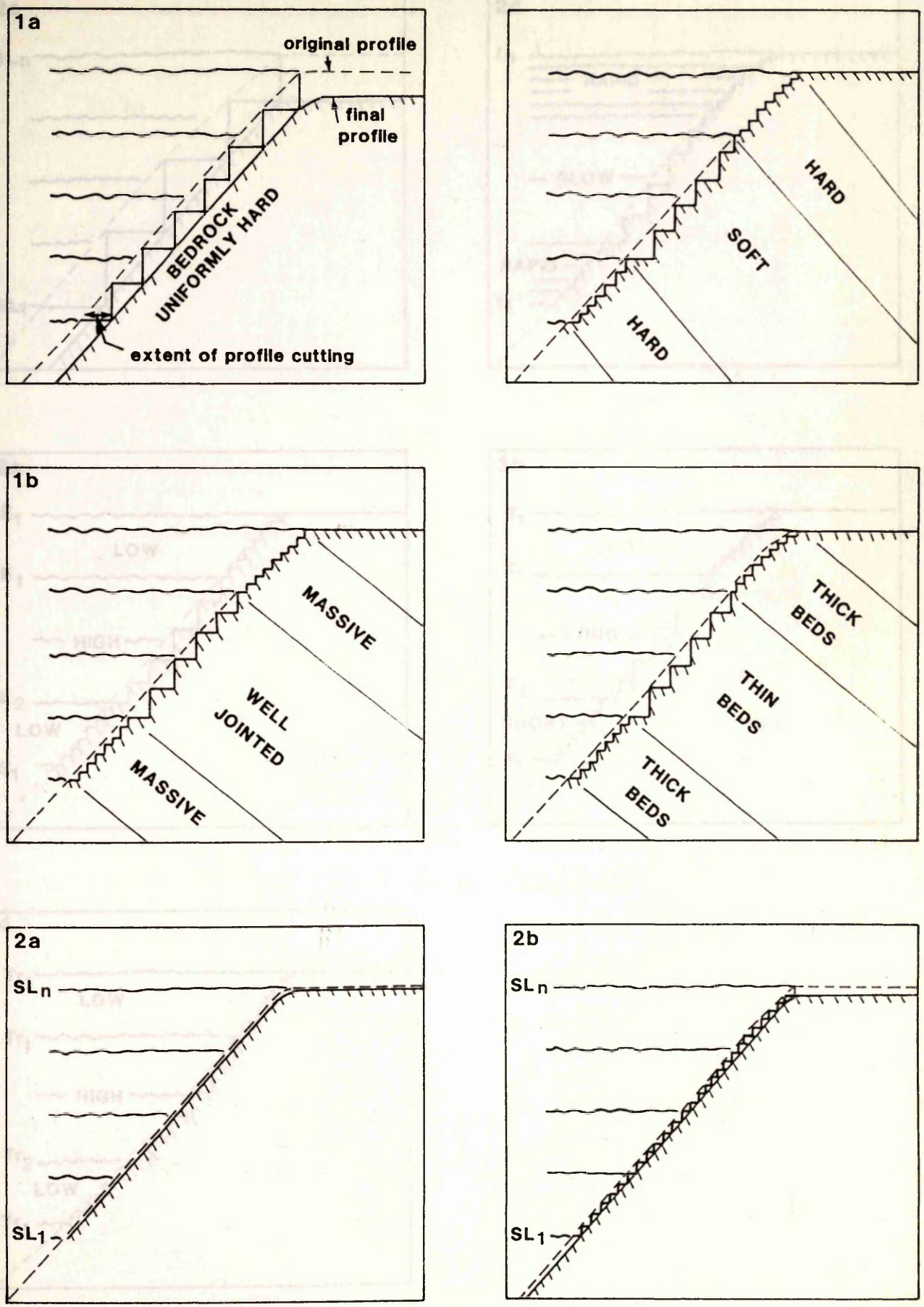

Fig. 4.11 Schematic representation of some of the important factors influencing shore platform morphology.

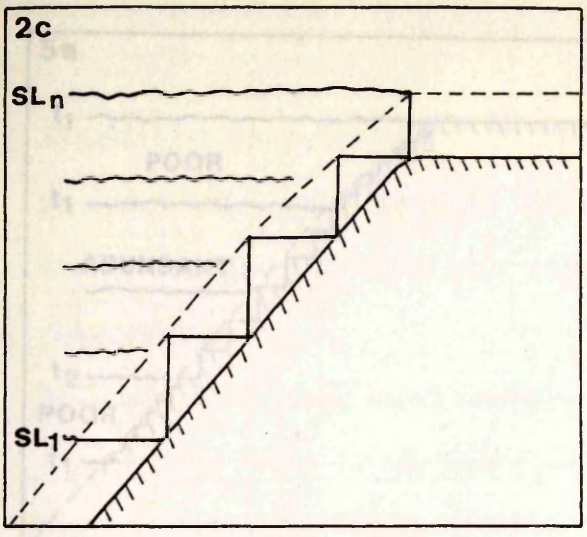
2c
SLn
SL1

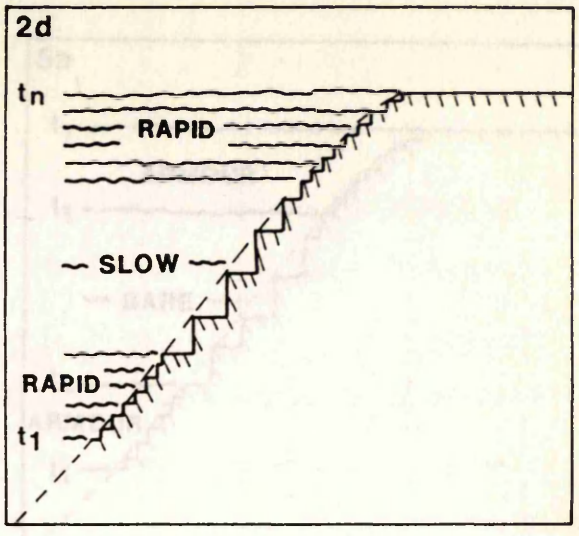
2d
tn
RAPID
SLOW
RAPID
t1

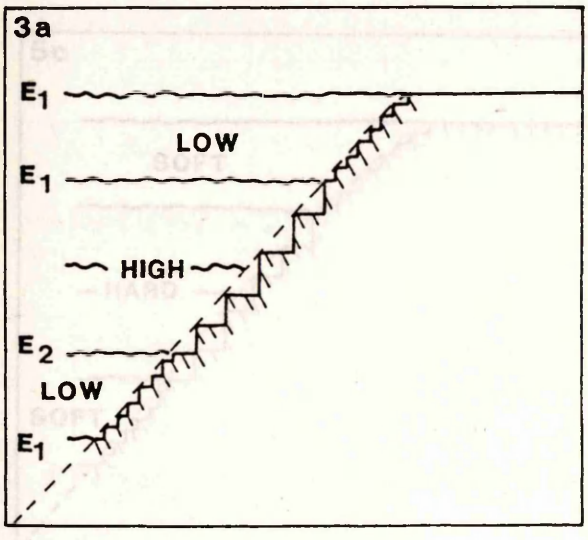
3a
E1
LOW
E1
HIGH
E2
LOW
E1

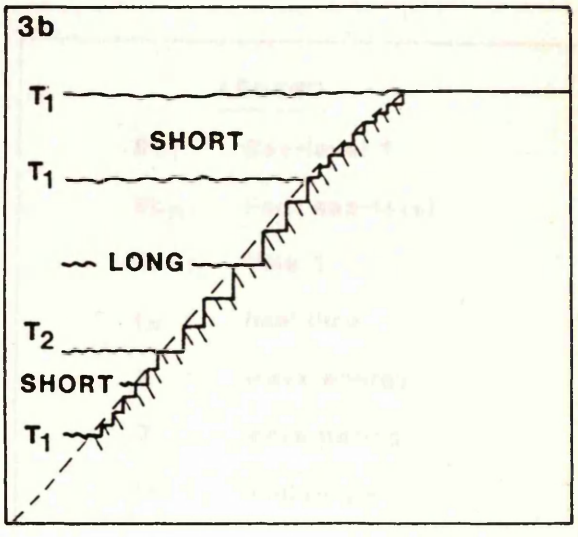
3b
T1
SHORT
T1
LONG
T2
SHORT
T1

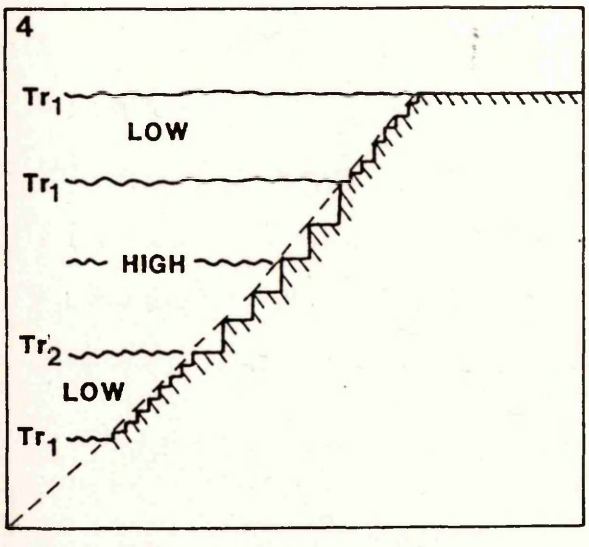
4
Tr1
LOW
Tr1
HIGH
Tr2
LOW
Tr1

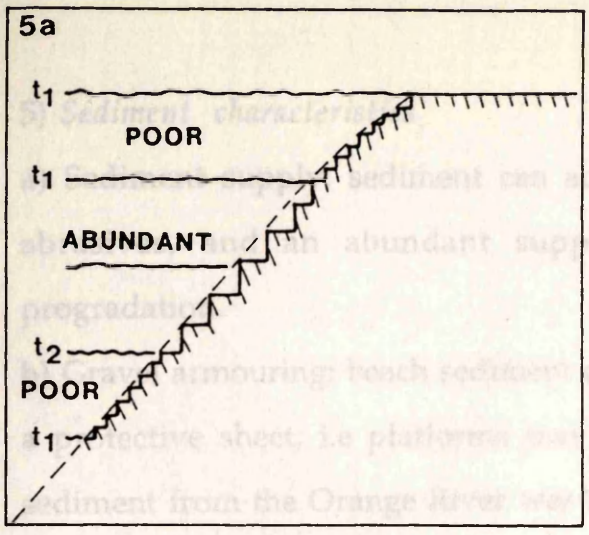

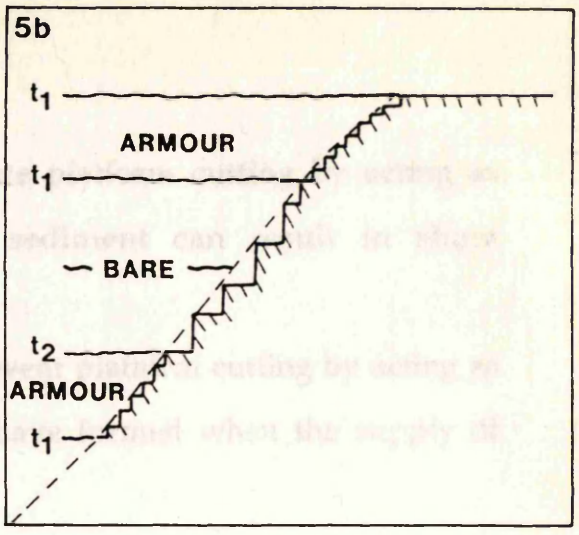

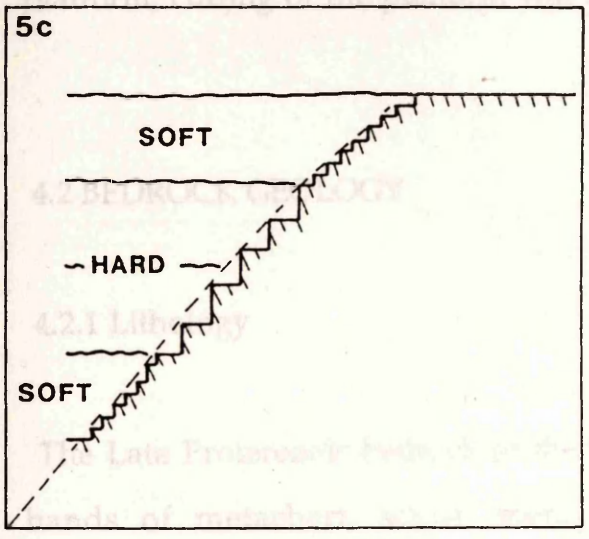

LEGEND

SL_1	:	Sea-level 1
SL_n	:	Final sea-level
t_1	:	time 1
t_n	:	final time
E	:	wave energy
T	:	wave period
Tr	:	tidal range

5) *Sediment characteristics*

a) Sediment supply: sediment can accentuate platform cutting by acting as abrasives, and an abundant supply of sediment can result in shore progradation.

b) Gravel armouring: beach sediment can prevent platform cutting by acting as a protective sheet, i.e platforms may only have formed when the supply of sediment from the Orange River was small.

c) Type of abrasive material: when the abrasive material is harder than the platform, cutting of the platform will be more effective.

4.2 BEDROCK GEOLOGY

4.2.1 Lithology

The Late Proterozoic bedrock of the Chameis Complex consists of alternating bands of metachert, schist, metagreywacke and phyllite (Frimmel and Hartnady, 1992; this study) (Fig. 4.12). Frimmel and Hartnady (1992) interpreted the Chameis Complex as a heterogeneous melange zone, i.e a highly tectonized, diverse metasedimentary envelope. This highly variable bedrock lithology and structure amongst others, would have either been responsible for or accentuated the formation of pocket beaches along this part of the Sperrgebiet coastline. The softer bands would have been eroded to form the embayments, while the more resistant lithologies form the headlands.

4.2.2 Petrographic description

The rock names used for the mineral descriptions here are largely adopted

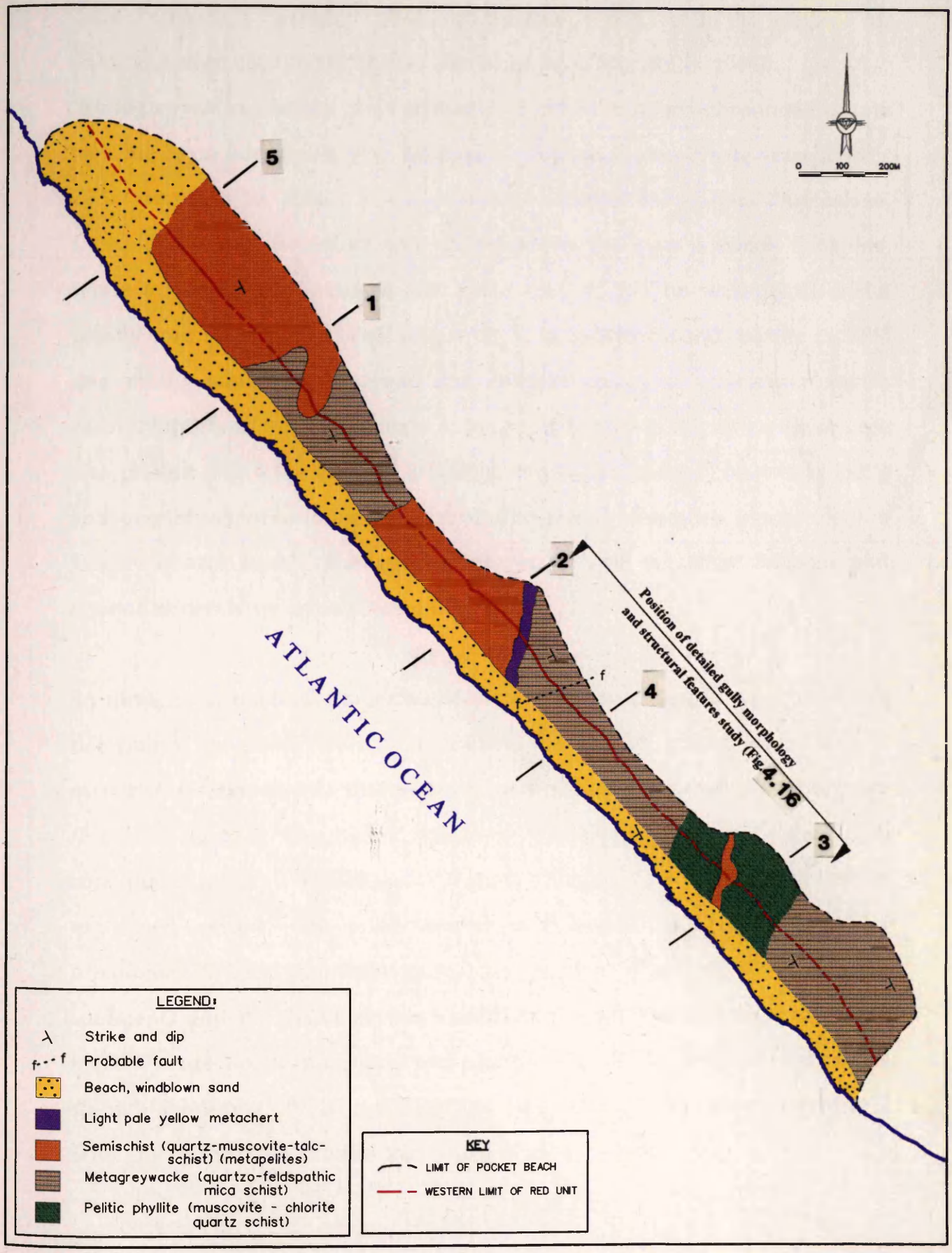

Fig. 4.12 Simplified geological map of the bedrock (Late Proterozoic) of study area (pocket beach no. 4) Chameis.

NAMDEB

from Frimmel & Hartnady (1992) and Frimmel (1995), while the symbols for mineral names used in the figures are taken from Miyashiro (1994).

Metagreywacke consists predominantly of polycrystalline subrounded quartz (± 60%), often intergrown with feldspar (± 15%), and subordinate muscovite (± 10%) occuring as flakes along preferred orientation planes. Plagioclase, microcline (tartan twinning) and orthoclase are the most common feldspars, while minor opaque minerals also occur (Fig. 4.13). The semi-pelitic **schist** mostly consists of polycrystalline quartz (50%), muscovite and chlorite (± 30%) and minor feldspar. Muscovite and chlorite are often intergrown which possibly indicates a slight increase in metamorphic grade. Opaque minerals are also present (Fig. 4.14). **Phyllite** is finer grained with abundant muscovite (60%) and possibly chlorite flakes along multidirectional orientation planes set in a largely quartz matrix. Subordinate biotite, as well as, minor feldspar and opaque minerals are again present (Fig. 4.15).

Although the physical properties of these dominant bedrock types were not determined quantitatively it is undoubtedly the much greater abundance of quartz in metagreywacke that makes it more resistant than schist and phyllite (Figs. 4.13 to 4.15). This higher resistance of metagreywacke as a result of its constituent minerals would make it more susceptable to intense jointing as explained earlier. The joints are then exploited, depending on their orientation, to form prominent gullies and potholes (Fig. 4.16) which trap the sediments and the diamonds associated with them. The less resistant rocks, mostly made up of muscovite and chlorite (Fig. 4.15), are planated into a smooth shore platform as can clearly be seen from a comparison of Profile 3, with any of the other profiles from areas of more resistant rock.

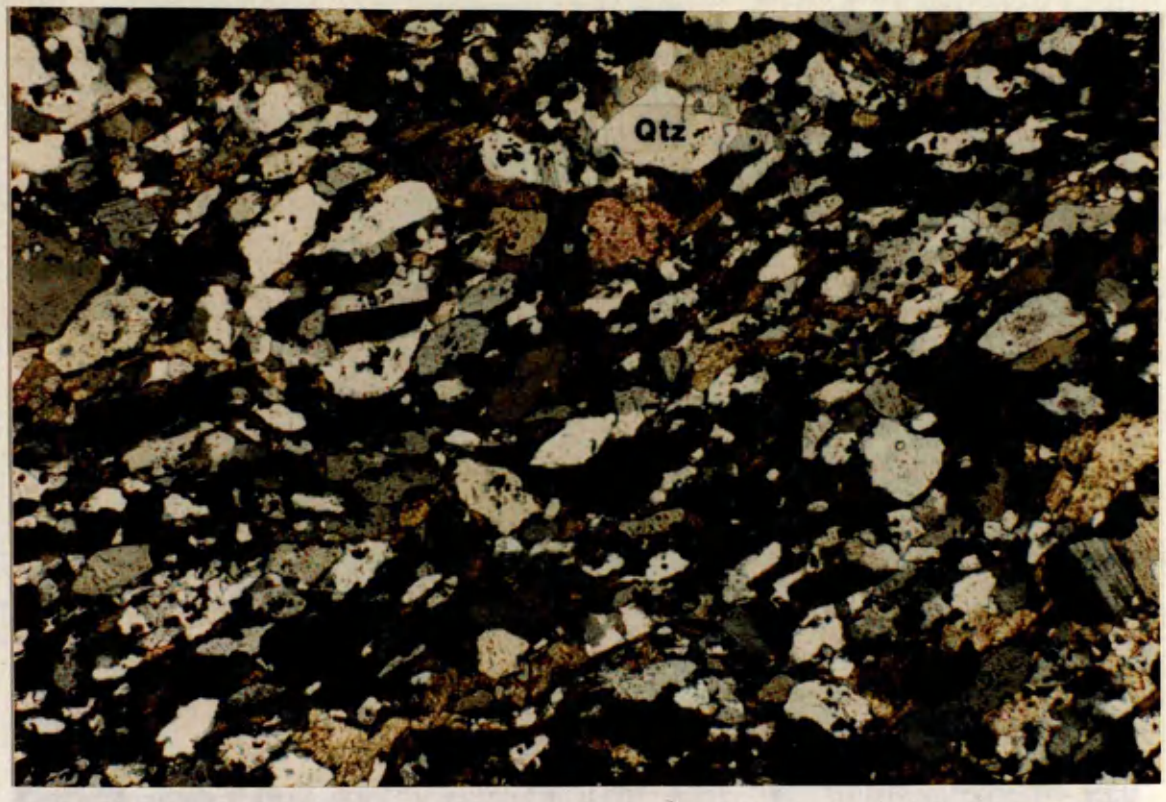

Fig. 4.13 Photomicrograph of metagreywacke predominantly made up of quartz (Qtz), K-feldspar (Kfs) and muscovite (Ms). Crossed polars. Magnification (x2.5).

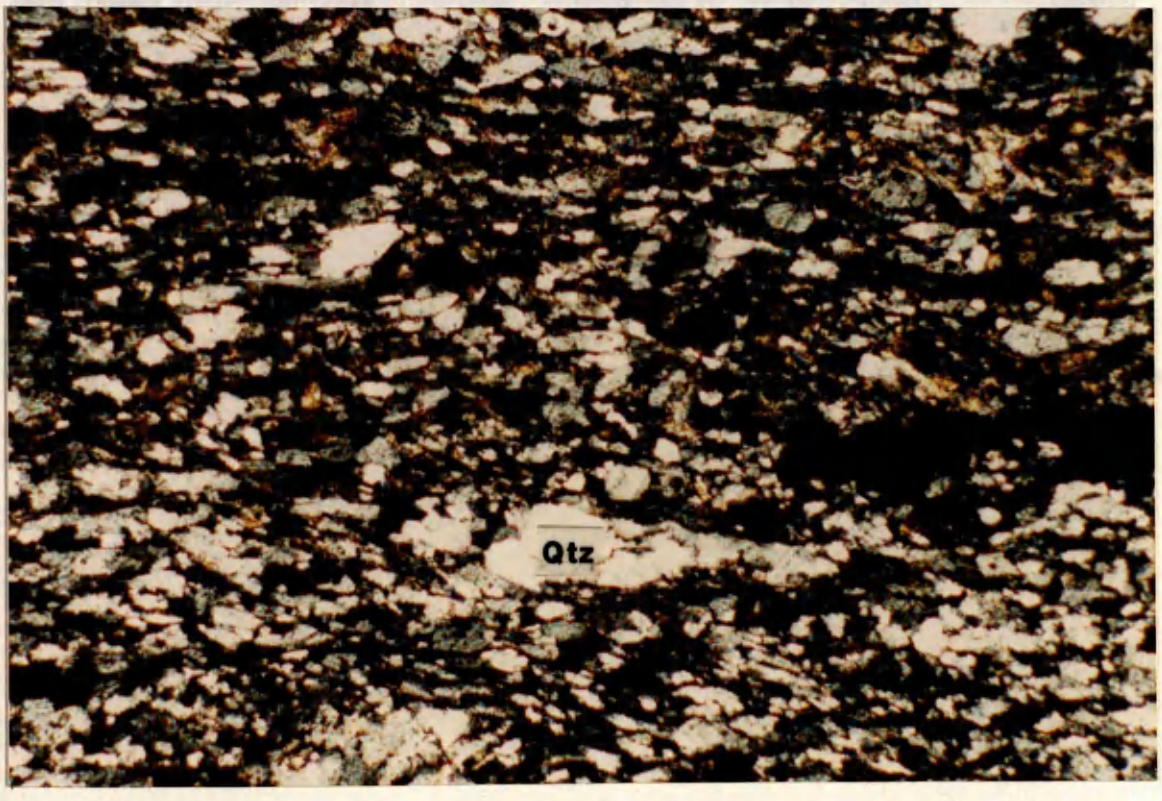

Fig. 4.14 Photomicrograph of semi-pelitic schist which mostly consists of quartz (Qtz), muscovite (Ms) and K-feldspar (Kfs). Crossed polars. Magnification (x2.5).

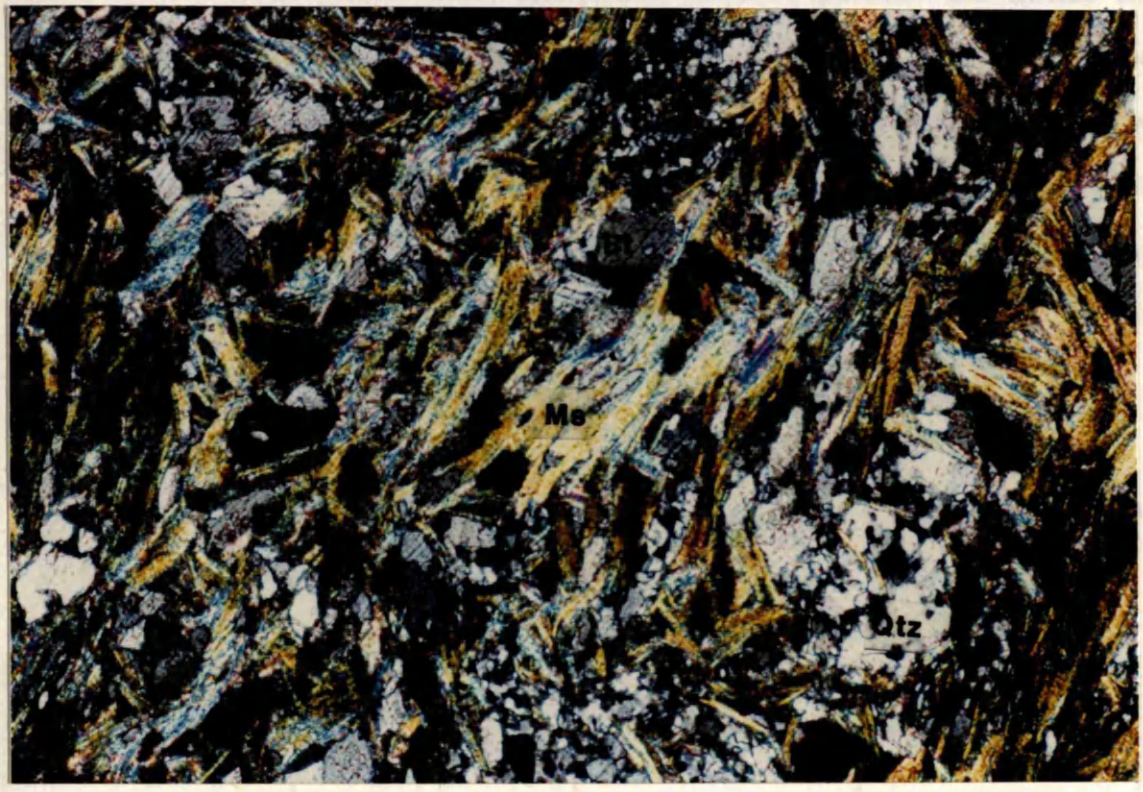

Fig. 4.15 Photomicrograph of micaceous phyllite, made up of muscovite (Ms) and chlorite (Chl) flakes showing multidirectional mineral growth probably as a result of polyphase deformation. Quartz (Qtz) and minor biotite (Bt) are also present. Crossed polars. Magnification (x2.5).

4.2.3 Structure

The strike of bedrock schistosity in the study area trends between 360° and 10°, and the bedrock dip angle is 65° towards the west (Fig. 4.16). The major joint directions in a section of the study area are shown in Fig. 4.16. The joints are generally more dense in the more resistant lithologies and their spacing varies between 25cm and 1m. Other structural features present are minor folds (mostly kink bands) and small faults. Bedrock varies from being of poor schistosity in the largely homogeneous metagreywacke and metachert to a well defined schistosity in the less resistant schist and phyllite. Preferential weathering caused the more resistant lithologies to stand proud as ridges whilst the weaker intervening beds form depressions, giving the shore platform alternating rough and smooth surfaces (see Table 4.1 and Fig. 4.17).

Table: 4.1 Platform spot elevations (metres above mean sea-level) within a section of the study area (as marked in Fig. 4.12).

ELEVATION	FREQUENCY	PERCENTAGE	CUMULATIVE %
< -4.00	0	0.00	0.00
-4.00 to -2.00	6	0.33	0.33
-2.00 to 0.00	424	23.06	23.39
0.00 to 2.00	856	46.55	69.94
2.00 to 4.00	449	24.41	94.35
4.00 to 6.00	93	5.06	99.41
6.00 to 8.00	11	0.60	100

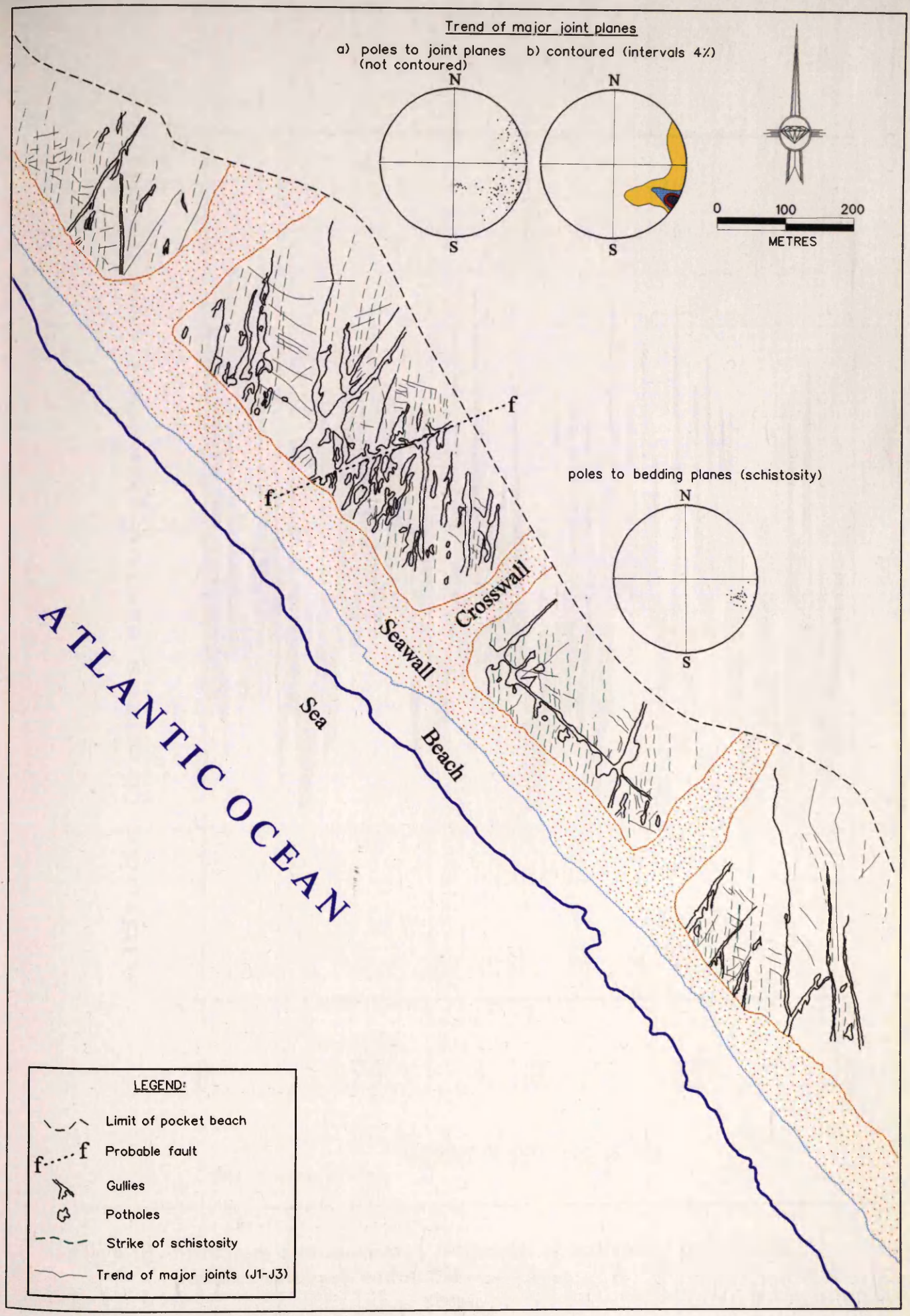

Fig. **4.16** Bedrock morphology map showing orientation of gullies and structural features within a section of the study area (pocket beach no. 4), Chameis. Compiled from vertical aerial photomosaics. Also shown are lower hemisphere equal area stereographic projections.

NAMDEB

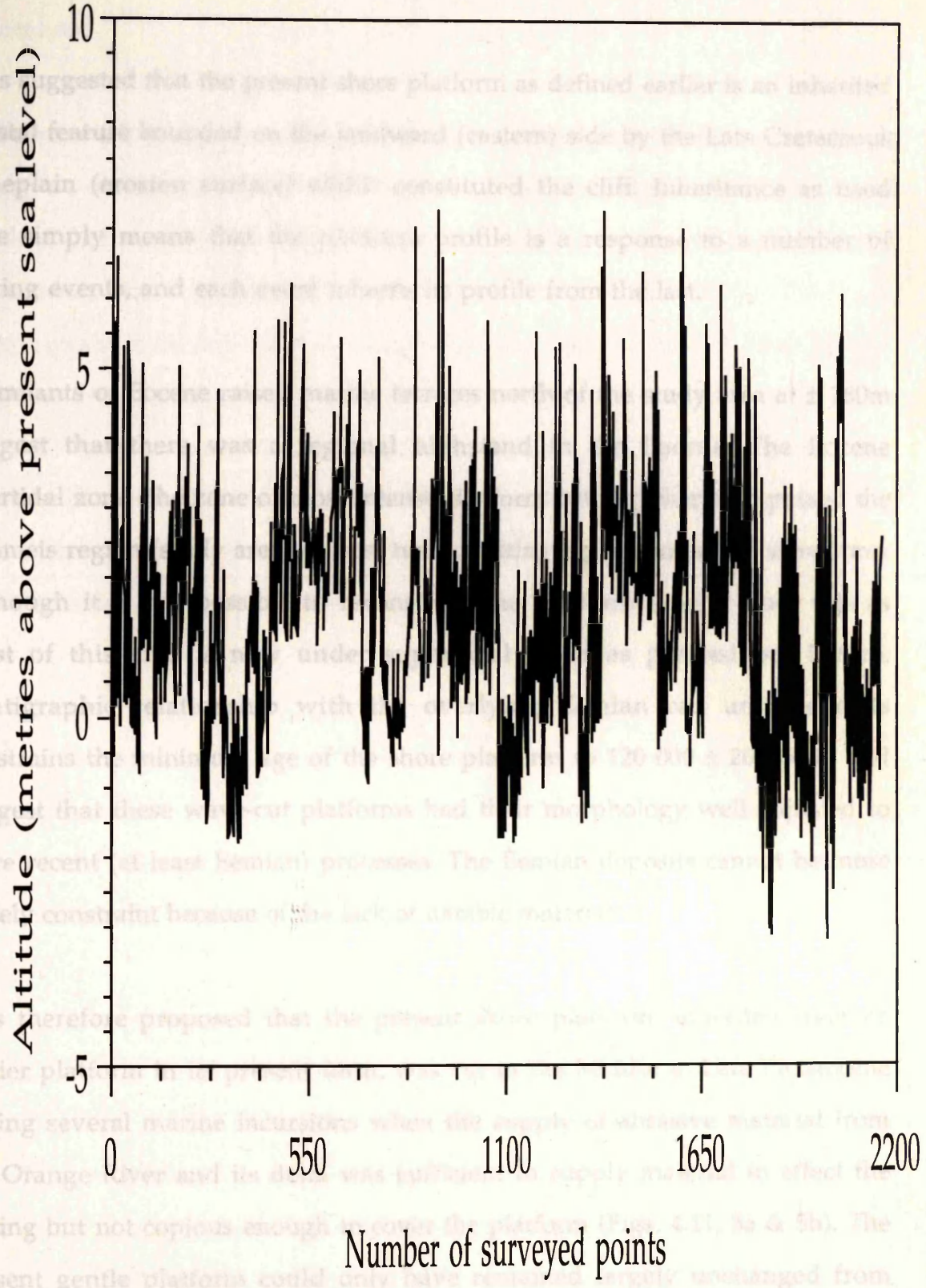

Fig. 4.17 Minimum and maximum elevations of individual gullies and potholes surveyed within the study area.

4.3 DEVELOPMENT OF THE SHORE PLATFORM

It is suggested that the present shore platform as defined earlier is an inherited coastal feature bounded on the landward (eastern) side by the Late Cretaceous peneplain (erosion surface) which constituted the cliff. Inheritance as used here simply means that the platform profile is a response to a number of cutting events, and each event inherits its profile from the last.

Remnants of Eocene raised marine terraces north of the study area at ± 160m suggest that there was a regional highstand in the Eocene. The Eocene intertidal zone (the zone of most intense platform cutting) therefore passed the Chameis region (study area) at least twice, cutting a platform at the same time. Although it is not possible to reconstruct the platform arising from this as most of this area is now under superficial cover as pointed out before. Stratigraphic relationship with the overlying Eemian red unit deposits constrains the minimum age of the shore platform to 120 000 ± 20 000BP and suggest that these wave-cut platforms had their morphology well adjusted to more recent (at least Eemian) processes. The Eemian deposits cannot be more closely constraint because of the lack of datable material.

It is therefore proposed that the present shore platform, inherited from an earlier platform in its present form, was cut in the Middle to Late Pleistocene during several marine incursions when the supply of abrasive material from the Orange River and its delta was sufficient to supply material to effect the cutting but not copious enough to cover the platform (Figs. 4.11, 5a & 5b). The present gentle platform could only have remained largely unchanged from some previous cycle if a rapid rise in sea-level without significant erosion of the platform (Fig. 4.11, 2a & 2b) is invoked or if the bedrock was highly resistant (Fig. 4.11, 1a). This is supported by Trenhaile (1987) who argues that

there is a general lack of evidence indicating long stillstands during the Pleistocene.

Alternatively the interruptions or gradient changes described earlier, in an otherwise continuously inclined shore platform planation surface, may have resulted from subsequent dissection and denudation controlled by structural weaknesses (Fig. 4.11, 1b) during more recent times (Miller, 1939b). This may have happened during the major regression (± 120m) of the c. 0.2 Ma Glacial maxima. The steadily falling elevation of intertidal red unit facies westwards (Fig. 3.5) is indicative of a regressive sea-level. This is however unlikely as not enough time would have been left after the cutting of these interruptions to concentrate diamonds in significant quantities during the accretion of the red unit deposits.

CHAPTER 5 DIAMONDS

INTRODUCTION

This chapter considers the spatial distribution of diamond concentration and the frequencies of occurrence of selected general characteristics of diamonds from the two stratigraphic units in the Chameis area. In addition, surface and abrasion features of the diamonds were determined. All these data are summarized in a series of pictorial illustrations and diagrams (Figs. 5.1 to 5.46). The main aim of this work is to evaluate whether any local differences in the distribution of diamond characteristics can be linked to variations of sediment texture, morphology and fabric. Such an approach may help then to explain the sedimentary processes that controlled the spatial arrangement of these parameters. Diamonds are therefore examined for 'fingerprints' that may have been left on them with regard to their source and subsequent sedimentary transport history. The diamond classification scheme of Robinson (1979) is used as a basis for this study and all the terminology related to the description of the diamonds is largely derived from this scheme.

5.1 GENERAL DISPERSAL PATTERNS

Fig. 5.1 shows the relative concentration of diamonds in the study area. The available evidence clearly shows that diamond concentrations are highest in the northern end of the pocket beach. This observation most probably reflects the higher energy conditions to the northern end of the beach which is related to sedimentary trends reported in Chapter 3. For example such trends as: a) maximum clast size; b) better sorting, and c) the greater abundance of higher

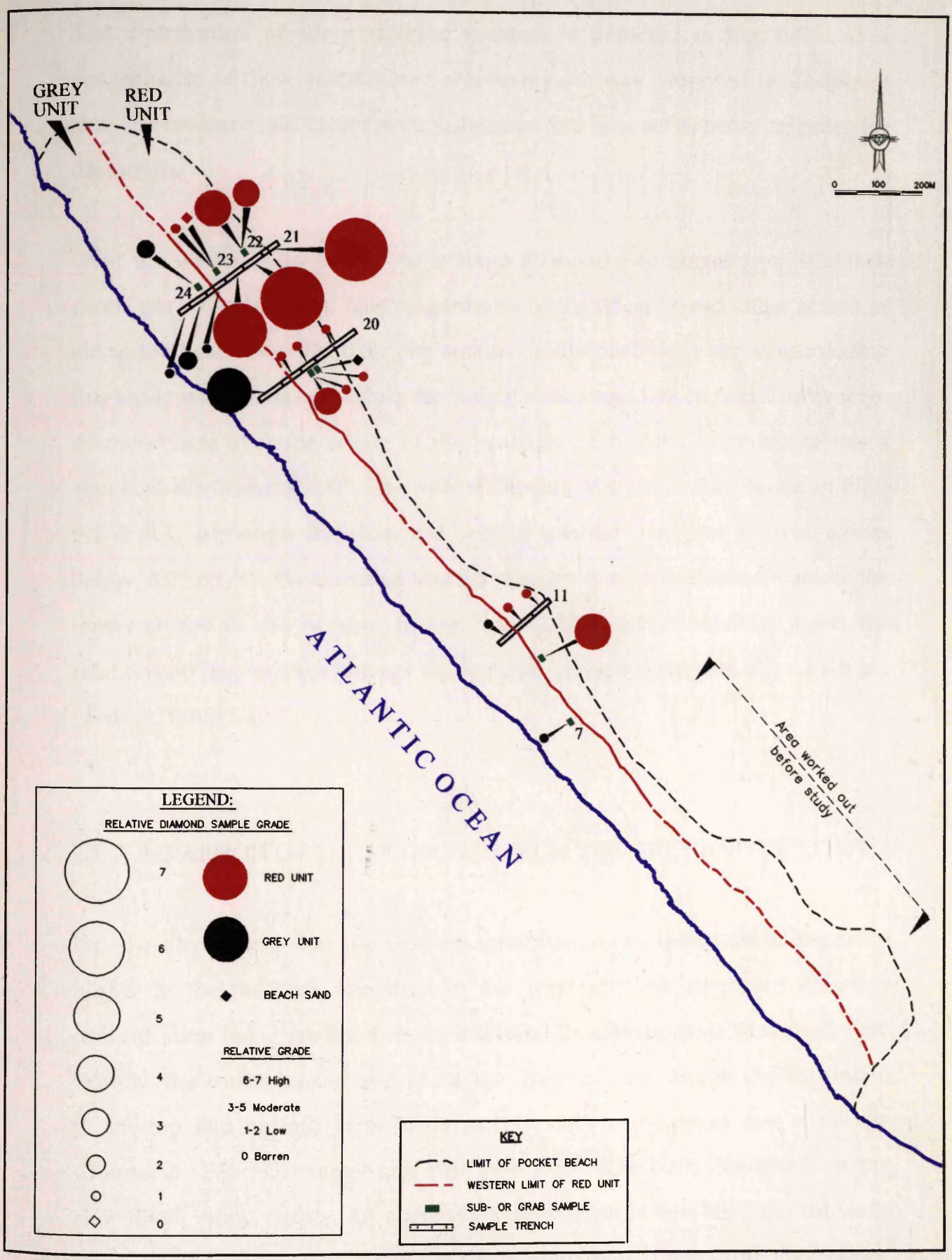

Fig. **5.1** The relative concentration of diamonds in the grey and red units within the study area (pocket beach no. 4), Chameis.

NAMDEB

The distribution of some of these features is depicted in Fig. 5.2. As a consequence of these sedimentary observations it was proposed in Chapter 3 that the coarser clasts create more turbulence and thus act as better trapsites for diamonds.

Over the whole of the beach, the average diamond size ranges from 0.22-0.60 carats per stone (cts/stn). This range shows no significant trend either across or along the beach (see Fig. 5.3). The smallest individual stone recovered during this study was 0.1 cts/stn, while the largest stone was 11.97 cts/stn. The average diamond size over the whole of the beach is 0.5 cts/stn but this size has a standard deviation of 0.47. The wide difference in sizes is also shown in Figs. 5.3 & 5.4. Although the diamond mining process does not recover stones below 0.07 cts/stn the diamond size distribution is slightly skewed towards the larger stones as can be seen in Fig. 5.4. Additional information about the relationship between the average and critical diamond size and sieve sizes are given in Table 5 1.

5.2 COMPARISON OF THE DIAMONDS FROM THE GREY AND RED UNITS

Fig. 5.1 also shows that the relative concentration of diamonds is generally higher in the red unit compared to the grey unit, the maximum diamond concentration being recorded in the intertidal (beachface) zone of the red unit. Within the intertidal red unit facies the diamonds are uniformly distributed in the top and bottom parts of the sedimentary sequence as was shown in Chapter 3 (Fig. 3.5), suggesting that they may have been deposited during short-lived storm events. An alternative explanation is that the constant wave action in the middle part of the beach moved the diamonds to the bottom, while those at the top were emplaced during storm or long period wave

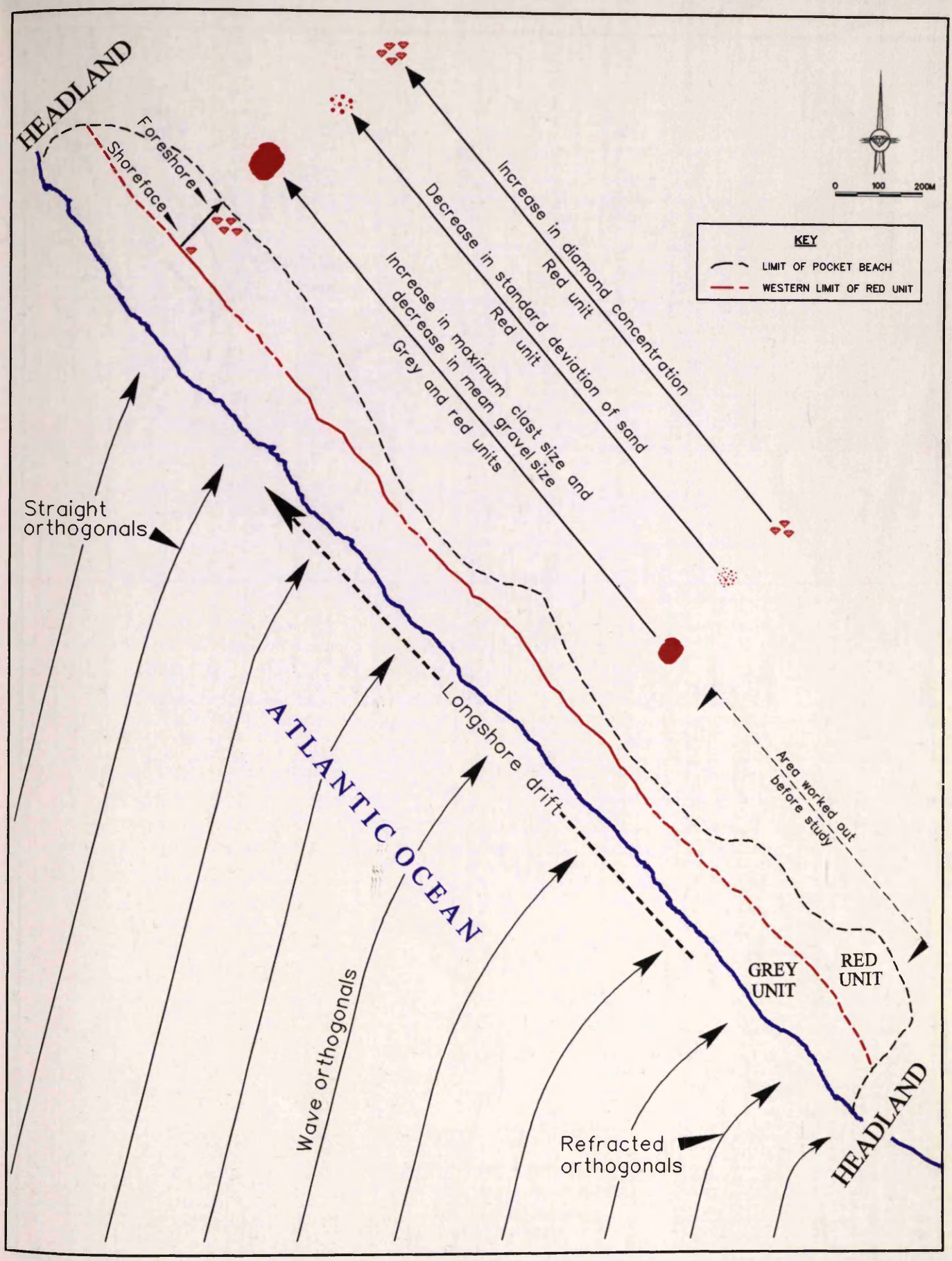

Fig. **5.2** The distribution of diamond concentration, standard deviation of sand and the maximum clast size in the red unit along a section of the study area (pocket beach no. 4), Chameis. Also shown is the distribution of maximum clast size of the grey unit.

NAMDEB

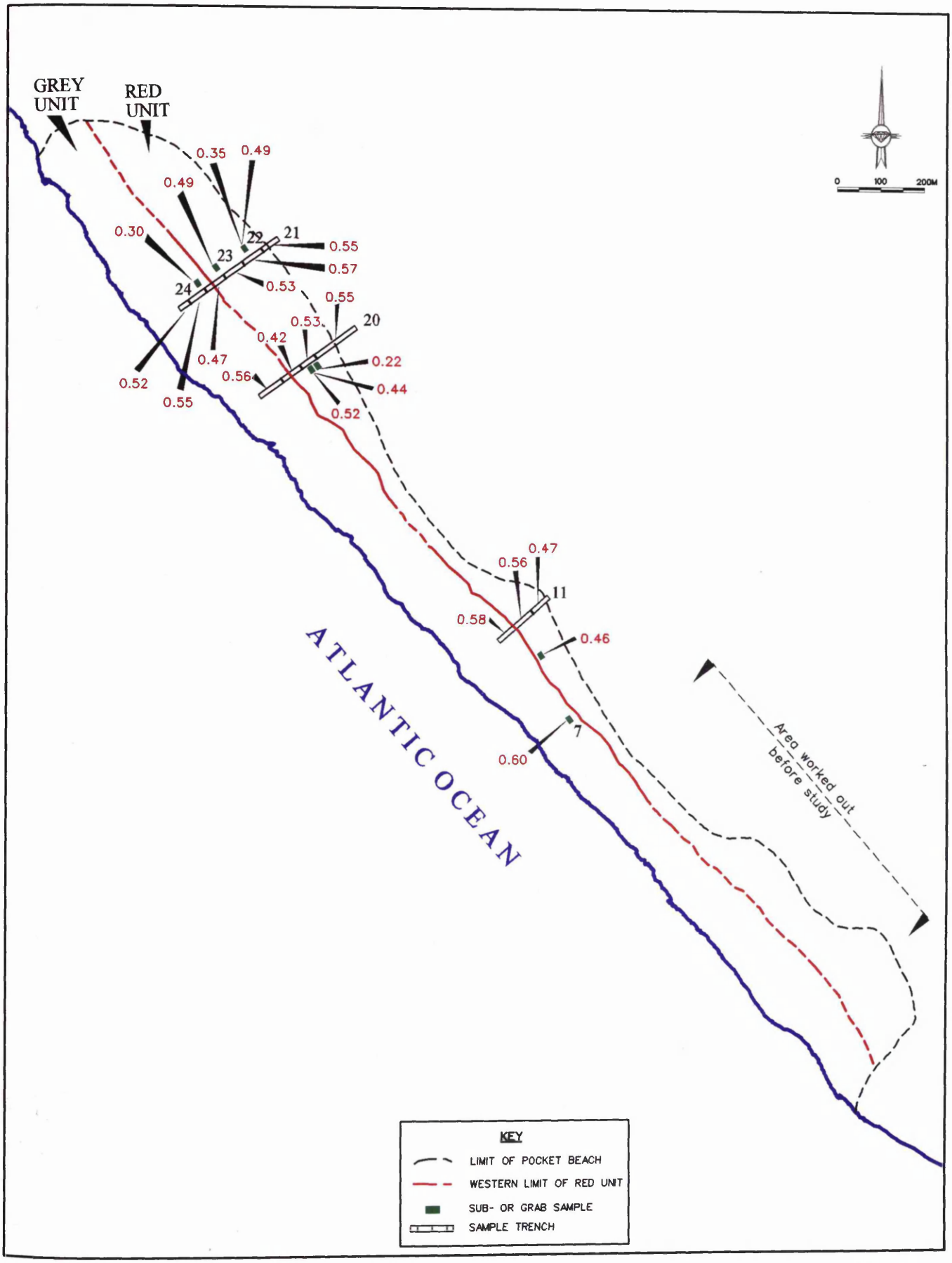

Fig. **5.3** The distribution of the average diamond size (carats per stone) within the grey and red units of the study area (pocket beach no. 4), Chameis.

NAMDEB

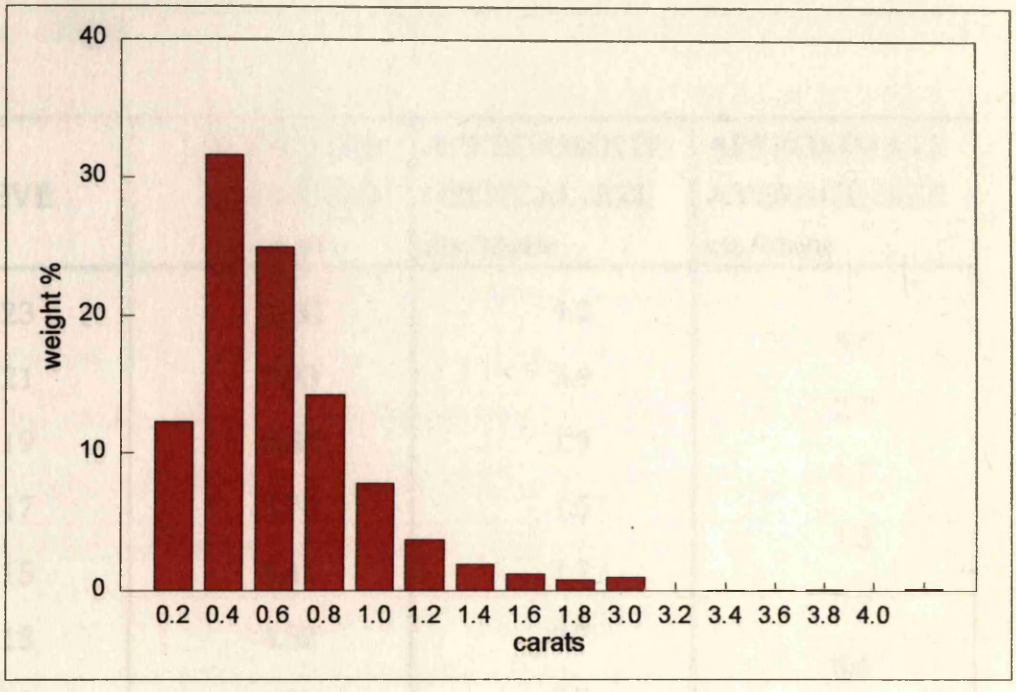

Fig. **5.4** The distribution of diamond size within the study area (pocket beach no.4), Chameis.

Table: 5.1 Diamond sieve aperture diameters, the approximate critical size of diamond passing through each sieve and the approximate average size of the diamonds in each sieve class (after Robinson, 1979).

SIEVE	APERTURE DIAMETER m m	APPROXIMATE CRITICAL SIZE cts/stone	APPROXIMATE AVERAGE SIZE cts/stone
+23	10.31	9.2	
			5.0
+21	7.93	3.9	
			2.7
+19	6.35	1.9	
			1.7
+17	5.74	1.5	
			1.3
+15	5.41	1.2	
			0.9
+13	4.52	0.7	
			0.6
+12	4.09	0.5	
			0.4
+11	3.45	0.32	
			0.23
+9	2.85	0.17	
			0.14
+7	2.46	0.12	
			0.10
+6	2.16	0.08	
			0.07
+5	1.83	0.05	
			0.04
+3	1.47	0.03	
			0.02
+2	1.32	0.02	
+1	1.09	0.01	

Note: Critical size is that size which will just pass through the appropriate screen. Critical size and average size depend on diamond shapes. Average figures are given. These vary slightly from one diamond sample to another.

events. This distribution is also consistent in both the sampling trench and the discrete facies subsample results. Diamonds in the grey unit concentrate best in the subtidal (shoreface) facies discussed in Chapter 3. Fig. 5.3 also shows that for both units there are no significant differences in the sizes of the diamonds, the average size for both being about 0.5 cts/stn indicating that the diamonds of both units would have travelled the same distance up the coast as was shown in Fig. 2.7.

Figs. 5.5 and 5.6 show representative samples of diamonds of the same size, from the red and grey units respectively. As can be seen, there is a close overall similarity of colour, with the majority of diamonds being dodecahedral. Fig. 5.7 shows that there is little difference in these characteristics within the red unit with a slight increase in diamond size.

The physical and abrasion characteristics of 243 diamonds in each of the two stratigraphic units, as a function of size, are presented in Table 5.2. The selected diamond characteristics are grouped per sample site and similar sieve size for the two stratigraphic units compared. An assesment of the diamond characteristics indicates that for a particular sample site, diamonds of the same size have similar characteristics irrespective of their stratigraphic unit. For example chi-square tests yielded the following results at the 95% confidence levels:

Sieve size	**Grey and red units**	**Degrees of freedom**	**Chi-square values**
-12 + 11	20(4) & 20(3)	12	7.604 (21.026)
-11 + 09	20(4) & 20(3)	16	6.062 (26.296)
-09 + 07	20(4) & 20(3)	9	3.749 (16.919)
-12 + 11	11(3) & 11(1)	9	0.953 (16.919)

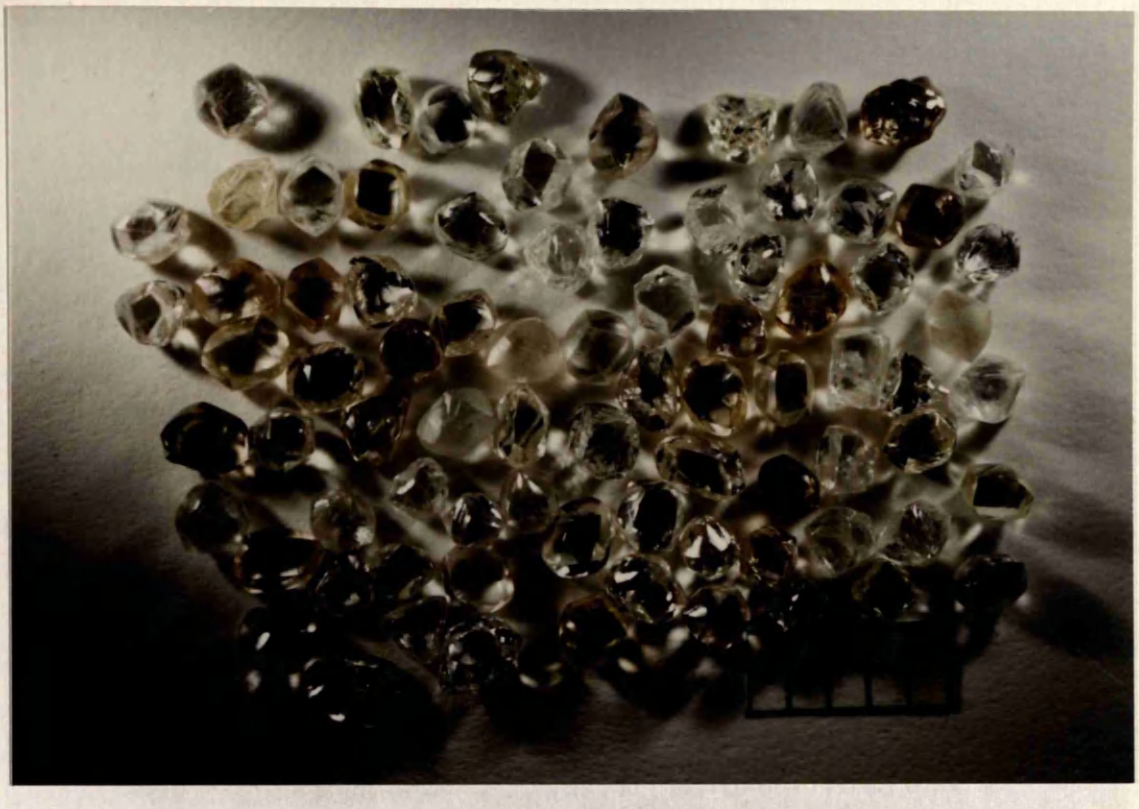

Fig. 5.5 From sieve size -11 + 09 a representative selection of mainly dodecahedral diamonds from the **red unit** at site 20. Note the different colours. Scale 10mm.

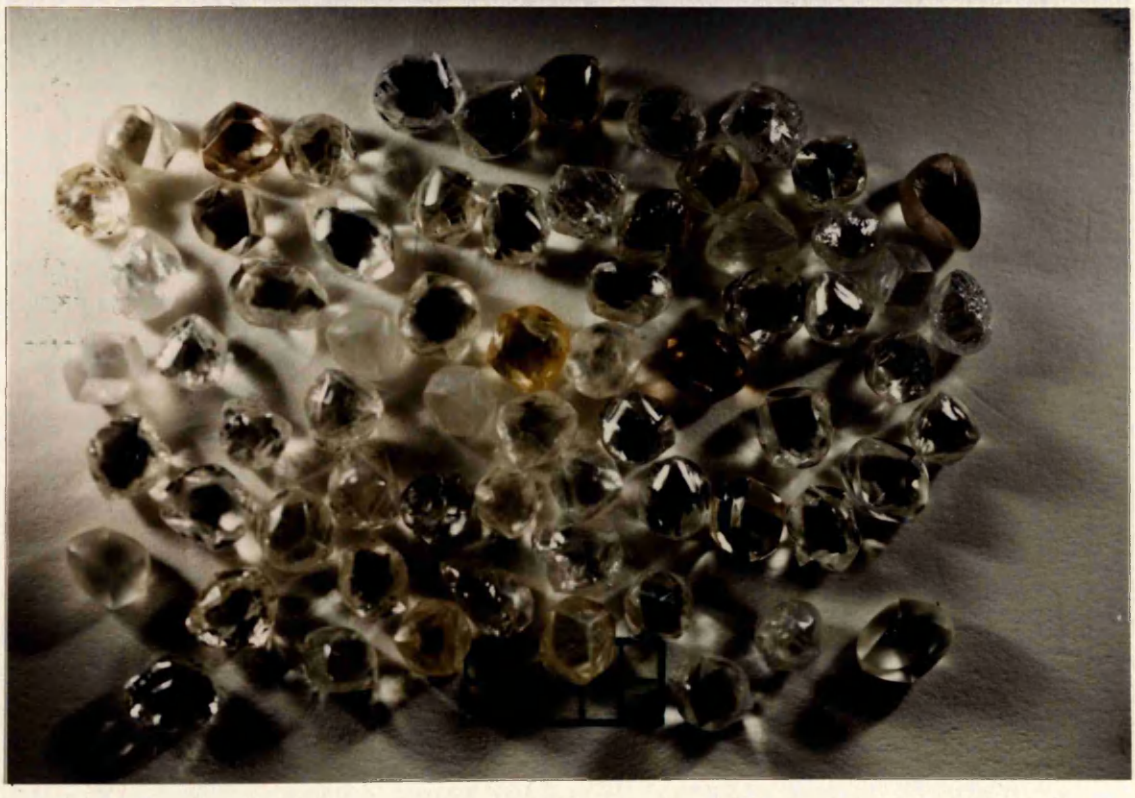

Fig. 5.6 From sieve size -11 + 09 a representative selection of mainly dodecahedral diamonds from the **grey unit** at site 21. Note the different colours. Scale 10mm.

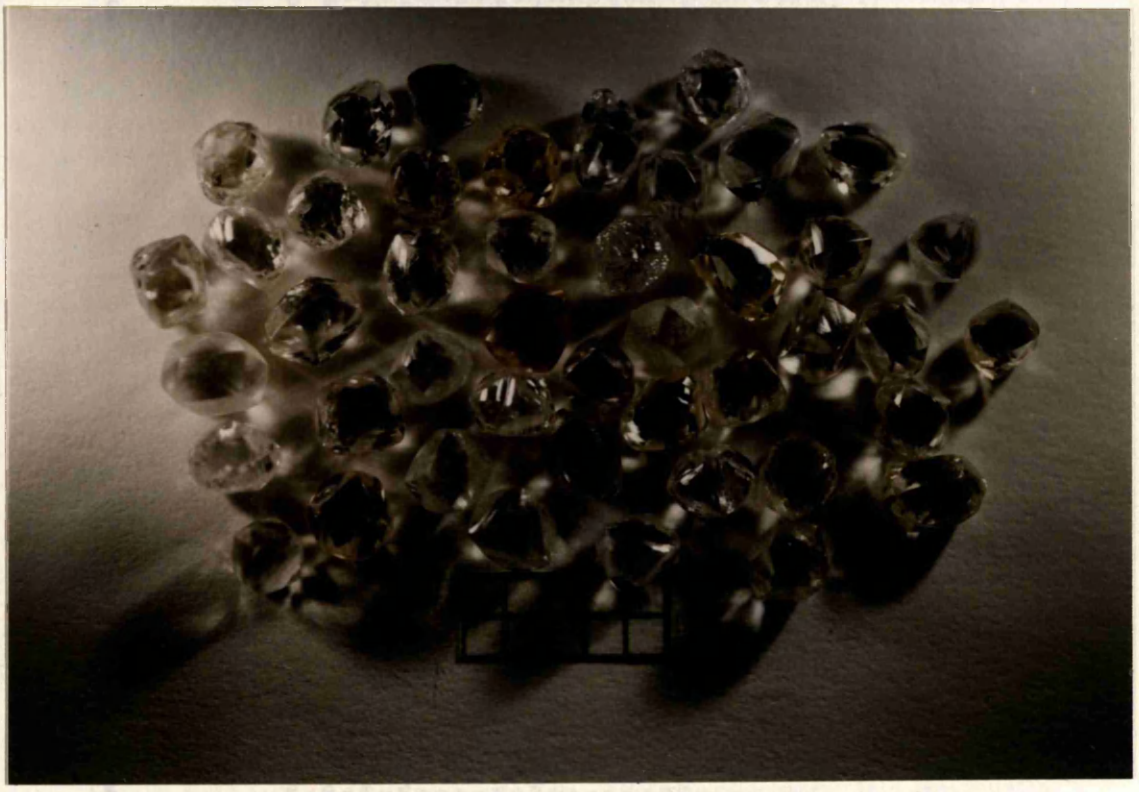

Fig. 5.7 Similar shapes and colour as in Fig. 5.5 for diamonds in the -12 +11 sieve size; **red unit**, site 20. Scale 10mm.

TABLE: **5.2** Comparison of the general characteristics and surface textures of the total diamonds studied from the red and grey units of pocket beach no.4, Chameis.

		GREY UNIT									RED UNIT								
		DIAMOND SAMPLE SITES																	
PARAMETERS		21(5&6)	21(5&6)	20(4)	20(4)	20(4)	20(4)	11(3)	11(3)	TOTAL	20(3)	20(3)	20(3)	20(3)	20(2)	20(2)	11(1)	11(1)	TOTAL
	no. of diamonds	25	25	19	50	50	25	24	25	243	19	50	50	25	25	25	24	25	243
	colourless	3	6	2	4	5	0	0	1	21	0	2	7	2	3	3	1	0	18
COLOUR	yellow	0	6	5	18	16	7	8	9	69	11	17	15	7	13	8	8	5	84
	brown	2	4	0	2	8	5	2	7	30	0	7	9	3	1	2	2	5	29
	green coated	20	9	12	26	21	13	14	8	123	8	24	19	13	8	12	13	15	112
	grey	0	0	0	0	0	0	1	0	1	0	0	0	0	0	0	0	0	0
SPOTS	green spotted	3	0	0	0	2	0	1	0	6	0	0	2	3	1	2	1	0	9
	brown spotted	0	0	0	0	3	2	0	0	5	0	0	0	0	0	0	1	0	1
	octahedron	1	0	6	2	4	0	1	3	17	3	6	4	0	0	0	1	0	14
MAIN FORM	rnd dodecahedron	24	25	13	48	46	25	23	22	226	16	44	45	25	25	25	23	24	227
	cube/frag./irregular	0	0	0	0	0	0	0	0	0	0	0	1	0	0	0	0	1	2
	octahedron	5	4	2	12	13	3	4	9	52	6	6	11	5	8	8	2	4	50
	rnd dodecahedron	1	0	5	2	4	0	0	3	15	3	6	5	0	0	0	1	0	15
SUBORDINATE FORM	cube	1	4	2	7	6	3	1	4	28	4	3	5	1	4	1	2	1	21
	broken	5	4	3	1	6	6	5	5	35	3	9	10	10	3	4	4	4	47
TWINNING	macles(octas,dodecs)	3	1	1	4	8	4	1	4	26	2	8	8	5	3	1	6	2	35
	aggregates	0	0	0	0	1	0	0	0	1	0	0	0	0	0	0	0	0	0
REGULARITY	flat	2	1	1	4	5	6	1	3	23	2	5	5	5	0	1	1	1	20
	irregular	0	0	0	0	0	0	0	2	2	0	0	2	0	1	0	0	0	3
	fine frost	8	6	6	19	17	8	11	5	80	9	17	12	12	6	8	9	11	84
UNRESTR. TEXTURES	coarse frost	5	2	6	8	8	2	6	4	41	2	7	6	4	1	4	4	3	31
	unabraded	10	14	4	22	30	20	9	18	127	3	30	33	20	12	9	8	14	129
	sharp points abraded	1	6	6	5	4	2	3	1	28	2	6	5	2	2	4	8	3	32
	points & sharp edges	3	1	3	4	4	1	6	2	24	3	2	2	2	5	3	6	2	25
DEGREE ABRADED	large percussions(few)	13	14	11	32	23	9	14	9	125	15	28	26	11	15	16	12	14	137
	small percussions(few)	5	10	4	9	8	2	9	5	52	11	17	15	6	5	5	11	4	74
	small percussions(many)	8	4	7	13	14	5	7	1	59	10	12	10	2	7	8	5	4	58
	no percussions	9	4	6	15	18	14	5	15	86	4	13	18	10	8	6	6	8	73
SIEVE CLASS		- 12 + 11	- 11 + 09	- 13 + 12	- 12 + 11	- 11 + 09	- 09 + 07	-12+11	-11+09		-13+12	-12+11	-11+09	-09+07	-12+11	-11+09	-12+11	-11+09	

NOTE: Number between brackets = no. of sample paddock from east to west

Table: **5.3** Comparison of the general characteristics and surface features of diamonds between the grey and red units within the study area (pocket beach no.4), Chameis.

GREY UNIT	RED UNIT
COLOUR	
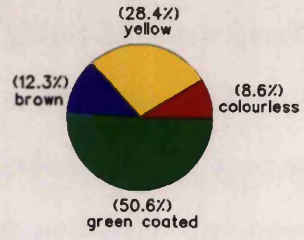	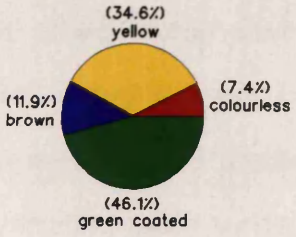
MAIN CRYSTAL SHAPE	
	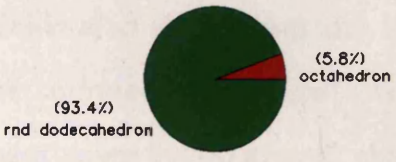
SUBORDINATE CRYSTAL SHAPE	
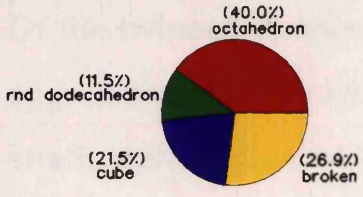	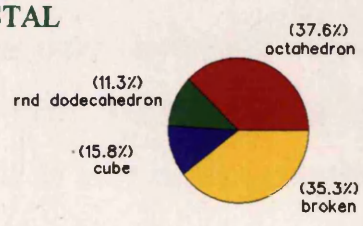
TWINNING	
	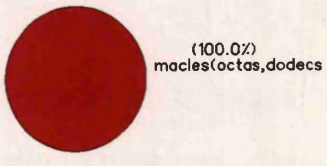
FROSTING	
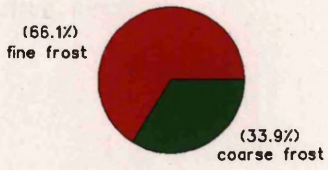	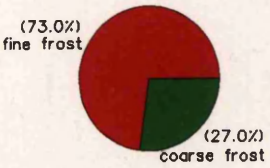
DEGREE OF ABRASION	
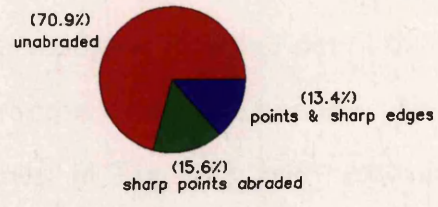	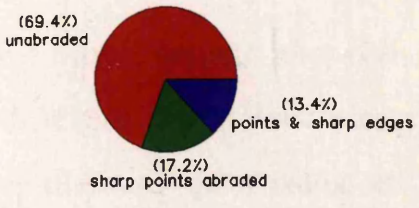
PERCUSSION	
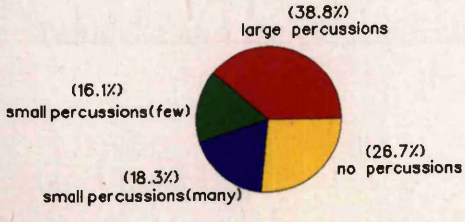	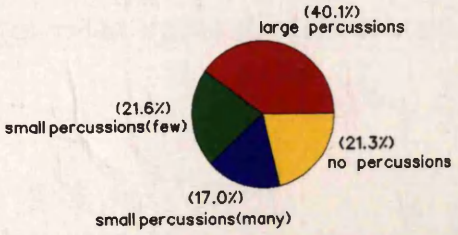

The large difference between the calculated chi-square value and the critical value given between brackets in column 4 above shows emphatically that their is no significant difference in the physical and abrasion characteristics of the diamonds from the grey and red units. This conclusion is reinforced pictorially for the principal diamond characteristics of the two stratigraphic units. The piecharts of Table 5.3 show that for both units about 50% of the diamonds are green coated, while about 30% are yellow. The Table also shows that the vast majority of the diamonds (94%) in both units are rounded dodecahedra with only 6% octahedra. The octahedra are the dominant subordinate crystal shape in both the grey and the red unit with broken diamonds second in abundance. Of the twinned diamond crystals macles are the most common with very few aggregates. Fine frosting is more common than coarse frosting in both stratigraphic units, while most of the diamonds in both units are unabraded. Large percussions are present in about 40% of the diamonds in each unit with about 25% showing no percussions.

As a consequence of these observations, no significant differences in diamond characteristics exist between the grey and the red units. Therefore, the characteristics of all the diamonds studied will be described as a whole in the ensuing section.

5.3 GENERAL CHARACTERISTICS OF DIAMONDS

To investigate in some detail the variations in physical properties and abrasion characteristics at Chameis, diamonds from the different beach localities, (shown in Fig. 5.1), were examined as a function of diamond size, using an adapted classification scheme by Robinson (1979). These data are presented in Table 5.4 and the principal characteristics are described under the following

TABLE: **5.4** The general characteristics and surface features of the total diamonds studied from pocket beach no.4, Chameis.

PARAMETERS		DIAMOND SAMPLE SITES																				
		21(5&6)	21(5&6)	21(5&6)	21(5&6)	21(5&6)	20(4)	20(4)	20(4)	20(4)	20(4)	20(3)	20(3)	20(3)	20(3)	20(2)	20(2)	11(1)	11(1)	11(3)	11(3)	TOTAL
	no. of diamonds	50	50	100	100	50	100	100	100	100	50	19	50	50	25	25	25	24	25	25	25	1093
	colourless	5	0	20	4	5	10	9	12	10	7	0	2	7	2	3	3	1	0	0	1	101
	yellow	6	9	33	31	11	29	31	36	36	13	11	17	15	7	13	8	8	5	8	9	336
COLOUR	brown	5	5	9	14	5	8	11	3	14	9	0	7	9	3	1	2	2	5	2	7	121
	green coated	33	36	38	51	29	48	49	49	40	21	8	24	19	13	8	12	13	15	14	8	528
	grey	1	0	0	0	0	3	0	0	0	0	0	0	0	0	0	0	0	0	1	0	5
SPOTS	green spotted	6	1	8	3	3	3	1	2	5	1	0	0	2	3	1	2	1	0	1	0	43
	brown spotted	0	0	0	2	0	1	0	0	4	1	0	0	0	0	0	0	1	0	0	0	9
	octahedron	13	5	3	0	0	18	18	4	5	1	3	6	4	0	0	0	1	0	1	3	85
MAIN FORM	rnd dodecahedron	37	45	97	100	50	82	82	96	95	49	16	44	46	25	25	25	23	24	24	22	1007
	cube/frag./irregular	0	0	0	0	0	0	0	0	0	0	0	0	0	0	0	0	0	1	0	0	2
	octahedron	17	14	24	21	12	36	22	24	29	8	6	6	11	5	8	8	2	4	4	9	270
	rnd dodecahedron	13	5	3	0	0	13	17	3	5	1	3	6	5	0	0	0	1	0	0	3	78
SUBORDINATE FORM	cube	11	8	8	14	2	20	11	13	15	8	4	3	5	1	4	1	2	1	1	4	136
	broken	13	10	15	14	8	22	11	14	13	10	3	9	10	10	3	4	4	4	5	5	187
TWINNING	macles(octas,dodecs)	8	4	15	14	6	12	9	8	14	5	2	8	8	5	3	1	6	2	1	4	135
	aggregates	0	0	0	1	1	1	0	0	1	0	0	0	0	0	0	0	0	0	0	0	4
REGULARITY	flat	1	2	8	9	2	5	5	5	8	9	2	5	5	5	0	1	1	1	1	3	78
	irregular	1	0	0	0	0	1	1	0	0	0	0	0	2	0	1	0	0	0	0	2	8
PERCULIARITY	concave faced	15	9	18	19	7	21	22	20	16	8	4	5	10	5	6	4	3	1	2	4	199
OCTA TEXTURES	trigons	27	17	23	13	6	45	34	20	26	7	7	11	10	3	5	6	3	4	5	10	282
	shield laminae	23	12	12	11	8	30	29	16	20	2	5	9	9	3	4	7	1	5	2	6	214
	terraces	7	12	42	43	14	24	28	38	38	21	5	23	19	8	13	15	7	8	12	8	385
	long hillocks	42	39	75	69	34	74	72	70	64	37	18	37	34	19	18	18	17	15	19	16	787
	short rounded hillocks	25	27	64	64	32	55	53	58	60	31	13	34	32	20	17	15	14	15	12	20	661
	flat triangular hillocks	8	12	22	26	14	23	17	25	18	10	5	13	15	7	9	5	6	3	6	10	254
	low- relief surface	2	3	13	11	7	6	9	11	14	8	1	2	1	4	3	3	2	5	2	3	110
	triangular pyramid	5	11	23	19	6	10	13	7	11	8	3	12	14	6	6	5	2	4	9	1	175
	ribbing	0	0	0	0	0	0	1	0	0	0	0	0	0	0	0	0	0	0	0	0	1
	discrete lam. lines	4	2	7	12	2	10	7	4	9	2	1	6	11	2	1	1	1	4	3	0	89
DODEC TEXTURES	fine lam.lines	16	13	25	32	13	28	30	39	31	20	6	19	20	8	8	7	6	12	8	8	349
	zig - zags	11	16	22	22	7	8	4	15	13	13	2	12	8	3	6	7	6	4	7	1	187
	microdisks	1	1	13	9	1	4	5	4	3	1	2	5	2	0	1	2	3	2	1	1	61
	corrosion sculpture	0	2	5	1	2	3	2	2	1	0	0	1	1	0	0	0	0	0	2	1	23
	shallow depressions	4	8	21	17	8	5	11	13	6	7	3	9	5	5	1	3	5	3	3	7	144
	fine frost	12	16	38	28	10	33	34	37	31	14	9	17	12	12	6	8	9	11	11	5	353
	coarse frost	11	9	18	13	8	17	18	15	16	5	2	7	6	4	1	4	4	3	6	4	171
	polish	2	0	7	7	1	3	2	8	6	2	1	3	1	1	2	2	2	1	0	2	53
UNRESTR. TEXTURES	network pattern(percu)	7	1	6	10	5	9	5	7	10	3	1	4	2	1	2	2	3	1	2	2	83
	arcuate groove	2	4	2	2	1	2	4	8	5	2	1	0	2	1	1	2	3	1	2	1	46
	scratch marking	8	3	27	9	2	10	8	15	12	3	3	4	6	0	4	5	3	1	2	1	126
	rut	4	10	19	14	3	9	17	10	11	10	2	8	4	3	3	4	2	2	3	1	139
	inclusion cavity	1	2	4	3	2	1	2	4	4	5	2	2	2	1	2	1	1	1	0	2	42
	unabraded	11	10	41	63	45	25	34	40	59	43	3	30	33	20	12	9	8	14	9	18	527
	sharp points abraded	5	8	11	13	3	16	22	12	12	4	2	6	5	2	2	4	8	3	3	1	142
	points & sharp edges	12	9	14	5	0	27	13	15	11	1	3	2	2	2	5	3	6	2	6	2	140
	A' edges ground	7	5	4	5	0	5	8	7	5	2	4	2	2	0	2	2	0	1	0	1	62
	C' edges ground	15	19	21	14	1	23	19	21	12	0	8	9	7	1	3	5	2	3	4	2	189
DEGREE ABRASION	large percussions(few)	37	35	61	52	24	59	58	57	44	21	15	28	26	11	15	16	12	14	14	9	608
	small percussions(few)	19	16	25	34	5	26	19	23	12	5	11	17	15	6	5	5	11	4	9	5	272
	small percussions(man	16	17	32	18	8	30	24	25	22	7	10	12	10	2	7	8	5	4	7	1	265
	no percussions	4	7	26	30	24	33	31	30	47	26	4	13	18	10	8	6	6	8	5	15	351
SIEVE CLASS		-15+13	-13+12	-12+11	-11+09	-09+07	-15+13	-13+12	-12+11	-11+09	-09+07	-13+12	-12+11	-11+09	-09+07	-12+11	-11+09	-12+11	-11+09	-12+11	-11+09	

NOTE: Number between brackets = no. of sample paddock from east to west.

headings.

5.3.1 Colour

The diamond colours recorded at Chameis are shown in Fig. 5.8. Although five colours are represented, only four are true body colours. Of these, yellow (31.2%) dominates over brown (11.2%) and colourless (9.4%), a very minor proportion being grey (0.5%). Figs. 5.9 and 5.10 show some of the typical colours for differently shaped diamonds from the grey unit and Figs. 5.11, 5.12 and 5.13 display specific colours from that unit. Overall, transparent green coated diamonds predominate at 47.7%. This colour shown in Fig. 5.14 arises as a consequence of alpha-particle irradiation which damages the diamond to a depth of about 20μm (Vance *et al.* 1973). With light coloured coats such as those at Chameis, the damage was probably inflicted during residency in the oxidized and mildly radioactive groundwater saturated upper part of the original kimberlites or lamproites from which these diamonds were eroded (see Harris, 1992). As a consequence of this damage the true body colour is disguised, but in order for the green to be seen, the body colour has to be colourless or light yellow. From Fig. 5.5 these colours are dominant among the non-coated stones. The proportion of alpha-particle damaged diamonds among brown stones is difficult to access if the body colour is anything other than weak. Occasionally, instead of a wholly green coated stone, single or clusters of green spots are noted on some of the diamond surfaces and an example is shown in Fig. 5.15. This blemish is also the result of alpha-particle damage, but this time, occurs when the adjacent radioactive source is particulate. This damage is likely to occur when the diamond has been eroded from the kimberlite and resides in an alluvial deposit in which there are radioactive particles. Experiments have shown (Vance *et al.*, 1973) that if heated to 600°C, the green coat or spot will turn irreversably to brown in less

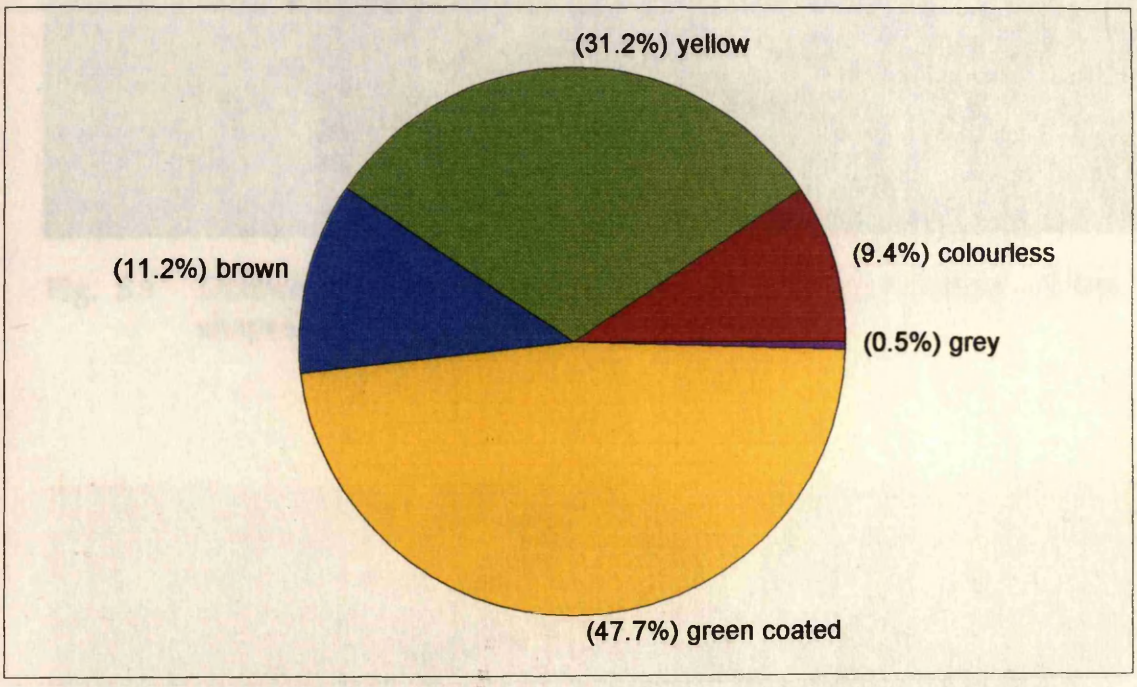

Fig. **5.8** The percentage of colours of the total diamonds studied from pocket beach no.4, Chameis.

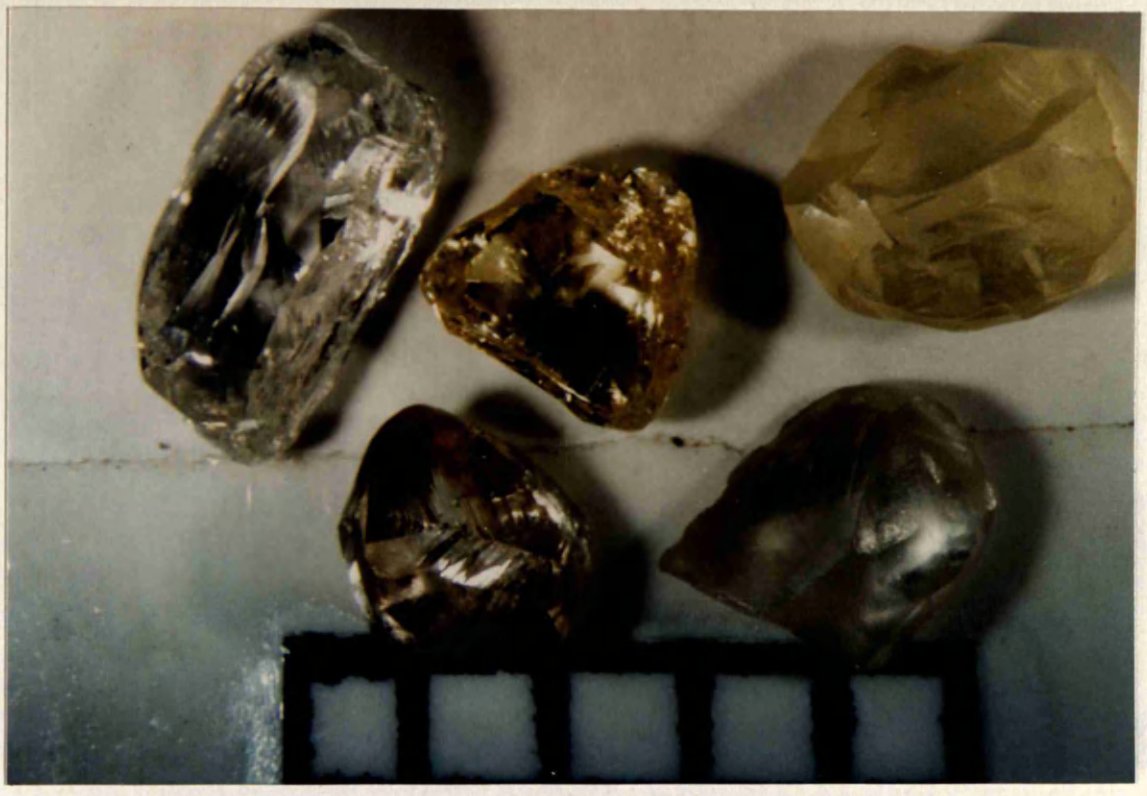

Fig. 5.9 Diamonds from the **grey unit**, site 7, showing different colours, shapes and levels of abrasion. Scale 10mm.

Fig. 5.10 Colourless, brown and a highly abraded light yellow diamond from the **grey unit**, site 20. Magnification (x6.5).

Fig. 5.11 A colourless octahedron with subordinate dodecahedral shape from the **grey unit**, site 21. Sieve size -15+13. Magnification (x10).

Fig. 5.12 A yellow dodecahedron, from the **grey unit**. Sieve size -15+13. Magnification (x10).

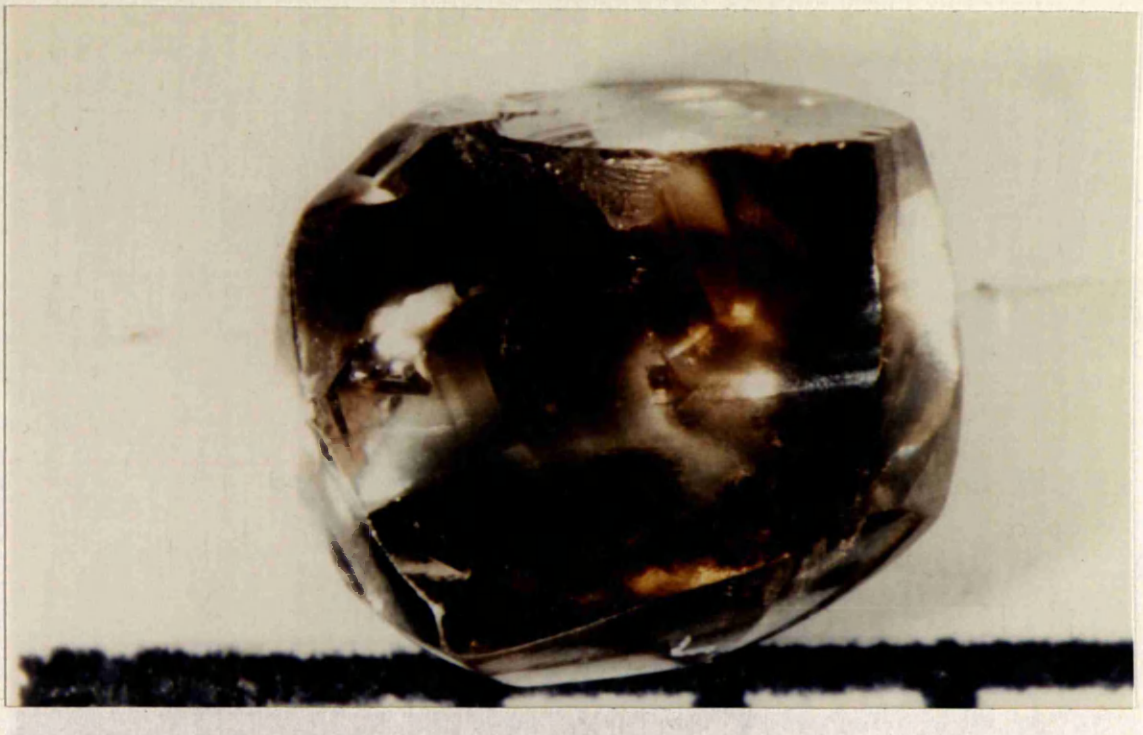

Fig. 5.13 A brown dodecahedron with plastic deformation and breakage, from the **grey unit**, site 21. Sieve size -15+13. Magnification (x10).

Fig. 5.14 A green coated dodecahedron from the **grey unit**, site 20. Size ± 6 cts/stn.

Fig. 5.15 An octahedron with a medium intensity green spot (arrowed) from the **grey unit**, site. 21. The diamond also exhibits shield laminae, trigons and a large percussion. Size + 1.30 cts/stn. Magnification (x10).

Fig. 5.16 A brown spotted broken diamond from the **grey unit**, site 21. Sieve size -15+13. Magnification (x10).

than 1 hour. Fig. 5.16 shows such a spot on a diamond from the grey unit. This observation may suggest that such diamonds have been subjected to great heat, but an alternative suggestion is that this colour change may be kinetically controlled, in which case, time may be an important parameter (Harris, 1992).

5.3.2 Crystal shape

As can be seen in Fig. 5.17, there is an overwhelming predominance of rounded dodecahedra (92%) amongst the main crystal shapes. Fig. 5.17 also shows that octahedra constitute 7.8%, and there are very few fragments or irregular diamonds (0.2%). No cubes were encountered during this study. Because of partial resorption during kimberlite or lamproite eruptions, many diamonds represent combinations of not only the main crystal shape, but also subordinate crystal shapes. The predominant subordinate crystal shape are octahedra (40.2%), with broken diamonds (27.9%), cubes (20.3%) and rounded dodecahedra (11.6%), as can be seen in Fig. 5.18. Figs. 5.19 shows a typically shaped octahedron with rounded edges and Fig. 5.20 a typically rounded dodecahedron from the grey unit. The octahedron from the red unit (Fig. 5.21) is also similar to the octahedron from the grey unit shown in Fig. 5.19. As an example of an irregular diamond, Fig. 5.22 shows a piece of boart, one of only three boarts that were reported during this study. Examples of combined crystal shapes are, rounded dodecahedron with a subordinate octahedron as shown in Fig. 5.23, and in Fig. 5.24 a rounded dodecahedron has subordinate cube corners.

The shape characteristics of the total diamonds studied indicate that the ratio of rounded dodecahedra to octahedra increases as diamond size decreases (see Fig. 5.25). For this result to occur in an alluvial environment the primary diamond population (s) would either need to be relatively heavily resorbed, or

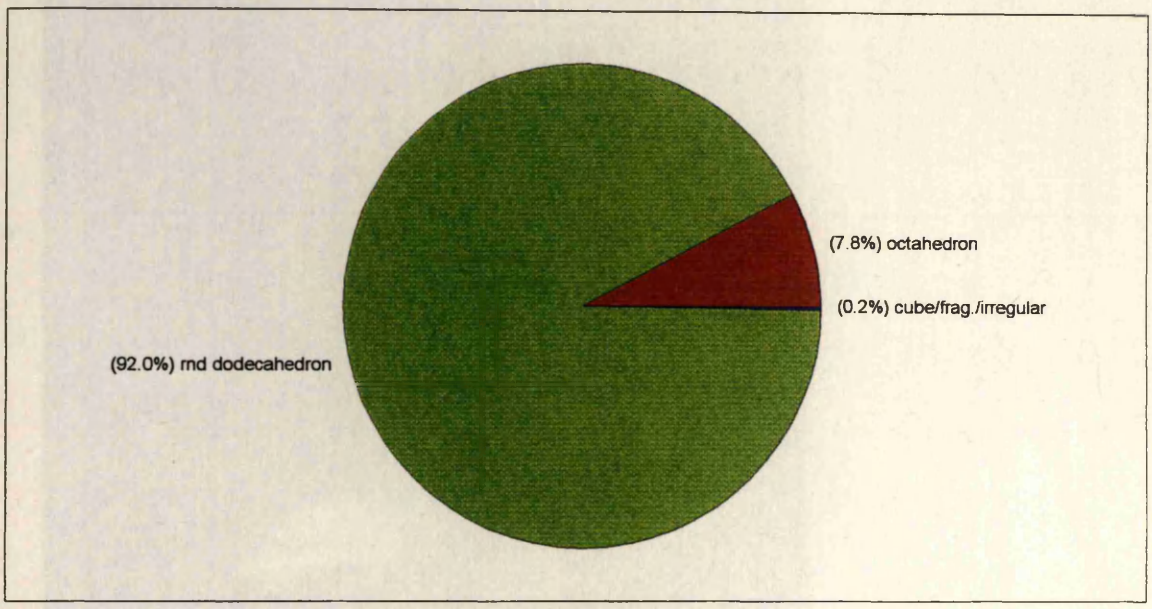

Fig. **5.17** Main crystal shapes of the total diamonds studied from pocket beach no.4, Chameis.

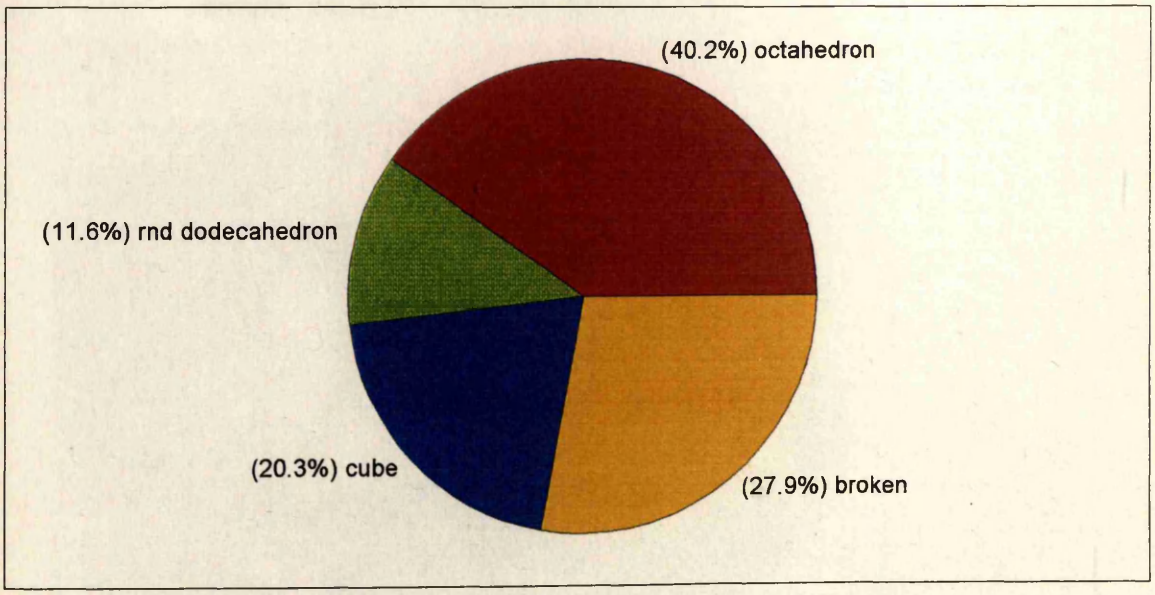

Fig. **5.18** Subordinate crystal shape of the total diamonds studied from pocket beach no.4, Chameis.

Fig. 5.19 A typically shaped octahedron from the **grey unit**, site 21; showing shield laminae. Magnification (x13).

Fig. 5.20 A slightly polished dodecahedron from the **grey unit**, site 21. Magnification (x10).

Fig. 5.21 A typically shaped octahedron from the **red unit**, site 20. Note the similarity of Fig. 5.19 with Fig. 5.21. Size ± 1.0 cts/stn. Scale 10mm.

Fig. 5.22 A piece of irregular boart from the **grey unit**, site 21. Size ± 1.0 cts/stn. Magnification (x10).

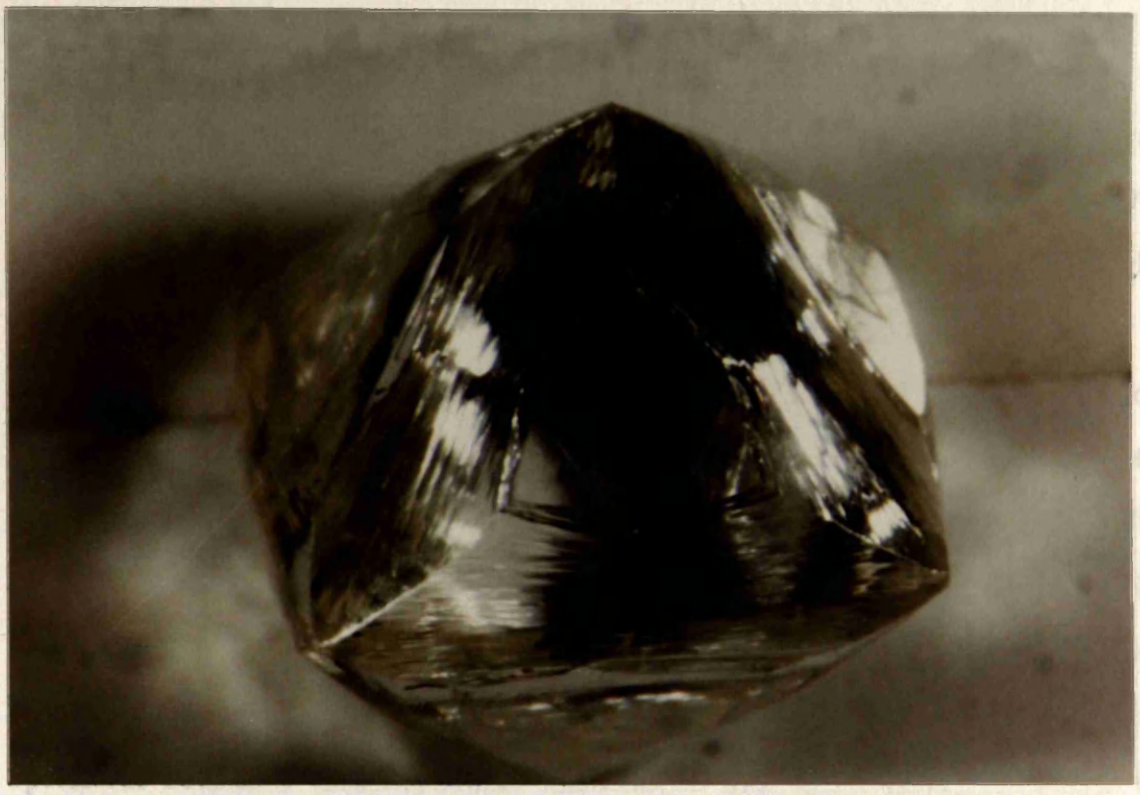

Fig. 5.23 Dodecahedron with shield laminae and trigons on subordinate octahedron face from the **grey unit**, site 21. Sieve size -15+13. Magnification (x6.5).

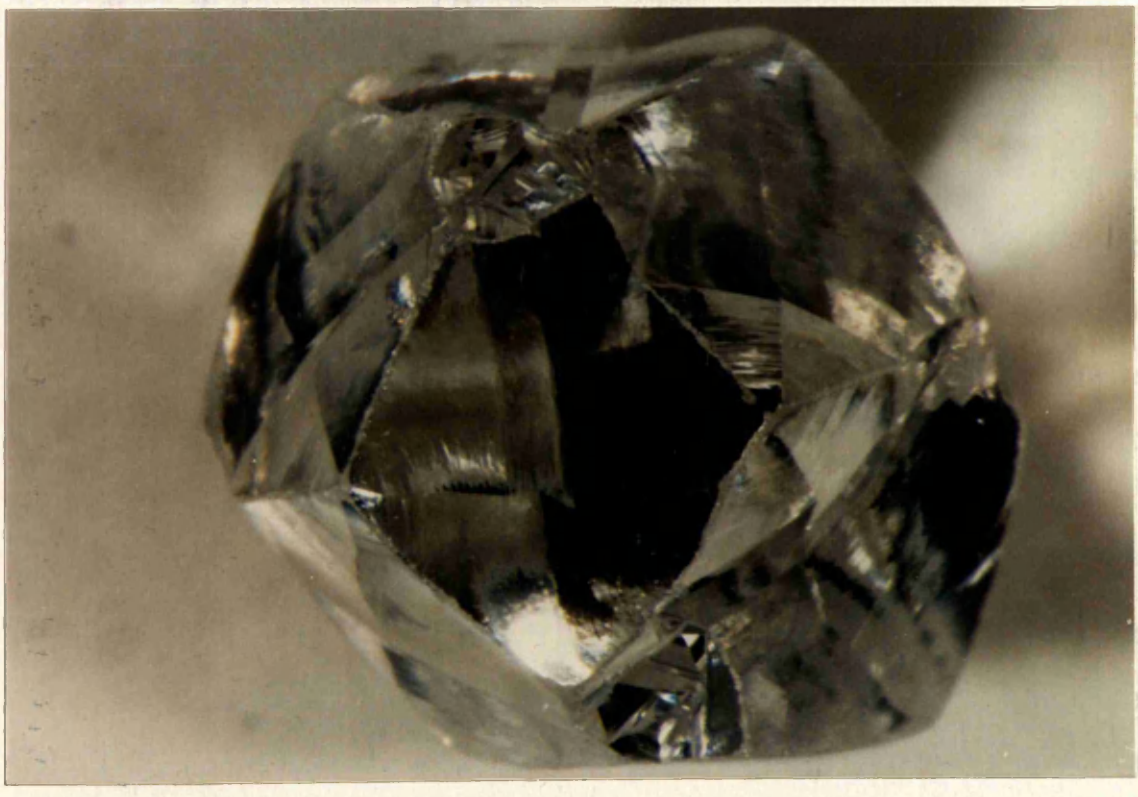

Fig. 5.24 A dodecahedron with subordinate cube corners and a slight polish from the **grey unit**, site 21. Size ± 1.3 cts/stn.

during transport, certain diamond shapes travel further than others. In the first of these possibilities and assuming that the Namibian diamonds are derived from the African hinterland, Harris *et al.*, 1975; Robinson, 1979; Robinson *et al.*, 1989 have all shown that there is a preponderance of rounded dodecahedral diamonds in most of the primary kimberlite deposits of southern Africa. The rounded dodecahedron (tetrahexahedroid) results from partial resorption of the octahedron, and Robinson (1979) determined that the diamond crystal weight loss during this conversion was about 45%. With respect to the second proposition, Sutherland (1982) ascribes the relative abundance of rounded dodecahedra with increasing distance away from a primary source, to the ease with which the generally smaller and more spherical rounded dodecahedron entrains in the sedimentary environment compared to the more regular octahedron. As either of these propositions are not mutually exclusive, it is not certain which process plays a dominant part in creating the graph shown in Fig. 5.25.

The extreme rarity of poor quality boart diamonds in this population suggests that they are probably progressively destroyed with transport distance. The percentage of broken diamonds is relatively low which might indicate that these diamonds are either few in number in the primary source or that they are also progressively eliminated during transportation. Both these observations further indicate that this diamond population has probably undergone considerable transport.

Table 5.4 also shows that up to 15% of the diamonds are macles, a twin form. Ideally, a macle is a spinel twin in the cubic system and a slightly rounded but typical example is shown in Fig. 5.26. Twinning can also occur with other crystal shapes such as dodecahedra and more rarely the octahedron, but in Chameis, these were less common than the spinel twin. The only other form

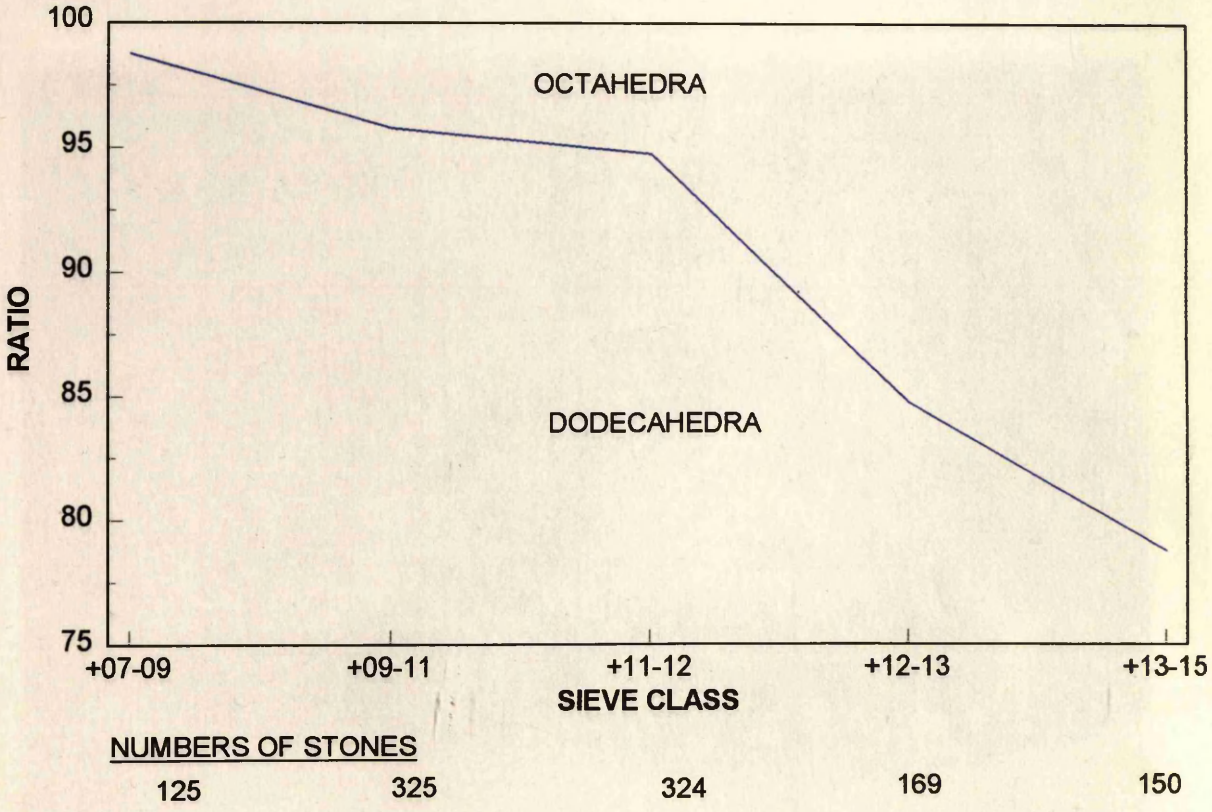

Fig. **5.25** The shape characteristics of total diamonds studied relative to their size, from pocket beach no.4, Chameis.

Fig. 5.26 A triangular macle with rounded edges from the **grey unit**, site 21. Size ± 1.0cts/stn. Magnification (x10).

of twinning recorded were aggregated crystals, but these constituted only a maximum of 1%.

5.3.3 Surface textures

Either whilst resident in the upper mantle or during kimberlite or lamproite evolution and movement to the surface, most primary diamond populations undergo resorption and/or etching, which gives rise to many different diamond surface textures. Once the diamonds have been released from the primary source by erosion, an additional suite of surface features may occur during alluvial transportation. An extensive classification scheme of these features has been developed by Robinson (1979) and in this section the textures noted on the Chameis diamonds are described.

a) *Primary textures*

The classification scheme by Robinson (1979) divides the surface textures into those which are specific to a particular shape and those that are unrestricted.

Figs. 5.27 & 5.28, respectively show the frequencies of occurrence of octahedral and dodecahedral surface textures. In Fig. 5.27 trigons and shield laminae are the only common octahedral surface textures and occur in approximately equal proportions. With the dodecahedra (Fig. 5.28), the surface textures are more numerous. More than 50% of the diamonds possess different types of hillocks. Terraces (12.3%) and fine lamination lines (11.1%) are also well represented. Six other dodecahedral surface textures are present in minor proportions and of these, triangular pyramids (5.6%), zig-zag patterns (6.0%) and shallow depressions were the most common (see below).

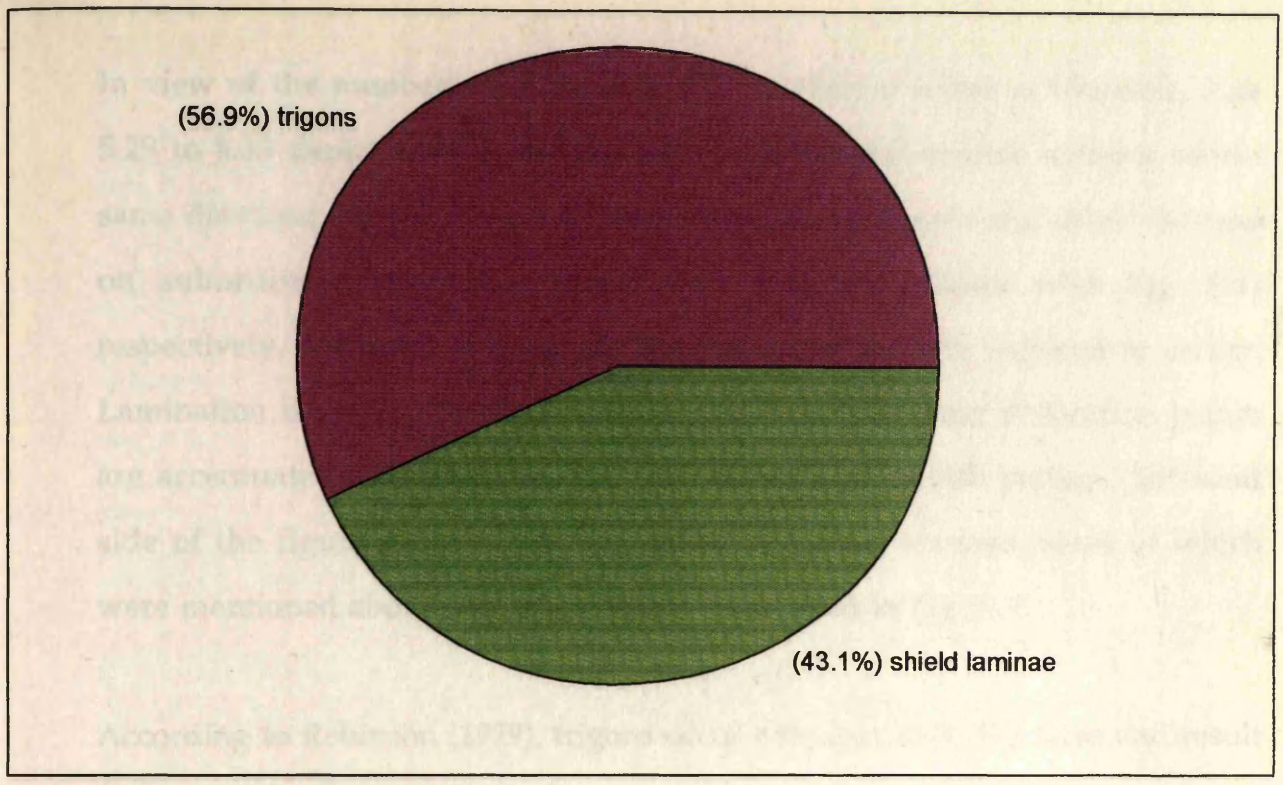

Fig. **5.27** Common octahedron surface textures of the total diamonds studied from pocket beach no. 4, Chameis.

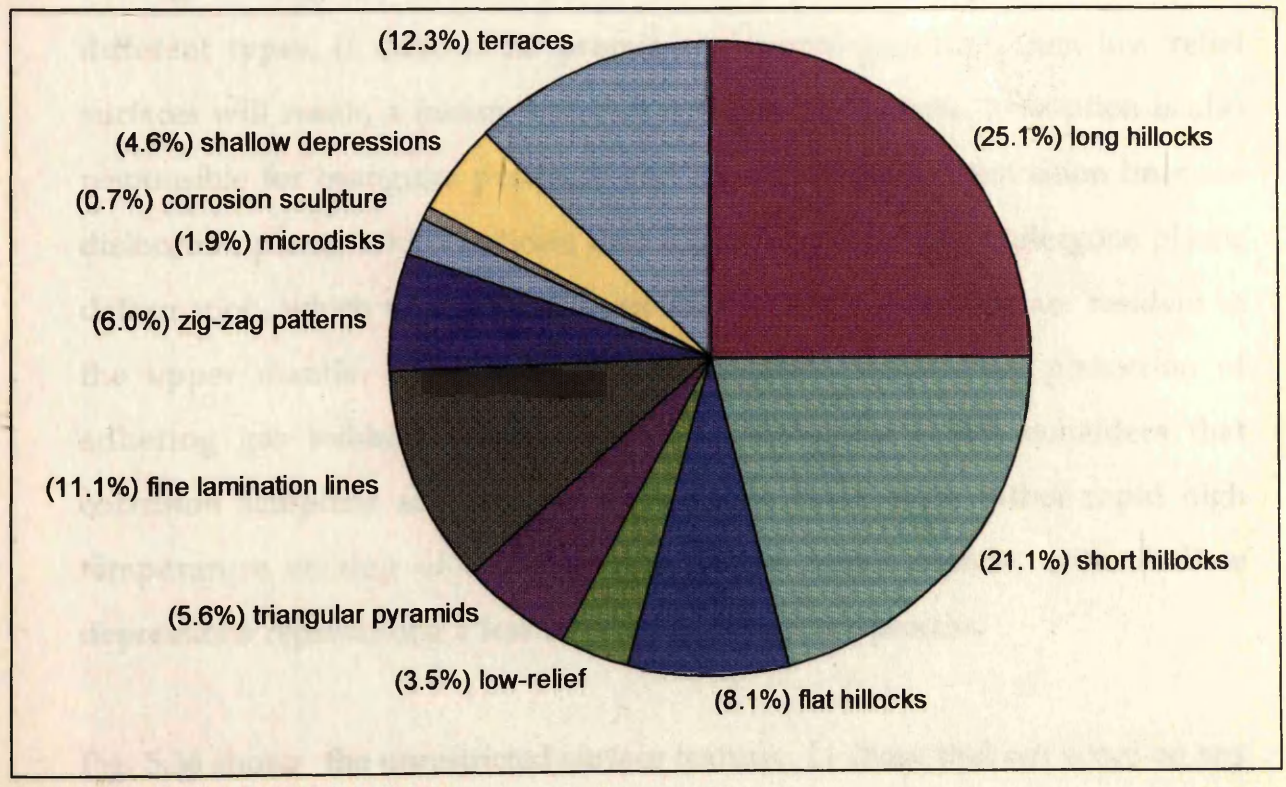

Fig. **5.28** Common dodecahedron surface textures of the total diamonds studied from pocket beach no. 4, Chameis.

In view of the numbers of diamonds with combined forms at Chameis, Figs. 5.29 to 5.33 depict both octahedral and dodecahedral surface textures on the same diamond. Figs. 5. 29 & 5.30 show examples of trigons and shield laminae on subordinate octahedral faces. Figs. 5.30 also shows with Fig. 5.31 respectively, examples of long and flat triangular hillocks, referred to earlier. Lamination lines can clearly be seen in Fig. 5.32, and these dislocation planes are accentuated by resorption. Fig. 5.33 shows a microdisk pattern (left-hand side of the figure). The minor dodecahedral surface textures, some of which were mentioned above, are schematically illustrated in Fig. 5.35.

According to Robinson (1979), trigons occur only on octahedral faces and result from an etch process which is governed by the three-fold crystallography of the octahedral face. Shield laminae result from the gradual exposure of usually thin octahedral layers during resorption. Such dodecahedral features as hillocks and terraces reflect internal structure picked out by resorption, but etching is thought to be more pronounced for hillocks which gives rise to the different types. If there is no prominent internal structure, then low relief surfaces will result, a feature not very common at Chameis. Resorption is also responsible for triangular pyramids and zig-zag textures. Lamination lines are dislocation planes which indicate that such diamonds have undergone plastic deformation, which most probably occurs whilst the diamonds are resident in the upper mantle. Microdisk patterns probably result from protection of adhering gas bubbles during resorption. Robinson (1979) considers that corrosion sculpture and shallow depressions result from rather rapid high temperature etching of static magma in the upper mantle, with shallow depressions representing a less severe product of this process.

Fig. 5.36 shows the unrestricted surface textures, i.e those that can occur on any crystal shape. At Chameis these features can be divided into two on the basis

Fig. 5.29 A very abraded dodecahedron with trigons on a residual octahedral face with shield laminae and hillocks elsewhere. From the **grey unit**, site 7. Size ± 1.0 cts/stn. Magnification (x12).

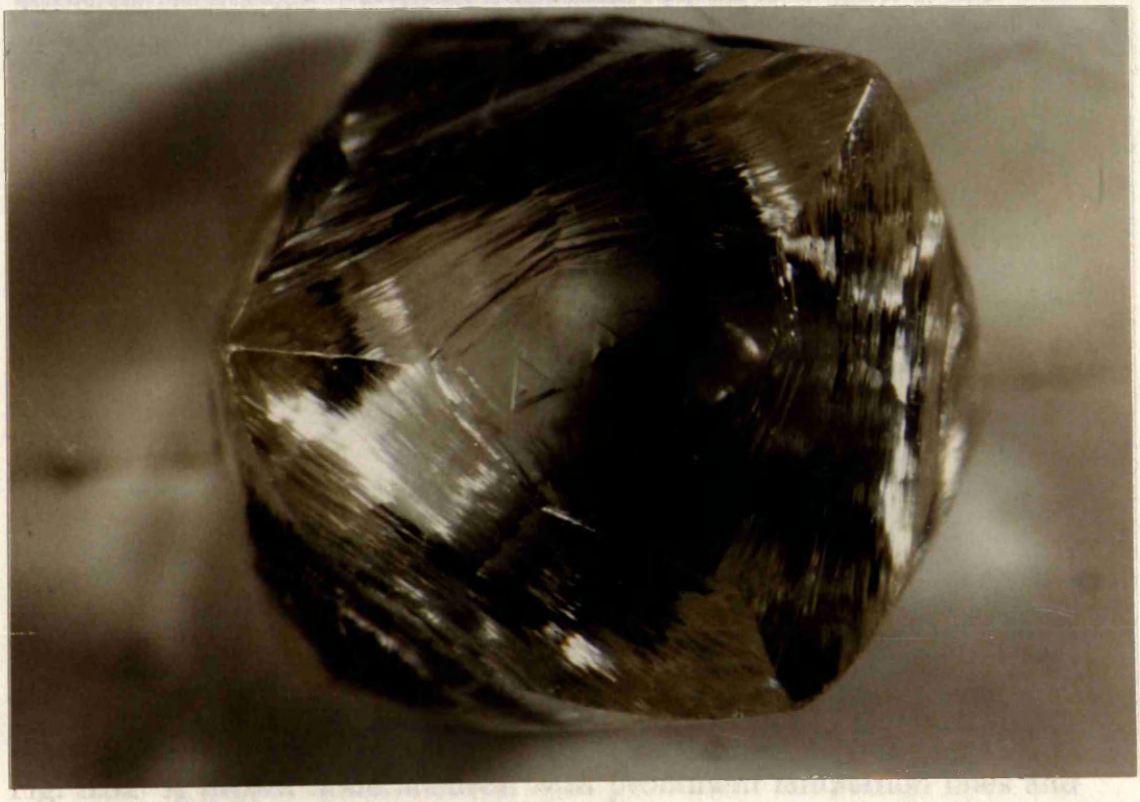

Fig. 5.30 A dodecahadron with long hillocks on dodecahedral surfaces from the **grey unit**, site 21. Sieve size -15+13. Magnification (x6.5).

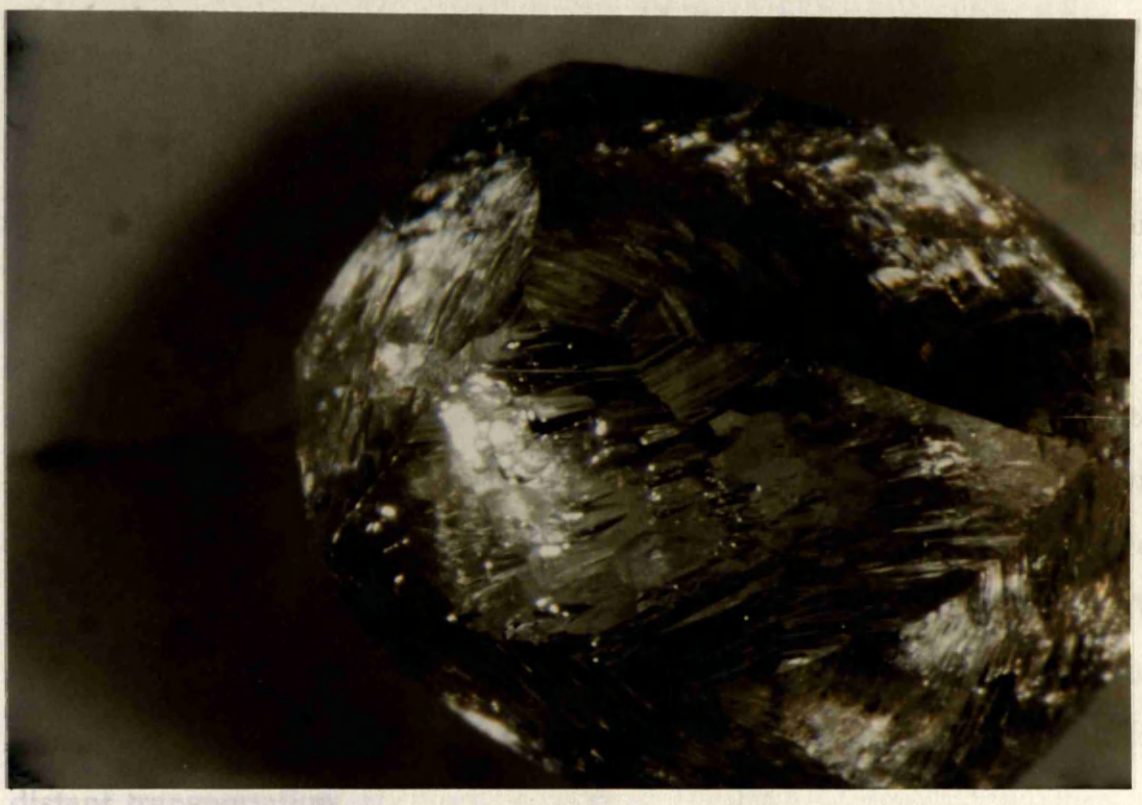

Fig. 5.31 Shield laminae and short hillocks on a dodecahedron from the **grey unit**, site 20. Size ± 1.3 cts/stn. Magnification (x12).

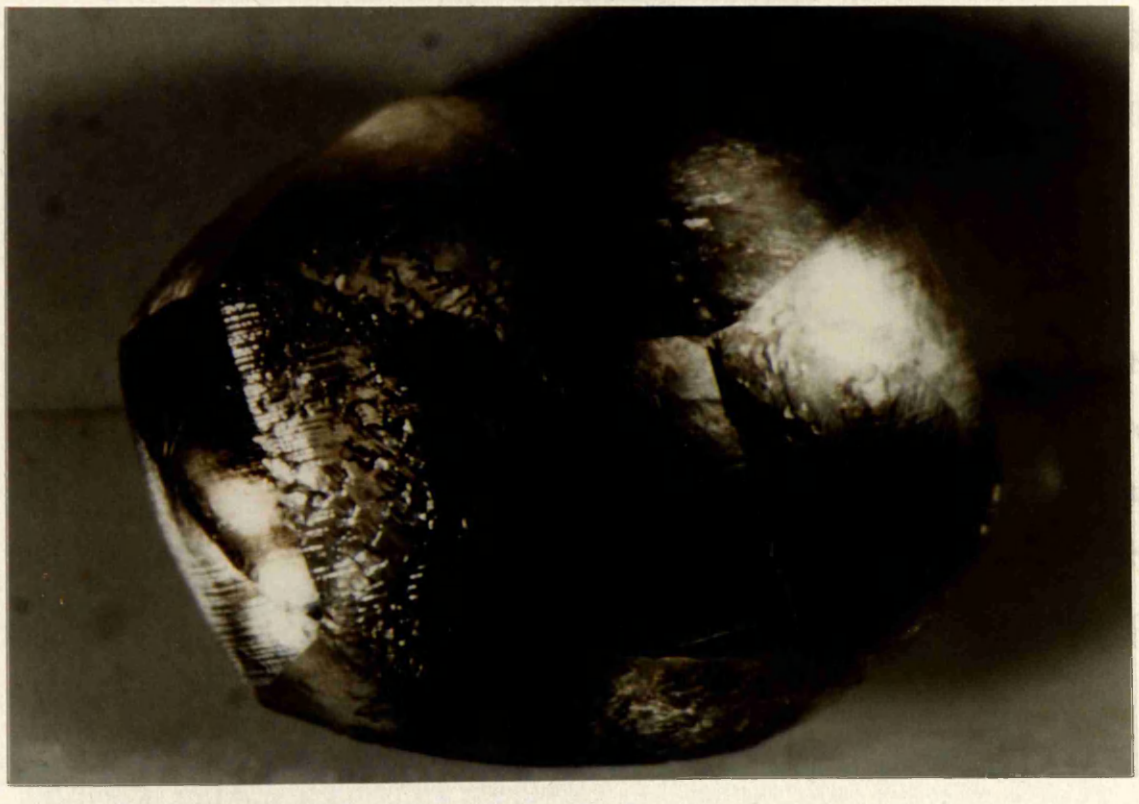

Fig. 5.32 A brown dodecahedron with prominent lamination lines and shallow depressions from the **grey unit**, site 21. Sieve size -15+13. Magnification (x13).

of whether or not they are primary, or likely to be the product of alluvial transport. For example, ruts (13.7%) and inclusion cavities (4.1%) are surface features most probably derived from kimberlite activity. The former are grooves running across the diamond surface which are often quite deep and not crystallographically controlled, the latter being cavities left after an inclusion has been released. The remaining features may or may not be products of transportation. Within this second group, the 12.4% of scratch markings and 4.5% of arcuate grooves are almost certainly caused by alluvial processes. The difficulty with the remaining features is that they can occur on diamonds recovered both from kimberlite pipes and alluvial deposits. The very high proportion of frosting (51.7%) suggests an alluvial derivation and Robinson (1979) believes that polish and network patterns are the result of distant transportation.

The right-hand half of Fig. 5.33, and Fig. 5.34 show examples of coarse frosting, Fig.5.37 shows a network pattern, Fig. 5.38 clear evidence of scratch-like markings and Fig. 5.39 an inclusion cavity associated with several large percussions.

b) *Secondary abrasion textures*

From the last part of the previous section, there is some uncertainty as to the origin of some surface features found on alluvial diamonds. However, considering the distance that these diamonds may have travelled and the battering they would have undergone during this transport it is likely that either a large percentage, or all, of the features to be described in this section, are alluvial transport related.

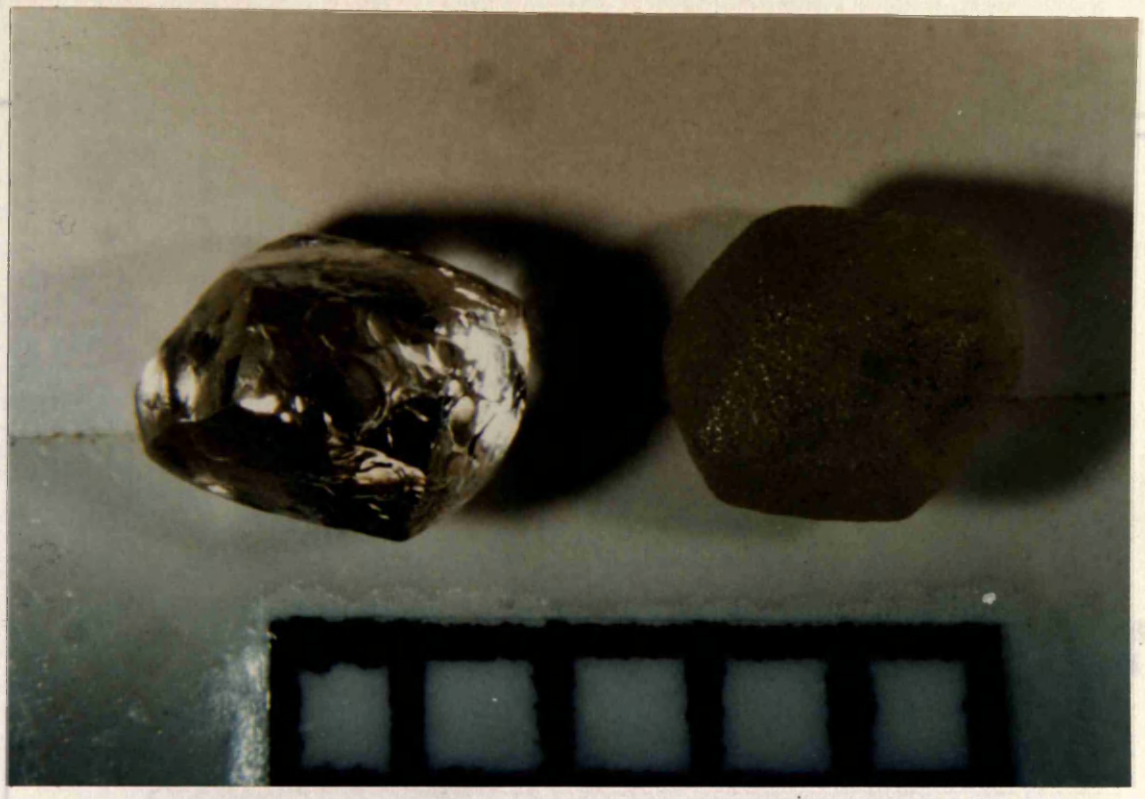

Fig. 5.33 A dodecahedron covered in a microdisk pattern (left) and a second dodecahedron exhibiting coarse frosting (right). From the **grey unit**, site 20. Scale 10 cm.

Fig. 5.34 A close-up of coarse frosting on a dodecahedron from the grey unit, site 21. Sieve size -15 +13. Magnification (x10).

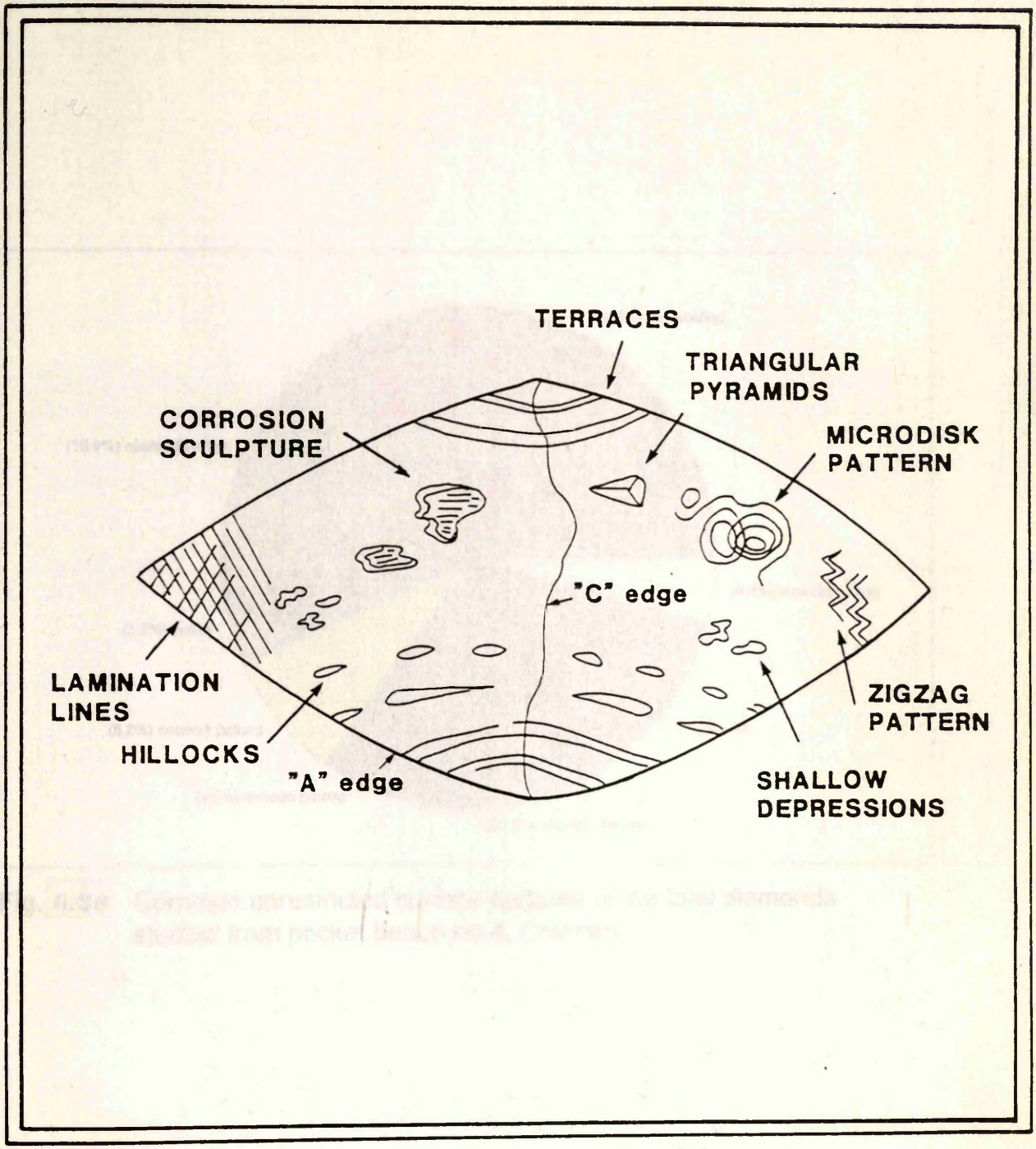

Fig. 5.35 Schematic diagram showing common surface textures on a dodecahedron face (after Robinson, 1979).

Fig 5

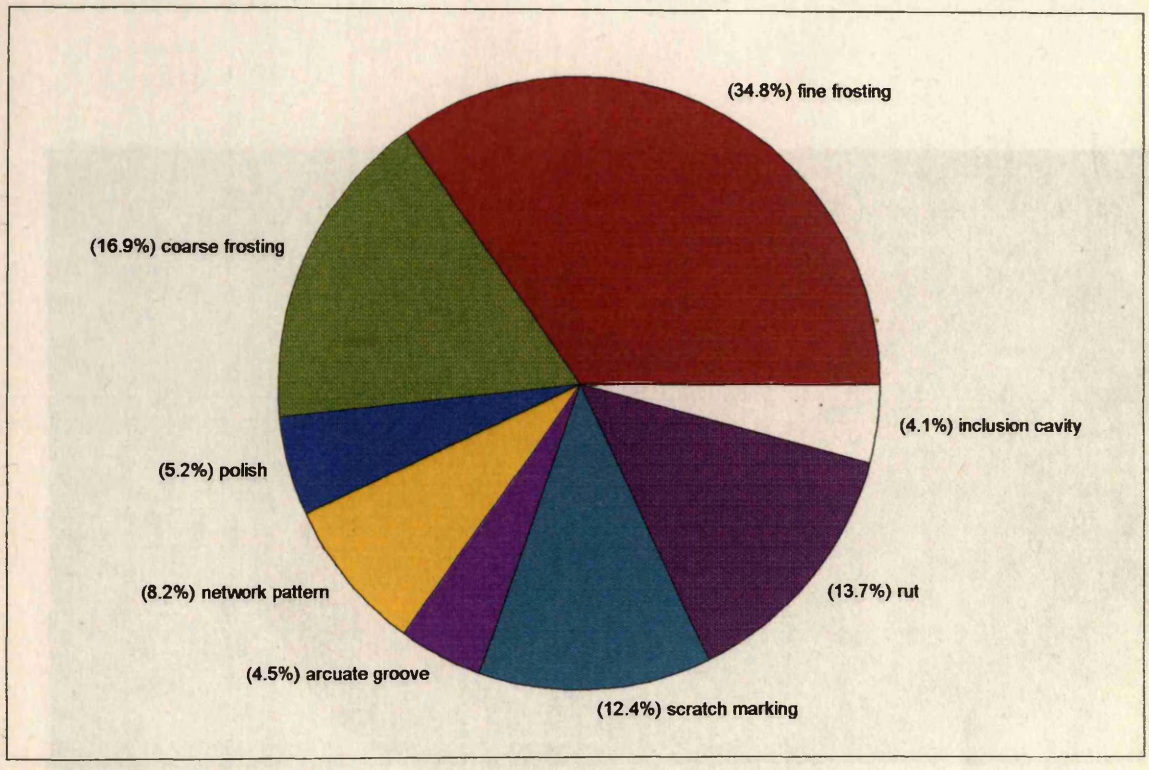

Fig. **5.36** Common unrestricted surface textures of the total diamonds studied from pocket beach no.4, Chameis.

Fig. 5.37 A strongly abraded cubododecahedron with a fine network pattern associated with percussions, from the **grey unit**, site 20. Size ± 1.5 cts/stn.

Fig. 5.38 Scratchlike markings and strong abrasion on a dodecahedron from the **grey unit**, site 21. Sieve size -15+13. Magnification (x10).

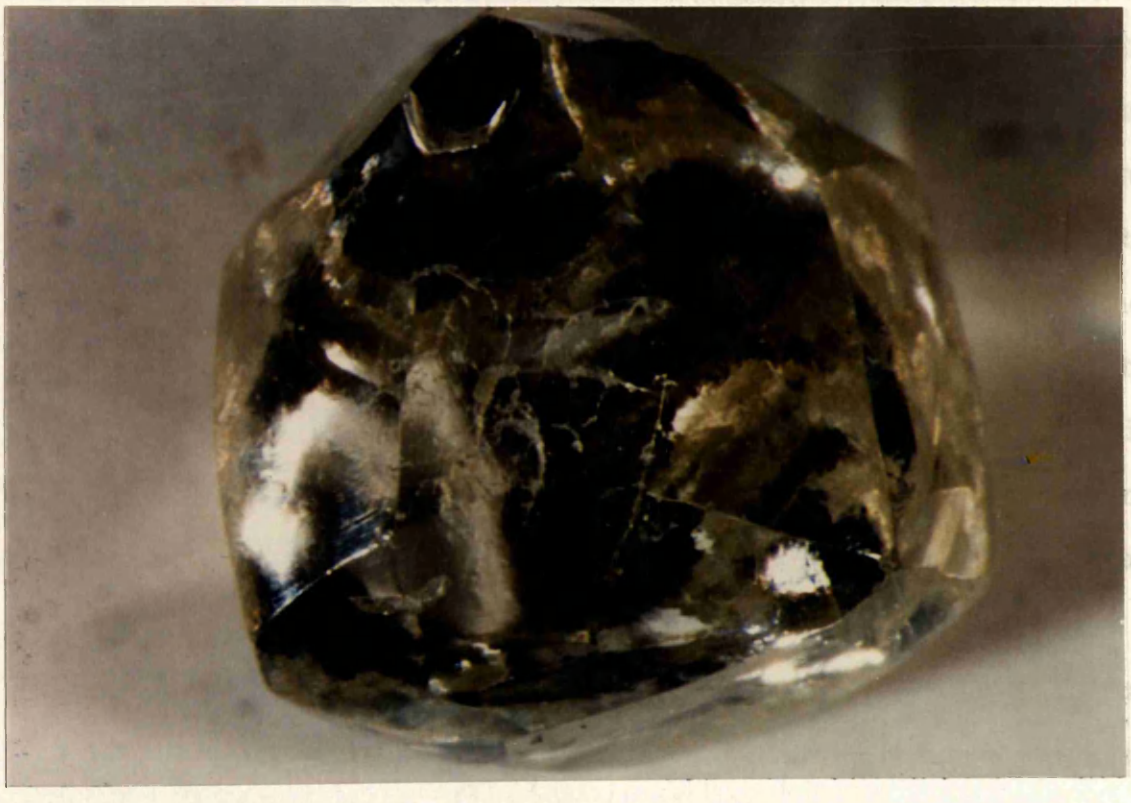

Fig. 5.39 Large percussions, an inclusion cavity (top centre) and slight polish on a dodecahedron from the **grey unit**, site 21. Size ± 1.5 cts/stn. Magnification (x10).

Fig. 5.40 shows that 49.7% of the total diamonds studied are unabraded. The remaining 50.3% having abraded edges and corners. The edges of diamonds are further subdivided into a "C" edge and an "A" edge. The relative positions of these edges on a dodecahedral diamond crystal are also illustrated in Fig. 5.35. In Fig. 5.40, diamonds are also subdivided into those that have only their sharp points abraded and those that have both their points and sharp edges abraded. Percussions as can be seen from Fig. 5.41 are very common, with only 23.5% of the diamonds showing no percussions. Large percussions predominate (40.6%), while 18.2% of the Chameis diamonds show at least a few small percussions. Fig. 5.42 shows an example of a diamond that has both "A" and "C" edges abraded, as well as, sharp points and edges. In Fig. 5.43 all edges of the diamond are abraded and it also shows a slight polish, discussed in the preceding section. Examples of numerous large percussions, as well as, scratch markings can be seen in Fig. 5.44 on this strongly abraded diamond. Fig. 5.45 shows a single large percussion running across the diamond crystal. The abrasion of diamonds around their edges and sharp points result from general wear, while percussions are impact scars from heavy blows. These features are created when diamonds are subjected to prolonged turbulence during transportation in fluviatile or marine environments. In Fig. 5.46, the degree of abrasion of individual Chameis diamonds vary as a function of their size and indicates that the larger diamonds are generally more prone to the effects of abrasion. Variable response to abrasion by different diamond size populations is apparently also known from other alluvial diamond sources (Sutherland, 1982). Robinson (1979) from a study of Orange River terrace diamonds, reported that 70% of the diamonds are unabraded. The degree of abrasion may therefore be a function of distance travelled from a primary kimberlite or lamproite source consistent with the widely held view that these

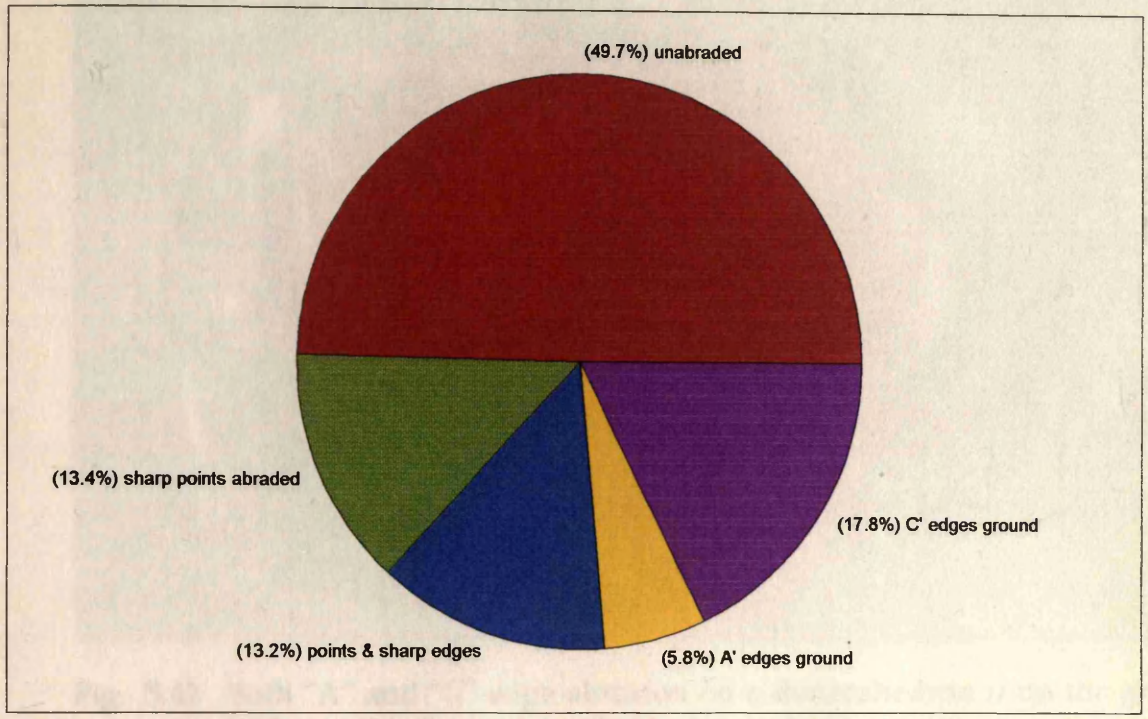

Fig. **5.40** Degree of abrasion of the total diamonds studied from pocket beach no.4, Chameis.

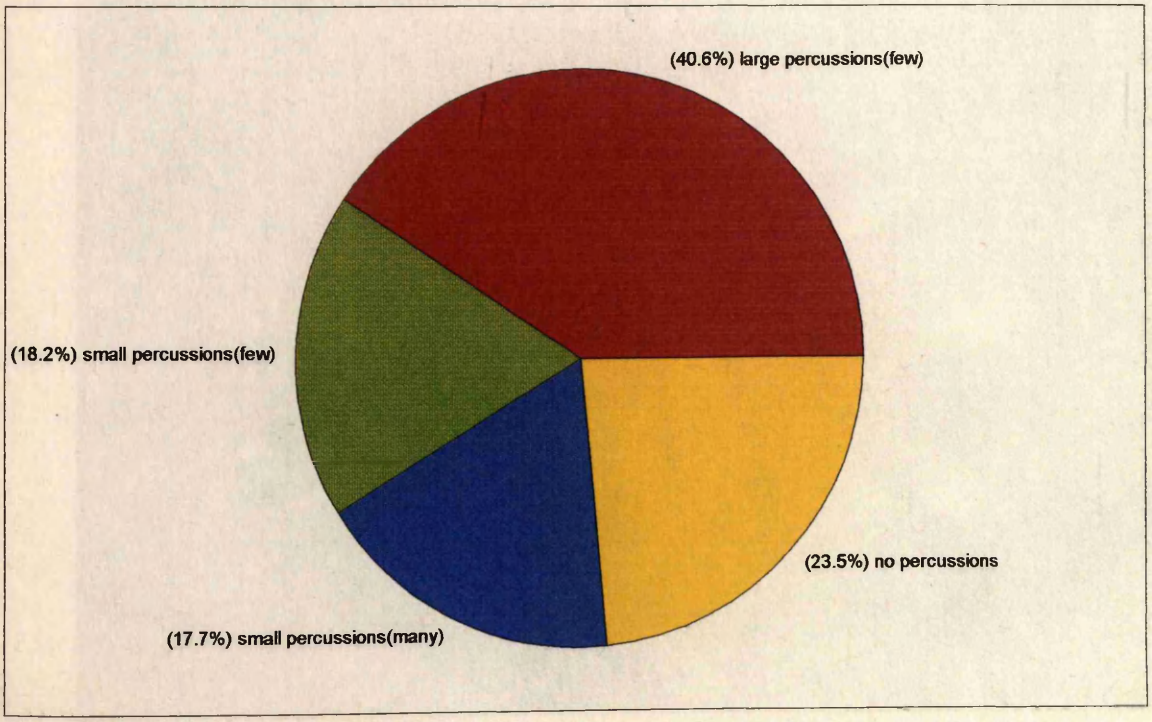

Fig. **5.41** Percussions on the total diamonds studied from pocket beach no.4, Chameis.

Fig. 5.42 Both "A" and "C" edge abrasion on a dodecahedron from the **grey unit**, site 21. Sieve size -15+13. Magnification (x13).

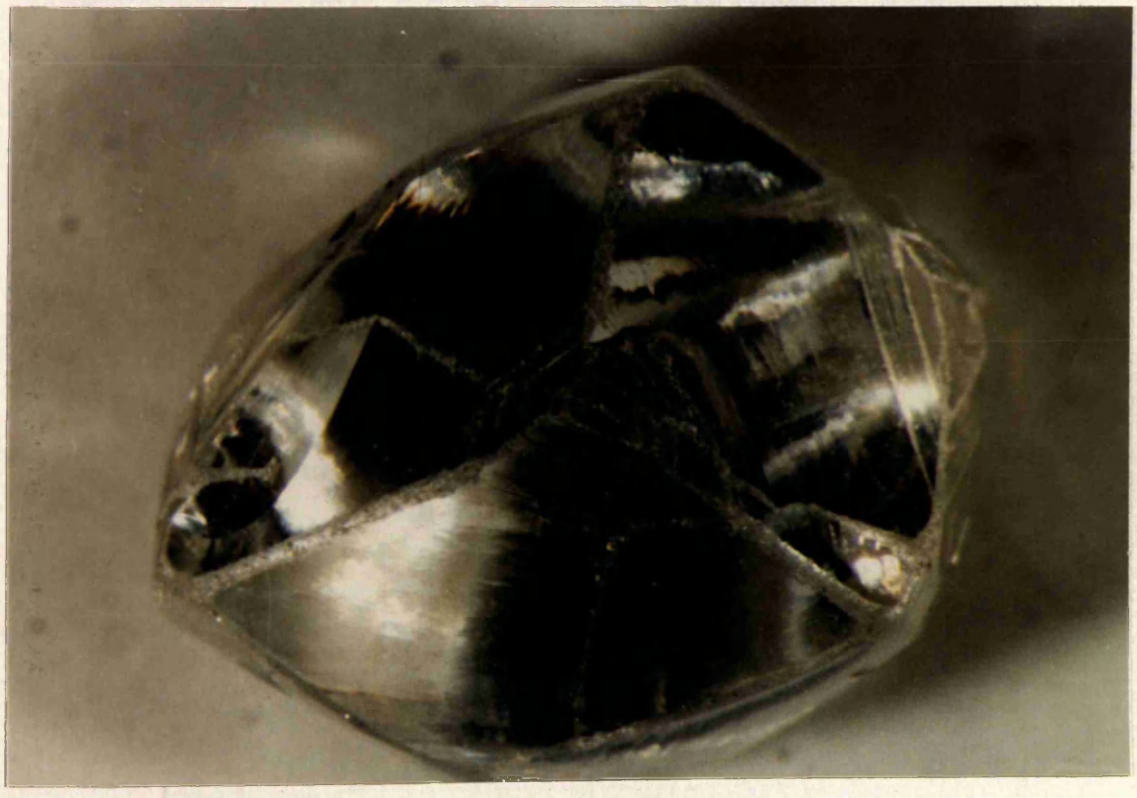

Fig. 5.43 A slightly polished dodecahedron with all edges abraded, from the **grey unit**, site 21. Magnification (x11).

Fig. 5.44 Large percussions, and scratch markings, on a strongly abraded diamond from the **grey unit**, site 20. Magnification (x11).

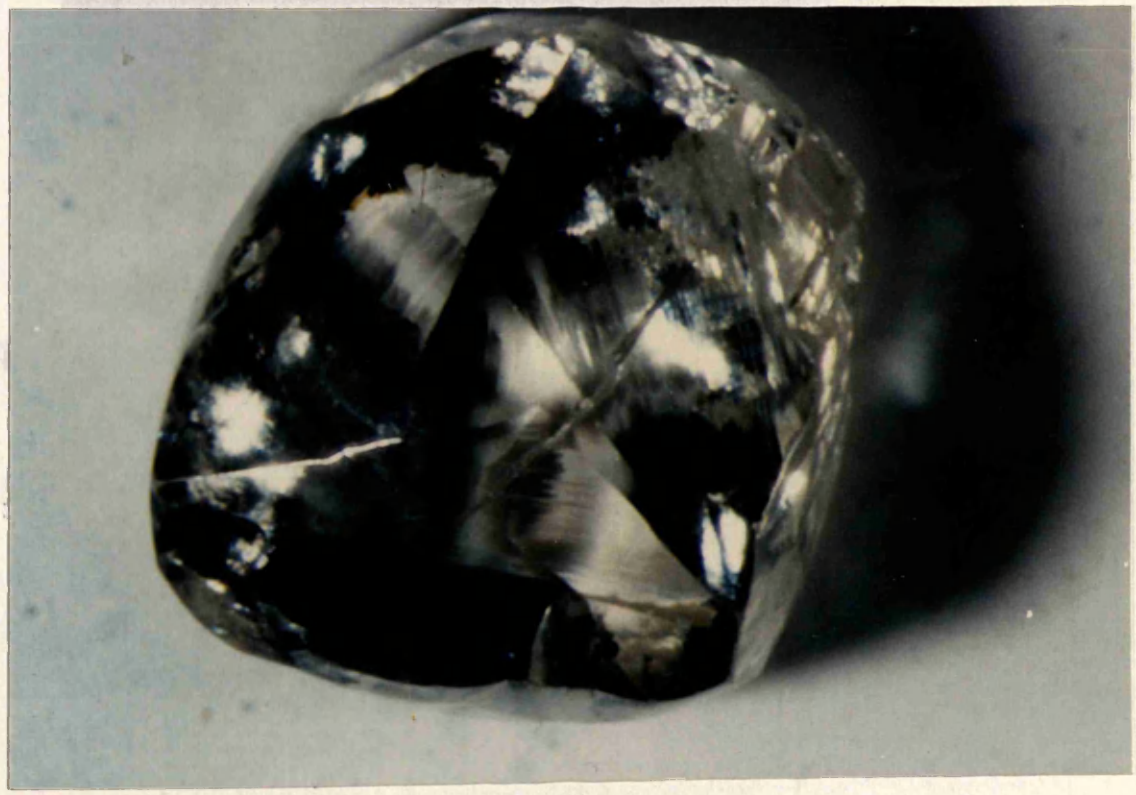

Fig. 5.45 A large percussion, on a slightly polished diamond from the **grey unit**, site 21. Size ± 1.5 cts/stn. Magnification (x10).

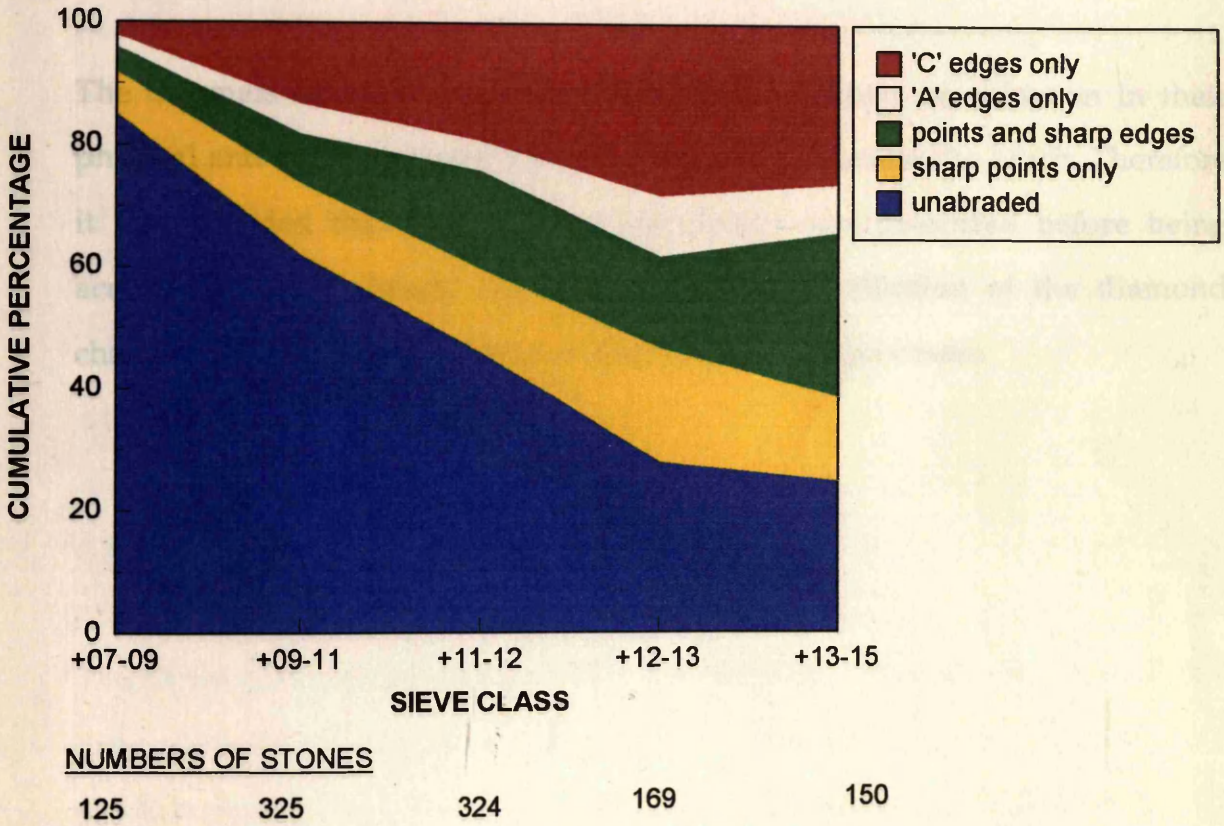

Fig. **5.46** The abrasion characteristics of total diamonds studied relative to their size, from pocket beach no.4, Chameis.

diamonds were transported to the Atlantic Ocean by the Orange River, and then to Chameis by longshore drift. A more systematic study of the diamonds all along the perceived course travelled by Namibian diamonds would however have to be carried out to confirm this.

5.4 CONCLUSION

The Chameis diamond population studied here shows no variation in their physical and abrasion characteristics either along or across the beach. Therefore it is concluded that this diamond population was presorted before being accreted onto the beach, and that the lateral distribution of the diamond characteristics was independent of local sedimentary processes.

CHAPTER 6 CONCLUSIONS

6.1 GROWTH OF BEACHES

Gravel beaches are poorly developed in this area which is at the distal end of a major dispersal system beginning at the mouth of the Orange River. The sediments which make up these beaches are predominantly supplied by local sources as well as from the regional dispersal system, and both transgressive and progradational beaches have low preservation potential as a consequence of the relatively low sediment supply. The beaches in the study area record the events of a major regressive phase which began at c. 120 000 BP and which was followed by a period of subaerial exposure and then by a much younger beach accretion phase at c. 5 000 BP.

6.2 SHORE PLATFORM

The shore platform record is a far more complex erosional history than had previously been recognized. Detailing this history, however has not been possible, but the complexity in the shore platform profile is clearly seen.

6.3 SOURCE OF DIAMONDS

Fom the study of Chameis diamond characteristics the following is deduced:

(1) The frequencies of occurrence of the diamond characteristics are independent of the sedimentary beach accretion processes in the study area.

(2) The incidences of occurrence of most characteristics observed are consistent with the general patterns reported from other alluvial diamond populations of

the west coast of southern Africa, suggesting at least a broadly similar origin on the Kaapvaal craton.

(3) The diamond size frequency diagram shows a limited distribution of sizes, and clearly these diamonds have been size-sorted along the beach system to the south prior to their arrival and deposition at Chameis.

6.4 ENTRAPMENT MECHANISMS FOR DIAMOND

(1) Other things being equal (rate of sediment supply, sea-level rise, etc.), diamonds concentrate best in intertidal Eemian in age beach facies on the northern side of southwest-facing pocket beaches of the Atlantic coast of the Sperrgebiet. These beaches themselves therefore contain appreciable diamonds and do not necessarily need shore platform trapsites, however they are likely to be poorly preserved in the stratigraphic record.

(2) Diamonds in these intertidal deposits do not necessarily gravitate to the bottom of the marine gravel sequence contrary to the widely accepted view, but may also be distributed uniformly throughout the marine gravel, subject to the sedimentary processes operating.

(3) The grain size of the gravel appears to be secondary in importance to processes of beach accretion in the concentration of diamonds in the intertidal beach facies and their associated wave energy levels.

(4) There appears to be a direct relationship between wave energy and the concentration of diamonds in the red unit beach deposits.

(5) In Holocene sediments, maximum diamond concentration is in the subtidal facies of areas with the highest density of gullies resulting from the preponderance of bedrock structural weaknesses. Therefore there appears to be a hierachical arrangement of the most important factors influencing the development of optimum trapsites at a particular locality. The rank of

importance of these factors is not always clear from the field evidence available.

(6) Shore platform morphology is highly dependent on local conditions of which bedrock geology, rate of sea-level change and wave intensity appear to be the most important, and therefore the assumption that there is a direct relationship between the heights of the shore platforms of the study area and the heights of other shore platforms within the region, is not necessarily true.

6.4 SUGGESTIONS FOR FUTURE WORK

Several questions not answered here have either arisen as a result of this study or the need for further work in some of the areas discussed below has been highlighted.

(1) The reason for the scarcity of the Orange River derived distinctive exotic suite in the red unit gravels compared to their overwhelming abundance in the grey unit at Chameis may be a significant indicator of where the diamonds in this unit were derived from. It may therefore also link these sediments to a time when very few of these exotic clasts were either transported down to the coast or along the coast. Therefore it is suggested that similar age deposits from a different locality in the Sperrgebiet be examined for possible compositional similarities.

(2) The detailed analysis of shore platform heights and the factors that are most likely to have influenced their morphology locally, from different areas in the Sperrgebiet may throw some light on how they form and provide further evidence for the sea-level history of the west coast of Namibia.

(3) A systematic detailed study of the physical characteristics and surface

features of statistically representative populations of diamonds from different placer deposits in the Sperrgebiet as well as from the offshore is suggested, to establish if these diamonds are at least broadly of similar origin.

REFERENCES

Aguirre, E. and Pasini, G. (1985). The Pliocene - Pleistocene boundary. Episodes, **8(2)**, 116-120.

American Geological Institute (1972). Glossary of Geology and related Sciences.

Beard, J.H., Sangree, J.B. and Smith, L.A. (1982). Quaternary chronology, palaeoclimate, depositional sequences and eustatic cycles. The American Association of Petroleum Geologists Bulletin, **66(2)**, 158-169.

Beetz, W. (1926). Die Tertiarablagerungen der Kustennamib. In: Kaiser, E., (Ed.) Die Diamantenwuste Sudwestafricas, **2**, 1-54. Dietrich Reimer, Berlin.

Bird, E.C.F. (1984). Coasts, 3nd edn. pp. 282. Australian National University Press, Canberra.

Bluck, B.J. (1967). Sedimentation of beach gravels: examples from South Wales. Journal of Sedimentary Petrology, **37**, 128-156.

Bluck, B.J. (1969). Particle rounding in beach gravels. Geological Magazine, **106**, 1-14.

Briggs, D.J. (1977). Sources and methods in geography. pp.190. Butterworth and Co. (Publishers) Ltd, London.

Carr, A.P. (1969). Size grading along the pebble beach: Chesil Beach, England. Journal of Sedimentary Petrology, **39**, 297-311.

Carr, A.P. (1971). Experiments on longshore transport and sorting of pebbles. Journal of Sedimentary Petrology, **41**, 1084-1104.

Censier, C. and Tourenq, J. (1995). Crystal forms and surface textures of alluvial diamonds from the Western Region of the Central African Republic. Mineralium Deposita, **30**, 314-322.

Clifton, H.E. (1969). Beach lamination: nature and origin. Marine Geology, **7**, 553-559.

Clifton, H.E., Hunter, R.E. and Phillips, R.L. (1971). Depositional structures and processes in the non-barred high-energy nearshore. Journal of Sedimentary Petrology, **41**, 651-670.

Coetzee, J.A. (1978). Climatic and biological changes in south-western Africa during the Late Cainozoic. Palaeoecology of Africa, **10**, 13-29.

Conybeare, C.E.B. and Crook, K.A.W. (1968). Manual of sedimentary structures. pp.327. Bureau of Mineral Resources, Geology and Geophysics, Canberra A.C.T., Bulletin no. **102**.

Corvinus, G. (1983). The raised beaches of CDM on the west coast of South West Africa/Namibia. Verlag C.H. Beck, Munich: 1-108.

Cotton, C.A. (1963). Levels of planation of marine benches. Zeitschrift fur Geomorphologie, **7**, 97-110.

CSIR (1995). CCGT Project- Oranjemund, Namibia.

Davies, J.L. (1964). A morphogenic approach to world shorelines. Zeitschrift fur Geomorphologie, **8**, 127-142.

Davies, O. (1973). Pleistocene shorelines in the westen Cape and South West Africa. Annals of Natal Museum, **21(3)**, 719-765.

Davis, R.A. Jr. and Ethington, R.L.(Eds.) (1976). Beach and Nearshore Sedimentation. pp.187. Society of Economic Palaeontologists and Mineralogists Special Publication, **24**, Tulsa.

Davis, R.A. Jr. (Ed.) (1985). Coastal Sedimentary Environments. pp.420. Springer - Verlag, New York.

Davis, R.A. Jr. and Clifton, H.E. (1987). Sea-level change and the preservation potential of wave-dominated and tide-dominated coastal sequences. In: Nummedal, D., Pilkey, O.H. and Howard, J.D., (Eds.) Sea-level fluctuation and coastal evolution. Society of Economic Palaeontologists and Mineralogists Special Publication, **41**, 167-178. Tulsa.

de Decker, R.H. (1988). The wave regime on the inner shelf south of the Orange River and its implications for sediment transport. South African Journal of Geology, **91(3)**, 358-371.

de Wit, M.C.J. (1993). Cainozoic evolution of drainage systems in the north-western Cape. Unpublished PhD thesis.pp.371. University of Cape Town.

Deacon, H.J. (1983). Another Look at the Pleistocene Climates of Southern Africa. South African Journal of Science, **79**, 325-328.

Dingle, R.V. and Scrutton, R.A. (1974). Continental Break-up and the Development of Post-Paleozoic Sedimentary Basins around Southern Africa. Geological Society of America Bulletin, **85**, 1467-1474.

Dingle, R.V., Siesser, W.G. and Newton, A.R. (1983). Mesozoic and Tertiary Geology of Southern Africa. pp.375. Balkema, Rotterdam.

Dupre, W.R. (1984). Reconstruction of palaeo-wave conditions during the Late Pleistocene from marine terrace deposits, Monterey Bay, California. In: Greenwood, B. and Davis, R.A. Jr., (Eds) Hydrodynamics and sedimentation in wave-dominated coastal environments. Marine Geology, **60**, 435-454.

Elliot, T. (1978). Clastic Shorelines. In Reading, H.G.(Ed.), Sedimentary Environments and Facies: Blackwell Scientific Publications, 143-177.

Elliot, I.G. and Clarke, D.J. (1986). Minor storm impact on the beachface of a sheltered sandy beach. Marine Geology, **73**, 61-83.

Emery, K.O. (1953). Grain size of marine beach gravels. Contribution of the Allan Hancock Foundation, no. **137**, 34-49.

Flemming, N.C. (1964). Form and relation to present sealevel of Pleistocene marine erosion features. Journal of Geology, **73**, 799-811.

Folk, R.L. and Ward, W.C. (1957). Brazos River bar: a study in the significance of grain-size parameters. Journal of Sedimentary Petrology, **27**, 3-26.

Folk, R.L. (1964). A review of grain-size parameters. Sedimentology, **6**, 73-93.

Forbes, D.L., Taylor, R.B., Orford, J.D., Carter, R.W.G. and Shaw, J. (1991). Gravel barrier migration and overstepping. Marine Geology, **97**, 305-313.

Frimmel, H.E. and Hartnady, C.J.H. (1992). Blue amphiboles and their significance for the metamorphic history of the Pan-African Gariep belt, Namibia. Journal of Metamorphic Geology, **10**, 651-669.

Frimmel, H.E. (1995). Metamorphic evolution of the Gariep Belt. South African Journal of Geology, **98(2)**, in press.

Gill, E.D. (1972). The relationship of present shore platforms to past sea-levels. Boreas, **1**, 1-25.

Greenman, L. (1964). The Geology of a portion of Chameis Bay, S.W.A. CDM Internal Report and Map 1-43.

Gurney, J.J. (1993). The diamondiferous roots of our wandering continent. South African Journal of Geology, **93(3)**, 424-437.

Hallam, C.D. (1964). The Geology of the coastal diamond deposits of Southern Africa. In: Haughton, S.H., (Ed.) The Geology of some Ore Deposits in Southern Africa. Geological Society of South Africa, pp. 671-728.

Hansom, J.D. (1983). Shore platform development in the South Shetland Islands, Antactica. Marine Geology, **53**, 211-229.

Harris, J.W., Hawthorne, J.B., Oosterveld, M.M. and Wehmeyer, E. (1975). A classification scheme for diamond and a comparitive study of South African diamond characteristics. Physics and Chemistry of the Earth, **9**, 765-784.

Harris, J.W. (1992). Diamond Geology. In: Field J.E.(Ed.) The Physical Properties of Natural and Synthetic Diamonds. Academic Press, London.

Haughton, S.H. (1931). Notes on the Occurrence of Upper Cretaceous Marine Beds in South West Africa. Transactions of the Geological Society of South Africa, **33**, 61-65.

Heller, P.L., Burns, B.A. and Marzo, M. (1993). Stratigraphic solution sets for determining the roles of sediment supply, subsidence, and sea-level on transgressions and regressions. Geology, **21**, 747-750.

Hendey, Q.B. (1981). Geological Succession at Langebaanweg, Cape Province, and Global Events of the Late Tertiary. South African Journal of Science, **77**, 33-38.

Hendey, Q.B. and Cooke, H.B.S. (1985). *Kolpochoerus paiceae* (Mammalia, Suidae) from Skurwerug, near Saldanha, South Africa, and its palaeo-environmental implications. Annals of the South African Museum, **97**, 9-56.

Higgs, R. (1979). Quartz-grain surface features of the Mesozoic-Cenozoic sands from the Labrador and western Greenland continental margins. Journal of Sedimentary Petrology, **49**, 599-610.

Hobday, D.K. and Banks, N.L. (1970). A coarse-grained pocket beach complex, Tanafjord (Norway). Sedimentology, **16**, 129-134.

Humbert, F.L. (1968). Selection and Wear of Pebbles on Gravel Beaches. pp.144. Geologisch Instituut, Groningen.

Imbrie, J. (1985). A theoretical framework for the Pleistocene ice ages. Journal of the Geological Society of London, **142**, 417-432.

Kaiser, E. (1926). Die Diamantenwüste Südwestafrikas, I. pp.321. Dietrich Reimer, Berlin.

Kensley, B. and Pether, J. (1986). Late Tertiary and early Quaternary fossil mollusca of the Hondeklip area, Cape Province, South Africa. Annals of the South African Museum, **97(6)**, 141-225.

King, C.A.M. (1972). Beaches and Coasts. pp.570. Edward Arnold, London.

Kirk, R.M. (1975). Aspects of surf and run-up processes on mixed sand and gravel beaches. Geografiska Annaler, **57A**, 117-133.

Komar, P.D. (1971b). The mechanics of sand transport on gravel beaches. Journal of Geophysical Research, **76**, 713-721.

Komar, P.D. (1976). Beach Processes and Sedimentation. Prentice Hall, Trenton, New Jersey.

Kraft, J.C. (1971). Sedimentary facies patterns and geologic history of a Holocene marine transgression. Geological Society of America Bulletin, **82**, 2131-2158.

Krumbein, W.C. (1941). Measurement and geological significance of shape and roundness of sedimentary particles. Journal of Sedimentary Petrology, **11**, 64-72.

Lancaster, N. and Ollier, C.D. (1983). Sources of sand for the Namib sand sea. Zeitschrift fur Geomorphologie, **45**, 71-83.

Larson, M. and Sunamura, T. (1993). Laboratory experiment of flow characteristics at a beach step. Journal of Sedimentary Petrology, **63(3)**, 495-500.

Lindholm, R.C. (1987). A practical approach to Sedimentology. pp.276. Allen & Unwin, London.

Martin, H. (1973). Palaeozoic, Mesozoic and Cenozoic deposits on the coast of South West Africa. In: Blant, G., (Ed.) Sedimentary Basins of the African Coasts, Part 2 south and east coast, Paris, Association of African Geological Surveys, 7-15.

Massari, F. and Parea, G.C. (1988). Progradational gravel beach sequences in a moderate - to high - energy, microtidal marine environment. Sedimentology, **35**, 881-913.

McCubbin, D.G. (1982). Barrier-Island and Strand-Plain Facies. In: Scholle, P.A. and Spearing, D., (Eds.) Sandstone Depositional Environments. The American Association of Petroleum Geologists, 247-279. Tulsa.

Merensky, H. (1909). The Diamond Deposits of Lüderitzland, German South West Africa. Transactions of the Geological Society of South Africa, **12**, 13-23.

Miller, A.A. (1939b). Attainable standards of accuracy in the determination of periglacial sea-levels by physiographic methods. Journal of Geomorphology, **2**, 95-115.

Mitchell, R.H. (1986). Kimberlites. pp.442. Plenum Press, New York.

Miyashiro, A. (1994). Metamorphic Petrology. pp.404. University College London Press, London.

Murray, L.G., Joynt, R.H. O'Shea, D.O.C., Foster, R.W., and Kleinjan, L. (1970). The geological environment of some diamond deposits off the coast of South West Africa. In: Delany, F.M., (Ed.) The geology of the East Atlantic continental margin. Report of the Institute of geological Science, **70**, 119-141.

Nordstrom, C.E. and Margolis, S.V. (1972). Sedimentary history of central California shelf sands as revealed by scanning electron microscopy. Journal of Sedimentary Petrology, **42**, 527-536.

Nordstrom, K.F. (1977). The use of grain size statistics to distinguish between high- and moderate-energy beach environments. Journal of Sedimentary Petrology, **47 (3)**, 1287-1294.

Orford, J.D. (1975). Discrimination of particle zonation on a pebble beach. Sedimentology, **22**, 441-463.

Orford, J.D. (1977). A proposed mechanism for storm beach sedimentation. Earth Surface Processes, **2**, 381-400.

Orford, J.D., Carter, R.W.G. and Jennings, S.C. (1991). Coarse clastic barrier environments: evolution and implications for quaternary sealevel interpretation. Quaternary International, **9**, 87-104.

Partridge, T.C. and Maud, R.R (1987). Geomorphic evolution of southern Africa since the Mesozoic. South African Journal of Geology, **90(2)**, 179-208.

Pether, J. (1986). Late Tertiary and early Quaternary marine deposits of the Namaqualand coast, Cape Province: new perspectives. South African Journal of Science, **82**, 464-470.

Pethick, J.S.(1984). An introduction to Coastal Geomorphology. pp.260. Edward Arnold, London.

Pettijohn, F.J. (1957). Sedimentary rocks. Harper and Brothers, New York.

Posamentier, H.W., Jervey, M.T. and Vail, P.R. (1988). Eustatic controls on clastic deposition I- Conceptual framework, In Wilgus, C.K., (Ed.) Sea-level changes; an intergrated approach. Society of Economic Palaeontologists and Mineralogists Special Publication, **42**, 109-124.

Postma, G. and Nemec, W. (1990). Regressive and transgressive sequences in a raised Holocene gravelly beach, southwestern Crete. Sedimentology, **37**, 907-920.

Powers M. (1953). A new roundness scale for sedimentary particles. Journal of Sedimentary Petrology, **325**, 117-119.

Ragan, D.M. (1985). Structural geology. An introduction to geometric techniques. pp. 393. Wiley.

Reineck, H.E. and Singh, I.B. (1973). Depositional Sedimentary Environments. pp.439. Springer-Verlag, Berlin.

Reuning, E. (1931). Der Ursprung der Kustendiamanten Süd-und Südwest Africas. Neuen Jahrbuch fur Mineralogie, no. **64**.

Robinson, D.N. (1979). Surface textures and other features of diamonds. Unpublished PhD thesis (vol. 1 & 2). pp.221. University of Cape Town.

Robinson, D.N., Scott, J.A., Van Niekerk, A. and Anderson, V.G. (1989). The sequence of events reflected in the diamonds of some southern African kimberlites. 4th International Kimberlite Conference. Kimberlites and Related Rocks, vol. 2, Geological Society of Australia Special Publication, **14**, 980-990.

Rouffaer, E.J.H.F. (1980). On the origin of alluvial diamonds along the Atlantic coast of South Africa and South West Africa. Unspecified.

Semeniuk, V. and Johnson, D.P. (1985). Modern and Pleistocene rocky shore sequences along carbonate coastlines, southwestern Australia. Sedimentary Geology, **44**, 225-261.

Sherman, D.J., Orford, J.D., and Carter, R.W.G. (1993). Development of cusp-related, gravel size and shape facies at Malin Head, Ireland.Sedimentology, **40**, 1139-1152.

Siesser, W.G. (1980). Late Miocene origin of the Benguela upwelling system off northern Namibia. Science, **208**, 283-285.

Siesser, W.G. and Dingle, R.V. (1981). Tertiary sea-level movements around southern Africa. Journal of Geology, **89**, 523-536.

Simpson, E.S.W. (1977). Evolution of the South Atlantic. Alex du Toit Memorial Lecture No.15, Annexure Transactions of the Geological Society of South Africa, **80**, pp.15.

Sneed, E.D. and Folk, R.L. (1958). Pebbles in the lower Colorado River, Texas, a study in particle morphogenesis. Journal of Geology, **66**, 114-150.

South African Committee for Stratigraphy (SACS) (1980). Stratigraphy of South Africa. Compiled by Kent, L.E., Part 1. Lithostratigraphy of the Republic of South Africa, and Namibia. Handbook of the Geological Survey of South Africa **8**, pp.690.

Stocken, C.G. (1978). A review of the later Mesozoic and Cenozoic deposits of the Sperrgebiet. Unpublised Report, pp.37. Geological Department, CDM.

Summerfield, M.A. (1991). Global Geomorphology. pp.524. John Wiley & Sons, New York.

Sunamura, T. (1975). A laboratory study of wave-cut platform formation. Journal of Geology, **83**, 389-397.

Sunamura, T. (1983). Processes of Sea Cliff and Platform Erosion. In Komar, P.D. and Moore, J.R., (Eds.) Handbook of Coastal Processes and Erosion. pp.305. CRC Press, Florida.

Sunamura, T. (1992). Geomorphology of Rocky Coasts. pp.302. John Wiley & Sons, Chichester.

Sutherland, D.G. (1982). The transport and sorting of diamonds by fluvial and marine processes. Economic Geology, **77(7)**, 1613-1620.

Swift, D.J.P., Figueiredo, A.G.Jr., Freeland, G.L. and Oertel, G.F. (1983). Hummocky cross-stratification and megaripples: a geological double standard? Journal of Sedimentary Petrology, **53**, 1295-1317.

Tacier, J.D. (1967). Bedrock morphology and diamond distribution at 81-84H, Affenrucken. Oceanographic Research Unit, 1-3.

Tankard, A.J. (1975). Cenozoic sea-level changes: a discussion. Annals of the South African Museum, 1-17.

Tankard, A.J., Jackson, M.P.A., Eriksson, K.A., Hobday, D.K., Hunter, F.T. and Minter, W.E.L. (1982). Crustal evolution of Southern Africa: 3.8 Billion years of Earth History. pp. 523. Springer-Verlag, Berlin.

Trenhaile, A.S. (1980). Shore platforms: a neglected coastal feature. Progress in Physical Geography, **4**, 1-23.

Trenhaile, A.S. and Bryne, L-M. (1986). A theoretical investigation of the Holocene development of rock coasts, with particular reference to shore platforms. Geografiska Annaler, **68A**, 1-14.

Trenhaile, A.S.(1987). The Geomorphology of Rocky Coasts. pp.384. Clarendon Press, Oxford.

Trenhaile, A.S. (1989). Sea-level oscillations and the development of rock coasts. In: Lakhan,V.C. and Trenhaile, A.S., (Eds.) Applications in Coastal Modeling, 271-295. Elsevier, Amsterdam.

Vail, P.R. and Hardenbol, J. (1979). Sea-level changes during the Tertiary. Oceanus, **22**, 71-79.

Vance, E. R., Harris, J.W. and Milledge, H.J. (1973). Possible origins of alpha-particle damage in diamonds from kimberlites and alluvial sources. Mineralogical Magazine, **39**, 349-360.

Wadell, H. (1932). Volume, shape and roundness of rock particles. Journal of Geology, **40**, 443-451.

Wagner, P.A. (1914). The diamond fields of Southern Africa. pp.347. The Transvaal Leader.

Walker, T.R., Waugh, B. and Crone, A.J. (1978). Diagenesis in first-cycle desert alluvium of Cenozoic age, southwestern United States and northwestern Mexico. Bulletin of the Geological Society of America, **89**, 19-32.

Ward, J.D., Seely, M.K. and Lancaster, N. and (1983). On the antiquity of the Namib. South African Journal of Science, **79**, 175-183.

Ward, J.D. and Corbett, I. (1990). Towards an Age for the Namib. In: Seely, M.K., (Ed.) Namib ecology: 25 years of Namib research, Transvaal Museum Monograph, no.**7**, 17-26.

Williams, A.T. and Caldwell, N.E. (1988). Particle size and shape in pebble-beach sedimentation. Marine Geology, **82**, 199-215.

Williams, D.F., Willard, S.M. and Fillon, R.H. (1981). Role of glacial Arctic Ocean ice sheets in Pleistocene oxygen isotope and sea-level records. Earth and Planetary Science Letters, **56**, 157-166.

Woods, A.J. (1980). Geomorphology, deformation, and chronology of marine terraces along the Pacific coast of central Baja California, Mexico. Quaternary Research, **13**, 346-364.

Wright, J.A. (1964). Gully pattern and development in wave-cut bedrock shelves north of the Orange River mouth, S.W.A. Transactions of the Geological Society of South Africa, **67**, 163-171.

Zenkovitch, V.P. (1949). Some factors in the formation of marine terraces. Dokl. Acad. Nauk. SSSR., **65**, 53-55.

Zenkovitch, V.P. (1967). Processes of Coastal Development. pp.738. Oliver and Boyd, Edinburgh.

Zingg, T. (1935). Beitrage zur Schott eranalyse. Schweizerische Mineralogisch-Petrographische Mitteilungen, **15**, 39-140.

APPENDICES

Table: AI.A CLAST SIZE, SHAPE AND COMPOSITION

SITE 14

obs	mean	a-axis	b-axis	c-axis	b/a	c/b	clasttype	shape	sphindex
1	66.00	120	48	30	0.40	0.63	vein quartz	blade	0.464
2	34.33	47	40	16	0.85	0.40	vein quartz	disc	0.662
3	83.67	120	76	55	0.63	0.72	vein quartz	rod	0.662
4	61.00	88	60	35	0.68	0.58	vein quartz	disc	0.647
5	87.33	110	80	72	0.73	0.90	quartzite	sphere	0.781
6	78.33	108	80	47	0.74	0.59	gneiss	disc	0.686
7	95.33	182	80	24	0.44	0.30	schist	blade	0.387
8	91.67	125	86	64	0.69	0.74	vein quartz	sphere	0.706
9	65.33	134	36	26	0.27	0.72	schist	rod	0.374
10	26.00	47	19	12	0.40	0.63	quartzite	blade	0.469
11	63.33	70	60	60	0.86	1.00	silcrete	sphere	0.902
12	143.33	220	155	55	0.70	0.35	quartzite	disc	0.561
13	73.33	100	85	35	0.85	0.41	quartzite	disc	0.668
14	22.67	35	18	15	0.51	0.83	vein quartz	rod	0.604
15	178.33	250	160	125	0.64	0.78	quartzite	rod	0.684
16	30.33	38	33	20	0.87	0.61	vein quartz	disc	0.770
17	146.67	215	140	85	0.65	0.61	quartzite	blade	0.636
18	18.67	27	19	10	0.70	0.53	quartzite	disc	0.639
19	226.67	285	265	130	0.93	0.49	quartzite	disc	0.751
20	51.00	60	50	43	0.83	0.86	vein quartz	sphere	0.842
21	116.67	170	130	50	0.76	0.38	quartzite	disc	0.608
22	32.00	37	30	29	0.81	0.97	vein quartz	sphere	0.860
23	102.00	160	90	56	0.56	0.62	quartzite	blade	0.582
24	46.00	70	48	20	0.69	0.42	quartzite	disc	0.581
25	128.33	200	135	50	0.68	0.37	quartzite	disc	0.553
26	33.33	52	26	22	0.50	0.85	silcrete	rod	0.596
27	178.33	255	170	110	0.67	0.65	quartzite	disc	0.660
28	211.67	270	205	160	0.76	0.78	quartzite	sphere	0.766
29	101.67	170	90	45	0.53	0.50	quartzite	blade	0.519
30	78.33	105	88	42	0.84	0.48	quartzite	disc	0.695
31	135.67	170	160	77	0.94	0.48	silcrete	disc	0.753
32	76.67	100	85	45	0.85	0.53	silcrete	disc	0.726
33	25.00	35	25	15	0.71	0.60	vein quartz	disc	0.674
34	13.33	19	12	9	0.63	0.75	vein quartz	rod	0.669
35	84.33	125	85	43	0.68	0.51	quartzite	disc	0.616
36	77.67	105	83	45	0.79	0.54	quartzite	disc	0.697
37	91.33	129	100	45	0.78	0.45	quartzite	disc	0.647
38	75.00	123	58	44	0.47	0.76	quartzite	rod	0.553
39	56.33	70	66	33	0.94	0.50	quartzite	disc	0.763
40	50.00	65	57	28	0.88	0.49	silcrete	disc	0.723
	83.93								

SITE 12

obs	mean	a-axis	b-axis	c-axis	b/a	c/b	clasttype	shape	sphindex
1	47.67	65	48	30	0.74	0.63	vein quartz	disc	0.699
2	30.67	50	22	20	0.44	0.91	schist	rod	0.560
3	43.33	82	34	14	0.41	0.41	schist	blade	0.414
4	40.33	65	40	16	0.62	0.40	vein quartz	blade	0.533
5	77.00	100	76	55	0.76	0.72	vein quartz	sphere	0.748
6	61.00	88	60	35	0.68	0.58	vein quartz	disc	0.647
7	87.33	110	80	72	0.73	0.90	quartzite	sphere	0.781
8	78.33	108	80	47	0.74	0.59	gneiss	disc	0.686
9	32.33	50	25	22	0.50	0.88	vein quartz	rod	0.604
10	81.67	120	75	50	0.63	0.67	quartzite	rod	0.639
11	95.33	182	80	24	0.44	0.30	schist	blade	0.387
12	77.67	126	64	43	0.51	0.67	schist	rod	0.558
13	65.33	134	36	26	0.27	0.72	schist	rod	0.374
14	26.00	47	19	12	0.40	0.63	quartzite	blade	0.469
15	86.33	120	102	37	0.85	0.36	quartzite	disc	0.640
16	76.67	101	94	35	0.93	0.37	quartzite	disc	0.686
17	105.33	144	118	54	0.82	0.46	silcrete	disc	0.675
18	68.33	116	64	25	0.55	0.39	quartzite	blade	0.492
19	88.00	119	101	44	0.85	0.44	quartzite	disc	0.680
20	89.00	124	119	24	0.96	0.20	schist	disc	0.571
21	73.00	100	65	54	0.65	0.83	vein quartz	rod	0.705
22	118.67	186	110	60	0.59	0.55	schist	blade	0.576
23	73.67	96	72	53	0.75	0.74	vein quartz	sphere	0.745
24	45.67	67	54	16	0.81	0.30	schist	disc	0.577
25	75.67	100	100	27	1.00	0.27	quartzite	disc	0.646
26	69.67	99	68	42	0.69	0.62	vein quartz	disc	0.663
27	128.33	202	119	64	0.59	0.54	silcrete	blade	0.571
28	173.00	267	150	102	0.56	0.68	quartzite	rod	0.599
29	49.33	64	50	34	0.78	0.68	vein quartz	sphere	0.746
30	255.67	368	276	123	0.75	0.45	schist	disc	0.631
31	137.00	231	120	60	0.52	0.50	schist	blade	0.513
32	50.00	56	50	44	0.89	0.88	vein quartz	sphere	0.889
33	83.33	139	85	26	0.61	0.31	quartzite	blade	0.485
34	129.67	217	121	51	0.56	0.42	quartzite	blade	0.508
35	182.00	289	159	98	0.55	0.62	quartzite	blade	0.571
36	61.67	96	69	20	0.72	0.29	quartzite	disc	0.531
37	157.33	288	122	62	0.42	0.51	schist	blade	0.450
38	120.33	181	130	50	0.72	0.38	quartzite	disc	0.583
39	60.00	75	53	52	0.71	0.98	quartzite	sphere	0.788
40	81.67	132	80	33	0.61	0.41	quartzite	blade	0.533
	87.08								

SITE 13

obs	mean	a-axis	b-axis	c-axis	b/a	c/b	clasttype	shape	sphindex
1	266.67	500	200	100	0.40	0.50	schist	blade	0.431
2	83.33	110	90	50	0.82	0.56	silcrete	disc	0.719
3	52.00	74	60	22	0.81	0.37	quartzite	disc	0.622
4	87.33	125	74	63	0.59	0.85	quartzite	rod	0.668
5	127.00	216	130	35	0.60	0.27	schist	blade	0.460
6	26.33	57	14	8	0.25	0.57	schist	blade	0.325
7	50.67	72	55	25	0.76	0.45	quartzite	disc	0.643
8	71.33	110	80	24	0.73	0.30	quartzite	disc	0.541
9	65.67	90	77	30	0.86	0.39	quartzite	disc	0.658
10	14.67	17	15	12	0.88	0.80	vein quartz	sphere	0.854
11	96.33	157	105	27	0.67	0.26	schist	disc	0.486
12	49.33	64	55	29	0.86	0.53	vein quartz	disc	0.730
13	323.33	560	220	190	0.39	0.86	schist	rod	0.511
14	97.67	195	65	33	0.33	0.51	schist	blade	0.384
15	60.33	88	73	20	0.83	0.27	quartzite	disc	0.573
16	125.00	190	145	40	0.76	0.28	schist	disc	0.544
17	34.67	68	27	9	0.40	0.33	schist	blade	0.375
18	44.67	60	47	27	0.78	0.57	quartzite	disc	0.706
19	47.67	65	48	30	0.74	0.63	vein quartz	disc	0.699
20	36.67	57	35	18	0.61	0.51	vein quartz	blade	0.579
21	86.00	135	105	18	0.78	0.17	schist	disc	0.470
22	49.33	75	50	23	0.67	0.46	vein quartz	disc	0.589
23	54.00	95	50	17	0.53	0.34	schist	blade	0.455
24	51.67	75	53	27	0.71	0.51	schist	disc	0.634
25	16.67	27	19	4	0.70	0.21	quartzite	disc	0.471
26	35.00	61	35	9	0.57	0.26	schist	blade	0.439
27	23.33	28	24	18	0.86	0.75	vein quartz	sphere	0.820
28	71.00	128	60	25	0.47	0.42	schist	blade	0.451
29	136.67	170	125	115	0.74	0.92	silcrete	sphere	0.792
30	82.67	110	100	38	0.91	0.38	vein quartz	disc	0.680
31	148.33	215	150	80	0.70	0.53	gneiss	disc	0.638
32	62.33	82	55	50	0.67	0.91	quartzite	sphere	0.742
33	22.00	32	24	10	0.75	0.42	vein quartz	disc	0.617
34	52.33	75	55	27	0.73	0.49	quartzite	disc	0.642
35	177.67	270	163	100	0.60	0.61	quartzite	blade	0.607
36	145.00	255	130	50	0.51	0.38	schist	blade	0.464
37	180.00	265	160	115	0.60	0.72	quartzite	rod	0.640
38	148.33	190	185	70	0.97	0.38	schist	disc	0.711
39	181.67	280	155	110	0.55	0.71	quartzite	rod	0.601
40	150.00	210	125	115	0.60	0.92	schist	rod	0.688
	90.87								

SITE 6

obs	mean	a-axis	b-axis	c-axis	b/a	c/b	clasttype	roundness	shape	sphindex
1	211.00	380	148	105	0.39	0.71	schist	0.49	rod	0.795
2	117.00	182	106	63	0.58	0.59	quartzite	0.49	blade	0.707
3	76.67	97	79	54	0.81	0.68	quartzite	0.49	sphere	0.776
4	87.33	137	82	43	0.60	0.52	vein quartz	0.49	blade	0.650
5	172.00	255	142	119	0.56	0.84	quartzite	0.7	rod	0.889
6	70.00	102	77	31	0.75	0.40	schist	0.35	disc	0.545
7	32.67	48	35	15	0.73	0.43	quartzite	0.7	disc	0.568
8	74.00	113	70	39	0.62	0.56	quartzite	0.35	blade	0.677
9	65.33	103	54	39	0.52	0.72	quartzite	0.7	rod	0.805
10	119.67	205	99	55	0.48	0.56	vein quartz	0.25	blade	0.676
11	15.33	22	15	9	0.68	0.60	vein quartz	0.49	disc	0.711
12	19.33	24	24	10	1.00	0.42	vein quartz	0.49	disc	0.558
13	93.33	156	91	33	0.58	0.36	schist	0.49	blade	0.509
14	46.00	64	56	18	0.88	0.32	quartzite	0.49	disc	0.469
15	17.33	27	16	9	0.59	0.56	vein quartz	0.25	blade	0.681
16	57.00	86	59	26	0.69	0.44	quartzite	0.49	disc	0.579
17	8.00	11	8	5	0.73	0.63	vein quartz	0.7	disc	0.731
18	26.33	47	22	10	0.47	0.45	quartzite	0.7	blade	0.591
19	38.67	59	29	28	0.49	0.97	quartzite	0.7	rod	0.977
20	49.33	75	51	22	0.68	0.43	schist	0.35	disc	0.571
21	39.67	67	35	17	0.52	0.49	vein quartz	0.49	blade	0.618
22	24.33	34	29	10	0.85	0.34	vein quartz	0.7	disc	0.492
23	32.33	43	33	21	0.77	0.64	vein quartz	0.49	disc	0.740
24	30.00	41	29	20	0.71	0.69	vein quartz	0.25	sphere	0.781
25	22.67	37	18	13	0.49	0.72	vein quartz	0.49	rod	0.805
26	22.33	40	17	10	0.43	0.59	quartzite	0.49	blade	0.702
27	20.00	29	21	10	0.72	0.48	vein quartz	0.49	disc	0.610
28	80.33	100	91	50	0.91	0.55	vein quartz	0.49	disc	0.671
29	41.33	52	45	27	0.87	0.60	vein quartz	0.49	disc	0.711
30	51.33	84	48	22	0.57	0.46	quartzite	0.7	blade	0.594
31	42.33	57	42	28	0.74	0.67	vein quartz	0.35	sphere	0.763
32	13.00	18	15	6	0.83	0.40	vein quartz	0.7	disc	0.543
33	73.67	112	84	25	0.75	0.30	schist	0.49	disc	0.446
34	34.67	50	40	14	0.80	0.35	vein quartz	0.49	disc	0.497
35	192.33	290	177	110	0.61	0.62	vein quartz	0.35	blade	0.728
36	108.00	177	111	36	0.63	0.32	schist	0.49	blade	0.472
37	313.67	689	172	80	0.25	0.47	schist	0.25	blade	0.600
38	124.00	200	114	58	0.57	0.51	quartzite	0.7	blade	0.637
39	64.67	93	67	34	0.72	0.51	quartzite	0.7	disc	0.636
40	83.33	99	81	70	0.82	0.86	quartzite	0.7	sphere	0.907
	70.26									

SITE 11

obs	mean	a-axis	b-axis	c-axis	b/a	c/b	clasttype	shape	sphindex
1	138.00	269	106	39	0.39	0.37	schist	blade	0.385
2	95.67	134	83	70	0.62	0.84	quartzite	rod	0.687
3	30.00	39	31	20	0.79	0.65	vein quartz	disc	0.741
4	18.33	28	20	7	0.71	0.35	vein quartz	disc	0.563
5	30.33	35	32	24	0.91	0.75	vein quartz	sphere	0.856
6	42.67	74	42	12	0.57	0.29	schist	blade	0.451
7	30.33	49	22	20	0.45	0.91	vein quartz	rod	0.568
8	9.33	14	9	5	0.64	0.56	vein quartz	blade	0.612
9	82.00	141	60	45	0.43	0.75	quartzite	rod	0.514
10	27.33	38	30	14	0.79	0.47	schist	disc	0.663
11	32.33	40	36	21	0.90	0.58	quartzite	disc	0.779
12	37.67	58	28	27	0.48	0.96	vein quartz	rod	0.608
13	34.00	53	27	22	0.51	0.81	vein quartz	rod	0.596
14	32.33	42	35	20	0.83	0.57	vein quartz	disc	0.735
15	14.67	18	14	12	0.78	0.86	vein quartz	sphere	0.803
16	130.33	253	94	44	0.37	0.47	schist	blade	0.401
17	62.33	110	42	35	0.38	0.83	quartzite	rod	0.495
18	36.67	59	29	22	0.49	0.76	vein quartz	rod	0.568
19	103.33	192	70	48	0.36	0.69	schist	rod	0.450
20	64.33	101	49	43	0.49	0.88	quartzite	rod	0.591
21	93.00	126	112	41	0.89	0.37	quartzite	disc	0.661
22	50.00	79	38	33	0.48	0.87	vein quartz	rod	0.586
23	37.33	50	35	27	0.70	0.77	vein quartz	sphere	0.723
24	37.33	58	34	20	0.59	0.59	vein quartz	blade	0.587
25	26.33	28	28	23	1.00	0.82	vein quartz	sphere	0.937
26	46.67	61	51	28	0.84	0.55	quartzite	disc	0.727
27	55.67	125	31	11	0.25	0.35	schist	blade	0.279
28	27.67	49	22	12	0.45	0.55	schist	blade	0.479
29	29.33	52	23	13	0.44	0.57	schist	blade	0.480
30	39.67	54	35	30	0.65	0.86	vein quartz	rod	0.711
31	25.00	39	24	12	0.62	0.50	vein quartz	blade	0.574
32	90.67	189	62	21	0.33	0.34	schist	blade	0.332
33	66.33	91	64	44	0.70	0.69	vein quartz	sphere	0.698
34	65.33	120	56	20	0.47	0.36	schist	blade	0.427
35	13.67	19	14	8	0.74	0.57	vein quartz	disc	0.677
36	25.67	32	25	20	0.78	0.80	vein quartz	sphere	0.787
37	89.00	104	99	64	0.95	0.65	quartzite	disc	0.837
38	147.00	245	100	96	0.41	0.96	schist	rod	0.543
39	85.33	135	79	42	0.59	0.53	quartzite	blade	0.567
40	134.33	169	150	84	0.89	0.56	quartzite	disc	0.761
	55.93								

SITE 22b

obs	mean	a-axis	b-axis	c-axis	b/a	c/b	clasttype	roundness	shape	sphindex
1	125.00	160	160	55	1.00	0.34	quartzite	0.49	disc	0.701
2	141.67	210	155	60	0.74	0.39	schist	0.49	disc	0.595
3	122.67	200	125	43	0.63	0.34	quartzite	0.49	blade	0.512
4	61.00	105	50	28	0.48	0.56	vein quartz	0.7	blade	0.503
5	188.33	320	175	70	0.55	0.40	schist	0.25	blade	0.493
6	103.33	150	100	60	0.67	0.60	quartzite	0.49	disc	0.644
7	43.33	55	40	35	0.73	0.88	vein quartz	0.35	sphere	0.774
8	150.00	245	140	65	0.57	0.46	silcrete	0.49	blade	0.533
9	166.67	295	125	80	0.42	0.64	schist	0.49	blade	0.486
10	57.00	80	56	35	0.70	0.63	vein quartz	0.35	disc	0.674
11	203.33	400	110	100	0.28	0.91	schist	0.49	rod	0.410
12	137.67	200	168	45	0.84	0.27	quartzite	0.7	disc	0.574
13	79.00	120	84	33	0.70	0.39	quartzite	0.7	disc	0.577
14	129.00	182	125	80	0.69	0.64	vein quartz	0.17	disc	0.671
15	70.00	90	70	50	0.78	0.71	vein quartz	0.35	sphere	0.756
16	110.33	155	96	80	0.62	0.83	vein quartz	0.49	rod	0.684
17	294.33	460	325	98	0.71	0.30	schist	0.25	disc	0.532
18	166.67	240	195	65	0.81	0.33	quartzite	0.35	disc	0.604
19	232.00	370	250	76	0.68	0.30	quartzite	0.35	disc	0.518
20	136.67	220	130	60	0.59	0.46	schist	0.35	blade	0.544
21	145.00	175	165	95	0.94	0.58	vein quartz	0.25	disc	0.800
22	163.33	285	140	65	0.49	0.46	quartzite	0.49	blade	0.482
23	205.67	380	132	105	0.35	0.80	schist	0.49	rod	0.458
24	325.00	635	230	110	0.36	0.48	schist	0.35	blade	0.397
25	66.00	95	76	27	0.80	0.36	silcrete	0.7	disc	0.610
26	310.00	490	320	120	0.65	0.38	quartzite	0.49	blade	0.543
27	421.67	760	320	185	0.42	0.58	schist	0.25	blade	0.468
28	143.67	273	103	55	0.38	0.53	schist	0.35	blade	0.424
29	230.00	395	175	120	0.44	0.69	schist	0.35	rod	0.512
30	124.33	182	145	46	0.80	0.32	quartzite	0.49	disc	0.586
31	149.33	240	155	53	0.65	0.34	quartzite	0.7	blade	0.522
32	268.00	565	145	94	0.26	0.65	schist	0.49	blade	0.350
33	148.67	250	139	57	0.56	0.41	vein quartz	0.25	blade	0.502
34	172.00	278	195	43	0.70	0.22	schist	0.17	disc	0.477
35	84.67	138	66	50	0.48	0.76	vein quartz	0.35	rod	0.558
36	45.33	70	36	30	0.51	0.83	vein quartz	0.49	rod	0.604
37	48.67	67	39	40	0.58	1.03	vein quartz	0.35	rod	0.703
38	91.67	141	80	54	0.57	0.68	vein quartz	0.25	rod	0.601
39	30.67	40	40	12	1.00	0.30	quartzite	0.7	disc	0.669
40	59.67	86	50	43	0.58	0.86	vein quartz	0.7	rod	0.662
	148.78									

SITE 23

obs	mean	a-axis	b-axis	c-axis	b/a	c/b	clasttype	roundness	shape	sphindex
1	141.67	220	140	65	0.64	0.46	quartzite	0.7	blade	0.573
2	83.00	93	57	24	0.61	0.42	schist	0.7	disc	0.551
3	121.67	190	125	50	0.66	0.40	schist	0.17	blade	0.557
4	107.00	157	116	48	0.74	0.41	quartzite	0.7	disc	0.609
5	89.67	130	115	24	0.88	0.21	schist	0.49	disc	0.547
6	68.33	102	76	27	0.75	0.36	vein quartz	0.49	disc	0.582
7	141.33	258	103	63	0.40	0.61	schist	0.49	blade	0.460
8	155.33	233	153	80	0.66	0.52	schist	0.35	blade	0.609
9	328.67	675	215	96	0.32	0.45	schist	0.35	blade	0.356
10	401.67	850	240	115	0.28	0.48	schist	0.25	blade	0.337
11	304.33	393	270	250	0.69	0.93	quartzite	0.35	sphere	0.759
12	218.00	390	240	24	0.62	0.10	schist	0.17	blade	0.336
13	336.67	540	370	100	0.69	0.27	schist	0.17	disc	0.503
14	66.33	105	62	32	0.59	0.52	vein quartz	0.35	blade	0.565
15	63.67	122	47	22	0.39	0.47	schist	0.49	blade	0.411
16	116.67	185	105	60	0.57	0.57	vein quartz	0.17	blade	0.569
17	52.33	75	47	35	0.63	0.74	vein quartz	0.7	rod	0.664
18	195.33	375	163	48	0.43	0.29	schist	0.17	blade	0.382
19	79.33	120	65	53	0.54	0.82	vein quartz	0.49	rod	0.621
20	116.67	155	145	50	0.94	0.34	quartzite	0.49	disc	0.671
21	117.33	177	130	45	0.73	0.35	quartzite	0.7	disc	0.572
22	103.33	140	103	67	0.74	0.65	vein quartz	0.17	disc	0.706
23	240.67	480	185	57	0.39	0.31	schist	0.17	blade	0.358
24	72.00	118	73	25	0.62	0.34	schist	0.49	blade	0.508
25	78.33	123	80	32	0.65	0.40	schist	0.35	blade	0.553
26	327.33	500	264	218	0.53	0.83	schist	0.17	rod	0.613
27	75.00	130	70	25	0.54	0.36	vein quartz	0.35	blade	0.470
28	393.33	615	410	155	0.67	0.38	schist	0.17	disc	0.552
29	121.33	210	117	37	0.56	0.32	schist	0.49	blade	0.461
30	49.67	60	54	35	0.90	0.65	vein quartz	0.49	disc	0.807
31	146.67	220	170	50	0.77	0.29	schist	0.17	disc	0.560
32	151.67	185	170	100	0.92	0.59	silcrete	0.7	disc	0.792
33	103.33	155	108	47	0.70	0.44	silcrete	0.7	disc	0.596
34	91.00	170	75	28	0.44	0.37	schist	0.35	blade	0.417
35	105.33	175	95	46	0.54	0.48	vein quartz	0.17	blade	0.523
36	145.00	232	122	81	0.53	0.66	schist	0.35	blade	0.568
37	86.33	122	90	47	0.74	0.52	silcrete	0.7	disc	0.657
38	108.33	150	105	70	0.70	0.67	vein quartz	0.17	sphere	0.689
39	47.67	76	53	14	0.70	0.26	schist	0.7	disc	0.505
40	101.00	173	110	20	0.64	0.18	schist	0.7	blade	0.419
	145.81									

SITE 24

obs	mean	a-axis	b-axis	c-axis	b/a	c/b	clasttype	roundness	shape	sphindex
1	98.33	205	46	44	0.22	0.96	quartzite	0.49	rod	0.364
2	119.00	246	66	45	0.27	0.68	schist	0.35	rod	0.366
3	61.67	105	48	32	0.46	0.67	vein quartz	0.7	rod	0.518
4	37.67	63	40	10	0.63	0.25	schist	0.49	blade	0.465
5	117.33	234	60	58	0.26	0.97	schist	0.49	rod	0.399
6	59.00	103	57	17	0.55	0.30	quartzite	0.7	blade	0.450
7	71.67	125	58	32	0.46	0.55	vein quartz	0.49	blade	0.492
8	36.67	52	43	15	0.83	0.35	quartzite	0.7	disc	0.620
9	104.33	213	75	25	0.35	0.33	schist	0.49	blade	0.346
10	66.67	110	60	30	0.55	0.50	schist	0.49	blade	0.530
11	64.00	83	66	43	0.80	0.65	vein quartz	0.7	disc	0.744
12	295.00	595	225	65	0.38	0.29	schist	0.17	blade	0.346
13	150.33	274	127	50	0.46	0.39	schist	0.49	blade	0.439
14	211.67	290	215	130	0.74	0.60	schist	0.49	disc	0.693
15	168.33	245	175	85	0.71	0.49	vein quartz	0.17	disc	0.628
16	211.67	265	260	110	0.98	0.42	quartzite	0.35	disc	0.741
17	128.33	180	140	65	0.78	0.46	vein quartz	0.49	disc	0.655
18	156.00	220	170	78	0.77	0.46	schist	0.35	disc	0.649
19	141.67	175	150	100	0.86	0.67	quartzite	0.35	disc	0.788
20	92.67	130	100	48	0.77	0.48	vein quartz	0.7	disc	0.657
21	69.67	130	67	12	0.52	0.18	schist	0.7	blade	0.362
22	99.33	150	100	48	0.67	0.48	vein quartz	0.49	disc	0.598
23	363.33	645	360	85	0.56	0.24	schist	0.17	blade	0.419
24	84.00	120	90	42	0.75	0.47	silcrete	0.7	disc	0.640
25	37.67	52	46	15	0.88	0.33	quartzite	0.7	disc	0.634
26	119.67	212	83	64	0.39	0.77	schist	0.7	rod	0.491
27	105.00	165	110	40	0.67	0.36	vein quartz	0.7	disc	0.545
28	598.33	1120	465	210	0.42	0.45	schist	0.35	blade	0.427
29	765.00	1460	510	325	0.35	0.64	schist	0.49	blade	0.427
30	152.67	225	158	75	0.70	0.47	quartzite	0.7	disc	0.616
31	211.67	400	155	80	0.39	0.52	schist	0.7	blade	0.426
32	57.00	80	55	36	0.69	0.65	vein quartz	0.7	disc	0.676
33	123.67	195	96	80	0.49	0.83	schist	0.35	rod	0.587
34	116.00	190	130	28	0.68	0.22	quartzite	0.49	disc	0.465
35	100.00	145	120	35	0.83	0.29	quartzite	0.35	disc	0.585
36	556.67	1150	360	160	0.31	0.44	schist	0.25	blade	0.352
37	70.00	105	83	22	0.79	0.27	vein quartz	0.7	disc	0.549
38	78.67	140	78	18	0.56	0.23	quartzite	0.7	blade	0.415
39	108.33	180	112	33	0.62	0.29	gneiss	0.49	blade	0.485
40	38.00	50	40	24	0.80	0.60	vein quartz	0.7	disc	0.727
	156.17									

SITE 22a

obs	mean	a-axis	b-axis	c-axis	b/a	c/b	clasttype	roundness	shape	sphindex
1	27.33	46	21	15	0.46	0.71	vein quartz	0.49	rod	0.530
2	26.67	37	26	17	0.70	0.65	vein quartz	0.49	disc	0.686
3	37.67	55	38	20	0.69	0.53	vein quartz	0.35	disc	0.631
4	70.00	105	60	45	0.57	0.75	vein quartz	0.17	rod	0.626
5	33.67	45	30	26	0.67	0.87	vein quartz	0.17	sphere	0.728
6	23.00	35	19	15	0.54	0.79	vein quartz	0.35	rod	0.615
7	30.33	45	36	10	0.80	0.28	gneiss	0.7	disc	0.562
8	52.00	77	42	37	0.55	0.88	vein quartz	0.35	rod	0.640
9	27.33	47	23	12	0.49	0.52	vein quartz	0.35	blade	0.500
10	76.33	154	55	20	0.36	0.36	schist	0.7	blade	0.359
11	20.67	33	16	13	0.48	0.81	vein quartz	0.35	rod	0.576
12	15.67	33	12	2	0.36	0.17	schist	0.7	blade	0.280
13	59.33	82	58	38	0.71	0.66	vein quartz	0.35	disc	0.689
14	35.00	45	38	22	0.84	0.58	vein quartz	0.7	disc	0.745
15	32.00	57	23	16	0.40	0.70	vein quartz	0.49	rod	0.484
16	59.67	110	43	26	0.39	0.60	vein quartz	0.17	blade	0.452
17	16.00	26	11	11	0.42	1.00	vein quartz	0.49	rod	0.564
18	52.67	73	55	30	0.75	0.55	vein quartz	0.35	disc	0.677
19	23.67	40	21	10	0.53	0.48	vein quartz	0.49	blade	0.508
20	30.00	40	28	22	0.70	0.79	quartzite	0.7	sphere	0.727
21	16.33	21	20	8	0.95	0.40	vein quartz	0.7	disc	0.713
22	33.00	60	25	14	0.42	0.56	vein quartz	0.49	blade	0.460
23	47.00	95	35	11	0.37	0.31	schist	0.49	blade	0.349
24	27.00	42	24	15	0.57	0.63	vein quartz	0.49	blade	0.589
25	22.67	32	23	13	0.72	0.57	vein quartz	0.7	disc	0.663
26	47.00	89	40	12	0.45	0.30	schist	0.7	blade	0.393
27	20.33	37	18	6	0.49	0.33	schist	0.7	blade	0.429
28	58.33	95	43	37	0.45	0.86	vein quartz	0.35	rod	0.561
29	69.33	98	72	38	0.73	0.53	vein quartz	0.35	disc	0.658
30	36.00	56	37	15	0.66	0.41	vein quartz	0.25	blade	0.561
31	34.33	53	30	20	0.57	0.67	vein quartz	0.49	rod	0.598
32	24.00	32	24	16	0.75	0.67	vein quartz	0.49	sphere	0.721
33	34.67	57	34	13	0.60	0.38	vein quartz	0.49	blade	0.514
34	45.33	72	37	27	0.51	0.73	vein quartz	0.35	rod	0.578
35	44.67	63	44	27	0.70	0.61	vein quartz	0.49	disc	0.669
36	20.00	35	18	7	0.51	0.39	quartzite	0.7	blade	0.469
37	31.33	39	31	24	0.79	0.77	vein quartz	0.35	sphere	0.788
38	20.33	31	22	8	0.71	0.36	vein quartz	0.49	disc	0.568
39	22.33	32	20	15	0.63	0.75	vein quartz	0.7	rod	0.664
40	30.33	41	25	25	0.61	1.00	vein quartz	0.25	rod	0.719
	35.83									

SITE 16

obs	mean	a-axis	b-axis	c-axis	b/a	c/b	clasttype	roundness	shape	sphindex
1	254.33	416	213	134	0.51	0.63	quartzite	0.35	blade	0.548
2	223.67	310	250	111	0.81	0.44	quartzite	0.35	disc	0.661
3	258.00	403	254	117	0.63	0.46	quartzite	0.25	blade	0.568
4	64.33	89	80	24	0.90	0.30	quartzite	0.70	disc	0.624
5	128.67	152	126	108	0.83	0.86	vein quartz	0.70	sphere	0.838
6	56.33	74	60	35	0.81	0.58	vein quartz	0.49	disc	0.727
7	78.00	113	92	29	0.81	0.32	silcrete	0.70	disc	0.593
8	75.67	118	80	29	0.68	0.36	quartzite	0.70	disc	0.550
9	114.67	232	89	23	0.38	0.26	schist	0.70	blade	0.336
10	110.00	157	120	53	0.76	0.44	vein quartz	0.70	disc	0.637
11	56.67	76	65	29	0.86	0.45	vein quartz	0.70	disc	0.688
12	103.67	149	114	48	0.77	0.42	quartzite	0.49	disc	0.627
13	177.67	227	173	133	0.76	0.77	quartzite	0.49	sphere	0.764
14	120.33	188	137	36	0.73	0.26	quartzite	0.49	disc	0.519
15	120.33	155	155	51	1.00	0.33	silcrete	0.70	disc	0.690
16	170.67	212	172	128	0.81	0.74	schist	0.49	sphere	0.788
17	255.33	378	279	109	0.74	0.39	vein quartz	0.35	disc	0.597
18	73.00	104	89	26	0.86	0.29	quartzite	0.70	disc	0.598
19	53.67	72	69	20	0.96	0.29	gneiss	0.70	disc	0.643
20	33.67	50	39	12	0.78	0.31	quartzite	0.70	disc	0.572
21	51.00	71	60	22	0.85	0.37	quartzite	0.70	disc	0.640
22	49.67	76	51	22	0.67	0.43	quartzite	0.70	disc	0.579
23	105.00	133	132	50	0.99	0.38	silcrete	0.70	disc	0.720
24	77.00	125	73	33	0.58	0.45	quartzite	0.70	blade	0.536
25	46.00	62	46	30	0.74	0.65	vein quartz	0.70	disc	0.711
26	99.00	148	99	50	0.67	0.51	gneiss	0.70	disc	0.609
27	21.33	28	22	14	0.79	0.64	vein quartz	0.70	disc	0.732
28	38.67	50	46	20	0.92	0.43	quartzite	0.70	disc	0.717
29	48.00	82	45	17	0.55	0.38	quartzite	0.70	blade	0.485
30	45.67	62	53	22	0.85	0.42	silcrete	0.70	disc	0.672
31	54.00	106	43	13	0.41	0.30	schist	0.70	blade	0.368
32	18.67	30	14	12	0.47	0.86	quartzite	0.70	rod	0.572
33	158.67	247	145	84	0.59	0.58	quartzite	0.35	blade	0.584
34	268.67	357	295	154	0.83	0.52	quartzite	0.49	disc	0.709
35	24.33	35	24	14	0.69	0.58	vein quartz	0.70	disc	0.650
36	134.00	182	137	83	0.75	0.61	quartzite	0.70	disc	0.700
37	38.00	63	37	14	0.59	0.38	quartzite	0.70	blade	0.507
38	40.67	48	43	31	0.90	0.72	vein quartz	0.70	sphere	0.833
39	75.67	157	47	23	0.30	0.49	schist	0.70	blade	0.353
40	150.67	179	178	95	0.99	0.53	vein quartz	0.70	disc	0.808
	101.83									

Table: AI.B EXOTIC CLAST SIZE, SHAPE AND COMPOSITION

SITE 16

obs	mean	a-axis	b-axis	c-axis	exotic clasttype	roundness
1	44	68	37	27	banded ironstone	0.70
2	22	33	20	13	banded ironstone	0.70
3	26	31	24	22	banded ironstone	0.70
4	27	42	26	14	banded ironstone	0.70
5	18	24	16	14	banded ironstone	0.70
6	28	45	26	14	banded ironstone	0.70
7	32	55	30	10	banded ironstone	0.70
8	38	56	40	17	banded ironstone	0.49
9	26	35	32	12	banded ironstone	0.49
10	26	42	22	13	banded ironstone	0.70
11	28	38	31	14	banded ironstone	0.70
12	27	43	25	12	banded ironstone	0.70
13	19	29	16	12	banded ironstone	0.70
14	20	25	20	14	banded ironstone	0.70
15	20	32	19	10	banded ironstone	0.70
16	28	39	31	13	banded ironstone	0.70
17	26	40	28	11	banded ironstone	0.70
18	22	27	21	17	banded ironstone	0.70
19	27	42	23	17	banded ironstone	0.70
20	11	14	13	6	jasper	0.70
21	14	18	14	9	jasper	0.70
22	24	31	29	13	banded ironstone	0.49
23	22	27	26	12	banded ironstone	0.70
24	25	39	19	17	quartz porphory	0.70
25	18	27	16	12	banded ironstone	0.70
26	17	23	18	10	riebeckite	0.70
27	17	25	17	9	riebeckite	0.70
28	19	29	20	7	banded ironstone	0.70
29	20	28	19	12	banded ironstone	0.70
30	26	33	32	13	quartz porphory	0.70

SITE 7

obs	mean	a-axis	b-axis	c-axis	exotic clasttype	roundness
1	39	54	37	26	quartz porphory	0.70
2	32	40	35	22	quartz porphory	0.70
3	29	40	30	16	banded ironstone	0.70
4	18	26	18	11	banded ironstone	0.70
5	23	34	20	16	banded ironstone	0.70
6	21	34	20	8	banded ironstone	0.70
7	19	27	20	9	banded ironstone	0.70
8	20	31	21	9	banded ironstone	0.70
9	9	12	10	6	banded ironstone	0.70
10	13	19	12	7	banded ironstone	0.70
11	10	15	10	4	banded ironstone	0.70
12	12	17	12	7	banded ironstone	0.70
13	15	24	14	6	banded ironstone	0.70
14	18	23	17	13	agate	0.70
15	11	15	11	8	agate	0.49
16	19	25	18	14	agate	0.70
17	15	17	15	14	agate	0.70
18	15	20	15	10	agate	0.70
19	16	24	14	11	agate	0.70
20	15	23	13	10	agate	0.70
21	18	25	18	10	agate	0.70
22	18	26	14	13	agate	0.49
23	13	19	10	10	agate	0.70
24	13	16	13	11	agate	0.70
25	13	18	12	9	agate	0.70
26	14	18	14	10	agate	0.70
27	9	11	9	7	agate	0.70
28	9	13	9	5	zeolite	0.70
29	10	15	9	6	zeolite	0.70
30	24	28	23	20	agate	0.70

SITE 24

obs	mean	a-axis	b-axis	c-axis	exotic clasttype	roundness
1	16	22	16	11	jasper	0.70
2	17	22	18	10	agate	0.70
3	11	15	11	8	agate	0.49
4	14	20	13	8	riebeckite	0.70
5	14	24	11	8	quartz porphory	0.25
6	21	35	18	11	banded ironstone	0.70
7	16	21	16	10	banded ironstone	0.70
8	13	20	13	5	banded ironstone	0.70
9	18	24	17	12	banded ironstone	0.70
10	14	18	15	8	banded ironstone	0.70
11	13	17	14	8	banded ironstone	0.70
12	52	71	60	24	quartz porphory	0.70
13	23	35	21	13	quartz porphory	0.70
14	9	12	9	5	banded ironstone	0.70
15	8	12	8	5	banded ironstone	0.70
16	22	31	25	10	banded ironstone	0.70
17	20	33	17	10	banded ironstone	0.70
18	21	33	22	9	banded ironstone	0.49
19	16	25	17	7	banded ironstone	0.49
20	15	20	15	10	banded ironstone	0.70
21	12	20	12	4	banded ironstone	0.70
22	11	17	11	6	banded ironstone	0.70
23	9	16	8	4	banded ironstone	0.70
24	17	24	15	13	banded ironstone	0.70
25	15	25	15	5	banded ironstone	0.70
26	22	27	23	17	agate	0.70
27	16	22	16	10	jasper	0.70
28	16	22	17	8	agate	0.70
29	11	15	11	8	agate	0.70
30	13	18	12	8	riebeckite	0.70

SITE 15

obs	mean	a-axis	b-axis	c-axis	exotic clasttype	roundness
1	36	46	38	23	quartz porphory	0.70
2	38	62	35	17	jasper	0.70
3	18	22	20	11	agate	0.70
4	16	23	16	9	agate	0.70
5	15	18	15	11	agate	0.70
6	16	21	17	10	agate	0.70
7	21	24	22	16	agate	0.70
8	25	40	26	9	riebeckite	0.70
9	17	23	16	13	riebeckite	0.70
10	22	35	17	13	banded ironstone	0.70
11	30	43	31	17	banded ironstone	0.70
12	16	26	14	9	banded ironstone	0.70
13	13	16	14	10	epidosite	0.70
14	26	38	28	11	banded ironstone	0.70
15	20	30	20	10	banded ironstone	0.70
16	20	28	18	13	banded ironstone	0.70
17	20	28	20	13	banded ironstone	0.70
18	27	35	27	18	banded ironstone	0.70
19	27	44	21	15	banded ironstone	0.70
20	26	38	30	11	banded ironstone	0.70
21	11	14	10	8	banded ironstone	0.70
22	22	34	20	12	banded ironstone	0.70
23	8	10	7	7	chalcedony	0.70
24	32	51	32	12	banded ironstone	0.70
25	15	20	17	7	banded ironstone	0.70
26	15	26	11	8	riebeckite	0.70
27	14	20	14	8	jasper	0.70
28	11	16	10	7	riebeckite	0.70
29	5	6	5	4	agate	0.70
30	9	10	9	8	agate	0.70

SITE 17

obs	mean	a-axis	b-axis	c-axis	exotic clasttype	roundness
1	21	33	22	8	banded ironstone	0.70
2	21	28	26	8	banded ironstone	0.70
3	19	27	23	8	banded ironstone	0.70
4	22	31	24	10	banded ironstone	0.70
5	20	26	21	14	banded ironstone	0.70
6	19	30	20	8	banded ironstone	0.70
7	25	31	24	20	agate	0.70
8	21	31	17	16	agate	0.70
9	22	23	21	21	agate	0.70
10	20	24	23	12	jasper	0.70
11	18	26	18	9	banded ironstone	0.70
12	15	25	14	6	banded ironstone	0.70
13	17	28	14	9	banded ironstone	0.70
14	15	26	10	9	banded ironstone	0.70
15	14	23	11	8	banded ironstone	0.70
16	16	18	18	12	banded ironstone	0.70
17	14	22	15	6	banded ironstone	0.70
18	13	21	11	8	banded ironstone	0.70
19	14	17	14	10	banded ironstone	0.70
20	10	17	8	5	banded ironstone	0.70
21	13	18	13	8	banded ironstone	0.70
22	13	17	11	10	banded ironstone	0.70
23	13	18	12	8	banded ironstone	0.70
24	10	16	10	3	banded ironstone	0.70
25	14	22	13	7	banded ironstone	0.49
26	13	17	14	7	banded ironstone	0.49
27	10	12	9	8	banded ironstone	0.70
28	10	13	10	8	banded ironstone	0.70
29	13	16	12	10	banded ironstone	0.49
30	12	17	11	8	banded ironstone	0.49

Table: AI.C PALAEOCURRENT ANALYSIS

SITE 22a

obs	facies	dip	azimuth
1	foreshore	6	235
2	foreshore	8	245
3	foreshore	2	256
4	foreshore	3	235
5	foreshore	8	220
6	foreshore	7	225
7	foreshore	5	233
8	foreshore	17	223
9	foreshore	6	230
10	foreshore	9	228
11	foreshore	8	245
12	foreshore	10	234
13	foreshore	9	235
14	foreshore	8	220
15	foreshore	5	248
16	foreshore	22	238
17	foreshore	20	232
18	foreshore	11	255
19	foreshore	25	246
20	foreshore	6	255
21	foreshore	16	254
22	foreshore	12	260
23	foreshore	22	252
24	foreshore	17	238
25	foreshore	6	254
26	foreshore	1	249
27	foreshore	5	245
28	foreshore	7	240
29	foreshore	5	245
	MEAN	10	241

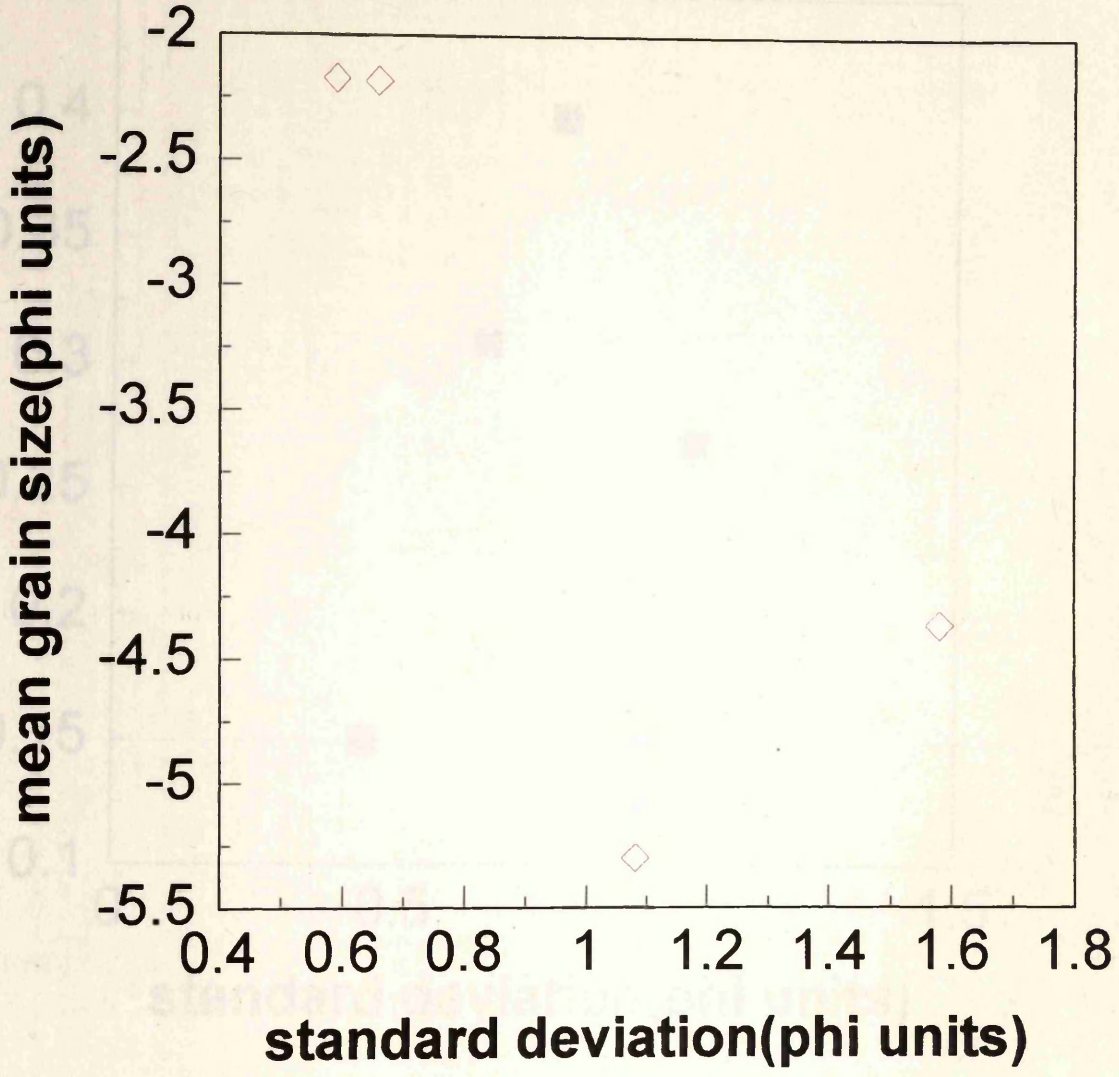

Fig.AI.1 The relationship between the standard deviation and mean grain size for red unit gravel within the study area(pocket beach no.4), Chameis.

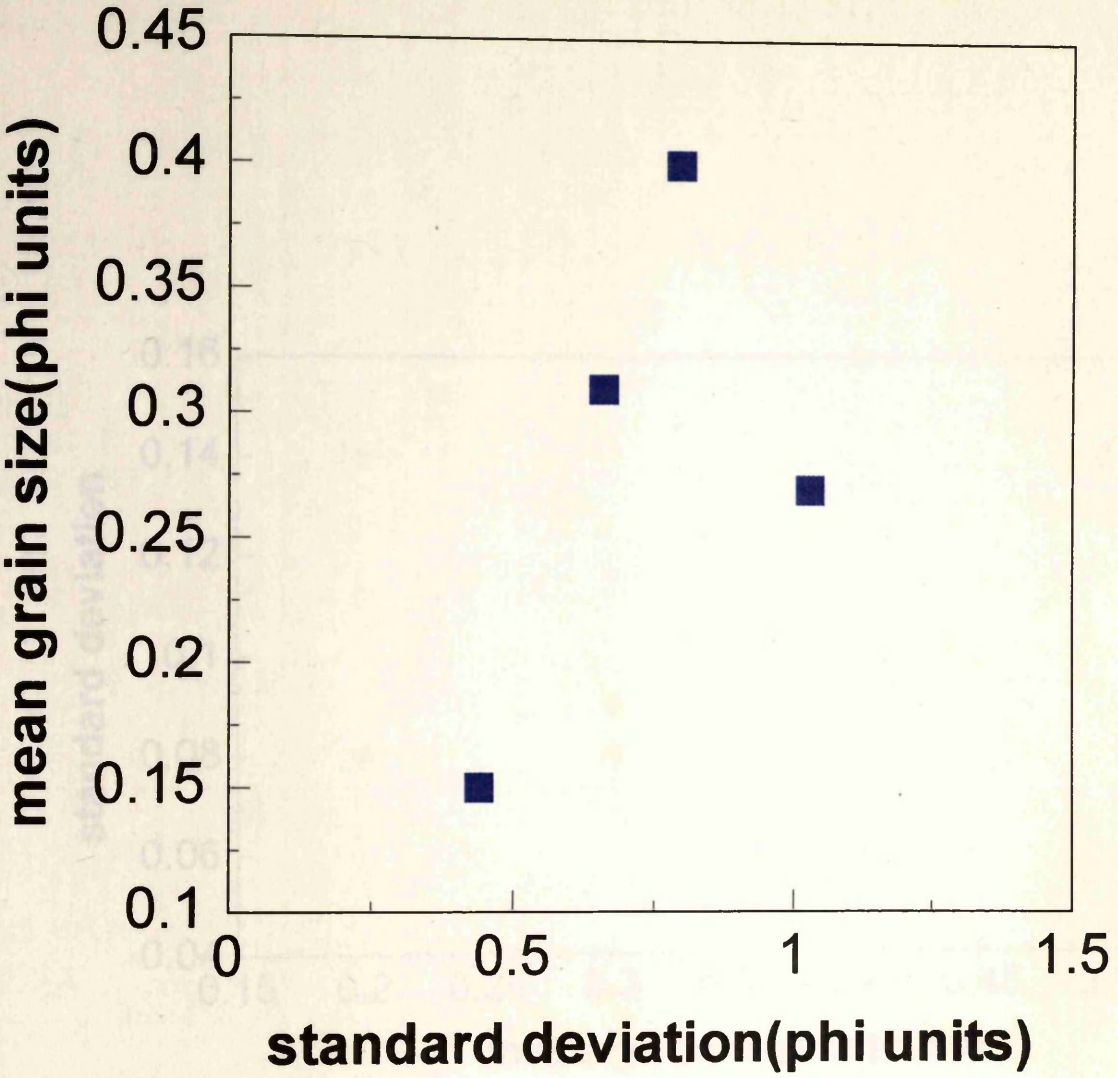

Fig. AI.2 The relationship between the standard deviation and mean grain size for red unit sand within the study area(pocket beach no.4), Chameis.

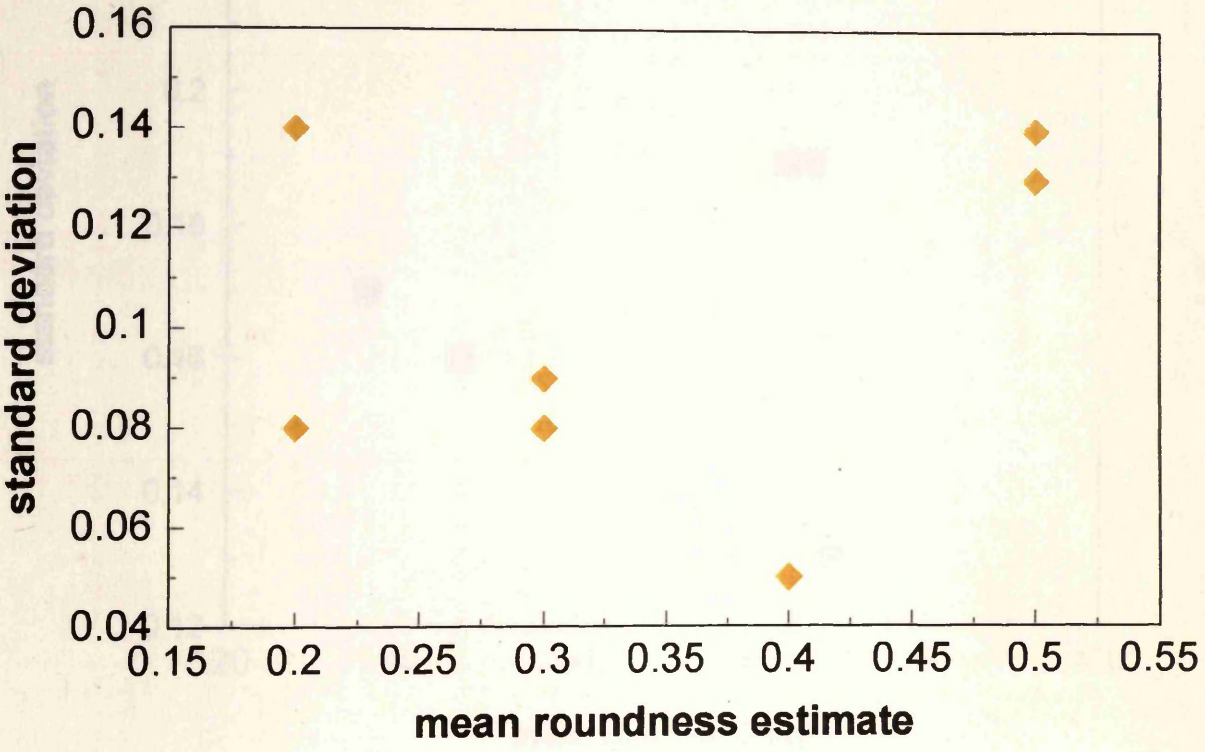

Fig. AI.3 The relationship between the mean roundness estimate and standard deviation for vein quartz: red unit at site 22a.

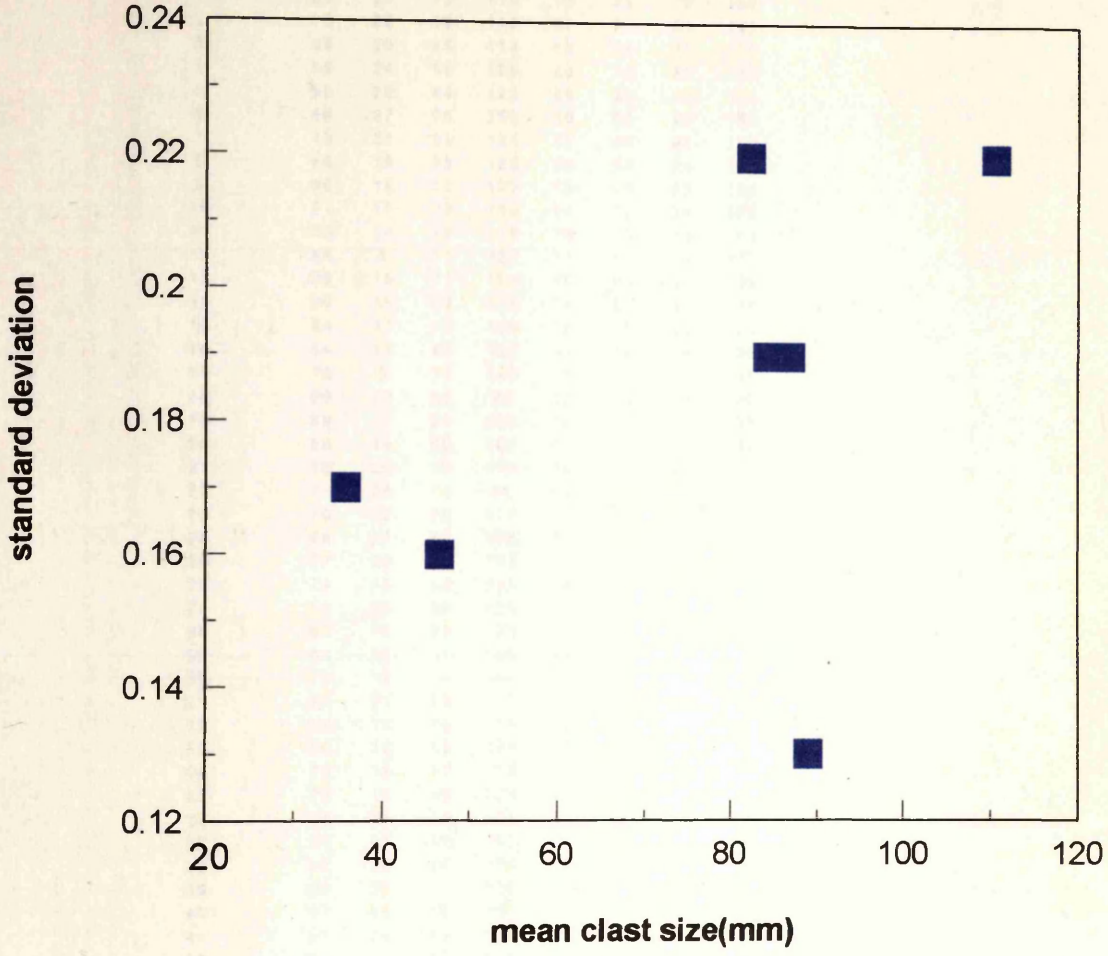

Fig. **AI.4** The relationship between mean clast size(mm) and the standard deviation of the roundness estimate for vein quartz of both the grey and red units within the study area.

Table: AII.A BEDROCK ORIENTATION DATA

obs	S1 dip	strike	J1 dip	strike	J2 dip	strike	J3 dip	strike
1	64	20	75	110	73	45	70	150
2	75	22	59	112	89	53	31	153
3	69	20	85	114	88	66	31	173
4	58	24	66	128	63	70	27	169
5	66	20	84	123	89	60	40	135
6	69	27	76	150	90	55	24	160
7	73	21	81	124	87	80	29	159
8	63	19	85	122	90	64	24	165
9	66	15	75	127	73	45	25	165
10	71	17	73	110	84	73	29	153
11	73	14	79	115	75	73	26	159
12	69	8	71	122	71	64	24	173
13	88	15	71	124	60	60	60	132
14	90	18	69	115	74	62	56	132
15	84	34	42	128	75	75	23	170
16	64	15	82	125	64	84	74	138
17	76	3	77	120	85	53	74	135
18	88	22	85	95	82	50	34	130
19	68	17	81	105	90	55	46	138
20	68	14	82	107	69	76	64	135
21	70	25	79	115	79	77	85	130
22	74	26	75	96	66	58	61	140
23	70	25	88	117	77	56		
24	68	27	90	105	74	57		
25	77	20	62	123	81	69		
26	74	15	54	120	90	66		
27	71	25	54	126	69	66		
28	64	18	58	120	90	49		
29	64	20	34	130	56	70		
30	73	15	74	104	81	81		
31	57	21	58	117	74	60		
32	55	14	59	118	90	72		
33	69	12	59	126	57	86		
34	73	15	51	105	81	55		
35	77	16	49	109	90	85		
36	60	20	50	123	75	85		
37	51	18	56	120				
38	81	25	83	105				
39	69	25	71	122				
40	77	20	60	90				
41	81	25	90	109				
42	64	27	87	102				
43			72	105				
44			74	105				
45			66	100				
46			66	95				
47			64	118				
48			49	110				
49			74	90				
50			61	112				
51			62	115				
52			90	113				
53			59	105				
54			90	115				
55			85	115				
56			90	119				
57			85	115				
58			90	118				
59			89	120				
60			90	120				
61			90	109				
62			90	115				
63			60	105				
64			81	112				
65			86	113				
66			90	118				
67			66	115				
68			62	126				
69			79	125				
70			60	126				

S1 = schistosity
J1-J3 = Major joints

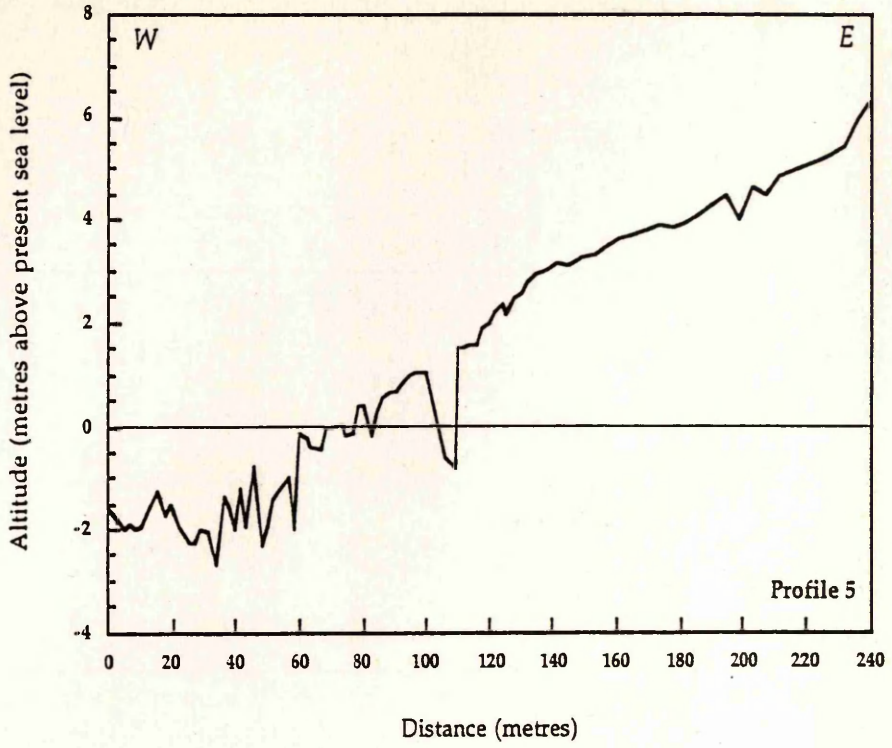

Fig. AII.1 Shore platform Profile 5 from site 20.

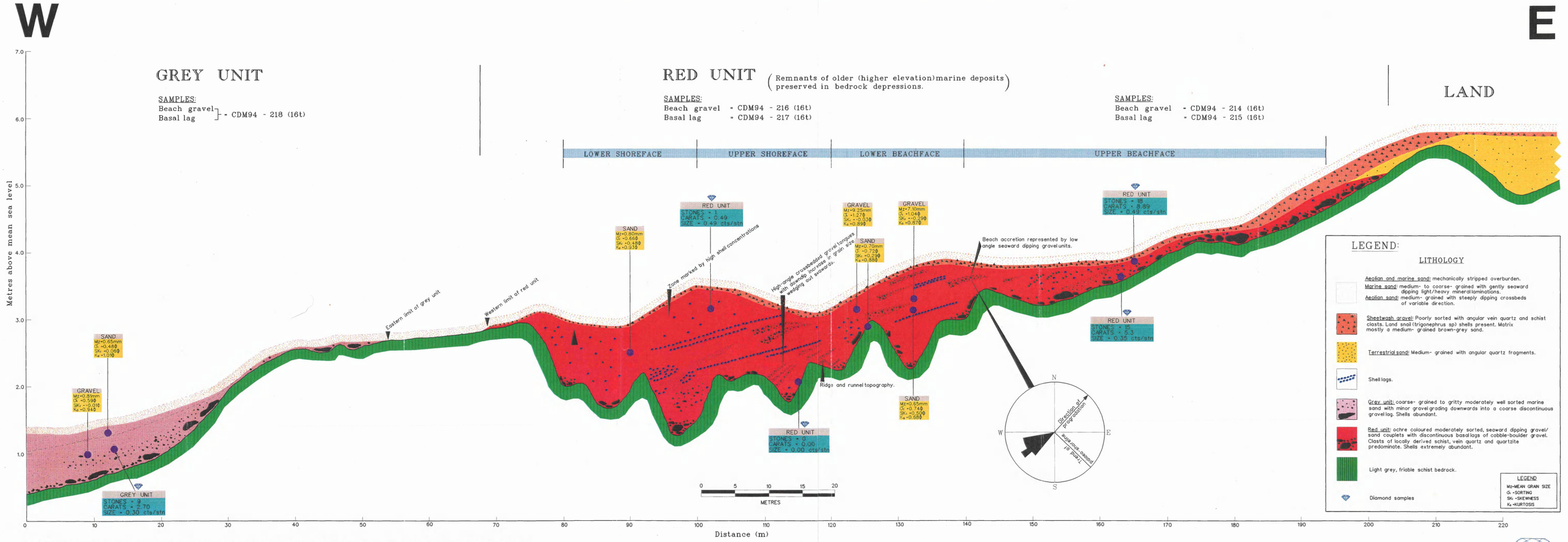

Fig.**3.5** Detailed cross-section across the grey and red units at site 21, within the study area (pocket beach no. 4), Chameis. Also indicated are diamond and grain size distributions across the beach, diamond size in carats per stone (cts/stn). A rose diagram showing directions of planar crossbeds relative to trend of palaeo-shoreline at site 22.